MARCH 1955

A.I.Ch.E. JOURNAL

Published by the American Institute of Chemical Engineers

CONTENTS

Effect of Fluid Properties on Mass Transfer in the Gas Phase
E. J. LYNCH AND C. R. WILKE

Phase Equilibria in Systems with Ethylene Above Its Critical Temperature
D. B. TODD AND J. C. ELGIN

Mass Transfer in Packed Beds
R. W. FAHIEN AND J. M. SMITH

Isobaric Integral Heat of Vaporization of Hydrocarbon Mixtures from Vapor-liquid *K* Values
W. C. EDMISTER

Fall of Single Liquid Drops Through Water
SHENGEN HU AND R. C. KINTNER

Absorption of Ethylene Oxide in a Packed Column with Various Solvents
C. F. BONILLA AND S. BARON

Transport of Momentum and Energy in a Ducted Jet
I. Experimental Study of a Nonisothermal Jet of Air Discharging into a Duct
II. Theoretical Study of Turbulent Transport of Momentum, Energy, and Matter in Ducted Coaxial Streams
III. Correlation of Profiles of Total Momentum and Energy Flux in a Nonisothermal Jet Discharging into a Duct
L. G. ALEXANDER, ARNOLD KIVNICK, E. W. COMINGS, AND E. D. HENZE

Laws of Corresponding States
L. G. NELSON AND E. F. OBERT

Upward Cocurrent Annular Flow of Air and Water in Smooth Tubes
SEYMOUR CALVERT AND BRYMER WILLIAMS

Enthalpy-concentration Diagrams for Binary Aqueous Mixtures of Hydrazine, Sodium Carbonate, and Glycerine
MACK TYNER

Enrichment Calculations in Gaseous Diffusion: Large Separation Factor
R. W. NAYLOR AND PAUL O. BACKER

Use of the Redlich and Kwong Equation of State in Calculating Thermodynamic Properties of Gases from Experimental Compressibility Data
HENDRICK C. VAN NESS

Controlling Mechanism in the Aqueous Absorption of Nitrogen Oxides
M. S. PETERS, C. P. ROSS, AND J. E. KLEIN

Approximate Equations for Time of Batch Fractionation
A. I. JOHNSON, CHEN-JUNG HUANG, AND F. D. TALBOT

Kinetics of the Catalyzed and Uncatalyzed Liquid-phase Hydration of Propylene Oxide
A. L. BENHAM AND F. L. KURATA

Performance of Small Herschel-Type Venturi Tubes
P. J. WALKER, JR., R. J. FORESTI, JR., F. RUSINKO, JR., AND B. W. MCCORMICK

ASSUMPTION UNIVERSITY LIBRARY

Foote LITHIUM HYDROXIDE

The basic lithium salt for industrial use, Foote lithium hydroxide provides chemically unique properties which are being applied to a host of products ranging from ceramic formulations to multi-purpose grease manufacture and welding rod coatings. Many other industrial uses of lithium are in the development stage.

Foote's integrated lithium facilities—raw material, production, research—are your assurance of an abundant supply of lithium for you and all industry.

We invite you to investigate and apply the unusual properties of lithium hydroxide and its derivatives in your products or processes.

Write for technical data sheets.

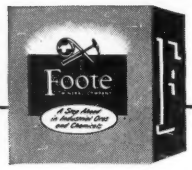

LITHIUM HYDROXIDE FOR INDUSTRY

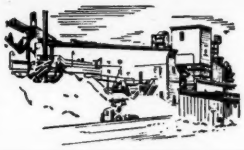

Kings Mountain, N.C. . . . where Foote is mining large deposits of spodumene.

Sunbright, Va. . . . the world's largest lithium chemical plant.

FOOTE MINERAL COMPANY

448 Eighteen West Chelten Building, Philadelphia 44, Pa.

RESEARCH LABORATORIES: Berwyn, Pa. • PLANTS: Exton, Pa.; Kings Mountain, N.C.; Sunbright, Va.

March
1955

A.I.Ch.E. JOURNAL

Vol. 1
No. 1

ADVISORY BOARD

C. M. Cooper, O. E. Dwyer,
W. C. Edmister, E. R. Gilliland,
A. N. Hixson, W. R. Marshall, Jr.,
R H. Newton, R. L. Pigford,
J. M Smith, Theodore Vermeulen,
R. R. White, R. H. Wilhelm

PUBLISHER

F. J. Van Antwerpen

EDITOR

Harding Bliss

The A.I.Ch. E. Journal, an official publication of the American Institute of Chemical Engineers, is devoted in the main to theoretical developments and research in chemical engineering and allied branches of engineering and science.

		Page
Greetings		7
Effect of Fluid Properties on Mass Transfer in the Gas Phase	E. J. Lynch and C. R. Wilke	9
Phase Equilibria in Systems with Ethylene Above Its Critical Temperature	D. B. Todd and J. C. Elgin	20
Mass Transfer in Packed Beds	R. W. Fahien and J. M. Smith	28
Isobaric Integral Heat of Vaporization of Hydrocarbon Mixtures from Vapor-liquid *K* Values	W. C. Edmister	38
Fall of Single Liquid Drops Through Water	Shengen Hu and R. C. Kintner	42
Absorption of Ethylene Oxide in a Packed Column with Various Solvents	C. F. Bonilla and S. Baron	49
Transport of Momentum and Energy in a Ducted Jet I. Experimental Study of a Nonisothermal Jet of Air Discharging into a Duct II. Theoretical Study of Turbulent Transport of Momentum, Energy, and Matter in Ducted Coaxial Streams III. Correlation of Profiles of Total Momentum and Energy Flux in a Nonisothermal Jet Discharging into a Duct	L. G. Alexander, A. Kivnick, E. W. Comings and E. D. Henze	55
Laws of Corresponding States	L. G. Nelson and E. F. Obert	74
Upward Cocurrent Annular Flow of Air and Water in Smooth Tubes	Seymour Calvert and Brymer Williams	78
Enthalpy-concentration Diagrams for Binary Aqueous Mixtures of Hydrazine, Sodium Carbonate, and Glycerine	Mack Tyner	87
Enrichment Calculations in Gaseous Diffusion: Large Separation Factor	R. W. Naylor and Paul O. Backer	95
Use of the Redlich and Kwong Equation of State in Calculating Thermodynamic Properties of Gases from Experimental Compressibility Data	Hendrick C. Van Ness	100
Controlling Mechanism in the Aqueous Absorption of Nitrogen Oxides	M. S. Peters, C. P. Ross, and J. E. Klein	105
Approximate Equations for Time of Batch Fractionation	A. I. Johnson, Chen-Jung Huang, and F. D. F. Talbot	111
Kinetics of the Catalyzed and Uncatalyzed Liquid-phase Hydration of Propylene Oxide	A. L. Benham and F. L. Kurata	118
Performance of Small Herschel-type Venturi Tubes	P. L. Walker, Jr., R. J. Foresti, Jr., F. Rusinko, Jr., and B. W. McCormick	125
A Note on the Additivity of Diffusional Resistances	T. K. Sherwood and K. F. Gordon	129
Books		130

89926

Publication office, Orange, Connecticut. Published quarterly in March, June, September, and December by the American Institute of Chemical Engineers, 25 West 45 Street, New York 36, New York. Manuscripts and other communications should be sent to the New York office. Correspondence with the editor may be addressed to him at Yale University, 225 Prospect Street, New Haven, Connecticut. Statements and opinions in the *A.I.Ch.E. Journal* are those of the contributors, and the American Institute of Chemical Engineers assumes no responsibility for them. Subscriptions: (member) $4.50 for one year, $7.50 for two years; (Nonmember) $9.00 for one year (applies to U.S. and possessions only). Single copies: $3.00. Application for second-class mail privilege is pending at Orange, Connecticut. Copyright 1955 by the American Institute of Chemical Engineers.

ADL Collins Helium Cryostat

an important tool for new research

- Operates from room temperature to 2°K.
- Liquefies helium and other low-boiling gases in a low-pressure cycle.
- Reliable, proved equipment.
- Easy to operate.
- Minimum maintenance.

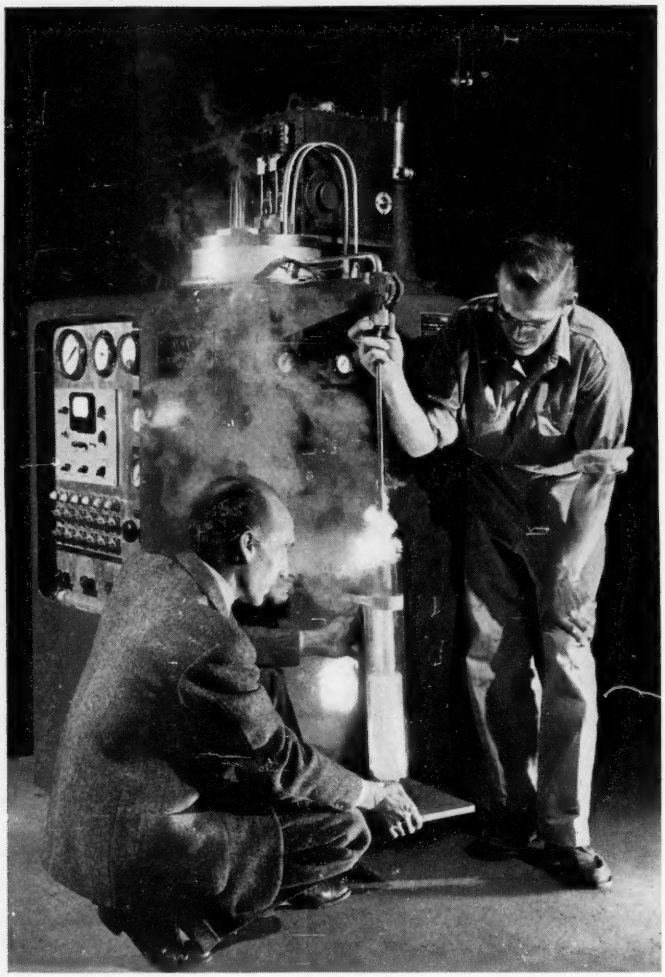

The ADL Collins Helium Cryostat has solved the major technical difficulties in producing extreme low temperatures and has opened up a new region for experiment . . . the region near absolute zero. At such low temperatures, extraneous thermal effects are reduced and atoms and electrons are in a more ordered state . . . Both pure and applied research laboratories are finding it profitable to extend their studies into this region.

Today with this equipment, CHEMICAL laboratories are carrying out new heat capacity and entropy measurements. Tomorrow look for a new type of chemistry using fragmentary molecules stabilized at extreme low temperatures. Well-known ELECTRONIC companies are studying the industrial possibilities of important phenomena such as superconductivity and perfect magnetic shielding. Orientation of radioactive nuclei at a fraction of a degree above absolute zero interests the NUCLEAR PHYSICISTS. New information on the hardening of metals, on the yield stress in steels is being obtained in METALLURGICAL laboratories. SOLID-STATE PHYSICISTS have discovered thermal conductivities at liquid helium temperatures 50 times greater than that of copper at room temperature . . .

For a review of the extreme low-temperature research being carried out in your field, fill out the coupon below and mail it to us.

Arthur D. Little, Inc.
MECHANICAL DIVISION
30 Memorial Drive, Cambridge 42, Mass.

NAME_____
ADDRESS_____
CITY_____ ZONE_____ STATE_____
FIRM_____

Application of Extreme Low Temperature to the field of

- ☐ CHEMISTRY
- ☐ NUCLEONICS
- ☐ ELECTRONICS
- ☐ METALLURGY
- ☐ List of laboratories using the ADL Cryostat

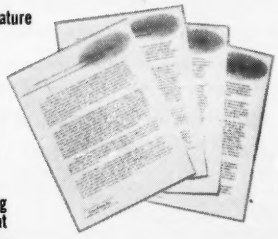

for rapid evaporation of solvents of low volatility

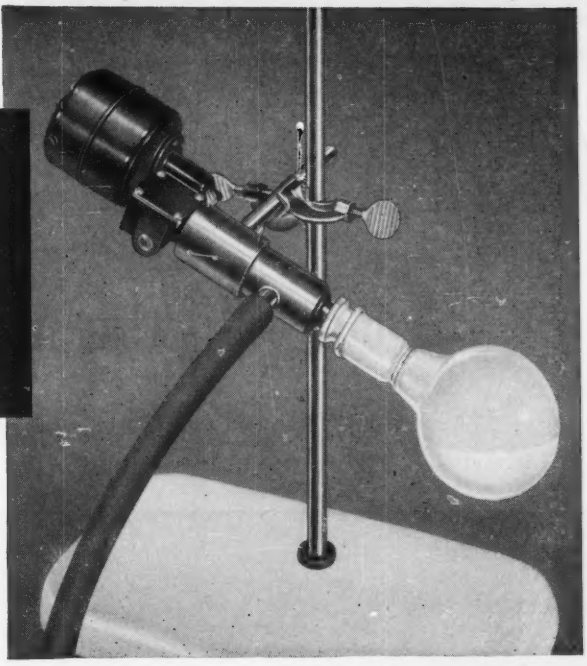

Use **THE**

RINCO ROTATING VACUUM-TYPE EVAPORATOR

(Patent Applied For)

● For speeding up routine evaporations. Handles volumes from 1 c.c. to 1000 c.c. Principle utilized — rotation of flask spreads out thin film over large area (diameter of flask) subjected to negative pressure. "Bumping" eliminated. Use of glass beads unnecessary. Rate of evaporation increased 4 to 5 times, depending on solvent used. Particularly advantageous with such solvents as water, dimethylformamide, etc. 30 ml. of water at 20° C will be evaporated in 30 minutes or less. Very useful with heat sensitive compounds and biological extracts since no temperature increases are necessary. Evaporator will, of course, operate satisfactorily at higher evaporation rates with increased temperature, when sample characteristics permit application of heat.

Evaporator consists essentially of a stainless steel shaft with a machined Standard Taper 19/38 joint at lower end. Shaft rotates on oilite bronze bearings within stainless steel housing having Standard Taper 12/30 take-off leading to vacuum pump or aspirator. Vacuum pump and trap are recommended for best results, but can be used with aspirator. Flask attached to Standard Taper joint at lower end of shaft rotates at approximately 60 r.p.m. by means of special motor. Standard Taper 19/38 joint accommodates smaller capacity flasks, i.e., 50 ml. H-63620 Reducing Adapters, Pyrex Brand Glass, permit use of larger flasks having Standard Taper 24/40, 29/42, etc. Entire apparatus can be easily disassembled for cleaning.

Can be adapted to single or multiple units.

H-21655 — Rinco Rotating Vacuum-type evaporator complete with motor and cord for use on 115V 60C, A.C. . . . **$96.50**

Note: Support stand, clamp and glassware are accessories and may be ordered separately.

HARSHAW SCIENTIFIC
DIVISION OF THE HARSHAW CHEMICAL CO.
CLEVELAND 6, OHIO

Cleveland 6, Ohio
1945 East 97th St.
Cincinnati 13, Ohio
6265 Wiehe Road
Detroit 28, Mich.
9240 Hubbell Ave.

HARSHAW

Houston 11, Texas
6622 Supply Row
Los Angeles 22, Calif.
3237 S. Garfield Ave.
Philadelphia 48, Pa.
Jackson & Swanson Sts.

WILMAD TUBING...

Product of Pride and Precision

• PRECISION BORE TUBING

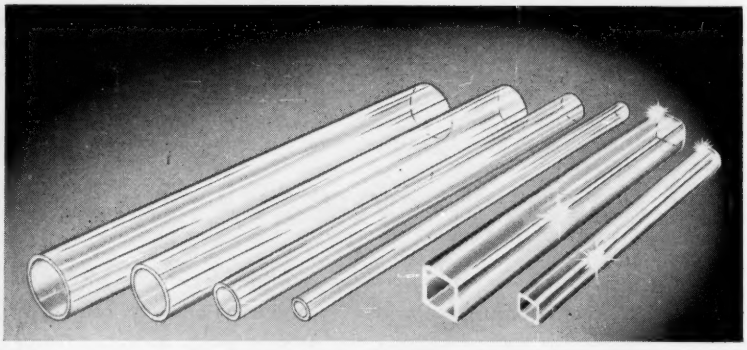

Many industrial and electronic engineers who need extreme accuracy in glass tubing use Wilmad Precision Bore Tubing exclusively. Ideal for use in barometers, bearings, dashpots, manometers, voltage regulators, capacitors, rotameter tubes, burettes, viscosimeters, wave guide tubes, UHF tuners and cavities, and hundreds of other applications.

Made in various shapes and sizes . . . square, rectangular, hexagonal, and tapered up to 7" ID. Fluted and other special shapes can be made to meet individual requirements. Available in Pyrex Brand, Vycor Brand and most of the electronic glasses.

• PRECISION BORE CAPILLARY TUBING

Our claim of consistently achieving an accuracy and uniformity hitherto considered impossible is no idle boast. In a size range that runs from .004" ID to .100" ID, our tolerance limits are set at ±.0002".

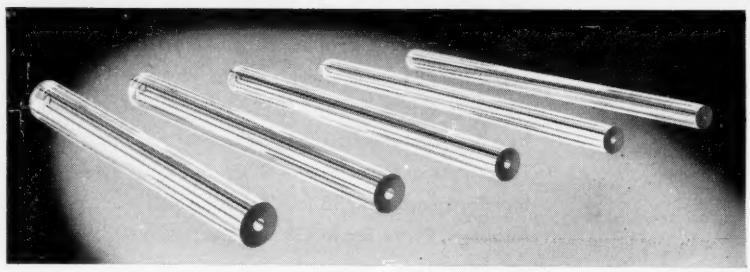

Send for this free catalog TODAY

We welcome the opportunity of discussing with your Engineering Department any particularly difficult problems they might have in the precision glass field. We will be glad to help you find a solution.

WILMAD GLASS COMPANY, INC.
DEPT. A
LANDISVILLE • NEW JERSEY
SPECIALISTS IN RESEARCH LABORATORY GLASSWARE

CHEMICAL - LABORATORY W GLASSWARE

Greetings--

FROM THE PRESIDENT

The appearance of this first issue of the A.I.Ch.E. Journal marks an important milestone in the publication history of the American Institute of Chemical Engineers. It has been evident for some time that the Institute needs two kinds of regular publications: one to meet the broad, general interests of chemical engineers by providing news, reviews, general articles, articles dealing with problems of management, economics, production, and the like, and the other to cover the more highly technical and theoretical phases of the profession. This dual treatment follows the pattern established by many other technical societies.

The new venture, however, was not undertaken without a good deal of debate and some misgiving about the future. Such a magazine is a gamble from a financial standpoint because it has to be offered to the membership below the actual cost of production. It is probable that the total return from subscriptions and advertising will always be less than cost, and this journal will have to be underwritten with other institute income.

Publication is probably the most important single activity of any engineering or scientific society from the standpoint both of service to its members and of its own prestige. This new journal has a great opportunity to promote both these ends, and I am confident that it will make the most of this opportunity.

I am happy to offer to the Editor and his staff my best wishes for success in this new venture. I have a particular pleasure in doing this since the Editor is a valued friend and close associate of many years. The Institute is fortunate in having the new journal under such competent guidance. In the final analysis the success of any publication depends to a large extent on the leadership provided by the editor.

As this new venture is launched, I am thinking of the analogy of a new ship gliding down the ways and I break a symbolic bottle of champagne on her bow as she leaves her berth and wish her "Bon Voyage."

B. F. DODGE

FROM THE SECRETARY

This is the second time I have been in on the beginning of a new publication for the American Institute of Chemical Engineers, and an old lesson is being reaffirmed—enterprises such as this are always acts of faith. At times during the preliminary studies leading to publication, which were carried out by Thomas K. Sherwood as chairman of the Publications Commmittee and by George Holbrook, chairman of the Committee on the Future of the Institute, it was often doubtful that the fiscal problems would allow us enough leeway. The plunge was taken, though, and like a swimmer diving into cold water, we are feeling the shock of our first immersion.

The doubt about beginning publications in this field is never, of course, a doubt of need or of quality. The chemical engineering profession requires many outlets for its theoretical and practical writings. The volume of valuable material which this magazine will ultimately attract would exceed the financial publishing ability of this society. By a process of selection, therefore, the Journal should become a leader in the field and a source of quality publications.

If this Journal is a success, it will be so because it serves a gaping need in the chemical field and thereby wins the financial support of the chemical engineers and the industries that employ them. The Council of the A.I.Ch.E. merits applause for its decision to publish. I know that the staff of the Institute will do their best to make this new vision a reality.

F. J. VAN ANTWERPEN

FROM THE EDITOR

With this first issue of the A.I.Ch.E Journal, the Institute begins a new venture of some magnitude and of much potential merit. The growth of the membership and the diversity of interests of the members have made inevitable this expansion of the publishing program. We plan to emphasize in the Journal those theoretical developments and research results which are immediately interesting to many and which it is hoped will be of great ultimate value to all, as the theory of today becomes the practice of the future.

The success of this venture will depend largely on the contributors of articles, and we hope to be able to give them every possible encouragement. We will try to accomplish the necessary editorial duties expeditiously.

It is to be hoped that our subscriber list will grow and that many readers will inform us of their views on the Journal, particularly how it can be improved. In such an undertaking it is impossible for those few of us directly concerned to think of all refinements, and the readers' opinions will certainly be welcomed.

The editor feels that particular recognition is due to the reviewers, that large and here nameless list of men whose efforts given so freely have made this issue possible. The help of the Publications Committee, the Advisory Board, the Publisher, and the Manuscript Editor is also acknowledged.

HARDING BLISS

FITZMILL
TRADE MARK

YOUR TRADEMARK GUARANTEE

OF CONTINUOUS RESEARCH AND DEVELOPMENT OF PROCESSING EQUIPMENT WHETHER FOR CONTINUOUS PRODUCTION, PILOT OR LABORATORY.

OUR STAFF OF EXPERIENCED CHEMICAL, MECHANICAL AND PROCESS ENGINEERS ARE AVAILABLE HAVING A WIDE KNOWLEDGE IN THE MANY INDUSTRIES TO WHICH EQUIPMENT ENGINEERED, DESIGNED AND MANUFACTURED BY THE COMPANY HAS BEEN APPLIED.

THE FITZMILL TRADEMARK APPLIES TO MANY KINDS OF STAINLESS OR NON-CORROSIVE EQUIPMENT RANGING FROM 3 - 300 HORSEPOWER, INCLUDING THE FOLLOWING TYPES OF PROCESSING EQUIPMENT:

COMMINUTING	**LANIATING**
MALAXATING	**DIVELLING**
TRITURATING	**RIVING**
THERMINUTING	**SLITTING**
CHILSONATOR	**HOMOLOID**

OUR MODERN LABORATORY IS MAINTAINED FOR THE DEVELOPMENT AND TESTING OF NEW MACHINES AND NEW METHODS OF PROCESSING.

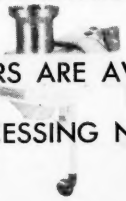

HIGHLY SKILLED, CAPABLE SALES ENGINEERS ARE AVAILABLE AT YOUR REQUEST TO ANALYZE YOUR EVERY PROCESSING NEED.

THE W. J. FITZPATRICK COMPANY

1009 W. WASHINGTON BLVD. • CHICAGO 7, ILLINOIS • CHesapeake 3-2800

NEW YORK • BOSTON • PHILADELPHIA • SPRINGFIELD • SAN JOSE • LOS ANGELES • SAN FRANCISCO • TORONTO • MONTREAL

REPRESENTATIVES IN FOREIGN COUNTRIES

EFFECT OF FLUID PROPERTIES ON MASS TRANSFER IN THE GAS PHASE

E. J. LYNCH and C. R. WILKE
University of California, Berkeley, California

Water was vaporized into air, helium, and Freon-12 in turbulent gas flow over a wet-bulb thermometer and through a 1-ft.-diam. tower packed with 1-in. Raschig rings.

The wet- and dry-bulb measurements indicate that the gas-film mass transfer coefficient varies with the Schmidt number to the —½ power for flow perpendicular to single cylinders.

Heights of a transfer unit, H.T.U., were measured in the packed tower for flow of the gases countercurrent to water over a range of gas and liquid rates. When compared at equal-gas-flow Reynolds numbers at constant liquid rate, H.T.U. varied as the 0.9 power of the Schmidt group. When compared at equal values of ρu^2 (ρ = gas density, u = velocity), H.T.U. varied as the 0.47 power of the Schmidt group. With reference to the psychrometric study, the latter method of comparison of H.T.U.'s seems preferable and indicates that further study of criteria for dimensional similitude in packed columns may be needed.

According to the two-film theory of Whitman(*50*), the resistance to mass transfer between a gas and a liquid stream can be divided into two additive resistances which result from hypothetical films of stagnant gas and liquid on either side of the interface. The liquid-film resistance in a packed column has been evaluated by Sherwood and Holloway(*41*) for the commonly used packings, but as yet a satisfactory correlation of gas-film absorption coefficients has not been made.

This investigation proposed to clarify the role of the gas-film resistance by determining the effect of the fluid properties on the rate of mass transfer in a packed tower. To do this, a twofold plan was followed. The most direct method was the actual measurement of mass transfer coefficients in a tower packed with 1-in. Raschig rings. To eliminate any influence from the liquid properties, it was decided to vaporize a single pure liquid into inert gases. The gases chosen were air, helium, and Freon-12. These gases, with water as the liquid, gave a thirtyfold variation in density, a twofold variation in viscosity, an eightfold variation in diffusivity, and a four-and-one-half-fold variation in Schmidt number.

As the Schmidt-number effect was of particular interest, the second method of approach utilized wet- and dry-bulb-thermometer measurements to determine the psychrometric ratio. As the Prandtl number of the gases is nearly constant, this method will give the variation of the mass transfer coefficient with the Schmidt number in evaporation from single cylinders. Although it is not necessary that the same Schmidt-number effect hold for single cylinders and packed towers, the effect should be of similar magnitude and should confirm the results obtained by the more direct method.

Complete tabular data are on file with the A. D. I. Auxiliary Publications Project, Photoduplication Service, Library of Congress, Washington 25, D. C., and may be ordered as Document 4473 for $1.75 for microfilm and $2.50 for photoprints.

THEORY

Approximate analytical solutions for the rate of mass transfer from an interface to a fluid moving in forced convection in a straight circular pipe have been developed by various authors(*5, 10, 34, 40*) through the use of the analogy between heat, mass, and momentum transfer. These solutions have indicated that the mass transfer coefficient, k_G for this case, is a function of the Reynolds number, $(du\rho/\mu)$, and the Schmidt number, $(\mu/\rho D)$. The Reynolds number ordinarily enters as a function replacing the friction factor. These solutions can be expressed generally by the equation

$$k_G M_m p_f / G = \phi'(du\rho/\mu), (\mu/\rho D) \qquad (1a)$$

where

ϕ' = some mathematical function
k_G = mass transfer coefficient, lb. moles/(hr.)(sq.ft.)
d = diameter of the tube, ft.
D = diffusion coefficient, sq. ft./sec.
u = velocity, ft./sec.
ρ = density, lb. mass/cu.ft.
μ = viscosity, lb. mass/(ft.)(sec.)
G = mass velocity of the gas, lb. mass/(hr.)(sq.ft.)
M_m = mean molecular weight, lb. mass/mole
p_f = film pressure factor(*51*); accounts for the presence and movement of the inert fluid

This equation can be expressed alternately in terms of the transfer unit defined by Chilton and Colburn(*8*):

$$a\text{H.T.U.}_G = \psi' (du\rho/\mu), (\mu/\rho D) \qquad (1b)$$

where

H.T.U.$_G$ = height of a transfer unit $= G/k_G a p_f M_m$, ft.
a = packing area/cu.ft. of packing, sq.ft./cu.ft.

These equations do not include the effect of the relative roughness on the mass transfer rate and consequently are limited to the particular pipe geometry for which the functions Φ' and Ψ'' are experimentally evaluated.

Mass Transfer in Packed Columns. Equations (1*a*) and (1*b*) have been frequently used to satisfy a need for some theoretical framework for the correlation of packed-column data; however, this extension of the functional relationship developed for simple pipe flow has

never been subjected to adequate experimental investigation to justify its general use. In an attempt to correlate the results of this work it was found that Equations (1*a*) and (1*b*) were not satisfactory, and an alternate method of correlation was therefore developed based on the following qualitative analysis.

In the study of mass transfer rates from single cylinders placed perpendicular to the flow stream (*29*), it has been found that the bulk of the mass transfer taking place occurs in the vicinity of the stagnation point and in the region of the turbulent wake. These same two sections of the cylinder are of primary concern in the loss of momentum of the gas stream as manifested by the pressure drop. Consequently, it might be expected that the two phenomena, transfer of momentum and transfer of mass, are to a large extent functions of the same properties of the flow field, particularly for gases in which the diffusivities for mass and momentum are of similar magnitude. Pressure-drop measurements made in flow past single cylinders (*15*) show that the drag coefficient becomes relatively constant at high values of the Reynolds number. Therefore, as a first approximation, the drag coefficient is independent of the Reynolds number and the pressure drop is dependent only upon the inertia of the gas stream, ρu_m^2. Since it is postulated above that the rate of mass transfer will depend on the same flow properties as does the pressure drop, it may follow that the mass transfer coefficient will also be a function of the inertia force and not the Reynolds number at high flow rates. With this modification, Equations (1*a*) and (1*b*) may be rewritten for application to single cylinders for conditions of high turbulence in the fluid:

$$k_G M_m p_f/G = \varphi(\rho u_m^2), \ (\mu/\rho\ D) \quad (2a)$$

$$a\text{H.T.U.}_G = \psi\ (\rho u_m^2), \ (\mu/\rho\ D) \quad (2b)$$

where u_m = mean velocity of the flowing fluid in feet per second. Pressure-drop measurements made in packed absorption towers (*37*) have also shown very little dependence on the Reynolds number over the usual operating range. A tower packed with Raschig rings being considered in a broad sense as a group of cylinders, the extension of Equations (2*a*) and (2*b*) to a packed tower would appear to follow.

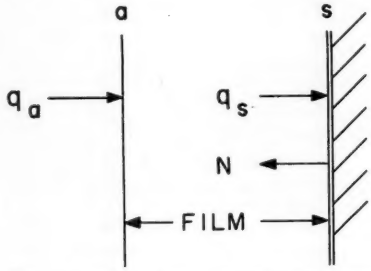

FIG. 1. SCHEMATIC REPRESENTATION OF HEAT AND MASS TRANSFER TAKING PLACE AT A WET-BULB THERMOMETER.

Psychrometry. If the vapor content of a gas stream is known, the psychrometer is a useful instrument for measuring the relative rates of heat and mass transfer from single cylinders. It has a distinct advantage over other methods for determining the dependence of k_G on Schmidt number in that no knowledge of the velocity-term dependence is required. If an exact analogy can be drawn between the two processes of heat and mass transfer, the velocity term should enter into both rates in the same manner, and the ratio of the mass transfer to the heat transfer coefficient should be a unique function of the Schmidt and Prandtl numbers.

Colburn (*10*), and Chilton and Colburn (*7*) have developed equations for the correlation of heat and mass transfer data in terms of the j number, a quantity which is analogous to the friction factor in momentum transfer. According to this concept,

$$j_h = [h/C_p G]\ (C_p\ \mu/k)^{2/3} \quad (3)$$

$$j_d = [k_G M_m\ p_{.m}/G]\ (\mu/\rho\ D)^{2/3} \quad (4)$$

where

h = heat transfer coefficient, B.t.u./(hr.) (sq.ft.) (°F.)

C_p = heat capacity of the gas, B.t.u./(lb. mass) (°F.)

k = thermal conductivity, B.t.u./(hr.) (sq.ft.) (°F./ft.)

If j_h is assumed to be equal to j_d, the psychrometric ratio is obtained:

$$(k_G M_m P_f/h) C_p = \left[\left(\frac{C_p \mu}{k}\right) \Big/ \left(\frac{\mu}{\rho D}\right)\right]^{2/3} \quad (5)$$

In the above j-number analogy the value of k_G is determined directly from the wet-bulb data, as it is multiplied by the term p_f, which corrects for variations in the partial pressure of the inert gas. The value of h, on the other hand, is the true heat transfer coefficient which would be obtained if there were no evaporation from the surface. To correct the wet-bulb data it is necessary to include a factor which will allow for the heat being carried away from the thermometer by the mass movement of the vapor molecules.

Figure 1 shows a model in which the transfer of heat and mass occurs only in the normal direction. With the surface temperature as a reference, it is seen that the heat transferred to the surface, q_s, is equal to the heat entering the film, q_a, minus the heat being carried out by the vapor flow, $NC_m(t_a - t_s)$, or

$$q_s = q_a - NC_m\ (t_a - t_s) \quad (6)$$

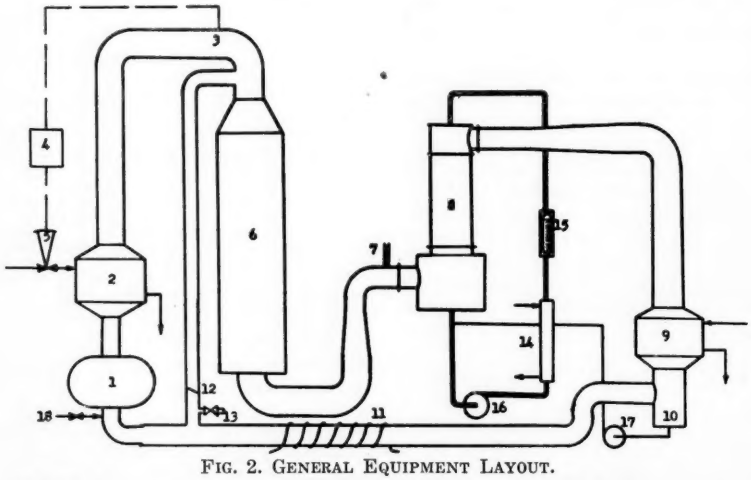

FIG. 2. GENERAL EQUIPMENT LAYOUT.

1. Blower
2. Heater
3. Thermocouple
4. Temperature recorder-controller
5. Motor valve
6. Flow-measuring chamber
7. Wet- dry-bulb assembly
8. Absorption tower
9. Cooling coil
10. Condensate receiver
11. Superheating coil
12. Butterfly valve—by-pass control
13. Vent valve
14. Liquid heat exchanger
15. Liquid flow meter
16. Liquid pump
17. Condensate return pump
18. Steam line for purging

where

N = number of moles diffusing per unit time per unit area, moles/(hr.) (sq.ft.)

C_m = molar heat capacity of the vapor, B.t.u./(lb. mole) (°F.)

t_a, t_s = gas and surface temperatures respectively, °F.

If there were no flow of vapor, q_s would equal q_a:

$$q_s = q_a = h\,(t_a - t_s) \qquad (7)$$

where h = heat transfer coefficient, assumed independent of the mass transfer movement.

The number of moles diffusing may be defined in terms of the mass transfer coefficient as

$$N = k_G\,(p_s - p_a) = k_G \Delta p \qquad (8)$$

Substituting from Equations (8) and (7) into Equation (6) gives

$$q_s = h(t_a - t_s) - C_m k_G\,\Delta p\,(t_a - t_s)$$

$$= h(t_a - t_s)\,(1 - C_m k_G \Delta p/h)$$

$$= h(t_a - t_s)\gamma \qquad (9)$$

where $\gamma = 1 - C_m k_G \Delta p/h \qquad (9a)$

If a new pseudo heat transfer coefficient, h', is defined as the total effective heat transfer coefficient including the convective transport of heat, then

$$h' = h_\gamma \qquad (10)$$

and the correct psychrometric ratio* is:

$$\beta = \frac{k_G M_m p_f \gamma}{h'} C_p = \text{function}$$

$$(\mu/\rho\, D),\ (C_p\mu/k) \qquad (11)$$

Colburn and Drew (*10a*) have developed a procedure for correcting the heat transfer coefficient for the effect of mass transfer in the case of condensation of mixed vapors. Their method could also be applied to the wet bulb thermometer. Experimental verification of these possible methods would be desirable.

*Heat transfer by radiation has been neglected in formulating the foregoing equations. As written, h is the usual forced convection coefficient for flow normal to cylinders (Ref. *36*, p. 473). To correct for radiation the factor $1 + \alpha$ may be introduced where α is the ratio of the radiation coefficient, h_r, to h. With this addition the psychrometric ratio, Equation (11), becomes

$$\beta = \frac{k_G M_m p_f C_p \gamma (1+\alpha)}{h'}$$

$$= \text{function}\left(\frac{\mu}{\rho D}\right), \left(\frac{C_p \mu}{k}\right)$$

$$= \frac{M_m\ p_f C_p \gamma\ (t_a - t_s)\ (1+\alpha)}{M_v\ \lambda_s\ (p_s - p_a)} \qquad (11a)$$

where λ_s = latent heat of vaporization of the liquid, B.t.u./lb. mass. The right-hand term has been added to indicate the quantities involved in experimental measurement or use of the psychrometric ratio.

EXPERIMENTAL

Physical and Thermodynamic Properties of Materials†. *Viscosity.* The viscosities of air, water, vapor, and helium were taken from a review article by F. G. Keyes (*27*) in which the available literature data for several gases are collected and formulated by means of an empirical equation. The viscosity of Freon-12 was taken from a paper by Buddenburg and Wilke (*6*) on the measured viscosity of several gases. It was extended over the desired temperature range by the use of the equation of Hirschfelder, Bird, and Spotz (*21*).

Thermal conductivity. The thermal conductivity of air, water vapor, and helium was taken from the review article by Keyes (*27*) quoted above. The thermal conductivity of Freon-12 is that reported by Sherratt and Griffiths (*39*) over the range from 33.3° to 216.2° C.

Heat capacity, C_p. The heat capacity of air and water vapor was taken from the book by Keenan (*26*) on the thermodynamic properties of air. The heat capacity of Freon-12 was calculated from the work of Justi and Langer (*25*), who reported the heat capacity at constant volume. The heat capacity of helium is reported in Perry's handbook (*36*) as constant for all temperatures.

Diffusivity. The diffusivities used were those measured by C. Y. Lee (*28*). The measured values were corrected to the desired temperature by the equation of Hirschfelder, Bird, and Spotz (*21*).

†Properties of pure gases were modified for the presence of water vapor by established methods.

Gas Specifications. The helium used, supplied by the U. S. Navy, was 99.9% pure, the major impurity being water vapor. The Freon-12 used was supplied by Kinetic Chemicals and was 99.95% pure; the major impurities were Freon-11 and Freon-13.

Equipment.

The general equipment arrangement is shown in Figure 2. Gas circulation was provided by means of a Roots-Connersville blower, and the flow rate was measured with a nozzle, made to the specifications of Bean, Buckingham, and Murphy (*3*), which was placed in a 20-in.-diam. section of ducting. The gas stream entering the absorption tower (Figure 3) was sampled for moisture content in the gas distributor; the stream leaving the tower was sampled in the exit ducting; and the inlet-gas temperature was measured at the top of one of the risers on the gas distributor.

The large section of the tower served as a liquid reservoir. Liquid circulation was provided by a centrifugal pump, the flow rate being measured by a calibrated rotameter. The liquid entered the top of the tower through a 44-point distributor, which discharged within 1/2 in. of the top of the packing. The temperature of the entering liquid was measured by a 4-couple thermopile placed in four of the distributing tubes. The liquid temperature at the bottom of the packing was measured by a single thermocouple placed in a small cup.

The wet- and dry-bulb thermome-

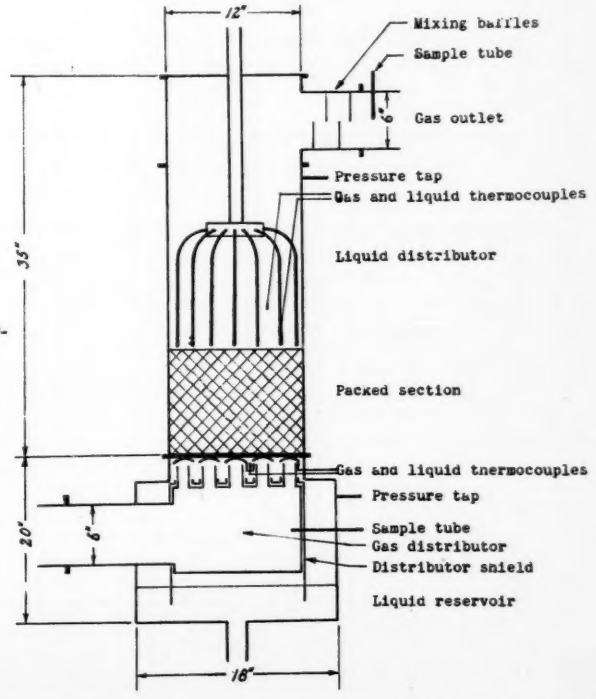

FIG. 3. ABSORPTION TOWER.

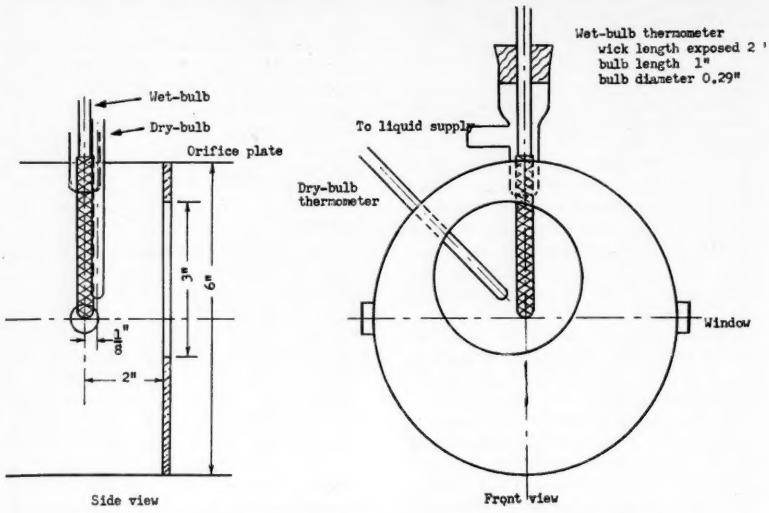

FIG. 4. WET- AND DRY-BULB-THERMOMETER ARRANGEMENT.

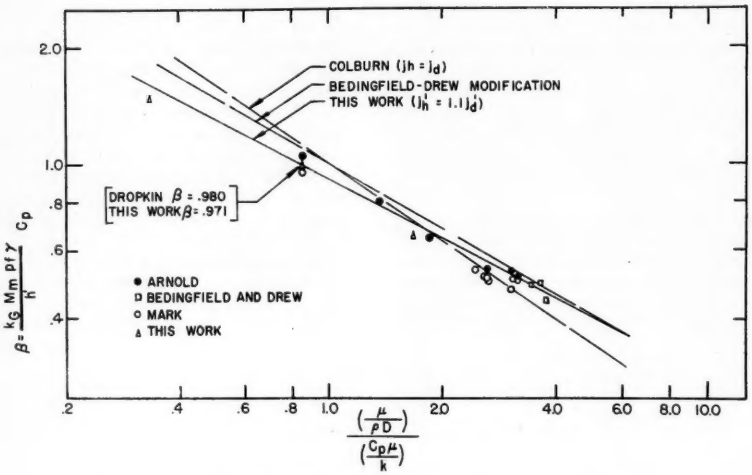

FIG. 5. THE PSYCHROMETRIC RATIO AS A FUNCTION OF Sc/Pr.

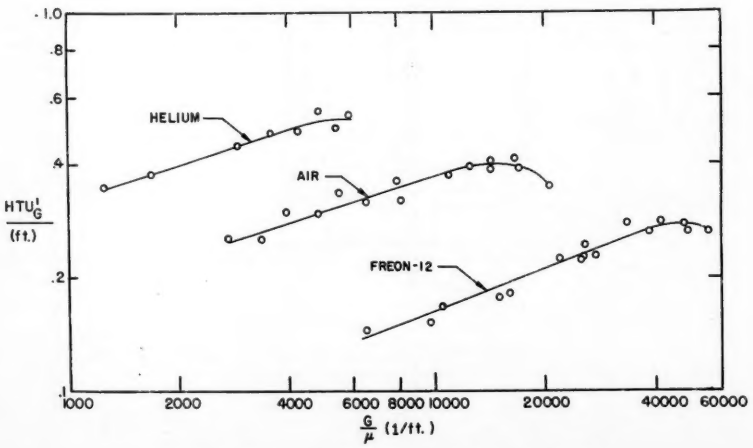

FIG. 6. H.T.U.'$_G$ AS A FUNCTION OF G/μ; $L = 1{,}575$.

ters for the psychrometic measurements (Figure 4) were placed in the ducting immediately before the tower and were preceded by an orifice which ensured a uniform high-velocity flow across the bulbs. Windows were provided in the duct wall so that positioning and wetting of the wick might be observed. A thermocouple was embedded in the duct wall to give the surface temperature for radiation corrections.

Procedure.

For all runs made with helium and Freon-12 it was necessary first to remove the air from the system. It was found that essentially complete removal could be effected by a single steam purge. The air concentration was checked by means of an Orsat analysis for oxygen, which was sensitive to $\pm$ 0.05%. When purging was complete, condensed steam was removed from the lines and the necessary adjustments were made to bring the equipment on stream. To prevent introduction of impurities into the gas stream, the equipment was operated with a slight positive pressure at the blower inlet.

After steady-state conditions were attained, gas samples were withdrawn simultaneously from the top and bottom of the tower by means of aspirator bottles of known volume. The moisture content was determined gravimetrically by drawing the samples through tubes filled with Drierite. During the sampling period the temperature of the inlet liquid stream was carefully controlled, to operate in general with the inlet- and exit-liquid temperatures less than 0.5° C. apart and with a variation of the inlet temperature of less than $\pm$ 0.05° C. during the run.

Immediately following sampling, water from an overhead supply was introduced to the wet-bulb wick and allowed to soak the cloth thoroughly. The water-supply rate was then reduced until a pendant drop could be observed on the tip of the wick. The wet- and dry-bulb temperatures were read. The water supply was stopped and the wet-bulb temperature checked for any further change. (Consecutive runs made at the same gas rate indicate that the moisture content of the gas stream remained essentially constant over long periods of time once steady-state conditions had been attained.)

All packed-bed data were taken with a 7 1/2-in. depth of packing with the exception of the runs made with air at heights of 2 and 13 1/2 in., which were used to determine the amount of transfer taking place outside the packed section. All runs were made at a liquid rate of 1,575 lb. mass/(hr.)(sq. ft.) except those made with air to check the effect of varying the liquid rate.

Details of equipment and procedure are available elsewhere (*30*).

RESULTS

Psychrometric.

The values of the psychrometric ratio obtained in this work for the three cases (Table 1) are shown plotted against the ratio Sc/Pr in Figure 6. This graph also includes the results of Arnold(*2*), Bedingfield and Drew(*4*), Mark(*31*), and Dropkin(*13*). These data can best be approximated by a straight line having a slope of —1/2, which satisfies a modified j-number analogy:

$$j'_h = 1.10\, j'_a$$

$$j'_h = \frac{h}{C_p G}\left(\frac{C_p \mu}{k}\right)^{\frac{1}{2}}$$

$$j'_d = \frac{k_G p_{j_m} M_m}{G}\left(\frac{\mu}{\rho D}\right)^{\frac{1}{2}} \qquad (12)$$

The equation for the psychrometric ratio* then becomes

$$\beta = \frac{k_G M_m p_f C_p \gamma}{h'} = 0.91\left(\frac{Pr}{Sc}\right)^{\frac{1}{2}} \qquad (13)$$

Since the value of the Prandtl group is nearly constant for the results shown here, the heat transfer coefficient may also be considered constant. The curve as plotted then represents the variation of the mass transfer coefficient with Schmidt number for flow of gas perpendicular to single cylinders; i.e., k_G is proportional to $Sc^{-\frac{1}{2}}$.

Packed Column

The packed-tower results are presented here in terms of the H.T.U. instead of k_G. In order to calculate the H.T.U. from the data, the following equation was used: (Representative data are presented in Table 2.)

$$H_2 - H_1 = \text{H.T.U.}_G \left[\left(\frac{y_f}{1-y}\right)_{avg} \ln\left(\frac{y_1 - y_i}{y_2 - y_i}\right)\right] \qquad (14)$$

where y = mole fraction and $y_f = p_f/P$. The expression in brackets is the number of transfer units, and its value can be computed from the data on the vapor concentrations at the inlet and exit of the tower and the temperature of the liquid stream. The height of the packed section, $H_2 - H_1$, when divided by the number of transfer units, gives the apparent height of a transfer unit.

*To include radiation effects, see footnote equation (11a).

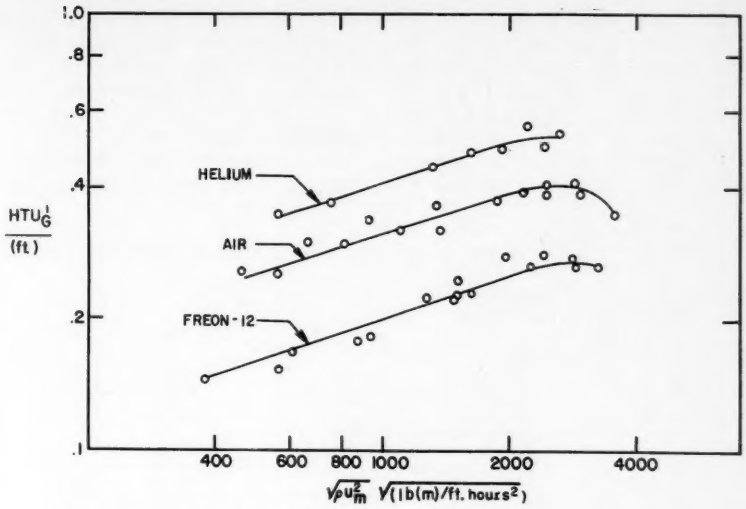

FIG. 7. H.T.U.'$_G$ AS A FUNCTION OF THE INERTIA GROUP; $L = 1{,}575$.

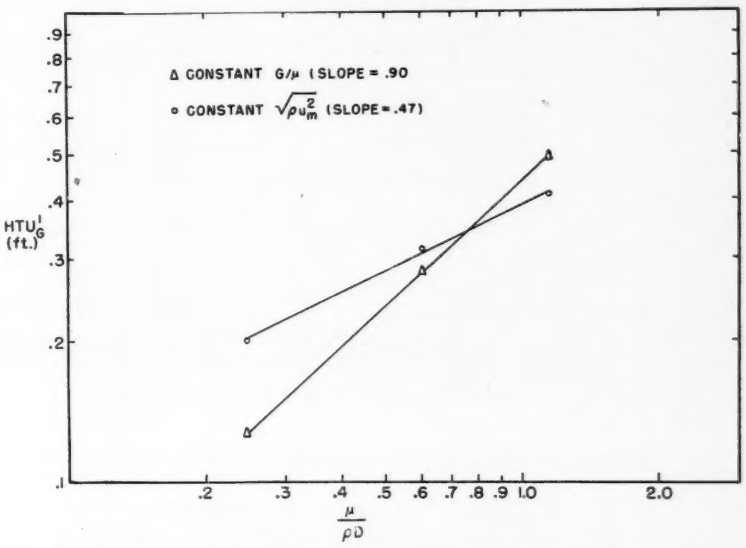

FIG. 8. H.T.U.'$_G$ AS A FUNCTION OF SCHMIDT NUMBER AT CONSTANT VALUES OF G/μ AND INERTIA GROUP; $L = 1{,}575$.

Figure 6 shows the apparent H.T.U. as a function of the group G/μ which is directly proportional to the Reynolds number for a given packing. Since only one packing size and shape was studied, the inclusion of a length dimension in the group was not warranted. The peaks of the curves correspond approximately to the flow rate at which the pressure-drop phenomenon known as "loading" occurs. This was determined by the simultaneous measurement of pressure drop across the packed section. The curves indicate that below the loading point the H.T.U. can be represented as varying with the mass velocity to the 0.33 power, with the power decreasing thereafter as the flooding point is approached. It will be noted that there is a slight difference in the slope for the three curves, but the differences are insignificant in view of the precision of the data.

The more obvious difference among the three curves is the lateral separation of the point of maximum H.T.U. The vertical separation of the curves might be expected and explained on the basis of Equation (1*b*) by the Schmidt-number differences, but the lateral separation would lead one to suspect that the Reynolds number may not be the proper correlating modulus in this case. If, instead, the group suggested by Equation (2*b*) is used, that is, ρu_m^2, the

curves of Figure 7 are obtained. (The group ρu_m^2/length has the dimensional significance of inertia force per unit volume of fluid (*47*), and therefore the group ρu_m^2 will be designated the *inertia group.*) The square root of the inertia group has been used in plotting in order to retain the first-power dependence on the velocity that exists in Figure 6. Similar usage in the correlation of flooding-velocity (*42*) and pressure-drop (*37*) data in packed columns would seem to justify the procedure. This group has also been used in the correlation of plate efficiencies (*20*), where it has been given the name *F* factor. The curves of Figure 7 are identical in shape with those of Figure 6, but with the inertia group as the correlating modulus, the lateral separation has now disappeared and the peaks of all three

TABLE 1.—SUMMARY OF WET-BULB DATA FOR VARIOUS INVESTIGATIONS*

Investigator and system	Pr	Sc	Sc/Pr	$\frac{k_G M_m p_f \gamma}{h'} C_p$
Mark				
air-benzene	0.702	1.71	2.44	0.532
air-chlorobenzene	0.704	2.17	3.08	0.502
air-toluene	0.704	1.86	2.64	0.511
air-carbon tetrachloride	0.700	1.87	2.67	0.499
air-ethylene tetrachloride	0.704	2.15	3.05	0.474
air-ethyl acetate	0.709	1.83	2.58	0.514
air-water	0.704	0.602	0.855	0.955
Arnold				
air-water	0.704	0.602	0.855	1.049
air-methal	0.706	0.970	1.37	0.800
air-propanol	0.705	1.30	1.85	0.642
air-toluene	0.704	1.86	2.64	0.537
air-chlorobenzene	0.704	2.17	3.08	0.531
air-*m*-xylene	0.704	2.24	3.18	0.514
Bedingfield and Drew				
air-naphthalene	0.704	2.56	3.64	0.494
air-*p*-dichlorobenzene	0.704	2.22	3.15	0.509
air-camphor	0.704	2.65	3.76	0.448
air-*p*-dibromobenzene	0.704	2.41	3.42	0.487
Dropkin				
air-water	0.704	0.602	0.855	0.980
This work†				
air-water	0.702	0.602	0.858	0.971
helium-water	0.687	1.15	1.673	0.650
Freon 12-water	0.740	0.248	0.335	1.482

*The physical properties used in the Schmidt and Prandtl numbers were evaluated at 25°C. Diffusivities for the systems studied by Bedingfield and Drew were recalculated by the method of Arnold (*2*).

†Individual results may be found in reference (*30*).

TABLE 2.—SAMPLE EXPERIMENTAL AND CALCULATED RESULTS FOR VAPORIZATION IN PACKED TOWERS*

Exp.	L	G	T_{AB}	T_{WT}	T_{WB}	y_{iT}	y_{iB}	Barometer	y_T	y_B	N.T.U.	H.T.U.′	H.T.U.	H.T.U./$Sc^{0.47}$	G/μ	$\sqrt{\rho}\,u_m^2$
4	1,575	123.2	30.76	29.16	29.43	0.04022	0.04084	753.2	0.03849	0.02153	2.453	0.225	0.375	0.476	2,764	461.4
6	1,575	571.0	40.97	31.30	31.44	0.04540	0.04573	752.2	0.04168	0.02759	1,585	0.394	0.579	0.735	12,686	2,158
9	1,575	292.9	34.14	28.69	28.62	0.03907	0.03891	753.7	0.03690	0.02354	1.958	0.319	0.469	0.595	6,559	1,099
10	1,575	215.5	32.48	28.57	28.15	0.03882	0.03788	753.7	0.03701	0.02305	2,104	0.297	0.437	0.555	4,832	807.7
14	1,575	775.4	40.86	31.41	31.28	0.04567	0.04527	750.4	0.04255	0.02980	1,601	0.390	0.573	0.727	17,227	2,930
15	1,575	934.9	41.10	31.66	31.54	0.04619	0.04578	750.4	0.04377	0.03134	1.787	0.350	0.515	0.654	20,780	3,531
20	1,010	255.3	32.71	28.52	28.52	0.03887	0.03887	750.5	0.03734	0.02363	2.300	0.272	0.400	0.508	5,724	958.7
21	1,995	255.3	32.58	28.37	28.62	0.03853	0.03909	750.5	0.03718	0.02387	2.423	0.258	0.379	0.481	5,724	958.7
22	3,850	255.3	32.24	28.34	28.44	0.03846	0.03868	750.5	0.03739	0.02365	2.643	0.236	0.347	0.440	5,724	958.7
36	575	254.8	33.52	29.40	29.20	0.04081	0.04034	752.4	0.03770	0.02357	1.685	0.371	0.545	0.692	5,712	956.8
1*H*	1,575	137.5	38.78	29.07	28.94	0.03990	0.03959	752.2	0.03691	0.02749	1.398	0.447	0.657	0.615	2,923	1,312
3*H*	1,575	255.5	42.24	30.36	30.24	0.04277	0.04244	752.2	0.03924	0.03010	1.252	0.499	0.734	0.687	5,420	2,431
7*H*	1,575	79.03	34.77	28.70	28.02	0.03898	0.03747	753.7	0.03661	0.02472	1,683	0.371	0.545	0.510	1,683	754.1
8*H*	1,575	58.85	33.36	28.49	27.84	0.03851	0.03708	753.7	0.03627	0.02359	1.796	0.348	0.512	0.479	1,252	562.1
3*F*	1,575	1,514	41.59	34.16	34.18	0.05314	0.05302	753.4	0.04998	0.02634	2.250	0.277	0.407	0.784	48,200	2,820
4*F*	1,575	1,745	42.16	34.39	34.37	0.05375	0.05349	753.4	0.05128	0.02706	2.370	0.264	0.388	0.748	55,430	3,257
9*F*	1,575	203.8	35.76	32.31	32.67	0.04813	0.04898	752.8	0.04776	0.02148	4.309	0.145	0.213	0.410	6,538	377.9
11*F*	1,575	329.4	34.74	33.48	33.57	0.05111	0.05137	753.5	0.05045	0.02399	3.726	0.168	0.247	0.476	10,574	610.0
14*F*	1,575	874.2	43.00	35.09	35.90	0.05592	0.05844	749.6	0.05395	0.02836	2.726	0.229	0.337	0.649	27,725	1,635
15*F*	1,575	1,216	41.10	34.06	34.12	0.05292	0.05306	749.6	0.05049	0.02738	2.358	0.265	0.390	0.752	38,730	2,269

*Complete results may be found in reference (*30*).

L = liquid flow rate, lb. mass/(hr.)(sq.ft.)

G = gas flow rate, lb. mass/(hr.)(sq.ft.)

T_{AB} = gas temperature at the bottom of the packed section, °C.

T_{WT} = water temperature at the top of the packed section, °C.

T_{WB} = water temperature at the bottom of the packed section, °C.

y_{iT} = interfacial mole fraction of water at the top of the packed section

y_{iB} = interfacial mole fraction of water at the bottom of the packed section

y_T = bulk mole fraction at the top of the packed section

y_B = bulk mole fraction at the bottom of the packed section

N.T.U. = number of transfer units

H.T.U.′ = apparent height of a transfer unit, ft.

H.T.U. = height of a transfer unit corrected for end effects, ft.

Sc = Schmidt number $\left(\frac{\mu}{\rho D}\right)$

G/μ = value proportional to the Reynolds number, 1/ft.

$\sqrt{\rho u_m^2}$ = inertia group, $\sqrt{\text{lb.mass/(ft.)(hr.)}^2}$

curves appear at the same value of the inertia group within the limits of experimental error.

Cross plots of the H.T.U. vs. Schmidt number at a constant value of G/μ of 4,000 in Figure 6 and at a constant value of $\sqrt{\rho u_m^2}$ of 1,000 in Figure 7 are presented in Figure 8. The cross plots indicate the Schmidt-number function by which the H.T.U. must be divided to cause a vertical alignment of the three curves of Figures 6 and 7. The plot based on the Reynolds number would require this function to be $Sc^{0.9}$. Correlation by the inertia-group plot, on the other hand, requires an exponent of 0.47 on the Schmidt group to align the three curves. This exponent is preferred in view of the good agreement with that obtained in the psychrometric study and with some results obtained in the vaporization of liquids and organic solids in packed beds (*9, 43*). A simple power function of the Schmidt group appears to be satisfactory for correlation over the present range of system properties and experimental conditions.

FIG. 10. H.T.U.$_G$ AS A FUNCTION OF THE INERTIA GROUP AND SCHMIDT NUMBER; $L = 1{,}575$.→

To obtain the true H.T.U., it is necessary to correct for "end effects," that is, that amount of transfer taking place outside the packed section. In the system under study, the amount of transfer is dependent primarily on the area of liquid exposed to the gas, which in turn depends on the liquid distribution and the manner in which the liquid drips from the bottom of the packing. This should be reasonably independent of the gas being used, so that the same end-effect correction might apply to all three gases. If it can also be assumed that the effect of the gas properties on mass transfer is the same in the end section and in the packed section, then the end effect can be expressed in terms of an equivalent length of packing, which should be constant for all gases and independent of the packed height. This procedure has been used by previous investigators (*18, 45*). If the end effect is constant, the apparent H.T.U. values obtained at a given packed height need only be multiplied by a constant value to obtain the true H.T.U. values; therefore the preceding analysis of the Schmidt-number effect is not dependent on

FIG. 11. H.T.U.$_G$ AS A FUNCTION OF THE LIQUID RATE.→

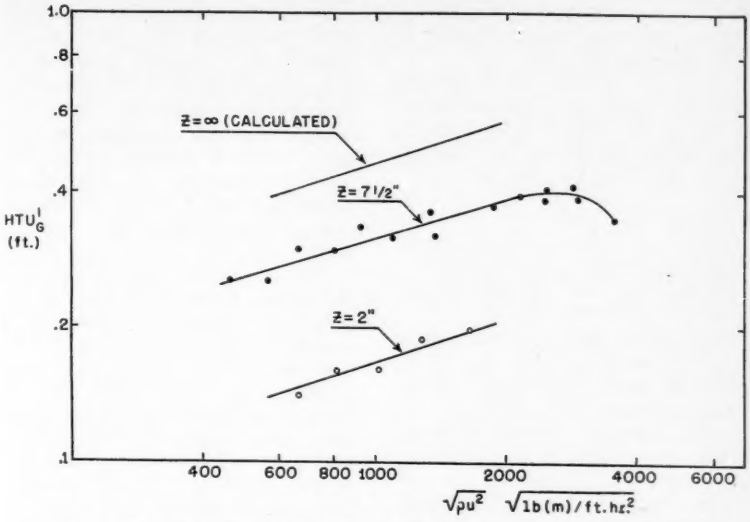

FIG. 9. THE APPARENT H.T.U. AS A FUNCTION OF PACKED HEIGHT FOR VAPORIZATION OF WATER INTO AIR; $L = 1{,}575$.

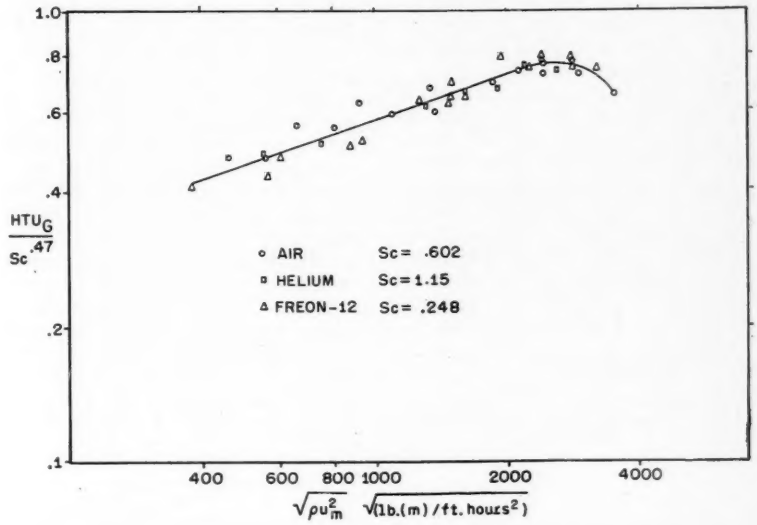

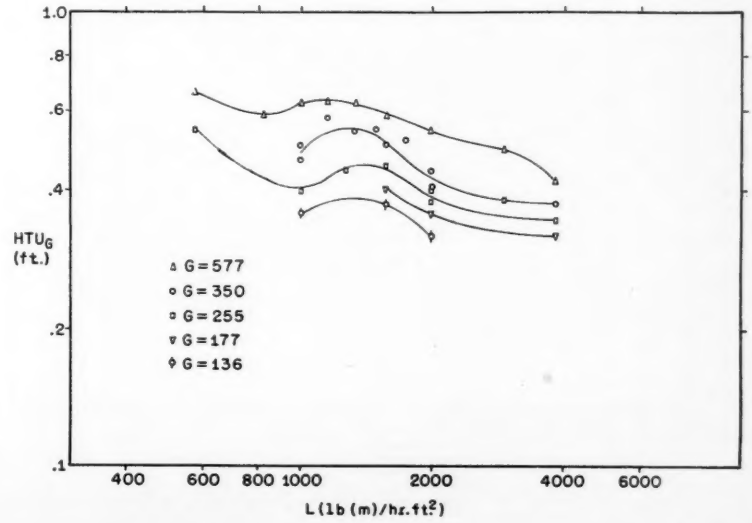

the use of true H.T.U. values, as all the data used were obtained at a single packed length.

It is possible to solve for the true H.T.U. if two apparent values H.T.U.'$_{23}$ and H.T.U.'$_{24}$ are known for two packed lengths Z_{23} and Z_{24} by use of Equation (30):

$$\text{H.T.U.}_{24} = \frac{\text{H.T.U.}'_{24}\ \text{H.T.U.}'_{23}\ (Z_{24}-Z_{23})}{Z_{24}\ \text{H.T.U.}'_{23} - Z_{23}\ \text{H.T.U.}'_{24}} \quad (15)$$

To evaluate the end effect in this work, bed lengths of 13 1/2, 7 1/2, and 2 in. were used. The 13 1/2-in. data scattered badly because the normal analytical errors were so greatly magnified by the approach to saturation at the top of the tower. These data therefore were not used in determining the end effect. The equivalent packed height was found to be essentially independent of gas rate (*see* Figure 9) with an average value of 3.51 in. This value was used to correct all the data for end effects.

All the H.T.U. data taken at a constant liquid rate of 1,575 lb. mass/(hr.)(sq. ft.) may be correlated by the single curve of Figure 10 which shows the effect of both gas velocity and gas properties on the gas film H.T.U. The average deviation of the data points from the line representing the mean is 4.25% with a maximum deviation of 12.5%; however, selection of $\sqrt{\rho u_m^2}$ in preference to G/μ as a basis for correlation cannot be conclusively justified with the present results. For example, in the region below the loading point the group $\rho^{0.2}$ (H.T.U.$_G/Sc^{0.5}$) can be expressed as a smooth function of G/μ which correlates the data nearly as well as Figure 10. Thus use of $\sqrt{\rho u_m^2}$ must be regarded as tentative pending further study. The effects of packing size and liquid properties also must be introduced into any general gas-film correlation.

The curves of Figure 11 show the effect of the liquid rate on the H.T.U. at several air rates. It is rather interesting that the H.T.U. does not bear a simple functional relationship to the liquid rate. It might be expected that as the liquid rate was increased the H.T.U. would decrease owing to the increased wetting of the packing. This would explain the shape of the curves at liquid rates below 900 lb. and above 1,500 lb. mass/(hr.)(sq.ft.). The sudden reversal of the liquid-rate dependence between these flow rates is difficult to explain on the basis of our present knowledge of flow distribution in a packed tower. One possibility is that the increased liquid flow over this range results in the blocking of some of the smaller flow passages, thereby preventing gas flow through these regions. This would effectively reduce the surface area available for transfer and result in higher values of the H.T.U.

It was observed that the average slope of the best straight line that could approximate each of the curves in Figure 11 is approximately the negative value of the slope of the curve of the H.T.U. vs. gas rate (below the loading point). This suggests that the group $(\sqrt{\rho u_m^2})_G/(\sqrt{\rho u_m^2})_L$ might serve as a parameter for general correlation as illustrated in Figure 12. This modulus has been used extensively for the correlation of flooding data. The average deviation of the data from the line representing the mean is 6.2% and the maximum deviation is 24%. In view of the limited scope of the liquid variables covered in this work, it is not possible to attach a final significance to this correlation. The influence of liquid density could enter in other ways, and the effect of other properties such as viscosity and surface tension remains to be considered.

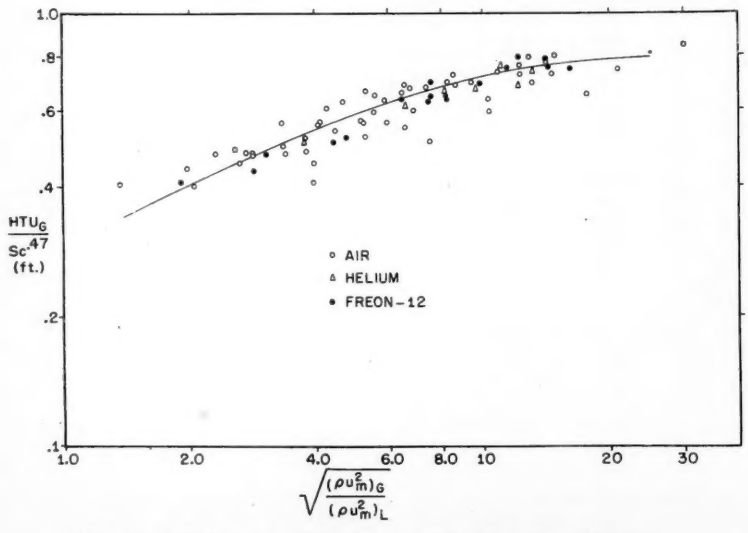

FIG. 12. H.T.U.$_G$ AS A FUNCTION OF THE FLOODING MODULUS.

DISCUSSION

In spite of the large volume of previous work on the subject, no completely reliable data exist for the resistance to mass transfer in the gas phase in a packed tower. From the numerous studies which have been made, a number of works have been selected to show the variation among investigators that has resulted even though they all used the same packing (1-in. Raschig rings) and inert carrier gas (air) and directed the experiments specifically toward the determination of gas-film data. The results plotted on the graph, Figure 13, for gas-film H.T.U. have been corrected for Schmidt-number effect to the system studied in this work (air-water), assuming the H.T.U. to be proportional to $Sc^{\frac{1}{2}}$. No correction was made for slight variation in packing properties since many of the investigators did not report these quantities.

Van Krevelin, Hoftijzer, and Van Hooren (*47*) reviewed a number of gas-film mass transfer studies to obtain a general equation. Since their equation is based largely on the absorption of NH_3 in water, it gives results similar to those found by Dwyer and Dodge (*14*), Vivian and Whitney (*49*), and Fellinger (*18*). The curve of Taecker and Hougen (*46*) pertains to systems without liquid flow and is not intended to be comparable to the other systems.

It will be noted that the technique of absorbing NH_3 and SO_2 in water has yielded much higher values of the H.T.U. than either the vaporization of liquids or the absorption of NH_3 and SO_2 in strong chemical solutions (absorption followed by a rapid chemical reaction). Fellinger found that

absorption of NH_3 in H_2SO_4 gave H.T.U.'s which were 1.5 to 2.5 times smaller than those for the absorption in water. These acid data scattered somewhat and were not published, but these results would seem to indicate that the nature of the liquid-phase resistance to mass transfer in the NH_3-water system may have been improperly evaluated.

An alternative explanation of the discrepancy is the existence of an interfacial resistance, postulated by some authors(*11, 12, 16*). Resistance to mass transfer usually has been considered to exist only in a gas film and a liquid film where equilibrium exists at the interface between them(*30*); however it is possible that a large mass transport in one direction might result in an increase in the concentration of vapor molecules at the interface if the accommodation coefficient were very different from unity. Thus the actual partial pressure at the interface could be much higher than the equilibrium value and would result in a lower transfer rate than would be expected. Only fundamental experiments on the rate of NH_3 absorption in water will determine whether either or both of these factors is involved in the wide difference in results obtained from the two types of experiments.

The discrepancy between the various studies based on the vaporization of water is probably the result of the analytical difficulties involved in this type of investigation. Saturation of the carrier gas with water occurs very rapidly so that it is difficult to determine the driving forces for mass transfer at the tower exit with the required precision. To alleviate this condition, it is necessary to use very short packed sections, and therefore large relative errors are introduced in the measurement of the bed length and the effect of the transfer which takes place outside the packed section is magnified.

Although there is a wide variation in the absolute value of the H.T.U., most of the investigators indicate that it will vary with approximately the 0.5 power of the velocity at flow rates below the loading point. There is also the growing realization that this portion of the curve is not exactly a straight line and that above the loading point the value of the H.T.U. undergoes a marked decrease for reasons which are not yet entirely clear. The data of Sherwood and Holloway(*41*) show that the liquid-film H.T.U. is independent of the gas rate until the loading point is reached. At the loading point rapid improvement in the rate of mass transfer would indicate that at this point there is a marked change in the liquid flow pattern, which results in an increased contact area. It is not known whether this change is simply an increase in the wetted area of packing caused by increased gas-pressure drop, a rippling of the liquid surface, or a more severe disintegration of the liquid streams, but it seems reasonable to assume that the effect is also responsible for the improved mass transfer rates in the gas film. Figure 13 gives some indication of the importance of the area effect. The curve of Taecker and Hougen(*46*) was obtained by using completely wetted porous packing without liquid flowing. The values of the H.T.U. that were obtained by this procedure are approximately one half those obtained in this work. This also suggests that there would be a great dependence of the gas-film H.T.U. on the liquid being used, since the fraction of the total available area that is wetted will depend on the characteristics of the wetting fluid.

The dependence of the gas-film H.T.U. on the liquid rate as determined by several investigators is shown in Figure 14. All the curves show a decrease in the H.T.U. with increase in liquid rate but the dependence on liquid varies widely. Dwyer and Dodge, Yoshida and Tanaka(*52*), and Vivian and Whitney indicate that the H.T.U.

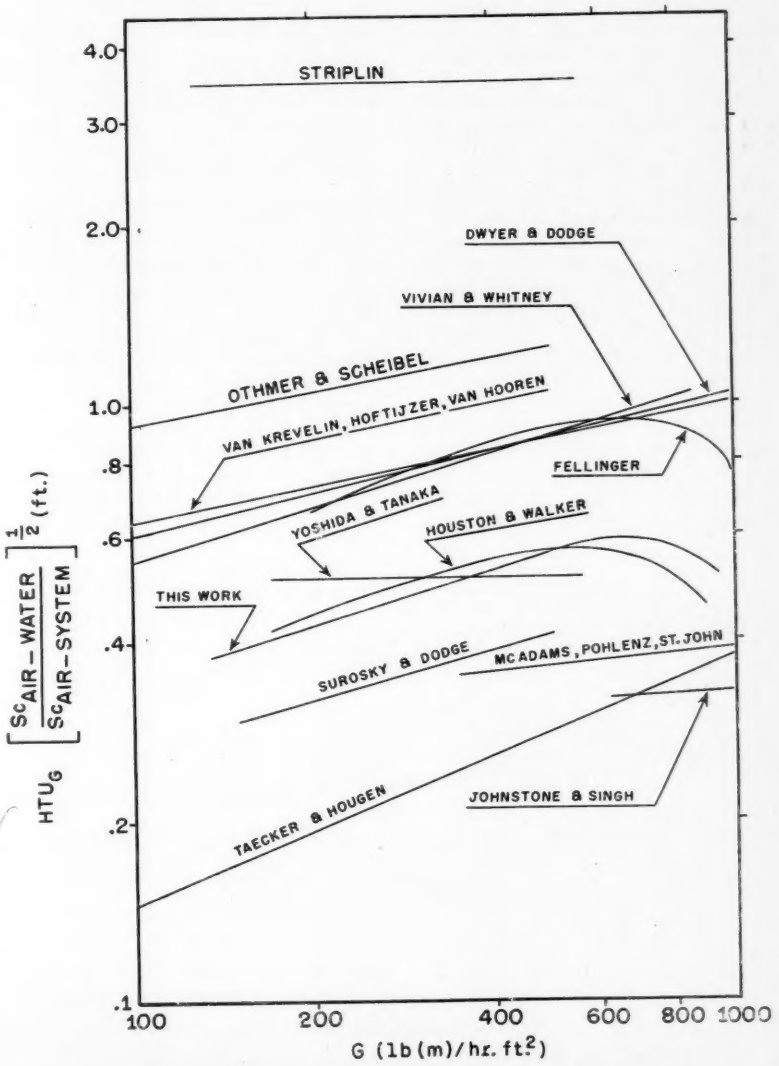

FIG 13. H.T.U.$_G$ AS A FUNCTION OF GAS RATE FOR VARIOUS INVESTIGATIONS.

varies as approximately $L^{-0.2}$ over the entire range of liquid rates measured. The curve of McAdams, Pohlenz, and St. John (*32*) is taken from their heat transfer results as their mass transfer results scattered excessively. The data of Surosky and Dodge (*45*) scatter too much to warrant the assumption that the H.T.U. is independent of liquid rate above a value of 1,200. Actually their data might be fitted as well by either a sloping line or an *S*-shaped curve. The curve of Fellinger based on liquid rates of 500, 1,500, and 4,500 shows the greatest dependence on liquid rate, the H.T.U. varying with $L^{-0.7}$ at low flow rates and changing gradually to $L^{-0.3}$ at high rates. The shape of the curve is almost identical with that suggested by Van Krevelin, Hoftijzer, and Van Hooren. Fellinger's three values could also be fitted by a curve of the type found in this work. It is difficult to draw a general conclusion from these studies or to say whether they offer either supporting or contradictory evidence for the unique liquid-rate dependence found by the authors.

The number of works devoted to the determination of the Schmidt-number effect is considerably more limited. Houston and Walker (*22*) absorbed NH_3, acetone, methanol, and ethanol from air into water and found that the H.T.U. was proportional to the diffusivity to the —2/3 power. Scheibel and Othmer (*38*) absorbed acetone and methyl ethyl ketone from air into water and obtained data which indicated that the H.T.U. was proportional to the diffusivity to the —1/2 power. However, in trying to correlate their data with the data of other investigators (*14*) on the absorption of NH_3, they were led to the final conclusion that the correct exponent on the diffusivity was —1. The results of both Houston and Walker and Scheibel and Othmer have possible sources of uncertainty in that it is necessary to correct for the liquid-film resistance which is present. In addition, the variation in diffusivity is small.

These difficulties can be avoided by the technique of vaporizing pure liquids into air. Mehta and Parekh (*33*) vaporized water, methanol, benzene, and toluene and found that the H.T.U. was proportional to $D^{0.17}$. Surosky and Dodge (*45*) used water, methanol, benzene, and ethyl butyrate as the liquids and found that their data could be correlated by use of H.T.U. proportional to $D^{0.15}$. The data of Simkin (*43*) and Chrisney (*9*) on the vaporization of solids and liquids from packed beds in the absence of liquid flow indicate that the H.T.U. is proportional to $D^{-0.36}$. This suggests that in the vaporization of pure liquids with liquid flow there are complications being introduced by the manner in which the various liquids wet and flow over the packing. The possible error from this source has been discussed previously.

It is possible to avoid the foregoing difficulties by the technique used in this work, that of using a single liquid for vaporization and varying the Schmidt number through the use of different carrier gases. It is necessary however to ascertain that the various gases do not have different effects on the liquid-flow pattern and effective mass transfer surface. If the gas does cause a change in the liquid flow, it should do so primarily by the pressure it exerts. Elgin and Weiss (*17*) and Jesser and Elgin (*23*) have found that the liquid holdup in a packed tower is independent of the gas-flow rate at constant liquid rate up to the flooding point. In addition, it was found in this work that the pressure drop across the packing was the same for all three gases at the same value of the inertia group. With this group as the correlating modulus, therefore, the relative mass transfer rates should be independent of the influence of the pressure drop on flow pattern and effective surface.

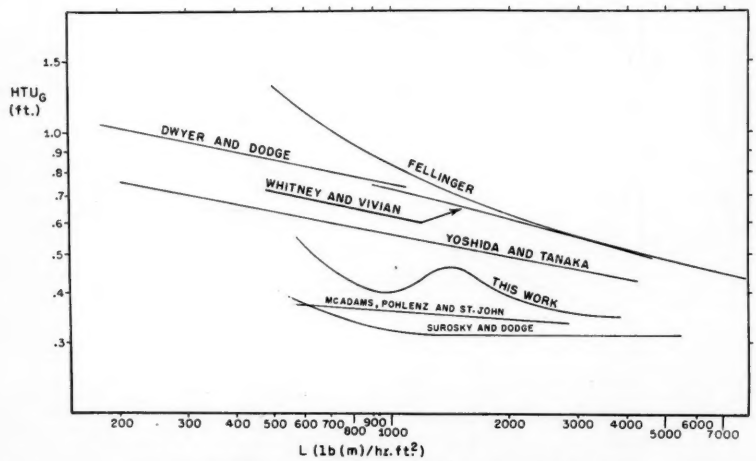

FIG. 14. H.T.U.$_G$ AS A FUNCTION OF LIQUID RATE FOR VARIOUS INVESTIGATIONS; $G = 200$.

ACKNOWLEDGMENT

The authors are indebted to the Shell Oil Company for financial aid in the course of this study and to the U. S. Atomic Energy Commission, under whose sponsorship the work was completed.

NOTATION

a = area available for mass transfer per unit volume of packing, sq.ft./cu.ft.

C_m = molal heat capacity at constant presure, B.t.u./(lb. mole) (°F.)

C_p = heat capacity at constant pressure, B.t.u./(lb. mass) (°F.)

D = diffusivity, sq.ft./sec.

d = diameter, ft.

G = mass velocity of the gas stream based on the superfiicial area, lb. mass/(hr.) (sq.ft.)

H = height, ft.

h = heat transfer coefficient, B.t.u./(hr.) (sq.ft.) (°F.)

h' = pseudo heat transfer coefficient defined by Equation (10)

H.T.U.$_G$ = height of a transfer unit for the gas film, ft.

H.T.U.'$_G$ = height of a transfer unit for the gas film not corrected for end effects, ft.

j_d = mass transfer factor defined by Equation (4)

j_h = heat transfer factor defined by Equation (3)

j'_d = mass transfer factor defined by Equation (12)

j'_h = heat transfer factor defined by Equation (12)

k = thermal conductivity, B.t.u./(hr.) (sq.ft.) (°F./ft.)

k_G = gas-film mass transfer coefficient, lb. moles/(hr.) (sq.ft.) (atm.)

L = liquid-flow rate based on the superficial tower area, lb. mass / (hr.) (sq.ft.)

M_m = mean molecular weight of the gas stream, lb. mass/lb. mole

M_v = molecular weight of the diffusing (evaporating) species, lb. mass/lb. mole

N = rate of transport of vapor, lb. moles/ (hr.) (sq.ft.)

N.T.U. = number of transfer units

P = total pressure, atm.

p = partial pressure, atm.

p_f = film pressure factor, atm.

q = heat transfer rate, B.t.u./ (hr.) (sq.ft.)

t = temperature, °F., °C.

u = velocity, ft./sec.

u_m = average velocity based on the total cross-section area, ft./ sec.

y = mole fraction

$y_f = p_f/P$

Z = packing length, ft.

Greek Letters

$\beta = \dfrac{k_G M_m p_f \gamma}{h'} C_p$

γ = a heat transfer factor defined by Equation (9a)

μ = viscosity, lb. mass/ (ft.) (hr.)

ϱ = density, lb. mass/cu.ft.

Dimensionless Groups

Re = Reynolds number, $du\varrho/\mu$

Sc = Schmidt number, $\mu/\varrho D$

Pr = Prandtl number, $C_p\mu/k$

Subscripts

a = main stream
avg = average
d = mass transfer
G = gas film
h = heat transfer
i = interface
m = mean
m =molal
s = surface

LITERATURE CITED

1. Arnold, J. H., *Ind. Eng. Chem.*, **22**, 1091 (1930).
2. Arnold, J. H., *Physics*, **4**, 225, 334 (1933).
3. Bean, H. S., E. Buckingham, and P. S. Murphy, *J. Research Natl. Bur. Standards*, **2**, 561 (1929).
4. Bedingfield, C. H., and T. B. Drew, *Ind. Eng. Chem.*, **42**, 1165 (1950).
5. Boelter, L. M. K., R. E. Martinelli, and F. Jonassen, *Trans. Am. Soc. Mech. Engrs.*, **63**, 447 (1941).
6. Buddenburg, J. W., and C. R. Wilke, *J. Phys. & Colloid Chem.*, **55**, 1491 (1951).
7. Chilton, T. H., and A. P. Colburn, *Ind. Eng. Chem.*, **26**, 1183 (1934).
8. Ibid., **27**, 255 (1935).
9. Chrisney, J. B., M.S. thesis, University of California (1948).
10. Colburn, A. P., *Trans. Am. Inst. Chem. Eng.*, **29**, 174 (1933).

10a. Colburn, A. P., and T. B. Drew, *Trans. Am. Inst. Chem. Engrs.*, **33**, 197 (1937).

11. Danckwerts, P. V., *Ind. Eng. Chem.*, **43**, 1460 (1951).
12. Drickamer, H. G., E. J. Scott, and L. H. Tung, *J. Chem. Phys.*, **19**, 1075 (1951).
13. Dropkin, D., *Cornell Univ. Eng. Expt. Sta., Bull.* **23**, (July 1936).
14. Dwyer, O. E., and B. F. Dodge, *Ind. Eng. Chem.*, **33**, 485 (1941).
15. Eisner, Das Widerstandsproblem, Third Int. Cong. App. Mech., Stockholm (1930).
16. Emmert, R. E., and R. L. Pigford, *Chem. Eng. Progr.*, **50**, 87 (1954).
17. Elgin, J. C., and F. B. Weiss, *Ind. Eng. Chem.*, **31**, 435 (1939).
18. Fellinger, L., Sc.D. Thesis, Mass. Inst. Technol. (1941).
19. Gamson, B. W., G. Thodos, and O. A. Hougen, *Trans. Am. Inst. Chem. Engrs.*, **39**, 1 (1943).
20. Gerster, J. A., A. P. Colburn, W. E. Bonnet, and T. W. Carmody, *Chem. Eng. Progr.*, **45**, 716 (1949).
21. Hirschfelder, J. O., R. B. Bird, and E. L. Spotz, *Trans. Am. Soc. Mech. Engrs.*, **71**, 921 (1949).
22. Houston, R. W., and C. A. Walker, *Ind. Eng. Chem.*, **42**, 1105 (1950).
23. Jesser, B. W., and J. C. Elgin, *Trans. Am. Inst. Chem. Engrs.*, **39**, 277 (1943).
24. Johnstone, J. F., and A. D. Singh, *Ind. Eng. Chem.*, **29**, 286 (1937).
25. Justi, E., and F. Langer, *Z. Tech. Phys.*, **21**, 189 (1940).
26. Keenan, J. H., "Thermodynamic Properties of Air," Wiley and Sons, Inc., New York (1945).
27. Keyes, F. G., *Trans. Am. Soc. Mech. Engrs.*, **73**, 589 (1951).
28. Lee, C. Y., and C. R. Wilke, *Ind. Eng. Chem.*, **46**, 2381 (1954).
29. Lorisch, *Forschungsarbeiten*, **322**, 46 (1929).
30. Lynch, E. J., and C. R. Wilke, Univ. of Calif. Rad. Lab. Report No. 2057 Rev.
31. Mark, J. G., *Trans. Am. Inst. Chem. Engrs.*, **28**, 107 (1932).
32. McAdams, W. H., J. B. Pohlenz, and R. C. St. John, *Chem. Eng. Progr.*, **45**, 241 (1949).
33. Mehta, J. J., and R. H. Parekh, M.S. Thesis, Mass. Inst. Technol. (1939).
34. Murphree, E. V., *Ind. Eng. Chem.*, **24**, 726 (1932).
35. Othmer, D. F., and E. G. Scheibel, *Trans. Am. Inst. Chem. Engrs.*, **37**, 211 (1941).
36. Perry, J. H., "Chemical Engineers' Handbook," 3 ed., p. 220, McGraw-Hill Book Company, Inc., New York (1950).
37. Sarchet, B. R., *Trans. Am. Inst. Chem. Engrs.*, **38**, 283 (1942).
38. Scheibel, E. G., and E. F. Othmer, *Trans. Am. Inst. Chem. Engrs.*, **40**, 611 (1944).
39. Sherratt, G. G., and E. Griffiths, *Phil. Mag.*, **27**, 68 (1939).
40. Sherwood, T. K., *Trans. Am. Soc., Chem. Engrs.*, **36**, 817 (1940).
41. Sherwood, T. K., and F. A. L. Holloway, *Trans. Am. Inst. Chem. Engrs.*, **36**, 39 (1940).
42. Sherwood, T. K., G. H. Shipley, and F. A. L. Holloway, *Ind. Eng. Chem.*, **30**, 768 (1938).
43. Simkin, D. J., M.S. Thesis, Univ. Calif. (1948).
44. Striplin, M. M., *Ind. Eng. Chem.*, **33**, 910 (1941).
45. Surosky, A. E., and B. F. Dodge, *Ind. Eng. Chem.*, **42**, 1112 (1950).
46. Taecker, R. G., and O. A. Hougen, *Chem. Eng. Progr.*, **45**, 188 (1949).
47. Van Krevelin, D. W., P. J. Hoftijzer, and C. J. Van Hooren, *Chem. Eng. Progr.*, **44**, 529 (1948).
48. Vennard, J. K., "Elementary Fluid Mechanics," p. 144, John Wiley and Sons, Inc., New York (1947).
49. Vivian, J. E., and R. P. Whitney, *Chem. Eng. Progr.*, **45**, 329 (1949).
50. Whitman, W. G., *Chem. & Met. Eng.*, **29**, No. 4, 146 (July 23, 1923).
51. Wilke, C. R., *Chem. Eng. Progr.*, **46**, 95 (1950).
52. Yoshida, F., and T. Tanaka, *Ind. Eng. Chem.*, **43**, 1467 (1951).

(Presented at A.I.Ch.E. Toronto meeting)

PHASE EQUILIBRIA in Systems with Ethylene Above Its Critical Temperature

DAVID B. TODD
and
JOSEPH C. ELGIN
Princeton University
Princeton, New Jersey

A study was made of the mutual solubility of ethylene with various polar and nonpolar relatively high-molecular-weight organic compounds at temperatures 1° and 10° C. respectively above the critical temperature of ethylene and at pressures up to 1,500 lb./sq.in.abs. For many compounds Henry's law was found to be applicable for the liquid phase up to approximately two thirds of the critical pressure of ethylene. In the critical region the solubility of ethylene was extremely sensitive to small changes in both temperature and pressure. The various types of phase behavior encountered were classified according to the nonideality involved. The results of this investigation indicate that a gas near its critical conditions is often capable of dissolving relatively nonvolatile materials in sufficient concentrations to warrant consideration of a separation process using such a gas as the extracting medium, namely fluid-liquid extraction.

Phase behavior and equilibrium between phases are the fundamental bases of any phase-change separation process. They are profoundly influenced by the temperature, pressure, and concentration region considered as well as by the relative chemical structures and physical properties of the substances involved. Although various investigators have explored certain regions of phase equilibria rather extensively, comparatively few studies have however been made where the equilibrium compositions of the phases were measured in the critical region for components differing widely in chemical structure, molecular weight, and critical temperature. From the results of previous studies a general classification of binary vapor-liquid-phase behavior in terms of the nonideality involved can be made as follows:

Ideal Solutions. This class has been generalized and dealt with by means of Raoult's, Henry's, Dalton's, and the ideal gas laws. Thus the compositions of the phases can be related to each other and to pressure and temperature algebraically or graphically. This situation is rarely met exactly but is approximated closely by a few systems such as similar hydrocarbons and is an important standard of comparison for other systems.

Nonideal Solutions at Low Pressures. This classification contains the large majority of liquid systems at normal and low pressures where the perfect-gas laws are approximately valid. Differing degrees of nonideality in the liquid phase lead to azeotropy and partial or complete immiscibility. Liquid-phase nonideality is usually measured in terms of an activity coefficient.

Nonideal Solutions at High Pressures. This class is the most difficult to treat thermodynamically, since both phases require correction factors, and comparatively more data are required for generalization. It is also probably the least investigated of the cases, especially at conditions favoring nonideality. For liquids this case involves components of differing molecular weight; differing size, shape, and structure; differing polarity; and differing hydrogen-bonding tendencies. For vapors this means operating in the critical region of the mixture of chemically dissimilar components. Such systems offer interesting possibilities for extending and generalizing the present knowledge of phase behavior and theoretical possibilities for developing new separation processes by deliberately making use of nonideal behavior.

Because processes often operate at constant temperature or pressure, the most common binary-phase diagrams are those of composition vs. temperature at constant pressure or composition vs. pressure at constant temperature. The general interrelations of these and other representations have recently been outlined by Ricci(4).

Further consideration of these phase diagrams permits subdivisions of the classes outlined above. For the less-well-known classification of nonideal solutions at high pressures, at least three types of behavior can be differentiated for binary systems. Basically a P-x diagram for a binary system of complete miscibility below the critical temperature of both components takes the familiar form shown in Figure 1. The intercepts on the P axis are the vapor pressures of the two components of the system at the specified temperature.

As the temperature is increased

D. B. Todd is at present with Shell Development Company, Emeryville, California.

above the critical for the more volatile component, a continuous loop (upper branch representing the liquid, lower branch the vapor phase) would be obtained originating from and ending with the vapor pressure of the less volatile component as in Figure 2. It is now possible to pass from a liquid to a vapor phase without crossing any phase boundaries. Above the critical temperature the material in equilibrium with a liquid phase is often referred to as a "fluid" phase.

As the dissimilarity in volatility and structure between the two components is increased, the two-phase area increases in spread and is distorted at low pressures, as depicted in Figures 3 and 4. These still represent a system of complete miscibility in the liquid phase and for purposes of reference are called here type 1.

With poorer liquid miscibility, the presence of the second component in the vapor, even in small amounts, materially increases the critical-pressure requirements for the system, leading to an "open" loop as in Figure 5. Here the slope of the P-x liquid line no longer steadily decreases, as was noticed in Figure 4. This system, with no maximum pressure of the two-phase region, has been called type 2.

It is possible that one component is sufficiently dissimilar to the other for partial immiscibility to develop in the critical region. This interference may arise owing to differences in molecular weight, hydrogen bonding, polarity, or other properties. The resultant P-x diagram, with partial immiscibility in the liquid phase, is shown in Figure 6 and is designated type 3.

The present investigation was undertaken as the initial study in a program of research designed to explore the nonideal-solution class in the region of high pressures, with the broad objective of systematizing behavior in this region and the ultimate goal of treating this information thermodynamically. A further objective was to explore the possibilities of applying unusual separation techniques such as fluid-liquid extraction or crystallization from a supercritical fluid. Particular systems and operating conditions were chosen that favored nonideality in both phases.

Ethylene was chosen for the gas because of its ready availability and its easily attained critical conditions (9.5° C. and 50.7 atm.). Other components, chosen for varying degrees of volatility, polarity, chain length, molecular weight, and chemical structure, were propionic, caproic, capric, stearic, and oleic acids; propyl, hexyl, decyl, and cetyl alcohols; decane, cetane, toluene, hexaldehyde, capronitrile, propyl propionate, and ortho and para dichlorobenzene. Generally compositions of the vapor and liquid phases were determined as a function of pressure at 1 and 10° respectively above the critical temperature of pure ethylene.

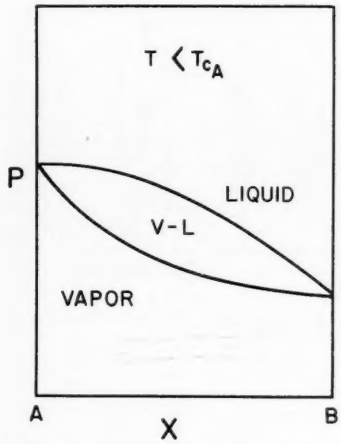

FIG. 1. HYPOTHETICAL P-x DIAGRAM FOR BINARY SYSTEM, $T<Tc_A$.

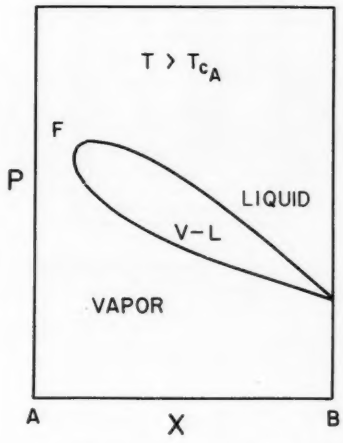

FIG. 2. HYPOTHETICAL P-x DIAGRAM FOR BINARY SYSTEM, $T>Tc_A$.

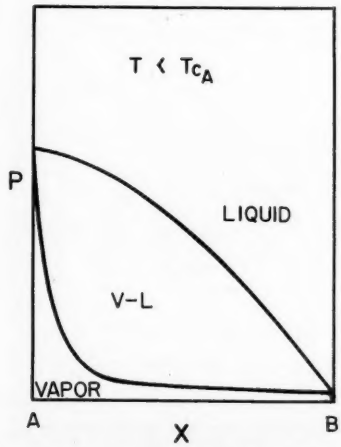

FIG. 3. P-x DIAGRAM FOR TYPE-1 SYSTEM, $T<Tc_A$.

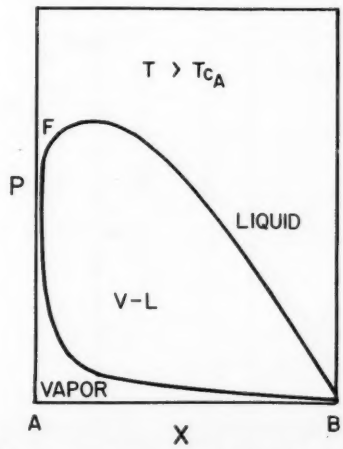

FIG. 4. P-x DIAGRAM FOR TYPE-1 SYSTEM, $T>Tc_A$.

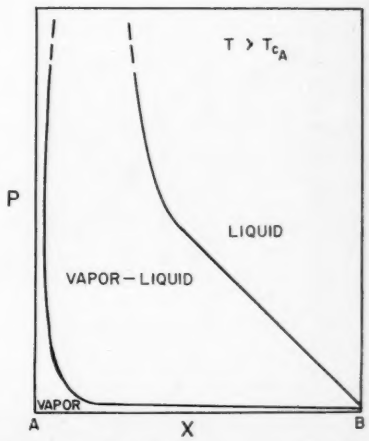

FIG. 5. P-x DIAGRAM FOR TYPE-2 SYSTEM.

EXPERIMENTAL METHOD

A modified Jerguson gauge equipped with a magnetic stirrer (*see* Figure 7) was used for the equilibrium determinations. Samples of vapor and

liquid phases were flashed into evacuated cartridges, *B*. Subsequent cooling in a dry-ice and acetone bath precipitated the component other than ethylene, permitting the ethylene to be withdrawn and measured volumetrically. The remaining part of the sample was flushed from the cartridge with a known amount of suitable solvent, the resulting concentration being determined by refractive index. Thus the composition of the original sample was readily calculated.

The procedure involved in bringing the system to equilibrium was as follows. The equilibrium chamber was completely dismantled and equipped with new gaskets before each series of runs. Solids to be studied were introduced during reassembly; liquids were introduced through line *A*. The mercury reservoir *F* was set to seal the bottom of the Jerguson gauge. Adjusting the height of the reservoir also permitted changing the level of either phase to the correct height for sampling through valve *D*. Ethylene was introduced directly from the cylinder. After long and vigorous stirring with the magnetic stirrer *E*, equilibrium was presumed attained when no further pressure change could be detected. The equilibrium chamber was kept at constant temperature (± 0.1° C.) by the cooling system *C*. Generally a judicious choice of the amount of solid or liquid originally introduced permitted operation in the visible range of the equilibrium chamber, with the amount of ethylene

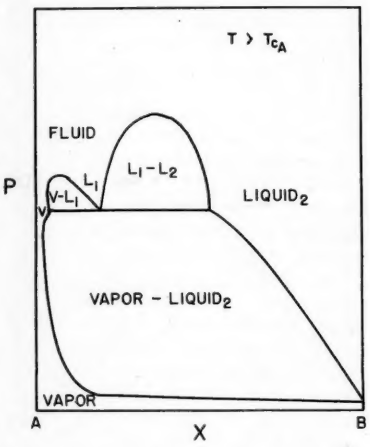

FIG. 6. *P-x* DIAGRAM FOR TYPE-3 SYSTEM.

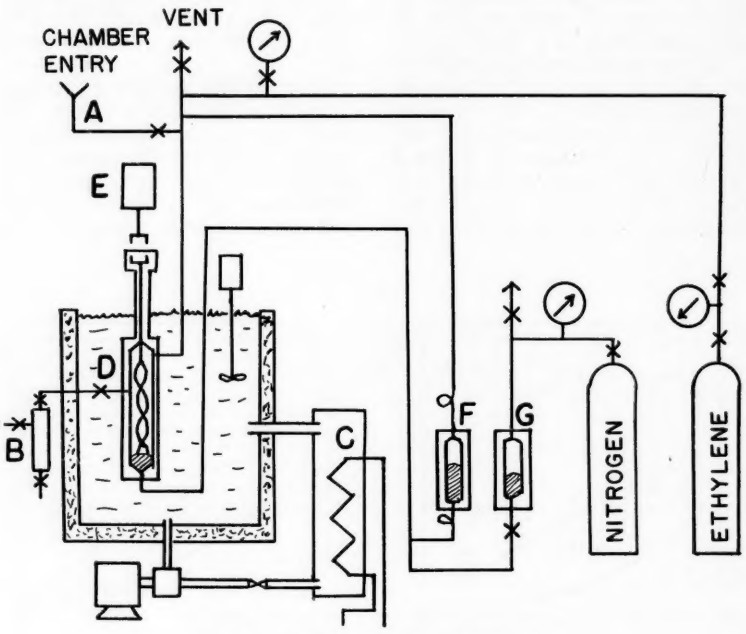

FIG. 7. EXPERIMENTAL APPARATUS.

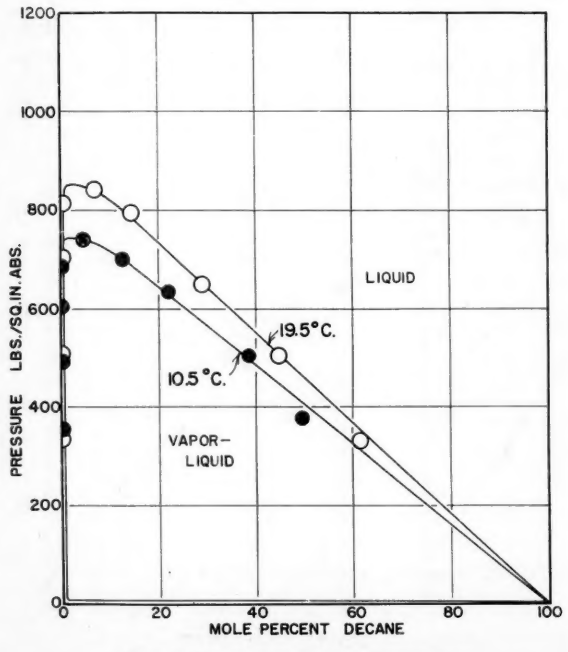

FIG. 8. DECANE-ETHYLENE ISOTHERMS.

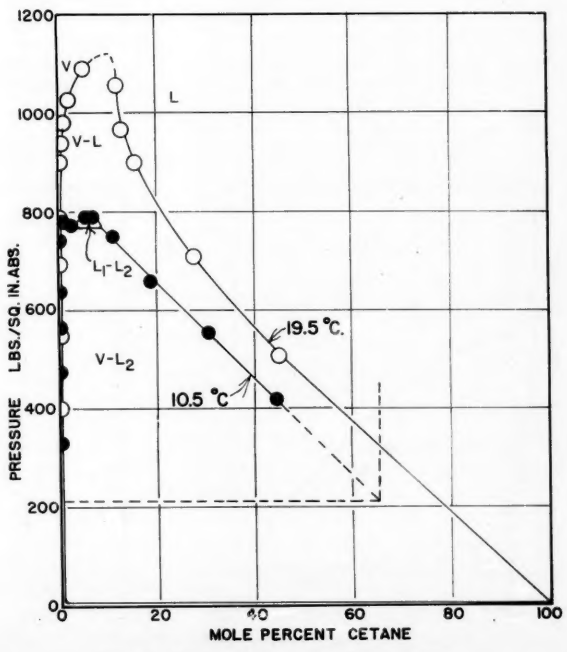

FIG. 9. CETANE-ETHYLENE ISOTHERMS.

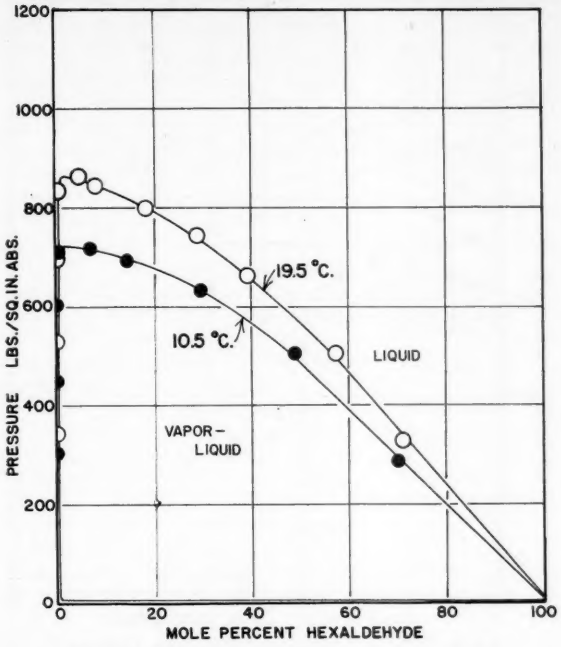

FIG. 10. HEXALDEHYDE-ETHYLENE ISOTHERMS.

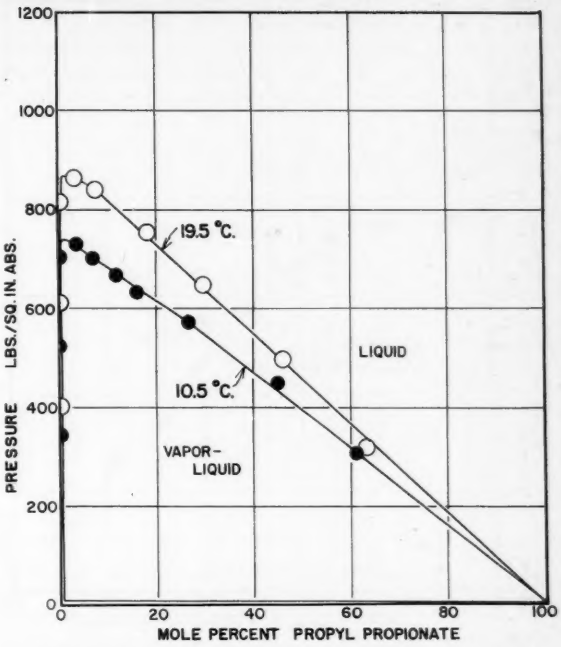

FIG. 11. PROPYL PROPIONATE–ETHYLENE ISOTHERMS.

determining the pressure. Changes in pressure could also be brought about by the back pressure of nitrogen against the second mercury reservoir *G*. During flashing, the volume occupied by the sample was simultaneously replaced by admission of mercury from reservoir *G*.

The source and purity of the compounds used in this investigation are listed in Table 3. The materials were used as obtained, without any attempt at further purification, and the effect of possible impurities on the absolute values reported was not determined.

RESULTS

The P-x diagrams for the various systems studied are represented in Figures 8 to 22.* At low pressures the composition of the vapor phase was not determined; however the vapor line has been illustrated as returning to the vapor pressure of the pure organic constituent. Subscript 1 refers to a liquid richer in ethylene than in

*Complete tabular data for experimentally measured values of phase compositions and pressures at each of the temperatures studied, Tables 4 through 19 of this paper, are on file with A.D.I., Auxiliary Publications Photoduplications Service, Library of Congress, Washington 25, D.C., as document 4476 and may be obtained for $1.75 for microfilm and $2.50 for photoprints.

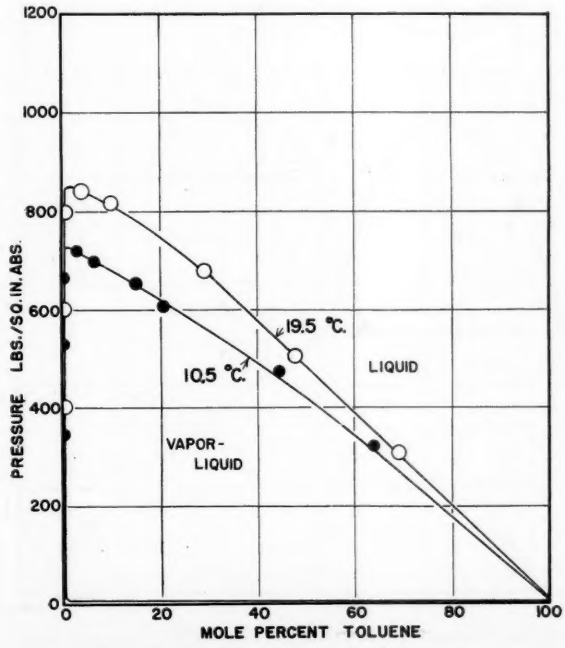

FIG. 12. TOLUENE-ETHYLENE ISOTHERMS.

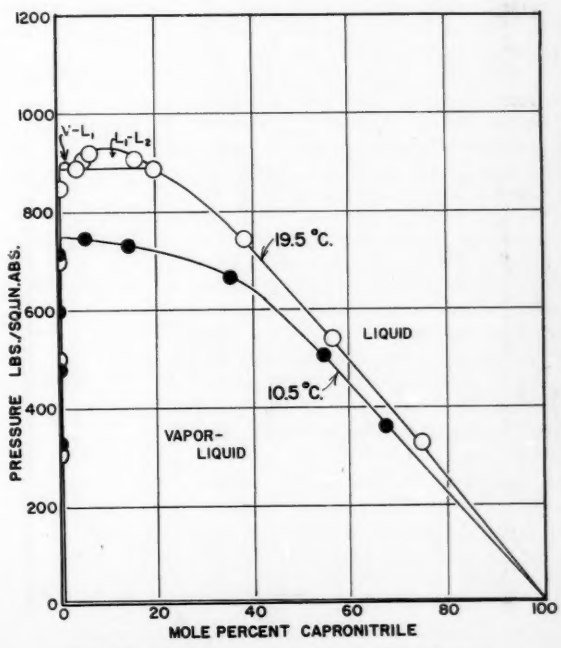

FIG. 13. CAPRONITRILE-ETHYLENE ISOTHERMS.

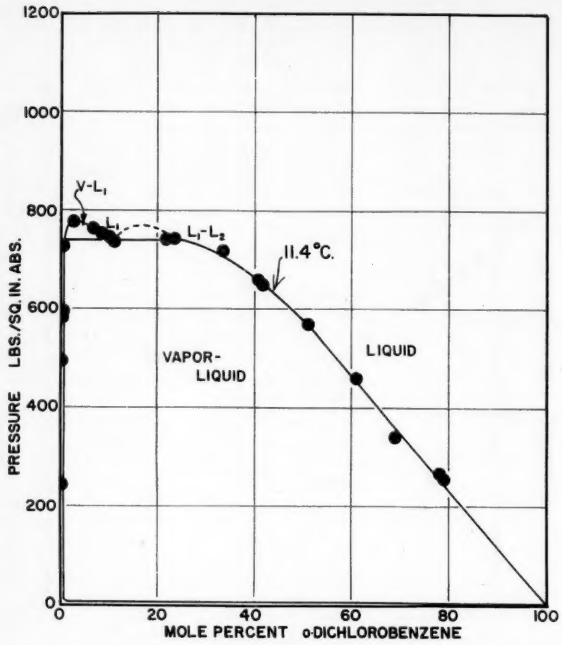

FIG. 14. *o*-DICHLOROBENZENE-ETHYLENE ISOTHERM.

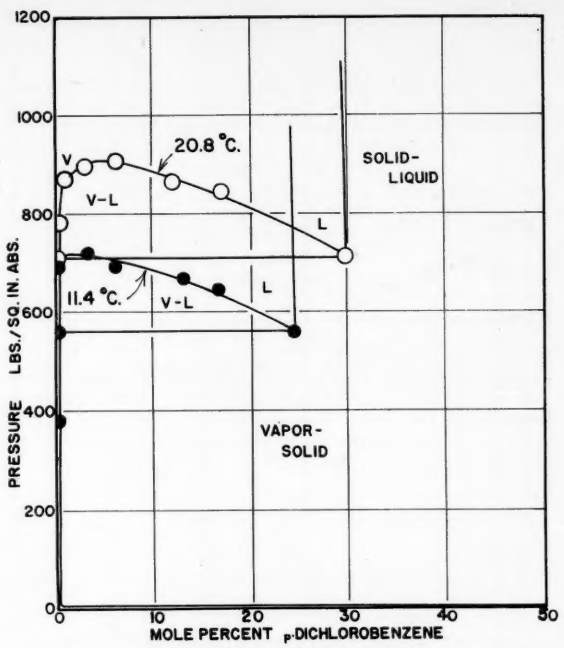

FIG. 15. *p*-DICHLOROBENZENE-ETHYLENE ISOTHERMS.

the liquid (subscript 2) which coexists with it.

The compounds forming the type-1 systems with ethylene are decane (Figure 8), hexaldehyde (Figure 10), propylpropionate (Figure 11), and toluene (Figure 12). At the temperatures studied, the variation of liquid composition with pressure was approximately linear over almost the entire pressure range. As the temperature is increased, the liquidus line is raised, and the critical point is reached at a high pressure and at a composition richer in the less volatile component. The phase diagram obtained for the ethylene-cetane system (Figure 9) indicates that this aliphatic system no longer strictly follows type-1 behavior. Since cetane is a solid at 10.5° C., no liquid was formed until the pressure of ethylene had been increased to 216 lb./sq.in.abs. Near the critical pressure of the mixture, a region of immiscibility occurred, indicating type-3 behavior. The formation of this ethylene-rich liquid is probably attributable to the nonideality arising from the great difference in molecular weight and volatility.

Regions of coexisting liquid phases near the critical pressure (type-3 behavior) were found also for the ethylene-capronitrile system at 19.5° C. (Figure 13), the ethylene-acetonitrile system at 10.5° C.(*2*), the ethylene-orthodichlorobenzene system at 11.4° C. (Figure 14), and the systems of ethylene with lower molecular-weight alcohols at 10.5° C. Figure 16 represents the composition in the three-phase region for the ethylene – *n*-propyl alcohol system (*3*). The secondary liquid exists over a narrower composition and pressure region in the ethylene – *n*-hexyl alcohol system (Figure 17). With decyl alcohol (Figure 18) formation of an ethylene-rich liquid could not be detected. Also, the critical pressures at these temperatures could not be attained with the present equipment indicating type-2 behavior. It is interesting that an ethylene-rich liquid phase can exist in these systems at temperatures above the critical temperature of ethylene.

Type-2 behavior was found also for the higher molecular weight acids. *P-x* isotherms are given for the ethylene–oleic acid system in Figure 22. Apparently at a pressure above 900 lb/sq.in.abs. the composition of the phases is relatively insensitive to further pressure change.

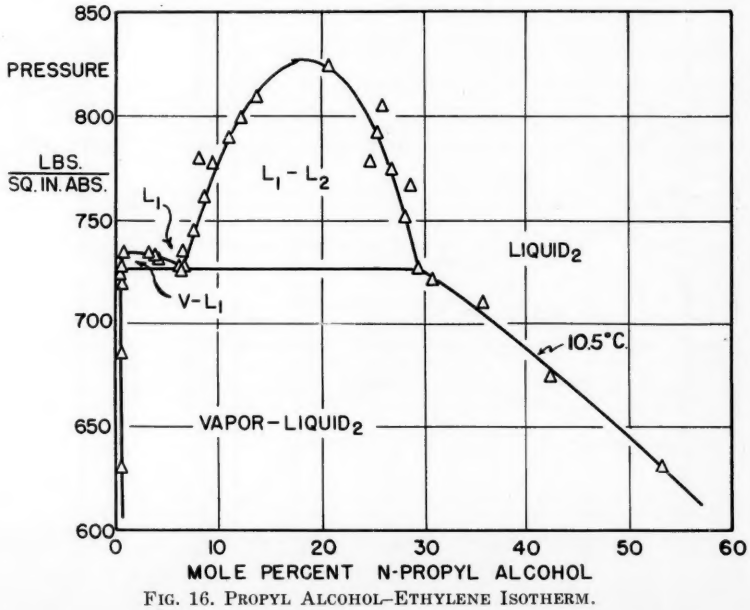

FIG. 16. PROPYL ALCOHOL–ETHYLENE ISOTHERM.

The lower molecular-weight acids fall into type-1 behavior (Figures 19 and 20); the transition to type 2 apparently depends upon the size of the acid molecule (Figure 21). As the chain length is increased, the melting point also is increased. Consequently not all the acids could be studied in this temperature region. The *P-x* diagram for the ethylene-caproic acid system (Figure 20) typifies the behavior for the lower molecular-weight acids. Here the increase of acid concentration at the critical pressure is much more noticeable. No liquid formation was detected in the ethylene–stearic acid system. A very narrow region of ethylene-rich liquid was obtained at 10.5°C. in the ethylene–cetyl alcohol system (*5*). Compression of ethylene on another solid, *p*-dichlorobenzene, caused formation of a liquid over a wide composition and pressure range (Figure 15). The effect of ethylene pressure on the melting point of this solid is noteworthy. The triple-point pressures determined here are some 25% lower than those reported by Diepen and Scheffer (*1*) possibly because of differences in the impurities present in the compounds used.

As the solubility of ethylene was found to increase linearly with pressure to about three fourths of the critical pressure for many of the systems, many of the data for the composition of the liquid phase can be represented in the form of Henry's law if it is assumed that the partial pressure of ethylene is equal to the total pressure of the system. Where applicable, Henry's law constants have been calculated and are listed in Table 1. At about the maximum valid pressure indicated, the slope of the composition vs. pressure curve decreases for type-1 and type-3 systems and increases for type-2 systems.

TABLE 1.—HENRY'S-LAW CONSTANTS FOR THE SOLUBILITY OF ETHYLENE

p_g = partial pressure of ethylene, lb./sq. in. abs.
N = mole fraction of ethylene in liquid phase
k = Henry's law constant, lb./sq. in. abs., $p_g = kN$

Solvent	Temp., °C.	k, lb./sq. in. abs.	Maximum valid pressure, lb./sq. in. abs.
Hexyl alcohol	10.5	149	590
	19.5	159	900
Decyl alcohol	10.5	100	300
	19.5	134	600
Decane	10.5	82	680
	19.5	92	800
Cetane	19.5	94	500
Hexaldehyde	10.5	98	500
	19.5	117	500
Capronitrile	10.5	113	500
	19.5	125	680
Propyl propionate	10.5	78	680
	19.5	92	800
Toluene	10.5	86	500
	19.5	97	680
Oleic acid	10.3	98	600
	20.0	114	680
o-Dichlorobenzene	11.4	118	580

DISCUSSION

From the phase diagrams it can be seen that the phase relations encountered in this investigation

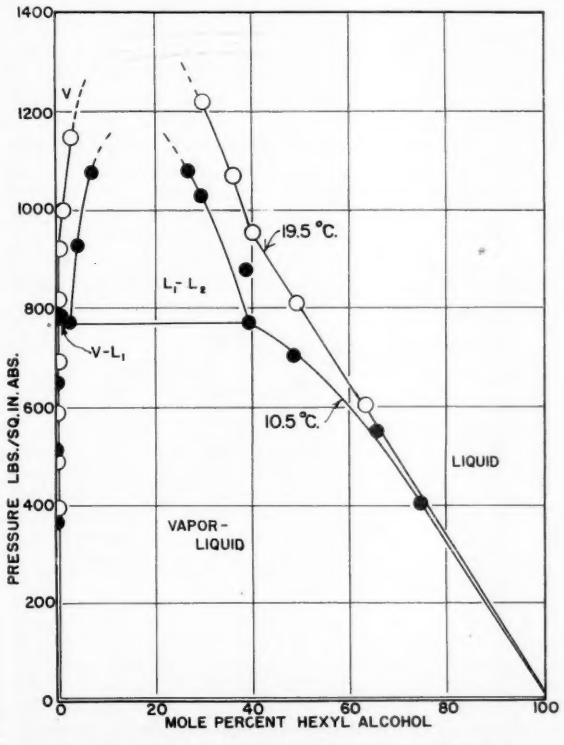

FIG. 17. HEXYL ALCOHOL–ETHYLENE ISOTHERMS.

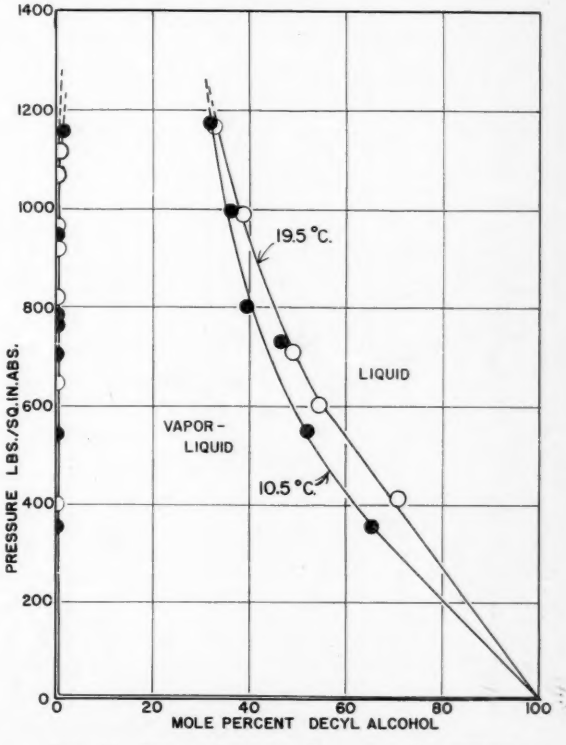

FIG. 18. DECYL ALCOHOL–ETHYLENE ISOTHERMS.

TABLE 2.—CONCENTRATION OF VAPOR PHASE IN SYSTEMS WITH ETHYLENE

Compound	Temp., °C.	Vapor pressure, mm. Hg	Pressure, lb./sq. in. abs.	Mole % in "vapor"	Wt. % in "vapor"
Capric acid.....	19.5	0.000003	1,200	0.47	2.8
Caproic acid.....	19.5	0.0035	1,014	3.2	12.1
Cetane.....	19.5	0.0017	1,090	4.9	29.3
Hexyl alcohol.....	19.5	0.69	1,150	2.6	9.0
Propyl alcohol.....	10.5	8.0	800	12.5	23.4

can be grouped into the three types of behavior enumerated under the classification of nonideal solutions at high pressures. Into which type any other system might fall may be estimated by a consideration of the factors involved in the systems already studied; for example, it is probable that combinations of a polar low-molecular-weight gas, e.g., ammonia or sulfur dioxide or carbon dioxide, with relatively high-molecular-weight nonpolar compounds such as hydrocarbons will exhibit behavior in the critical region analogous to that of these classes.

Type-1 behavior would be expected where differences in chemical structure and molecular size are not great. Systems of paraffins or olefins with other similar paraffins, aldehydes, or esters would probably be classed in this type.

For minor differences in chain length, type-3 behavior would be produced by differences in chemical structure, polarity, or hydrogen-bonding tendencies. The ethylene-alcohol and ethylene-nitrile systems are evidence of this. Although the acids are strongly polar and tend to form relatively strong hydrogen bonds, it is believed that these molecules act as dimers and thus somewhat nullify these strong effects. For members of a homologous series, sufficient dissimilarity in chain length could also cause type-3 behavior (for example ethylene and cetane).

With dissimilar components either Type 2 or 3 behavior would be expected. Difference in volatility and size of molecule would eventually lead to type 2. The two-liquid-phase phenomena (type 3) can occur only if the less volatile component is sufficiently volatile to enter the vapor phase in a high enough concentration to interfere with the densely packed molecules of the more volatile component and thus to lead to gas-phase nonideality similar to that of the liquid phase.

When one of the components is a solid, compression of a super critical gas upon it may cause a liquid to form or may yield a region of increased solids solubility manyfold greater than that predicted from vapor pressure alone (*1*).

Besides the theoretical interest in the unusual phase behavior encountered in these systems, the principles involved can be applied in operations wherein the nonideality is intentionally created. The magnitude of solubility of a compound of low volatility in a gas above its critical temperature (*see* Table 2) is sufficient to consider the gas as an extracting medium, that is fluid-liquid or fluid-solid extraction analogous to liquid-liquid extraction and leaching. In this case the solute is removed and the solvent recovered by partial decompression. For the cases cited in Table 2, decompression to 900 lb./sq.in. abs. at 19.5° C. or to 700 lb./sq.in.abs. at 10.5° C. reduces the nonvolatile-component concentration in the vapor phase to less than 1% by weight. Thus compression of a gas over a mixture of compounds could selectively dissolve one compound, permitting it to be removed from the mixture. Partial decompression of the fluid

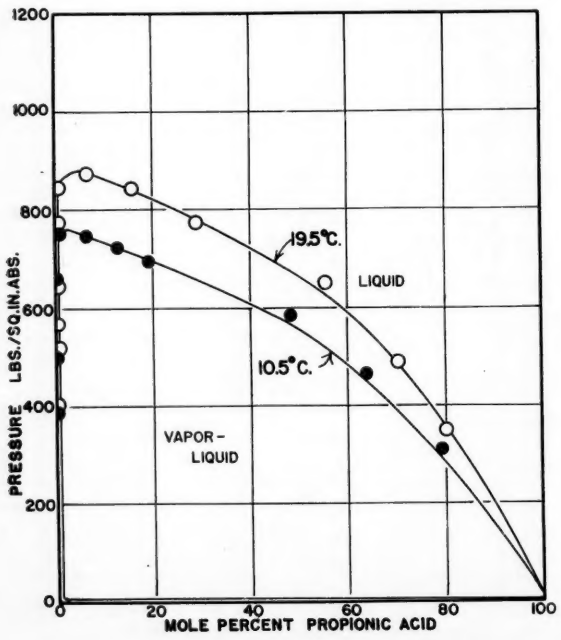

FIG. 19. PROPIONIC ACID–ETHYLENE ISOTHERMS.

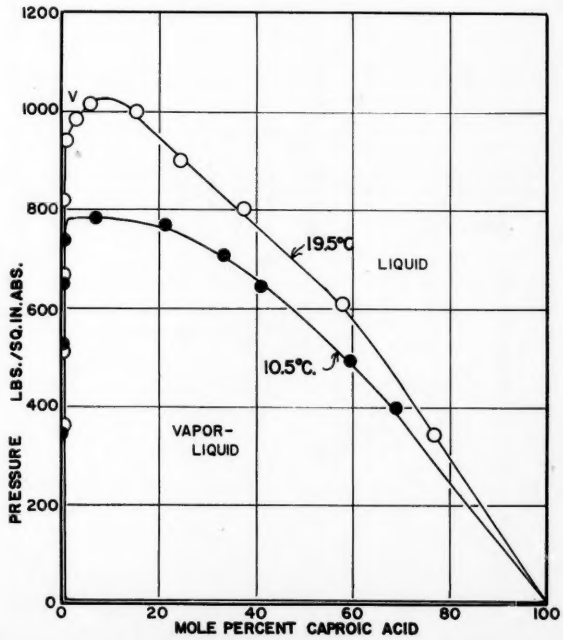

FIG. 20. CAPROIC ACID–ETHYLENE ISOTHERMS.

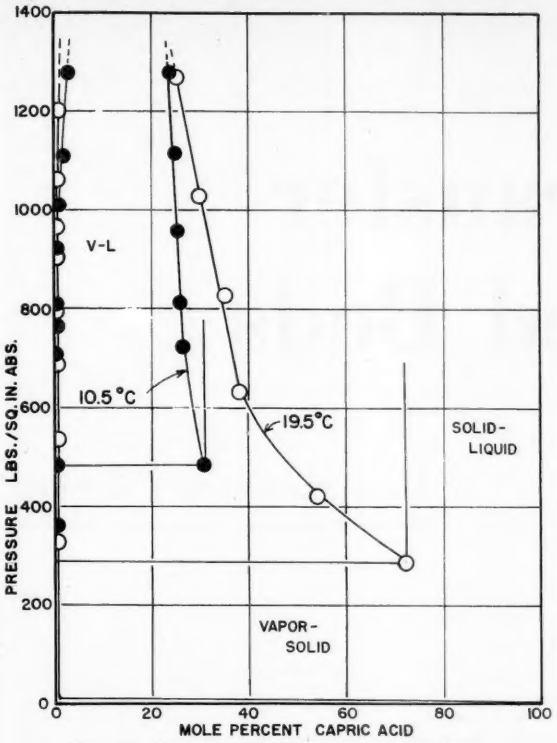

FIG. 21. CAPRIC ACID–ETHYLENE ISOTHERMS.

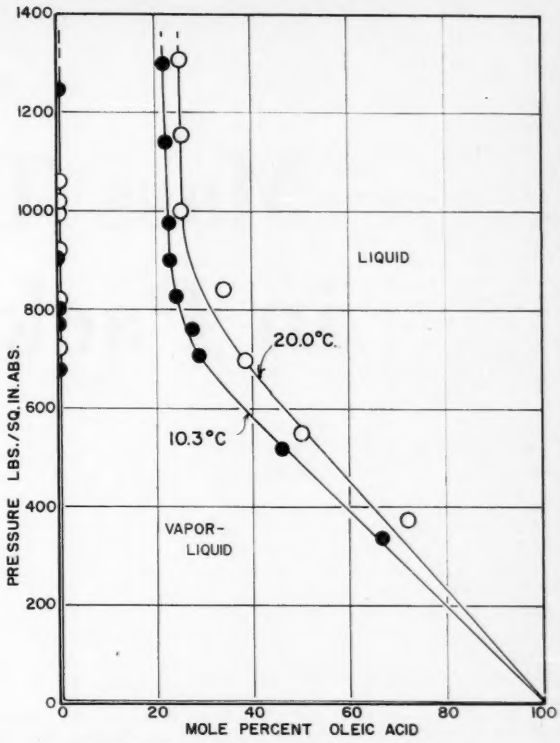

FIG. 22. OLEIC ACID–ETHYLENE ISOTHERMS.

elsewhere would drop out the dissolved compound, and the gas could be reused for further extraction.

Weinstock(*6*) has recently completed a study of ternary systems involving ethylene and water with various organic liquids wherein the ethylene under pressure is used to force a phase separation, splitting out the water from the organic solution. The behavior with supercritical ethylene is analogous to the use of a solid such as sodium chloride as a "salting-out" agent.

Supplying the energy for phase creation in the form of pressure rather than heat would also provide a means of separation and purification of those temperature-sensitive materials not suited for normal distillation. Because of the relatively high densities involved in such a process, the capacity would be greater than for the molecular distillation now frequently in use. A range of temperature regions is available because of the various extractant gases that might be chosen.

ACKNOWLEDGMENT

The authors gratefully acknowledge the support of the American Cynamid Company, whose fellowship was held by one of them during this investigation.

NOTATION

A = substance in binary system with high volatility
B = substance in binary system with low volatility
F = fluid phase
L = liquid phase
P = pressure
T = temperature
T_c = critical temperature
V = vapor phase
x = composition

TABLE 3.—MATERIALS USED

Compound	Source	Purity
Propionic acid	Matheson Co.	C.P. grade
n-Caproic acid	Matheson Co. 2756	98%, B.P. 94-95°C./8 mm.
n-Capric acid	Matheson Co. 5168	98.5%, M.P. 29-30°C.
Stearic acid	Merck & Co. 0.04282	U.S.P. triple pressed
Oleic acid	Merck & Co. 0.03221	U.S.P.
n-Hexyl alcohol	Matheson Co. P5236	95.0%, B.P. 153-156°C.
n-Decyl alcohol	Matheson Co. P5189	94.0%, B.P. 90% 229-233°C.
Cetyl alcohol	Matheson Co. 2602	98.5%, M.P. 48-49°C.
n-Decane	Matheson Co. 5845	99.0%, B.P. 173-175°C.
Cetane	Matheson Co. P5829	95.0% M.P. 15-17°C.
n-Hexaldehyde	Matheson Co. P5169	95%, B.P. 90% 124-130°C.
n-Capronitrile	Matheson Co. 6612	98.0%, B.P. 161-163°C.
n-Propylpropionate	Matheson Co. 4296	98.5%, B.P. 122-125°C.
Toluene	Merck & Co. 74951	A.C.S. Specs., B.P. range 1°C.
p-Dichlorobenzene	Matheson Co. 2779	99.0%, M.P. 52-5-53°C.
o-Dichlorobenzene	Matheson Co. 1289	99.5%, B.P. 53-55°C./10 mm.
Ethylene	U.S. Industrial Chem.	99.5%

LITERATURE CITED

1. Diepen, G. A. M., and F. E. C. Scheffer, *J. Am. Chem. Soc.*, 70, 4085 (1948); *J. Phys. Chem.*, 57, 575 (1953).
2. Gottschlich, C., M. S. E. Thesis, Princeton Univ. (1953).
3. Jaglom, J., M. S. E. Thesis, Princeton Univ. (1953).
4. Ricci, J. E., "The Phase Rule and Heterogeneous Equilibrium," Van Nostrand Co., New York (1951).
5. Todd, D. B., Ph. D. Thesis, Princeton Univ. (1951).
6. Weinstock, J. J., Ph. D. Thesis, Princeton Univ. (1954).

(Presented at A.I.Ch.E. San Francisco meeting)

Mass Transfer in Packed Beds

R. W. FAHIEN AND J. M. SMITH
Purdue University, Lafayette, Indiana

Although considerable work has been done on the problem of heat transfer radially in fixed beds through which gases are flowing, the data available for mass transfer are limited to one pipe size and one packing size and refer to average diffusivities for the entire bed. The present study was undertaken to determine: (1) diffusivities over a range of pipe and packing sizes and (2) the effect of radial position in the bed.

The measurements were made by introducing carbon dioxide into an air stream and analyzing the resultant mixture at various positions in the bed downstream from the point of injection. Pipe sizes of 2, 3, and 4 in. were packed with spherical particles of 5/32-, ¼-, ⅜-, and ½-in. nominal diameter.

The differential equation describing the concentration in a packed bed when diffusivity E and the velocity u are permitted to vary with radial position was solved by use of an I.B.M. card-programmed calculator for the computations.

The results show that the Peclet number $D_p u/E$ increases from the center toward the wall of the pipe and that the increase is significant when D_p/D_t is greater than 0.05. Empirical correlations are then presented for both point Peclet numbers, which vary with radial position, and average Peclet numbers for the entire bed.

The variations in Peclet number with radius can be explained in terms of the corresponding variation in void fraction for 81% of the radius of the bed. At modified Reynolds numbers above 40 to 100 the equation $Pe = 8.0 + 100\ (\delta - \delta_w)$ correlates the effects of pipe and packing size and radial position. At radial positions greater than 0.81 wall friction influences turbulence conditions and the Peclet number.

In the design of fixed-bed catalytic reactors a knowledge of both heat and mass transfer rates in the radial direction is important. The heat transfer problem has received considerable attention, but data for mass transfer in gaseous systems are limited. The main objective of this study was to provide such information for a variety of tube and packing sizes.

Mass transfer is important not only in itself, but also because of its relation to the heat transfer process which occurs simultaneously under the influence of the temperature gradient existing radially in the packed bed. Although the mass transfer process takes place primarily by the mechanism of convection, heat transfer can occur by a variety of other mechanisms also. Hence a study of mass transfer provides a means of breaking down the more complex heat transfer process, at least partially, into its component parts.

Previous heat transfer studies (*1, 10*) have indicated that effective thermal conductivities vary with radial position. Since it seemed likely that effective diffusivities would also show such variations, a further purpose of this study was to determine point values of the diffusivity at different positions in the bed.

Because of the possible variation in both diffusivity and velocity with radial position, a complex differential equation must be used to relate the variables. One method of handling the problem is to obtain data at a number of packing-bed depths and solve the equation for the diffusivity, or Peclet number, by differentiating the data rather than integrating the equation. This procedure has been used in attacking the analogous heat transfer problem (*10*). To eliminate both the necessity for measuring concentrations at multiple bed depths and the errors associated with graphical differentiation, in the present study the complex equation was solved with the aid of an I.B.M. card-programmed calculator. Hence another purpose of the study was to demonstrate the use of an automatic computing ma-

R. W. Fahien is at present with the Ethyl Corporation, Baton Rouge, Louisiana.

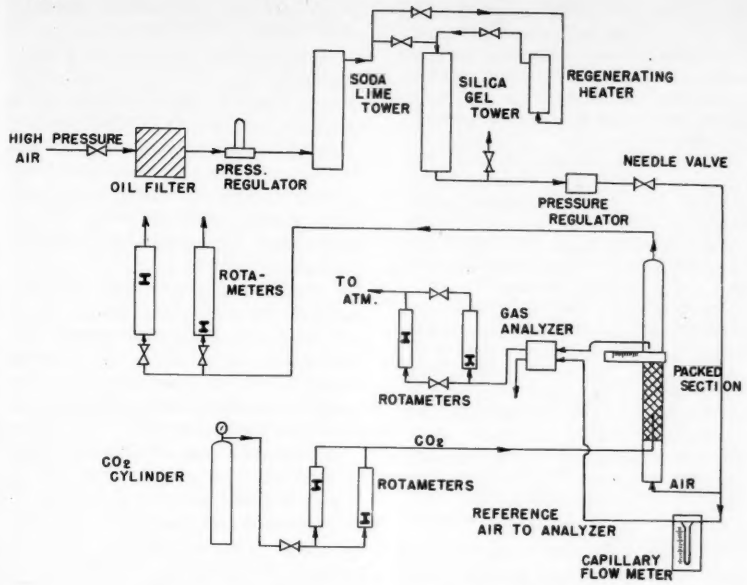

FIG. 1. FLOW SHEET OF AIR–CARBON DIOXIDE SYSTEM.

chine in chemical engineering calculations of this type. The details of setting up such calculations on the C.P.C. machine will be described in a separate paper.

The experimental technique consisted of injecting carbon dioxide into an air stream flowing through the vertical packed bed. At some height above the point of injection, samples of the air–carbon dioxide mixture were withdrawn and analyzed. A knowledge of the concentration and velocity [available from Schwartz and Smith(*11*)] across the diameter of the bed at a single bed depth provided sufficient information to yield effective diffusivity values at any point in the bed.

PREVIOUS WORK

The first measurements of mass transfer by turbulent diffusion in gaseous systems were carried out by Sherwood and Towle(*14*). Although their work was done in an empty pipe, the results are important for fixed-bed diffusion, as it was shown that the diffusivity was not influenced by the molecular weight of the diffusing component.

Bernard and Wilhelm(*3*) reported considerable data on radial mass transfer rates in liquid systems and also the only published values for gaseous systems, i.e., for carbon dioxide diffusing across an air stream flowing through an 8-in. diam. pipe packed with 3/8-in. spheres.

Singer and Wilhelm(*13*) have assembled data on heat and mass transfer in terms of the Peclet group, Reynolds number, and the ratio of particle-to-tube diameter. These results show that the Peclet group for heat transfer is generally smaller than the corresponding group for mass transfer.

From theoretical considerations Baron(*2*) has predicted that the Peclet number should be between 5 and 13. The basis for this prediction is the random-walk theory, in which a statistical approach is employed. Latinen(*7*) has extended the random-walk concept to three dimensions and demonstrates the applicability of his theory to a body-centered cubic packing arrangement. For fully developed turbulence a Peclet number of 11.3 is predicted. These methods of prediction do not take into account effects of radial variations in velocity and void space.

Ranz(*8*), postulating a different orientation in the bed and also assuming that the Peclet number does not depend upon the velocity or void space, proposed another method of prediction. When applied to a system of spherical particles, packed with their centers at the corners of tetrahedrons, this approach gives $Pe = 11.2$.

The availability of data showing the variation of void fraction with radial position(*9*) makes possible a clearer interpretation of the present mass transfer study.

SCOPE OF WORK

The following variables were studied:

Pipe size: 2, 3, 4 in.

Mass velocity: 125, 250, 500, 1,000 and 1,500 lb./(hr.) (sq. ft. of total pipe area). In some cases 40, 775, and 1,500 values were also used.

Packing size: 5/32-, 0.30-, 0.36-, and 0.58-in. spheres.

For each combination of the foregoing variables, three diameters across the bed were traversed, and between twenty-four and fifty-one samples of carbon dioxide were taken and analyzed. The range of modified Reynolds numbers was from 12 to 1,180, and the range of particle-to-tube diameter, D_p/D_t, from 0.038 to 0.175.

APPARATUS AND EXPERIMENTAL PROCEDURE

Figure 1 shows a schematic diagram of the entire apparatus, consisting of an air-cleaning and purifying section, an air-metering section, the test section, a carbon dioxide metering section, and a gas-analyzing section.

Carbon dioxide and water vapor were removed from the incoming air by soda lime and silica gel towers.

The test section in detail is shown in Figure 2. Straightening vanes were inserted just above the elbow leading into the section. The carbon dioxide injection tube entered the section above the straightening vanes and passed through a wire screen supporting the packing. In the 2-in. pipe runs, the 0.135-in. I.D. injection tube terminated at a point 23 in. above the screen. The upper tip of the tube was ground to a thin edge. In the 3-in. pipe runs, a 0.183-in. I.D. injection tube was used, and its tip extended 13.5 in. above the screen holding the packing. For the 4-in.-

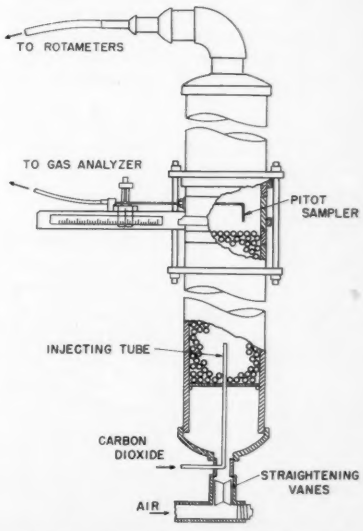

FIG. 2. DETAILS OF TEST SECTION.

pipe setup, the 0.183-in. injection tube extended 10.6 in. above the screen.

The height of packing above the tip of the injection tube was varied in the 2-in.-pipe runs, but the final data were taken at a height of 9 1/2 in. for the 5/32-in. spheres and 6 3/8 in. for the 3/8-in. spheres. The corresponding values for the 3- and 4-in.-pipes were 9.6 and 12.4 in. A statistical analysis, described in the next section, was used to arrive at these bed heights.

The bed was packed by pouring the spheres slowly from the top, using a rotating motion. This normal packing, as described by Furnas (*4*), was found to give more reproducible results than methods involving tapping. A similar conclusion was reached by Schwartz and Smith (*11*) in their velocity investigation.

Samples of carbon dioxide were removed from the top of the packed bed through a 1/16-in. O.D. Pitot tube. The tube was housed in a brass ring (Figure 2) that permitted samples to be taken from any radial position and across any diameter of the pipe.

The samples were passed through one side of an M/T-T-8 thermal-conductivity analyzer, supplied by the Gow-Mac Company. Reference air for this instrument was taken from a point just before the bed so that the measured values represented differences in concentration between the point in the bed and the inlet air.

The M/T-T-8 analyzer is an eight-filament unit containing two cells in each of four arms of a Wheatstone's bridge circuit. A constant bridge current of 100 ma. was supplied from lead storage batteries. The unbalanced e.m.f. from the bridge circuit was measured and recorded on a Leeds and Northrup Model *S* Micromax. The difference between the chart readings when a sample was passing through one cell and when reference air was in both cells was a measure of the concentration of the sample.

The flow rate through the sampling cell was fixed at a value such that the velocities inside and outside the sampling tube were the same. A number of special experiments were made to determine how rapidly samples could be withdrawn without causing appreciable mixing, and optimum values were obtained for each set of conditions.

Likewise the carbon dioxide was admitted at a speed designed to maintain an undisturbed velocity profile within the bed. This average velocity in the injection tube was found by experiment to be approximately the same as in the test section.

The analyzer was calibrated by preparing mixtures of air and carbon dioxide by use of the rotameters in the apparatus for a measure of the concentration. In order to increase the accuracy of the calibration, all concentrations were referred to a reference value, C_A, which was the measured average effluent concentration from the test section. The calibration curve could then be expressed by the equation.

$$\frac{\Delta Y}{\Delta Y_A} = \left(\frac{C}{C_A}\right)^{1/b} \qquad (1)$$

where ΔY refers to the difference in chart reading and b is the calibration constant. The use of the effluent concentration as the reference value minimized errors due to temperature changes and similar variables which might change from day to day. In substance this procedure amounted to checking one point on the calibration curve with each run.

Pellet sizes were measured by two methods: (1) measuring the diameter of several units with a micrometer and (2) measuring the volume of water displaced by approximately 100 units and computing the diameter equivalent to a perfect sphere. The 5/32-in. steel balls were nearly uniform with an average diameter of 0.156 in. The 1/4-, 3/8-, and 1/2-in. particles were alumina-catalyst-support pellets and were somewhat irregular spheres. Their actual average diameters were 0.30, 0.36, and 0.58 in.

STATISTICAL ANALYSIS AND REPRODUCIBILITY

Reproducibility. Concentrations measured in a packed bed are subject to large variations from point to point as a result of the random packing distribution within the bed. Hence samples removed from points on different radii, but at the same radial position, r/r_o, will be distributed randomly about a mean concentration which is characteristic of that radial position. The extent of the variations which occur are shown in Figure 3, where concentration ratios, C/C_A, at constant radial position are plotted vs. an angular position corresponding to the diameter traversed.

In view of these results and since the effect of radial variation on Peclet number was an objective, it was deemed necessary to measure carefully concentrations over a number of diameters. To carry out this program most efficiently a statistical analysis of typical sets of data was undertaken. The results from four runs (4,141, 4,142, 4,143, and 2,141) made in the 2-in. pipe with 5/32-in. packing were employed and measurements were made at a packing-bed depth of 8.13 in. (above the injector-tube tip) and across three diameters 120° apart. The results are plotted in Figure 4. The deviations from the mean range from 3% at the center to 2.5% at the wall.

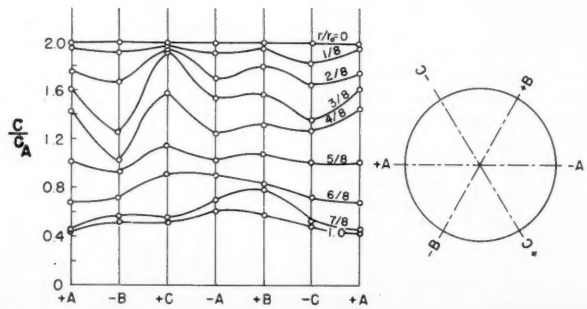

FIG. 3. VARIATION OF CONCENTRATION WITH RADIAL AND ANGULAR POSITION, 8.09-IN. BED DEPTH.

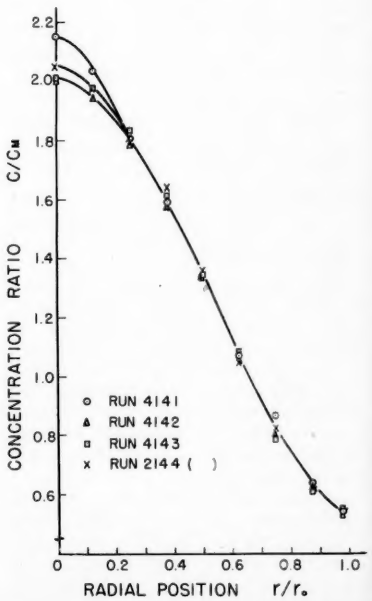

FIG. 4. REPRODUCIBILITY OF CONCENTRATION PROFILES, 2-IN. TUBE, 5/32-IN. SPHERES.

Effect of Repacking the Bed. An analysis of variance using the data in Figures 3 and 4 showed that the error resulting from taking data over three different diameters was not significantly different from that of taking data over one diameter and repacking the bed three times. Hence all data were obtained over three diameters with but one bed packing for each set of conditions.

Effect of Bed Height. At low heights of packing, errors would be expected owing to the presence of the injector tube. On the other hand, the concentration profile flattens out at high bed depths and introduces errors in the analysis of the data. Hence an optimum packing height exists for each set of conditions. To test these factors, Kurihara(*6*) has measured concentration profiles for packing depths ranging from 1.69 to 11.03 in. for 5/32-in. pellets in the 2-in. pipe. The data are shown in Figure 5 and the computed Peclet numbers in Figure 6. The fact that the graphical differentiation technique was used to obtain the Peclet numbers explains some of the variation in the values; however it is clear that at bed heights above 6 in. the effect of bed height is not large in comparison with random errors due to packing distribution. On the basis of these data were determined the bed heights given in the section on Apparatus.

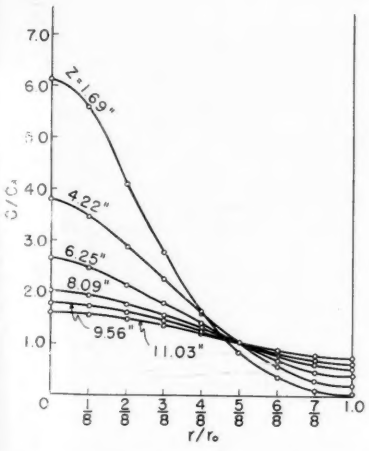

FIG. 5. VARIATION OF CONCENTRATION WITH RADIAL POSITION.

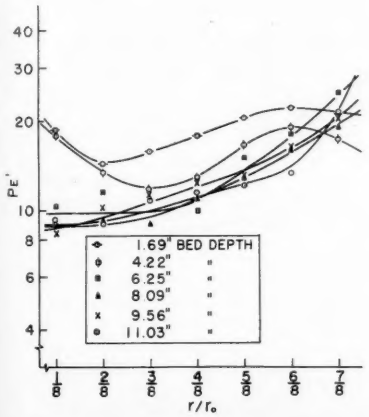

FIG. 6. VARIATION OF MODIFIED *Pe* WITH RADIAL POSITION OBTAINED BY THE GRAPHICAL METHOD.

Error in Carbon Dioxide Analysis. The statistical analysis showed that differences between diameters were significant at the 5% confidence level when compared with the residual variation. The randomness of the packing therefore was the primary cause of the differences between different sets of data, such as shown in Figure 4, and not errors in carbon dioxide analysis and errors due to other assignable causes.

Since the effluent concentration was measured for each run, it is possible to compare this value with the integrated average concentration. This comparison however involves more than the error in the carbon dioxide analysis, for the velocity data of Schwartz and Smith(*11*) must be employed in obtaining the integrated value. For all the data the deviation between the two quantities averaged 4.8%. It is worth while to note that assuming a uniform velocity profile rather than using the available data would have led to much greater deviations between the integrated and measured average concentrations. It is believed that the 4.8% value represents the degree of correspondence between the velocity and concentration measurements which were made with the same packing materials but in different equipment.

Effect of Height of Pitot Tube above Top of Bed. In taking samples from the top of the packed bed, it was important that random variations were minimized so that average concentrations might be obtained from a minimum amount of data; hence it was not desirable to withdraw samples from directly above the packing. On the other hand, experiments indicated that appreciable mixing occurred if the distance above the packing became great. On the basis of several trial runs it was decided that a distance above the packing of 1/4 to 1/2 in. represented the optimum condition, and this spacing was used in taking the final data.

The velocity data of Schwartz and Smith(*11*), used in analyzing the results of the present investigation, were obtained at a height of 2 in. above the top of the packing. This larger distance was necessary because of the hot-wire–anemometer technique employed to measure velocities. At distance of 1/4 to 1/2 in. velocity components perpendicular to the direction of flow affected the anemometer readings. It was found that if the distance was increased to 2 in., these velocity components were negligible, and the velocity in the direction of flow still was not affected by the empty pipe length of 2 in. In the concentration measurements, perpendicular velocity components were of no significance, and so accurate data could be obtained by sampling the gas at the much smaller distances of 1/4 to 1/2 in. above the packing.

CALCULATION OF RESULTS

Development of Equation. It is usually assumed that a differential equation can be written to describe the temperature and concentration in a packed bed, an assumption that presupposes that it is possible to choose a differential element large enough to represent average conditions over an area involving both packing and void space, yet small enough to assume continuity of temperature and concentration gradients. This approach therefore assumes that heat and mass transfer are occurring continuously and uniformly across each radius of the packed bed. The actual process takes place to a large extent in the form of discrete displacements controlled by the dimensions of the packing. Under these conditions it can be argued that the abstraction of a differential equation need not be employed to describe processes occurring in finite steps but that these processes might better be described in terms of difference equations which could be solved numerically with high-speed computing equipment.

Although such an argument has much to recommend it, the past development of reactor-design methods and treatment of heat transfer data has been entirely in terms of the differential-equation approach. Accordingly, in this present study

the differential equation for mass transfer has been used as a starting point, although its solution has been obtained by substitution of difference equations and with the aid of computing machines. Thus the concept of an effective diffusivity, E, has been retained as defined by the expression

Rate of mass transfer per unit area $= -E\dfrac{dC}{dr}$ (2)

Under these conditions the basic differential equation for mass transfer in the bed may be written

$$\frac{\partial\left(Er\,\dfrac{\partial C}{\partial r}\right)}{\partial r} = r\,\frac{\partial\,(Cu)}{\partial z} \qquad (3)$$

This expression is based upon two additional assumptions besides Equation (2); i.e., (1) angular symmetry is everywhere present, and (2) diffusion in the axial direction can be neglected. Axial diffusion is probably unimportant at all except the lowest mass velocities because the mass transfer due to the bulk velocity of the gas is predominant. It is not possible to introduce an accurate longitudinal term in the differential equation because of inadequate knowledge of the diffusivity in the axial direction.

Schwartz and Smith(*11*) have found that the variation of velocity u with bed height is not large compared with random variations at a given radial position. With this simplification, and introducing the radial position coordinate $\theta = r/r_o$, Equation (3) becomes

$$\frac{\partial\left(E\,\theta\,\dfrac{\partial C}{\partial\,\theta}\right)}{\partial\,\theta} = r_o^{\,2}u\,\theta\,\frac{\partial C}{\partial z} \qquad (4)$$

The boundary conditions are

$$\left(\frac{\partial C}{\partial\,\theta}\right)_{\theta=0} = 0 \text{ angular symmetry} \qquad (5)$$

$$\left(\frac{\partial C}{\partial\,\theta}\right)_{\theta=1} = 0 \text{ no mass transfer at wall} \qquad (6)$$

$$\begin{aligned} C(\theta,\,0) &= C_f \qquad 0 < \theta < t \\ C(\theta,\,0) &= .0 \qquad\;\; t < \theta < 1 \end{aligned} \qquad (7)$$

Boundary condition(*7*) represents the physical situation at zero bed depth where pure carbon dioxide of concentration C_f is introduced into the bed through an injection tube of radius tr_o.

Solution of Equation. Equation (4) cannot be solved analytically unless the relationship between the diffusivity E and the radial position r is known. Since this was one objective of the work, numerical methods had to be used. It may be noted that if both E and u are assumed constant the coefficients are constant and an analytical solution in terms of Bessel functions is possible.

Point values of the diffusivity and the Peclet number at various radial positions were obtained by using the available velocity data (*11*) and replacing Equation (4) with a set of homogeneous linear difference equations which could be solved with the aid of an I.B.M. card-programmed calculator.

The general method of solution can be outlined as follows:

1. It is postulated that the concentration C can be considered the product of two functions R and Z, the first of which is a function of r only and the second a function of z only. Two ordinary differential equations are obtained: one involving Z and one involving R.
2. The equation containing Z is solved analytically by ordinary methods.
3. The equation involving R is a complex differential equation whose analytical solution, if possible, would be extremely difficult. This equation may be replaced by a system of difference equations, each written about a point in the region from $r = o$ to $r = r_o$.
4. This system of difference equations is actually a set of homogeneous linear equations involving the values of an eigen function on R at each interval in the region and an eigen value, λ.
5. This set of linear equations can be solved by trial and error for values of R and λ at each radial position by use of the velocity and concentration

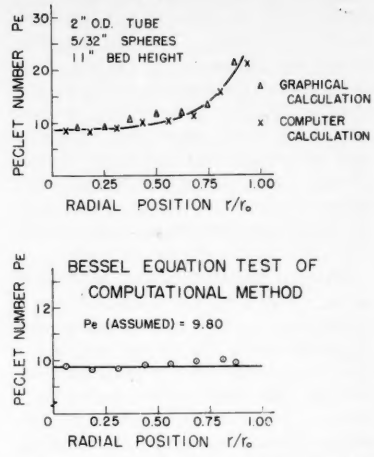

FIG. 7. COMPARISON BETWEEN MACHINE AND GRAPHICAL CALCULATION.

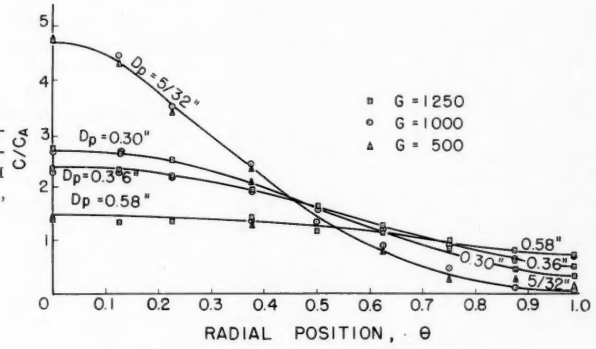

FIG. 8*a*. VARIATION OF CONCENTRATION WITH RADIAL POSITION, 4-IN. PIPE.

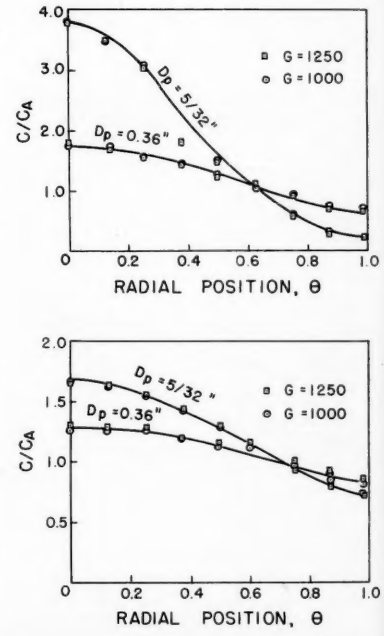

FIG. 8*b*. CONCENTRATION VS. RADIAL POSITION; 3-IN. PIPE ABOVE, 2-IN. PIPE BELOW.

data. The form of the solution is

$$C = \sum_{0}^{n} A_n R_n \exp\left(-4\lambda_n^2 z/D_t^2\right) \quad (8)$$

where A_n are constants, R_n are the eigen functions depending upon radial position only, and λ_n are the eigen values determined by the boundary conditions.

The procedures for carrying out the calculations on the I.B.M. machine are described in a separate paper.

The measured concentration data across three diameters of the pipe gave six individual values at each radial position. These were averaged arithmetically to obtain the mean concentration used in the calculations. The diameter of the pipe was divided into eight intervals, so that Peclet numbers were obtained at values of θ equal to 1/16, 3/16, 5/16, 7/16, 11/16, and 13/16 and 15/16.

To test the computation method the Bessel Test was carried out; that is, the velocity and diffusivity were assumed constant, and an arbitrary value of the Peclet number of 9.8 was chosen. Then the concentration profile for this hypothetical case was obtained from the Bessel solution. These concentrations were used in the computation method to compute Peclet numbers at each radial position. If there is no error in the method, the value of Pe should be 9.8 in each case.

The results of the test are shown in the lower half of Figure 7 and indicate the validity of the method. In the upper part of the figure is a comparison of Peclet numbers computed graphically by Kuriahra (*6*) and by the computational method.

For some purposes, particularly simplified reactor-design procedures, average values of the Peclet number across the entire diameter of the bed are useful. Various methods might be used to obtain such results. Bernard and Wilhelm (*3*) assumed that both velocity and eddy diffusivity were constant and used a Bessel solution of Equation (4) to obtain mean Peclet numbers. Another assumption is that the ratio u/E is constant. This second approach was used in this work and Equation (4) again solved with the C.P.C. machine to obtain average values of Pe.

The values of the velocity u used in the calculations and the values of E computed are based upon the superficial area, rather than on an area determined from the actual void fraction.

TABLE 2.—AVERAGE VALUES OF PECLET NUMBER, $D_p u/E$

Tube size, in.	Pellet size, in.	Mass velocity, lb./(hr.) (sq. ft.)						
		40	125	250	500	1000	1250	1500
4	5/32	6.00	12.3	9.86	7.80	8.42		
4	0.30	....	8.68	9.30	8.55	8.80	8.48	
4	0.36	9.67	9.67	....	9.00	9.43	9.90	
4	0.58	....	11.2	11.1	12.7	12.7	12.9	
3	5/32	....	9.35	9.58	8.13	8.41	8.27	
3	0.36	....	11.6	10.5	9.50	9.88	9.78	
2	5/32	....	10.7	10.7	10.1	10.1	....	10.0
2	0.36	....	13.5	12.3	12.1	12.9	....	13.0

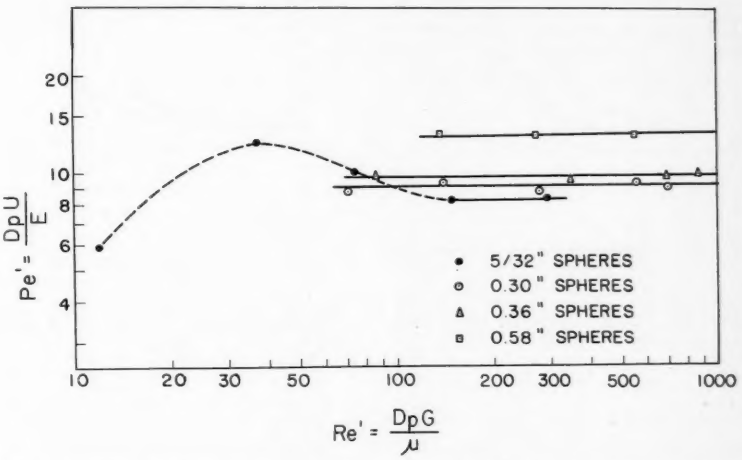

FIG. 9. AVERAGE PECLET NUMBER CALCULATED BY METHOD *A* (CONSTANT U/E), 4-IN. PIPE.

TABLE 4.—POINT VALUES OF PECLET NUMBER, $D_p u/E$

G = 125 lb./(hr.) (sq. ft.)

Radial position	2-in. Pipe		3-in. Pipe		4-in. Pipe			
	5/32 in.	0.36 in.	5/32 in.	0.36 in.	5/32 in.	0.30 in.	0.36 in.	0.58 in.
3/16	9.3	9.0	7.0	9.4	7.0	9.3	7.8	8.1
5/16	8.3	10.5	8.5	10.2	8.0	8.0	7.8	8.2
7/16	8.9	11.1	10.8	9.8	8.1	8.2	7.6	7.6
9/16	9.2	13.2	11.7	9.6	10.3	9.2	10.6	11.7
11/16	11.0	16.3	11.7	11.0	9.9	11.3	16.7	14.9
13/16	12.8	24.2	12.3	13.4	9.9	21.2	22.6	18.5
15/16	32.2	36.5	14.0	38.5	10.9	35.0	38.1	44.3

RESULTS

The measured concentration ratios, shown as mean values with respect to angular position, are presented in Table 1*. Typical concentration profiles across the radius of the bed are shown for the 4-in. pipe in Figure 8*a* and for the 2- and 3-in. pipes in Figure 8*b*. It is interesting to note that the concentration does not vary with mass velocity in the range covered by the graph.

Average values of the Peclet number, computed on the assumption that u/E does not vary with radial position, are given for all conditions in Table 2, and in Figure 9 for the 4-in. pipe. Because the concentration profiles are nonvariant with mass velocity, it is seen from Figure 9 that the Peclet

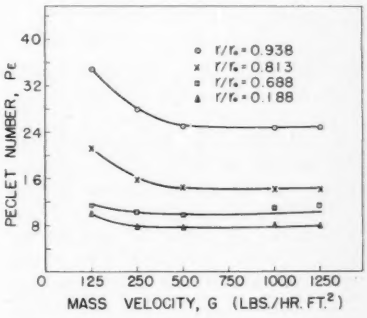

FIG. 10. EFFECT OF MASS VELOCITY ON PECLET NUMBER, 4-IN. PIPE, 0.30-IN. SPHERES.

*Tables 1 and 3 are on file with the American Documentation Institute, Auxiliary Publications Photoduplication Service, Library of Congress, Washington 25, D. C., and may be ordered as document 4475 on remission of $1.25 for microfilm or photoprints.

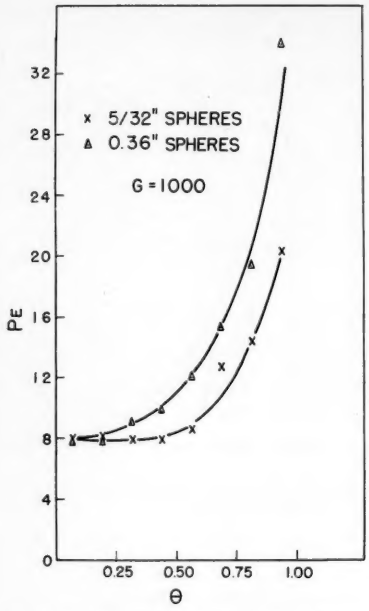

FIG. 11. PECLET NUMBER IN A 2-IN. PIPE.

fluid dynamics. A satisfactory theory of fluid dynamics for a packed bed has not been developed. The theories of Prandtl, Von Karman, and Taylor, which have been applied in simple cases of homoge-

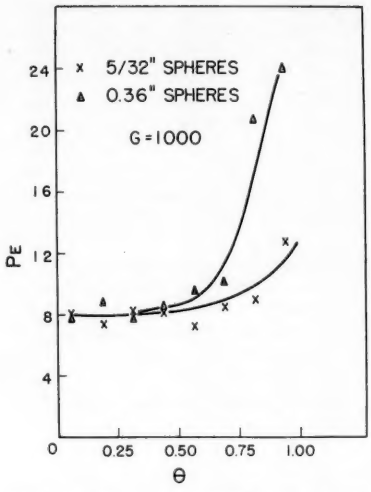

FIG. 12. PECLET NUMBER IN A 3-IN. PIPE.

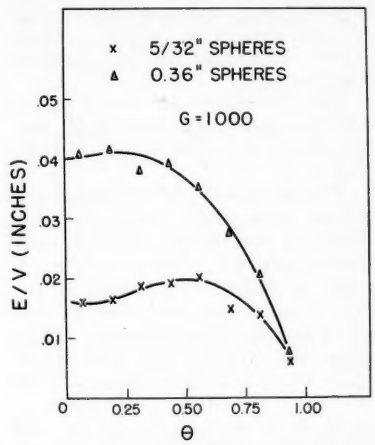

FIG. 14. EFFECTIVE DIFFUSIVITY IN A 2-IN. PIPE.

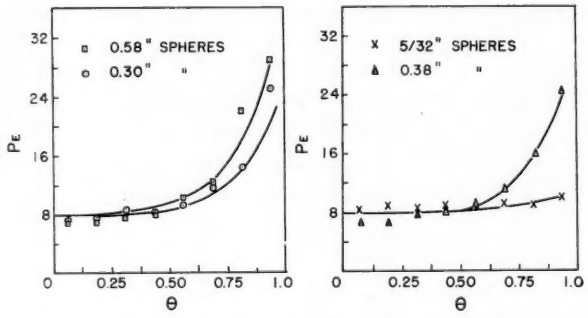

FIG. 13*a* AND *b*. PECLET NUMBER IN A 4-IN. PIPE.

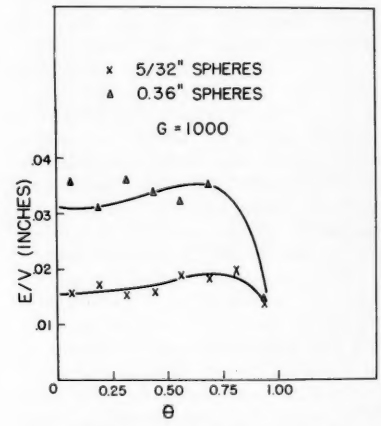

FIG. 15. EFFECTIVE DIFFUSIVITY IN A 3-IN. PIPE.

numbers are also essentially constant above $G = 500$ lb./(hr.) (sq. ft.).

Point values of the Peclet number also show little variation with mass velocity at the higher levels, as indicated in Figure 10 for 4-in.-pipe data. In Table 3* are shown point Peclet numbers for mass velocities above 500 lb./(hr.) (sq. ft.). Table 4 gives the results at 125 lb./(hr.) (sq. ft.).

DISCUSSION OF RESULTS

A quantitative explanation of diffusion on a theoretical basis is difficult because the problems involved are so closely connected with

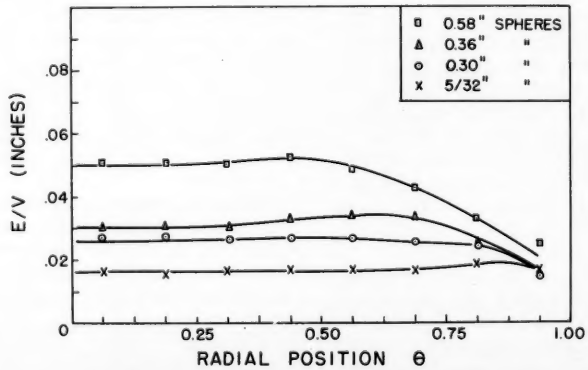

FIG. 16. EFFECTIVE DIFFUSIVITY IN A 4-IN. PIPE.

* See footnote on page 33.

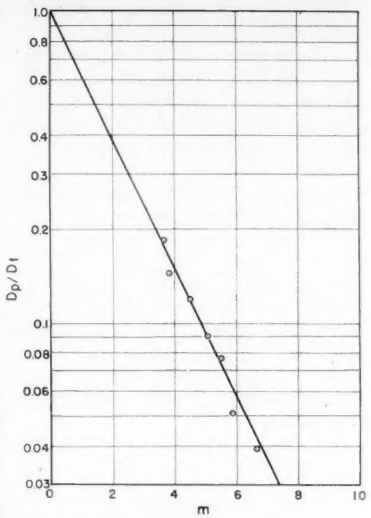

FIG. 17. CORRELATION OF m WITH D_p/D_t.

neous flow, are difficult to extend to packed beds because of the random arrangement and sizes of the channels and the numerous irregularly arranged surfaces. Hence a sound theoretical interpretation of the variation of Peclet number with radial position does not seem possible at present; nevertheless, a method of predicting Peclet numbers from the known bed parameters is important in reactor-design problems. Accordingly, first are presented empirical equations which correlate the data obtained, and then in the next section the theoretical implications, particularly with respect to void space, are considered. The interpretation of the data is aided by the availability of velocity (*11*) and void fraction (*9*) information for the same bed conditions.

Correlation of Point Peclet Numbers. Perhaps the most important result of this study is the significant increase of the Peclet number with an increase in radial position, an increase that depends upon the ratio D_p/D_t and is significant when the ratio is above about 0.05. These conclusions are evident from Figures 11, 12 and 13. For the 5/32-in. particles in the 4-in. pipe ($D_p/D_t = 0.038$) the Peclet number profile is almost flat (*see* Figure 13). At the other extreme, Figure 11, the increase in Peclet number begins at the center of the pipe. The value of Pe at the center in all cases is essentially 8.0.

A second interesting result is that values of the eddy diffusivity for different particle sizes are different near the center of the pipe but similar as the wall is approached. This is seen in Figures 14, 15, 16, where the eddy diffusivity divided by the average velocity, V, over the whole pipe is plotted vs. radial position. At the center the diffusivity is proportional to the particle size, but near the wall it is largely determined by the tube size.

Mathematically these conclusions regarding the Peclet number can be represented by an expression of the form

$$Pe = Pe_o + F\ \theta^m \qquad (9)$$

where F and m depend upon particle and tube sizes and Pe_o is the value of the Peclet number at the center of the tube and is equal to 8.0. Values of m and F were obtained from Equation (9) and the tabulated values of Pe. The resulting correlations for F and m in terms of D_p/D_t are shown in Figures 17 and 18. These two graphs, along with Equation (9), correlate all the data at mass velocities above $G = 500$ lb./(hr.) (sq. ft.) within 10%. Values of the Peclet number at lower mass velocities are higher, as indicated by Figure 10, but the increase is only of the order of 10 to 20%.

Equation (9) predicts a continual increase in Peclet number as D_p/D_t is increased and a value of 108 may be estimated for an empty tube ($D_p/D_t = 1.0$) by logarithmic extrapolation. This is in reasonable agreement with Sherwood and Towle's result of 118 $(Re)^{0.1}$, considering the extrapolation involved.

Correlation of Average Peclet Numbers. The effect of particle size on average Peclet numbers can be correlated by a function involving $(D_p/D_t)^2$. The result is shown in Figure 19. The data of Bernard and Wilhelm, obtained assuming E and u were constant, are also included.

THEORETICAL CONSIDERATIONS

It has been mentioned that the random-walk theory has been applied to packed beds (*2, 7*). This is essentially an extension of the

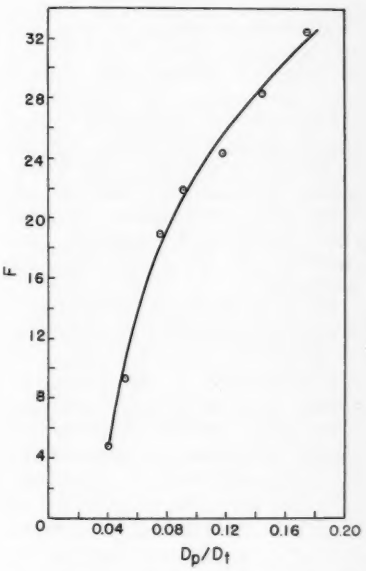

FIG. 18. CORRELATION OF F WITH D_p/D_t.

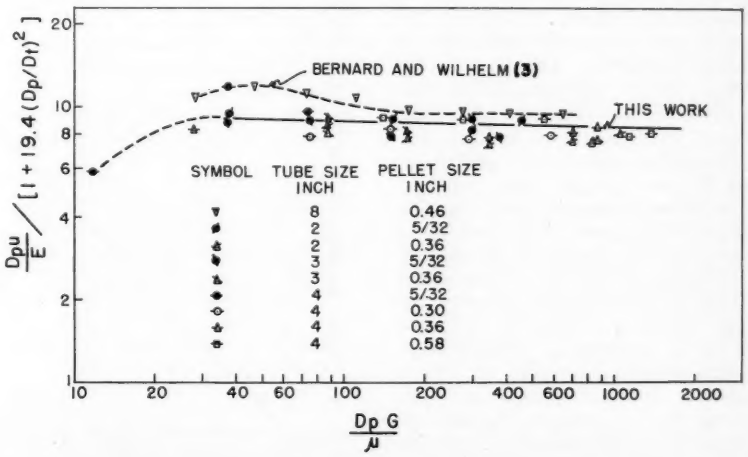

FIG. 19. CORRELATION OF AVERAGE PECLET NUMBER WITH D_p/D_t AND REYNOLDS NUMBER.

Einstein equation for diffusion in Brownian motion. Taylor(5) originally applied the concept of a relationship between the eddy diffusivity and the mean-square lateral displacement to homogeneous fluid systems. Baron's(2) and Latinen's(7) developments are logical extensions to packed-bed arrangements. The radial displacement of the fluid stream in a bed is determined largely by the dimensions of the channels, which are themselves randomly arranged. The application of the Einstein equation to the process requires the following chief assumptions: (1) mixing within each interstice is substantially complete so that a fluid element within a void has an equal probability of leaving by any of several exit paths; (2) the number of radial displacements is sufficiently large that statistical principles may be employed to estimate the mean-square displacement; and (3) effects due to changes in void fraction, velocity variations, and presence of the tube wall are neglected.

From assumption (3), the theory would be expected to be successful in predicting the point values of the diffusivity at the center of almost any packed-tube arrangement, and also the point values across the entire diameter when D_p/D_t is small. Such is indeed the case, for the value of $Pe = 8.0$ at the center of the bed, determined in this study, is almost midway between the limits of 5 and 13 predicted by Baron. Also, where D_p/D_t is small, as in the lower curve of Figure 13*b*, the entire range of Peclet numbers is within the prediction interval. These conclusions are sound as long as the mass velocity is sufficiently high to make assumption (1) valid. As the mass velocity is decreased, the Peclet number will first increase as the effect of incomplete mixing becomes significant and finally decrease to zero at zero velocity where molecular diffusion is the controlling factor. This maximum in the Peclet number is illustrated in Figure 9 and also to a slight extent in the average Peclet numbers shown in Figure 19. It is not valid to postulate a critical Reynolds number at which the Peclet number becomes dependent upon mass velocity, because the particle diameter and void fraction are also factors which affect this transition. However from the available data it appears that Reynolds numbers from 40 to 100 constitute the critical range.

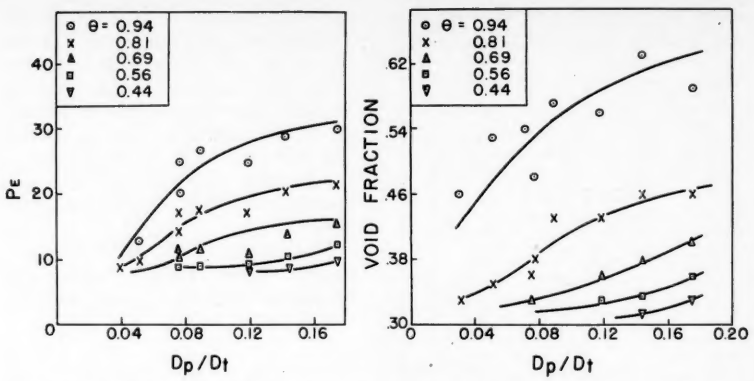

FIG. 20. LEFT: EFFECT OF D_p/D_t ON PECLET NUMBER; RIGHT: EFFECT OF D_p/D_t ON VOID FRACTION.

Effect of Void Fraction and Pipe Wall. Returning to the variation in Peclet numbers with radial position, it seems clear that the fundamental factors involved are the void fraction and the influence of the pipe wall. A comparison of the radial variation in both void fraction(9) and Peclet number as presented in Figure 20 is striking.

The similarity in shape of the two sets of curves lends substance to the belief that internal changes in void space have a large effect on the Peclet number. However, void-space changes cannot explain the variation in Peclet number over the entire pipe radius. Near the wall, tube-generated turbulence becomes important with respect to particle-generated turbulence, and this has its effect on the Peclet number.

These conclusions are shown graphically in Figure 21, where the increase in Peclet number above the value at the center of the tube is plotted vs. the corresponding increase in void fraction. Up to a radial position of 0.81 the Peclet number is proportional to the void fraction; hence for 81% of the pipe radius the empirical correlation of Equation (9) in terms of radial position and D_p/D_t can be replaced by the more fundamental relation

$$Pe = 8.0 + 100\ (\delta - \delta_o) \quad (10)$$

(limited to $\theta < 0.81$ and $Re > 100$) in terms solely of void fraction δ.

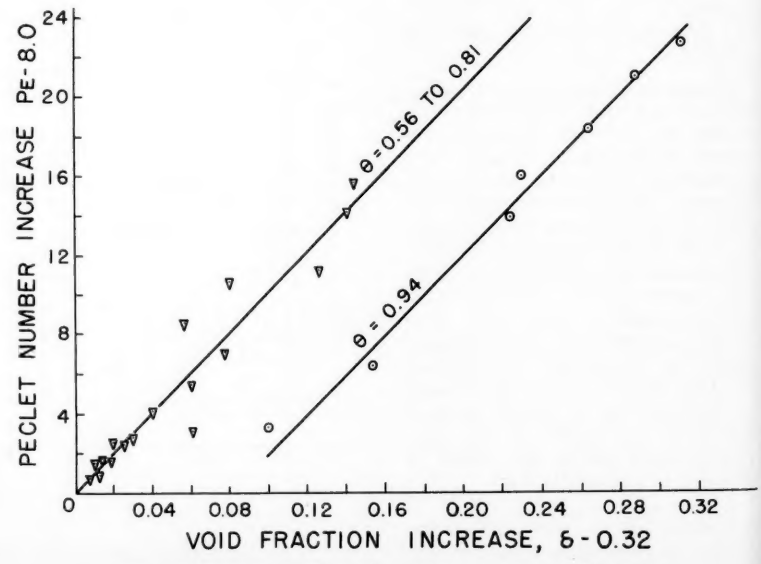

FIG. 21. EFFECT OF VOID FRACTION ON PECLET NUMBER.

The effect of the tube wall is also evident from Figure 21, where the line for a radial position of 0.94 is seen to be displaced from that for θ from 0 to 0.81. At this radial position near the wall the velocity is decreasing rapidly owing to wall friction. Hence the void fraction alone is not sufficient to describe the turbulence conditions and therefore the Peclet number.

Explanation in Terms of Existing Theories. The increase in Peclet number can be qualitatively considered by modification of the random-walk concept, as extended by Latinen. This theory predicts that

$$Pe = \frac{4}{C_1 C_2^2}\left[\frac{1 - R_x}{1 + R_x}\right] \quad (11)$$

where C_1 and C_2 are constants and R_x is the correlation coefficient between successive displacements. This coefficient is a measure of the degree of turbulence within a void space. If the flow is streamline, there will be very little mixing and R_x will approach -1, and Pe infinity. If instead mixing is complete within the void, R_x will be zero and the Peclet number constant. The increase in Peclet number with radial position can therefore be attributed to a change in the correlation coefficient from a value near zero at the center of the bed to negative values as the wall is approached. This decrease in correlation coefficient is brought about mainly by an increase in the probability of a deflection toward the direction of an increasing void space and increasing velocity. Both these quantities have been found experimentally to increase as the radial position increases; however there is some uncertainty in using Latinen's expression here since it is based upon the Einstein equation, which itself is dependent upon the assumption that the correlation coefficient is zero (complete mixing).

Qualitative interpretation of the results in terms of the Prandtl mixing-length concept is also of interest. It can be postulated that in the central core of the bed the scale of turbulence is proportional to the particle size and the mean-square deviating velocity is proportional to the superficial velocity in the direction of flow. If the eddy diffusivity is the product of a mixing length (scale of turbulence) and deviating velocity, it is evident that the Peclet number will be constant. As the wall of the pipe is approached, the void fraction increases and it is reasonable to assume that the scale of turbulence also increases. It follows that the decrease in diffusivity, observed as the radial position increases, corresponds to a large decrease in deviating velocity. This conclusion is consistent with the concept that empty pipe behavior is approached near the wall of a packed bed, for in empty pipes the intensity of turbulence, or deviating velocity, is much less than in packed beds. Thus Bernard and Wilhelm (*3*) have estimated that the intensity is about 40% in fully developed turbulence in packed beds, while the corresponding value in empty pipes is of the order of 2.5 to 5%.

SUMMARY

1. Measured point values of the Peclet number in packed beds increase with radial position. This increase depends upon the particle and pipe size and is significant when D_p/D_t is greater than 0.05.

2. Above modified Reynolds numbers of 40 to 100, the Peclet number is independent of superficial velocity in the pipe and at the center of the bed has a constant value of about 8.0.

3. The change in Peclet number with radial position is due to the increase in void fraction and to the influence of the pipe wall. At up to 81% of the radius the Peclet number could be correlated in terms of void fraction alone, independent of particle size, tube size, and radial position.

4. From a theoretical point of view the increase in Peclet number can be qualitatively explained on the basis of a decreasing intensity of turbulence as the void fraction increases and the pipe wall is approached.

ACKNOWLEDGMENT

Hiroo Kurihara assisted in the experimental phase of the project. Professors S. H. Gould, A. J. Perlis, and I. W. Burr of Purdue University gave freely of their counsel in the mathematical and statistical problems. The work was carried out with the financial assistance of the Purdue Research Foundation.

NOTATION

A = constant in series solution of differential equation
C = concentration at a point in the bed, lb./cu.ft.
C_A = measured average effluent concentration, lb./cu.ft.
C_t = concentration of pure carbon dioxide in injection tube
D_p = particle size
D_t = pipe size
E = total effective diffusivity, based upon total area including packing and including the molecular-diffusion contribution
F = function of D_p/D_t used to correlate Pe
G = superficial mass velocity, lb./(hr.) (sq.ft.)
m = function of D_p/D_t used to correlate Pe
Pe = Peclet number, $D_p u/E$
Pe_o = Peclet number at center of bed
r = distance from center of bed
r_o = radius of pipe
R = eigen function
R_x = correlation coefficient between successive displacements
Re = modified Reynolds number, $D_p G/\mu$
t = radial position of radius of injection tube; i.e., radius of injection tube = tr_o
u = superficial velocity at a point in the bed
V = average effluent velocity (superficial)
Y = reading on Micromax recorder for concentration
z = height of packed bed above tip of injection tube

Greek Symbols

δ = void fraction
λ = eigen value
θ = radial position, r/r_o
μ = viscosity of gas flowing through bed

LITERATURE CITED

1. Argo, W. B., and J. M. Smith, *Chem. Eng. Progr.*, 49, 443 (1953).
2. Baron T., *Chem. Eng. Progr.*, 48, 118 (1952).
3. Bernard, R. A., and R. H. Wilhelm, *Chem. Eng. Progr.*, 46, 233 (1950).
4. Furnas, C. C., *U.S. Bur. Mines Rept.* 307 (1929).
5. Goldstein, S., "Modern Developments in Fluid Mechanics," Oxford University Press (1938).
6. Kurihara, H., M.S. thesis, Purdue University (August, 1953).
7. Latinen, Ph. D. thesis, Princeton (December, 1951).
8. Ranz, W. E., *Chem. Eng. Progr.*, 48, 247 (1952).
9. Schaffer, M.R., M.S. thesis, Purdue University (June, 1953).
10. Schuler, R. W., V. P. Stallings, and J. M. Smith, *Chem. Eng. Progr. Symposium Ser.* No. 4, 49, 19 (1953).
11. Schwartz, C. E., and J. M. Smith, *Ind. Eng. Chem.*, 45, 1209 (1953).
12. Sherwood, T. K., and B. B. Woertz, *Trans. Am. Inst. Chem. Engrs.*, 35, 517 (1939).
13. Singer, E., and R. H. Wilhelm, *Chem. Eng. Progr.*, 46, 343 (1950).
14. Towle, W. L., and T. K. Sherwood, *Ind. Eng. Chem.*, 31, 457 (1939).

(Presented at A.I.Ch.E. New York meeting)

ISOBARIC INTEGRAL HEAT OF VAPORIZATION of Hydrocarbon Mixtures from Vapor-liquid *K* Values

WAYNE C. EDMISTER, California Research Corporation, Richmond, California

The isobaric integral heat of vaporization is the difference between the enthalpy values for a given mixture at its dew and bubble points taken at the same pressure but different temperatures. In terms of partial enthalpies

$$\Delta H_V = (H^V - H^L)_P = \Sigma z \overline{\Delta H}_V = (\Sigma y \overline{H}^V)_2 - (\Sigma x \overline{H}^L)_1 \quad (1)$$

where H is enthalpy of the mixture, $\overline{H}$ is the partial enthalpy of a component of the mixture, superscript V or L designates the phase (vapor or liquid), subscript V (after ΔH) designates heat of vaporization, subscripts 1 and 2 designate the temperatures of the bubble and dew points, respectively, and x, y, and z are mole fractions for liquids, vapors, and mixtures in general [all numerically the same in Equation (1)]. In terms of partial enthalpies referred to ideal-gas-state values,

$$\Sigma z \overline{\Delta H}_V = \Sigma z (\overline{\Delta H}^V_2 - \overline{\Delta H}^L_1) + \Sigma z \Delta H^\circ \quad (2)$$

where $\overline{\Delta H} = \overline{H} - H^\circ$, H° is the enthalpy of a component of a mixture in the ideal gas state, and $\Delta H^\circ = H^\circ_2 - H^\circ_1$.

The summations of Equation (2) are illustrated in Figure 1, where T_1 is the bubble-point temperature and T_2 the dew-point temperature.

The partial-enthalpy differences, $\overline{\Delta H}^V_2$ and $\overline{\Delta H}^L_1$, are related to the fugacity coefficients as are the vapor-liquid equilibria K values. An equation for $\Sigma z \overline{\Delta H}_V$ in terms of the temperatures and K values at the bubble and dew points is derived below.

From the definition of fugacity f, the following equation has been obtained and appears in thermodynamic texts:

$$\overline{\Delta H} = \overline{H} - H^\circ = -RT^2 \left(\frac{\delta \ln f}{\delta T}\right)_{P,\ N} \quad (3)$$

where subscript N means at constant composition and P at constant pressure. Equation (3) is general and applies to either a liquid or vapor phase. This differential form can be approximated by a difference form by integrating with a constant value of $\overline{\Delta H}$ for a small temperature interval. If at the same time fugacity is divided by mole fraction to give fugacity coefficient,

$$\overline{\Delta H} = \frac{RT_1T_2}{T_2 - T_1} \ln \frac{(f/z)_1}{(f/z)_2} \quad (4)$$

Equation (4) may be applied to a component of any phase, whether it be a liquid or vapor, at constant pressure and composition, so long as $\overline{\Delta H}$ is assumed constant. Figure 1*A* shows graphically the partial enthalpies of propane in a liquid and vapor of fixed composition as given by mole average boiling point at 300 lb./sq. in. abs. compared to the ideal-gas-state values. Points 1^L and 2^V represent the bubble and dew points of a certain mixture that is considered later in an illustrative example. In the application of Equation (4) to propane vapor from 1^V to 2^L, it is assumed that $\overline{\Delta H}^V$ remains constant at $\overline{\Delta H}^V_2$ even though it obviously is greater at $\overline{\Delta H}^V_1$. Correspondingly it is assumed that $\overline{\Delta H}^L$ remains constant at $\overline{\Delta H}^L_1$ when Equation (4) is applied to the liquid from 1^L to 2^L.

Figure 1*B* shows how the fugacity of propane in the liquid and vapor at two compositions and at 300 lb./sq. in. abs. does vary with temperature. Applying Equation (4) to any component of a mixture, as required in Equation (2), gives

$$\overline{\Delta H}^V_2 - \overline{\Delta H}^L_1 = \frac{RT_1T_2}{T_2 - T_1} \left[\ln \frac{(f^V/y)_1}{(f^V/y)_2} - \ln \frac{(f^L/x)_1}{(f^V/x)_2}\right]_P \quad (5)$$

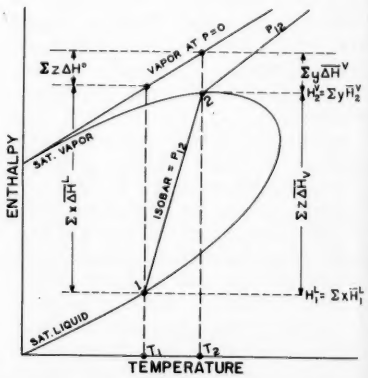

FIG. 1. ENTHALPY-TEMPERATURE DIAGRAM FOR MIXTURE ILLUSTRATING ISOBARIC INTEGRAL HEAT OF VAPORIZATION.

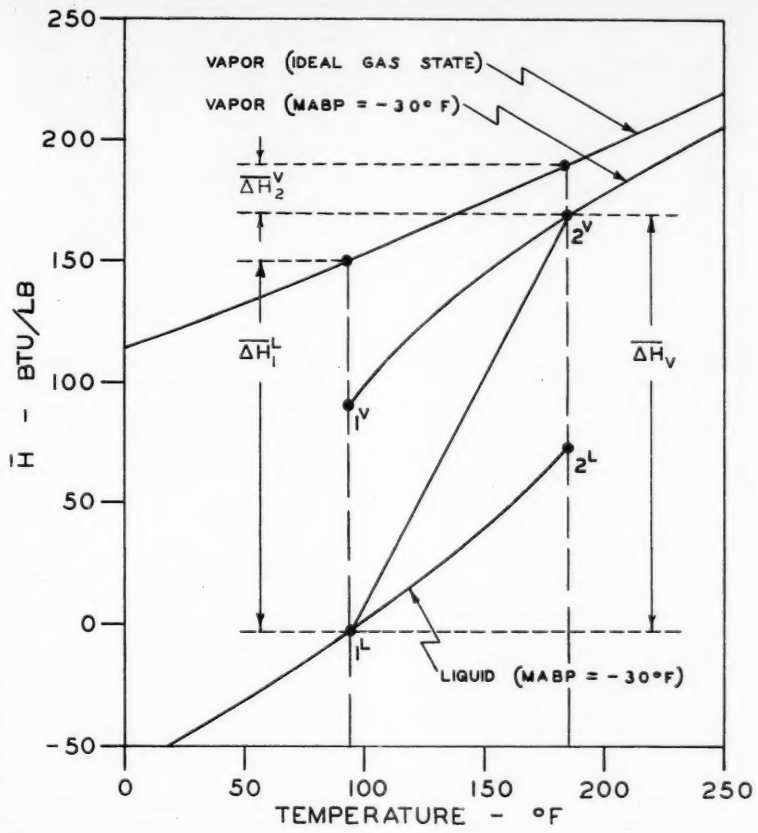

FIG. 1A. TYPICAL VALUES OF H FOR PROPANE AT 300 LB./SQ. IN. ABS.

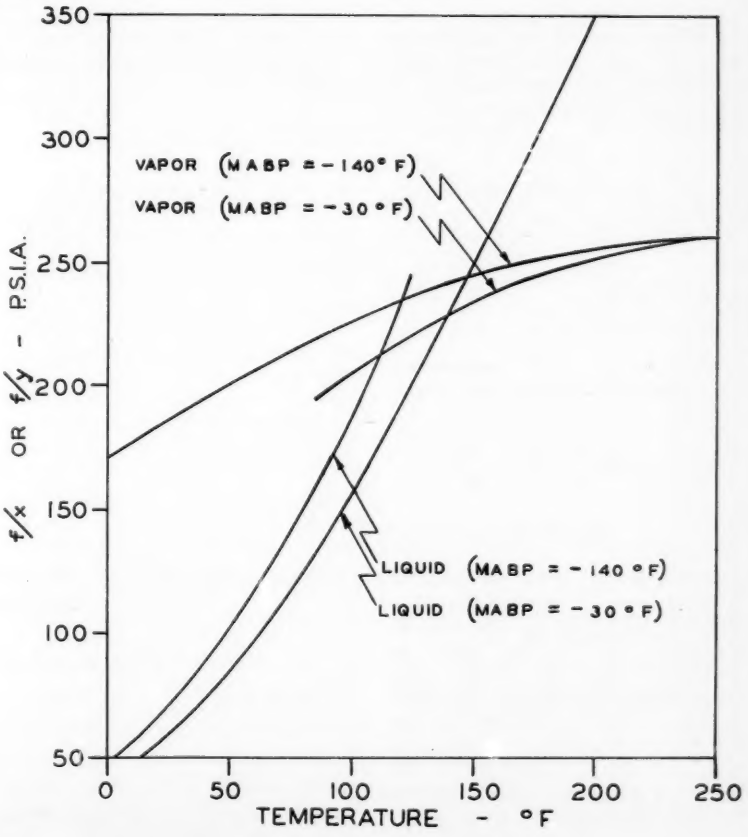

FIG. 1B. TYPICAL VALUE OF FUGACITY FOR PROPANE AT 300 LB./SQ. IN. ABS.

where, as before, x and y are numerically the same.

The equilibrium vapor and liquid phases at T_1 and T_2 will now be considered so that the K values may be introduced into Equation (5). If the composition of the liquid which would be in equilibrium with the dew-point vapor is denoted by x^* and the composition of the vapor which would be in equilibrium with the bubble-point liquid is denoted by y^*, the definition of K gives

$$K_2 = \frac{(f^L/x^*)_2}{(f^V/y)_2} \text{ at } T_2 \qquad (6a)$$

$$K_1 = \frac{(f^L/x)_1}{(f^V/y^*)_1} \text{ at } T_1 \qquad (6b)$$

Combining Equations (5) and (6) gives for any one component:

$$\overline{\Delta H}_2^V - \overline{\Delta H}_1^L = \frac{RT_1T_2}{T_2-T_1}$$

$$\left[\ln\frac{K_2}{K_1} + \ln\frac{(f^V/y)_1}{(f^V/y^*)_1} + \ln\frac{(f^L/x)_2}{(f^L/x^*)_2}\right]_P \qquad (7)$$

Summing for all components according to Equation (2) gives

$$\Sigma z\overline{\Delta H}_V = \frac{RT_1T_2}{T_2-T_1}\left[\Sigma z \ln\frac{K_2}{K_1} + \Sigma y \ln\frac{(f^V/y)_1}{(f^V/y^*)_1} + \Sigma x \ln\frac{(f^L/x)_2}{(f^L/x^*)_2}\right]_P + \Sigma z\,\Delta H^\circ \qquad (8)$$

The second and third terms in the bracket of Equation (8) will next be examined from the point of view of the Gibbs-Duhem equation for changes in composition at constant temperature and pressure. In terms of fugacities this equation is

TABLE 1.—SOLUTION OF ISOBARIC HEAT OF VAPORIZATION EXAMPLE BY K-VALUE METHOD

Component	Moles	K values at 300 lb./sq. in. abs. At D. P. 185° F. K_2	At B. P. 95° F. K_1	Ratio K_2/K_1	$\frac{RT_1T_2}{T_2-T_1}\ln\frac{K_2}{K_1}$ M B.t.u./lb. mole	$H°$ M B.t.u./lb. mole 185° F.	95° F.	$\Delta H°$	$\overline{\Delta H}_V$ M B.t.u./lb. mole	$(\overline{\Delta H}_V)$ (moles) M B.t.u./100 moles mixture
C_1	5	8.48	7.76	1.093	0.70	5.266	4.466	0.800	1.500	7.5
C_2	15	2.94	1.86	1.581	3.62	6.593	5.367	1.266	4.886	72.7
C_3	30	1.36	0.695	1.956	5.37	8.375	6.643	1.732	7.102	213.1
nC_4	50	0.685	0.258	2.655	7.75	11.073	8.783	2.290	10.040	502.0
	100									795.3

$$\Sigma z\, d\ln f = 0 \qquad (9)$$

Since the sum of the z's is unity,

$$\Sigma z\, d\ln (f/z) = 0 \qquad (10)$$

For small changes in composition the differential form is approximated by the difference form,

$$\Sigma z \ln \frac{(f/z)'}{(f/z)''} = 0. \qquad (11)$$

where the prime and double prime designate two different compositions for the same phase, temperature, and pressure. This equation may be applied to either vapor or liquid phases.

Assuming the approximate form of the Gibbs-Duhem relationship with the composition factor of the logarithm taken at one end of the interval, the second and third summations in the brackets of Equation (8) are zero, or

$$\Sigma y \ln \frac{(f^V/y)_1}{(f^V/y^*)_1} = 0 \qquad (12a)$$

$$\Sigma x \ln \frac{(f^L/x)_2}{(f^L/x^*)_2} = 0 \qquad (12b)$$

Equation (8) now becomes by combination with Equation (12)

$$\Delta H_V = \Sigma z\left[\frac{RT_1T_2}{T_2-T_1}\ln\frac{K_2}{K_1}\right] + \Sigma z\, \Delta H° \qquad (13)$$

Equation (13) gives the isobaric integral heat of vaporization of a mixture. The term in brackets of Equation (13) is the same as Dodge's (*2*, Equation IV-208, page 142) which was derived for ideal solutions with the assumption that $\overline{\Delta H}$ was independent of temperature. As shown above, it is not necessary to restrict this equation to ideal solutions, but it is necessary to assume that $\overline{\Delta H}$ is independent of temperature for the bubble- to dew-point interval. Also it has been necessary to assume that the changes in composition in going from the bubble-point liquid to its equilibrium vapor and from the dew-point vapor to its equilibrium liquid are such that the Gibbs-Duhem equation can be applied in an approximate form.

Equation (13) has been derived primarily for application to multicomponent hydrocarbon mixtures, particularly for cases in which composition effects on vapor-liquid K values are represented satisfactorily by average boiling points of the equilibrium phases. Figure 2 has been prepared to aid in the evaluation of the bracketed term in Equation (13). Liquid-bubble-point temperature, ΔT, and K_2/K_1 are required, and the dashed lines and arrows illustrate the way the chart is read. A typical example follows:

ILLUSTRATIVE EXAMPLE

Find the heat required to vaporize a mixture of 5 moles methane, 15 moles ethane, 30 moles propane, and 50 moles n-butane from bubble to dew points at 300 lb./sq. in.

The K values were found from De Priester's P-T-C charts (*1*), and the bubble and dew points computed as 95° and 185°F. by conventional methods.

Table 1 gives the solution by the K-value method [Equation (13)], and Table 2 gives the solution by the partial-enthalpy method (*3*). The results are compared in Table 3.

DISCUSSION

It will be noted from examination of the values in Table 3 that the partial-heat-of-vaporization quantities for different components found from K values by Equation (13) differ from the values found from the more reliable partial-enthalpy values but that the totals are in agreement. Evidently

TABLE 2.—SOLUTION OF ISOBARIC INTEGRAL HEAT OF VAPORIZATION EXAMPLE BY PARTIAL-ENTHALPY METHOD

Component	Moles	Partial enthalpies at 300 lb./sq. in. abs. M B.t.u./lb. mole* $\overline{H}^V$ at 185	$\overline{H}^L$ at 95	$\overline{\Delta H}_V$	$(\overline{\Delta H}_V)$ (moles) M B.t.u./100 moles mixture
C_1	5	5.71	3.23	2.48	12.4
C_2	15	6.37	0.96	5.40	81.1
C_3	30	7.45	—0.09	7.54	226.2
nC_4	50	9.36	—0.41	9.77	488.2
	100				807.9

Gas at O lb./sq. in. abs. and 0° R.

TABLE 3.—COMPARISON OF METHODS FOR ISOBARIC HEAT OF VAPORIZATION OF HYDROCARBON MIXTURES

Component	$(\overline{\Delta H}_V)$ (moles), M B.t.u./100 moles mixture Via $\overline{H}$ values	Via K Values	% Dev. of $\overline{\Delta H}_V$ by K-value method
C_1	12.4	7.5	—39.5
C_2	81.1	72.7	—10.4
C_3	226.2	213.1	—5.8
nC_4	488.2	502.0	+3.7
Σ	807.9	795.3	—1.6

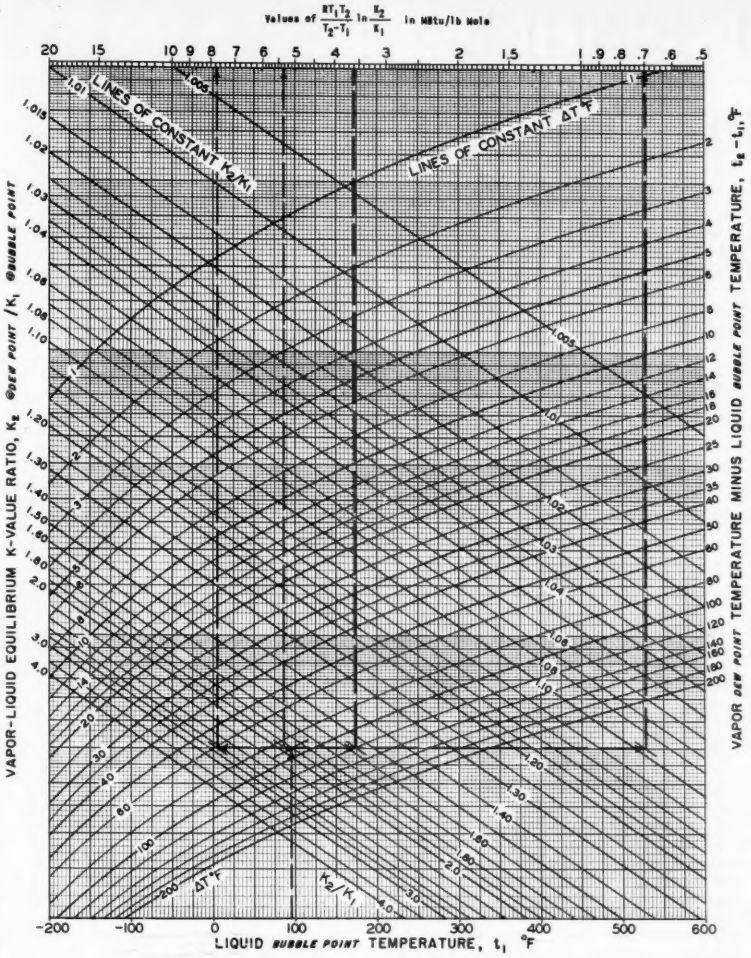
Values of $\frac{RT_1T_2}{T_2-T_1}\ln\frac{K_2}{K_1}$ in MBtu/lb Mole
LINES OF CONSTANT K_2/K_1
LINES OF CONSTANT ΔT, °F
VAPOR-LIQUID EQUILIBRIUM K-VALUE RATIO, K_2 @DEW POINT /K_1 @BUBBLE POINT
VAPOR DEW POINT TEMPERATURE MINUS LIQUID BUBBLE POINT TEMPERATURE, t_2-t_1, °F
LIQUID BUBBLE POINT TEMPERATURE, t_1, °F

FIG. 2. ISOBARIC INTEGRAL HEAT OF VAPORIZATION OF MIXTURES FROM K VALUES.

the values of ln K_2/K_1 for each component cannot be used to obtain accurate partial heats of vaporization or condensation, as the results are too high for high-boiling compounds and too low for lower boiling compounds. In getting the heat of vaporization for the whole mixture, however, these opposite deviations tend to compensate for each other.

Twelve sets of calculations were made on two other mixtures of light hydrocarbons at 400 and 600 lb./sq. in pressure. For each mixture and pressure ΔH values were found for complete vaporization, partial vaporization (i.e., vaporizing a portion of a mixture under steady-state conditions), and partial condensation.

The two partial cases were included to determine whether the difference in liquid (or vapor) boiling points for the same mixture showed the correct effect on heat of vaporization through the effects of average boiling point on K values and the bubble and dew points.

These calculations showed that the isobaric heats of vaporization found by Equation (13) were consistently lower than the more precise values by an average of 3.7%. No effects of pressure, width of mixture (i.e., bubble- to dew-point temperature interval), or presence of large amounts of unvaporized liquid or uncondensed vapor were noted. This would indicate that the assumption of constant average $\overline{\Delta H}$ for the bubble- to dew-point temperature interval, made in obtaining Equation (4), is justified.

De Priester's *P-T-C—K*-value correlations, which were used in these calculations, have an average deviation of 6.4% from observed K values. As the partial-enthalpy values used in the comparisons are of comparable accuracy, this evaluation of the proposed equation indicates that the K and $\overline{H}$ values used are not consistent. The $\overline{\Delta H}$ values of Edmister and Canjar (*3*) may be 3 to 4% high, or the temperature coefficient of De Priester's (*1*) K values may be low. Experimental vapor-liquid equilibria and isobaric integral heat of vaporization data, taken simultaneously, are required to establish which is the case.

CONCLUSIONS

Equation (13) may be used to estimate the isobaric integral heat of vaporization of hydrocarbon mixtures from K values. K values cannot be used to obtain heats of solution of partial heats of vaporization for mixture components.

NOTATION

f = fugacity of a component of a mixture
H = enthalpy of a mixture
$\overline{H}$ = partial enthalpy of a component of a mixture
$\triangle H_V$ = isobaric integral heat of vaporization
$\overline{\triangle H}$ = partial-enthalpy difference referred to ideal gas state, $\overline{H}$-H°
$\overline{\Delta H_V}$ = isobaric partial heat of vaporization
ΔH° = difference in ideal-gas-state enthalpy at T_1 and T_2
R = gas constant
T = absolute temperature, °R.
x = mole fraction of a component of a liquid
y = mole fraction of a component of a vapor
z = mole fraction of a component in any mixture

Superscripts

V = vapor
L = liquid
$^\circ$ = ideal gas state
* = equilibrium vapor at bubble point or equilibrium liquid at dew point on y or x

Subscripts

N = constant composition on a partial derivative
P = pressure
V = vaporization change
1, 2 means at T_1 or T_2

LITERATURE CITED

1. De Priester, C. L., *Chem. Eng. Progr. Symposium Series* No. 7, 49, 1, (1953).
2. Dodge, B. F., "Chemical Engineering Thermodynamics," McGraw-Hill Book Company, Inc., New York (1944).
3. Edmister, W. C., and L. N. Canjar, *Chem. Eng. Progr. Symposium Series* No. 7, 49, 73, 85 (1953).
4. Rossini, F. D., et al., *Am. Petroleum Inst. Research Project* 44.

THE FALL OF SINGLE LIQUID DROPS THROUGH WATER

SHENGEN HU AND R. C. KINTNER
Illinois Institute of Technology, Chicago, Illinois

The steady motion of single drops of ten organic liquids falling through a stationary water field is discussed. A correlation is presented for nine systems with the exception of the aniline-water system, in the form of a single curve relating the drag coefficient, Weber number, Reynolds number, and a physical property group. The curve can be used directly to predict the terminal velocity, drag coefficient, Reynolds number, and Weber number for any given equivalent drop size.

A break point in the curve serves to predict the peak velocity and its related quantities. The critical drop size is predicted from the pertinent physical properties alone. All these estimations were accurate within 10% for the systems used. The interfacial tensions ranged from 24 to 45 dynes/cm. and the drop densities from 1.100 to 2.947g./ml., the latter resulting in a twentyfold range of density differences. The drop viscosities had no apparent effect.

With the exception of extended-surface units and packed towers, which operate by the film-contact mechanism, nearly all types of liquid-liquid–extraction equipment used today secure contact through the dispersion of one phase as drops (*23*). Even in packed towers, drop formation has been found to prevail when the dispersed phase does not wet the packing (*4*). It is thus apparent that a study of the motion of liquid drops in a second liquid medium should provide basic information for the design of most liquid-liquid extractors, as drop size is directly related to stage efficiency and terminal velocity to the capacity of the equipment.

The hydrodynamic aspect of the problem is so complex that even for the more simple cases analyzed (*15*) many assumptions have to be made in order to render any mathematical solution possible. It is generally assumed, for instance, that the drop is of a simple spherical or ellipsoidal shape regardless of its size and velocity or of the physical properties of the system. From the fragmentary experimental results obtained by previous workers it has been found that a liquid drop does not always behave like a rigid sphere or ellipsoid. This discrepancy should be easily anticipated inasmuch as the nature of a liquid-liquid interface is not the same as that of a liquid-solid boundary and the shape of the drop is not always rigid and spherical or ellipsoidal. With these considerations the present investigation has been initiated with the simple objective of experimentally studying the behavior of single liquid drops falling under steady-state conditions in a stationary water field as governed by the pertinent physical properties of the system, i.e., densities, viscosities, and interfacial tensions. No mass transfer was involved.

Shengen Hu is with the Institute of Gas Technology, Chicago, Illinois.

PREVIOUS WORK

The translation of a solid sphere in an infinite mass of a perfect liquid was first analyzed by Stokes (*30*) in 1845 and was later reduced to the case of viscous flow by neglecting the inertial-force terms in the Navier-Stokes equations of motion (*15*). The simple Stokes' law of resistance thus obtained is $F = 3\pi\mu du$, which holds only at Reynolds numbers of less than two (*3, 24, 32*).

The question of the existence of slipping at the boundary surface of a solid sphere moving in a liquid medium within the Stokes'-law range has been treated by Basset (*6*), but experimental evidence obtained by various workers seems to indicate that there is no slipping at the solid-liquid boundary (*2, 3, 13*).

TABLE 1.—PHYSICAL PROPERTIES, C. G. S. UNITS

	System	ρ_o	ρ	$\frac{\Delta\rho}{\rho}$	$\mu_o \times 10^2$	$\mu \times 10^2$	σ_i	P	T
1	Aniline	1.0176	0.9979	0.0197	3.5416	0.9471	2.8*	1.41×10^9	25.0
2	Tetrabromoethane	2.9474	0.9973	1.9553	9.2888	0.8968	35.9	3.73×10^9	24.9
3	Dibromoethane	2.1541	0.9966	1.1614	1.5852	0.8968	31.9	4.39×10^9	25.0
4	Ethyl bromide	1.4478	0.9977	0.4511	0.4908	0.8814	30.0	1.01×10^{10}	26.2
5	Nitrobenzene	1.1947	0.9972	0.1981	1.7379	0.8835	24.1	1.18×10^{10}	25.6
6	Bromobenzene	1.4881	0.9971	0.4924	1.0719	0.8958	37.9	1.75×10^{10}	25.0
7	*o*-Nitrotoluene	1.1576	0.9970	0.1609	2.0360	0.8996	26.5	1.80×10^{10}	24.7
8	Tetrachloroethylene	1.6143	0.9970	0.6192	0.8903	0.8946	44.4	2.25×10^{10}	25.1
9	Carbon tetrachloride	1.5770	0.9957	0.5838	0.8702	0.7797	40.6	3.14×10^{10}	30.4
10	Chlorobenzene	1.0995	0.9969	0.1029	0.7606	0.9036	36.7	7.30×10^{10}	24.8

Symbols:

ρ = density
μ = viscosity
σ_i = interfacial tension
Sub o = organic phase
Others = water phase

$$P = \frac{\sigma_i^3 \rho^2}{g \mu^4 \Delta\rho}$$

T = temperature, °C.
*System unstable.

The case of a liquid sphere was analyzed by Rybczynski (*25*) in 1911 and independently by Hadamard (*11*) in the same year. Lamb (*15*) has given a detailed discussion by considering the internal as well as the external motions and has given the following correction factor for Stokes' law when steady-state conditions prevail:

$$F = K_1 \cdot 3\pi\mu\, a\, U_o$$

and

$$U_o = (1/K_1)\, g\, d^2 \Delta\rho/18\mu$$

$$= \text{terminal velocity}$$

where

$$K_1 = (3\mu_o + 2\mu)/(3\mu_o + 3\mu)$$

Bond (*7*) and Bond and Newton (*8*) made further investigations on this subject. By taking into account the interfacial tension at the drop-medium boundary, they speculated at a critical drop size at which the drop motion would start to deviate from that of a rigid sphere. Unfortunately their results were too few and too erratic to substantiate their postulations.

Allen (*2*) proposed to explore relatively high Reynolds numbers by means of dimensional analysis. By analogy with the flow of liquids through pipes (*26*) he assumed that the resistance to the motion of a sphere was proportional to the *n*th power of the velocity:

$$U_o \propto d^{(3/n)-1} \Big/ v^{(2/n)-1}$$

Thus if n is 1.0 and K is 3π, Stokes' law is obtained and U_o varies as the square of the drop diameter. If n is 1.5, U_o is proportional to d, and

$$F = k\rho^{\frac{1}{2}} \mu^{\frac{1}{2}} d^{3/2} u^{3/2}$$

If n is 2.0, U_o varies as $d^{\frac{1}{2}}$, and the resistance is independent of viscosity. This is the so-called "Newton's law of motion":

$$F = k\rho a^2 u^2$$

Allen has verified these equations with his own data for all three ranges.

Characterization of drop motion by Reynolds-number ranges was also done by Smirnov and Ruban (*28*), who worked on eleven organic liquid-water systems, using water as the field liquid in most of their experiments. The highest Re they reached was less than 1,000.

THEORETICAL CONSIDERATIONS

Deformation and Oscillation. The main reasons for the differences between the motion of liquid drops and that of rigid spheres are believed to be the deformation and oscillation of the drops as well as the flow on the drop surface and the circulation inside the drops. The effects of the last two factors on the motion of liquid drops have been the subjects of many experimental investigations and theoretical analyses in the past (*2, 3, 7, 8, 13, 15*), covering Re ranges both within and beyond the Stokes'-law region. Unfortunately no definite conclusions have been reached to date.

Previous workers (*15, 24, 29, 31*) have also analyzed the deformation of moving drops without oscillation and the oscillation of deformed drops without gross drop motion. Solutions for such ideal cases are expressed in terms of the eccentricity of the drops, the amplitude and frequency of their oscillations, and the time of oscillation decay, as related to drop size and velocity and the physical properties of the system. Despite these mathematical formulations, the exact nature of drop motion still remains to be determined by experimental methods because of the inseparableness of the two interfering factors in the actual situation.

Terminal Velocity. Under steady-state conditions, the gravity force on a falling spherical drop is exactly balanced by the resistance it encounters:

$$\frac{\pi d^3}{6} \Delta\rho g = C_D \frac{\pi d^2}{4} \frac{U_o^2 \rho}{2}$$

from which

$$C_D = (4/3)\, (\Delta\rho/\rho)\, (dg/U_o^2$$

$$= (4/3)\, (\Delta\rho/\rho)\, (1/Fr)$$

If the drop starts to fall from rest, it will accelerate for a short distance before reaching its terminal velocity. It can be shown that (*15*),

$$\frac{\pi d^3}{6}\left(\rho_o + \frac{\rho}{2}\right)\frac{du}{dt} = \frac{\pi d^3}{6}\Delta\rho g - C_D \frac{\pi d^2 u^2 \rho}{4 \times 2}$$

When solved

$$u = U_o \tanh\left(\frac{U_o t}{\alpha}\right),$$

$$S = \alpha \ln\cosh\left(\frac{U_o t}{\alpha}\right)$$

where

$$U_o = \sqrt{(4/3)\, (\Delta\rho/\rho)\, (dg/C_D)}$$

$$\alpha = (2/3)\, (d/C_D)\, (2\rho_o + \rho)/\rho$$

hence

$$u = U_o\left[1 - \exp\left(-\frac{3C_D \rho S}{(2\rho_o + \rho)d}\right)\right]^{\frac{1}{2}}$$

The relationship between C_D and U_o has been experimentally established for various rigid shapes (*10*), but to date no generalized correlation has been obtained for liquid drops.

Dimensional Analysis. As the objective of the present work is to characterize drop motion by means of the pertinent physical properties of the systems concerned, it would appear that the best way to correlate the experimental results is by dimensional analysis in a manner similar in many respects to that used by Peebles and Garber (*23a*) for gas bubbles. One may consider

$$f(\mu_o, \mu, \rho, \Delta\rho, \sigma_i, d, U_o, g) = 0$$

or

$$K.\ \mu_o^a.\ \mu^b.\ \rho^c.\ \Delta\rho^e.\ \sigma_i^f.\ d^h.\ U_o^i.\ g^k = 1$$

If the equation is solved dimensionally,

$$\left(\frac{\mu_o}{\mu}\right)^a \left(\frac{\Delta\rho}{\rho}\right)^b (Re)^c (We)^d (M)^e = 1$$

where

$$M = \frac{g\mu^4}{\rho\sigma^3} = \frac{3\rho C_D\ We^3}{4\Delta\rho Re^4}$$

A short history of the M group as well as a resumé of the attempts made by previous workers to use it for correlating experimental data can be found in the literature (*1, 27*). In the data analysis of the present work, however, a modified form of the M group, called the P group, has been found to give better correlations than the M group:

$$P = \frac{1}{M} \frac{\rho}{\Delta\rho}$$

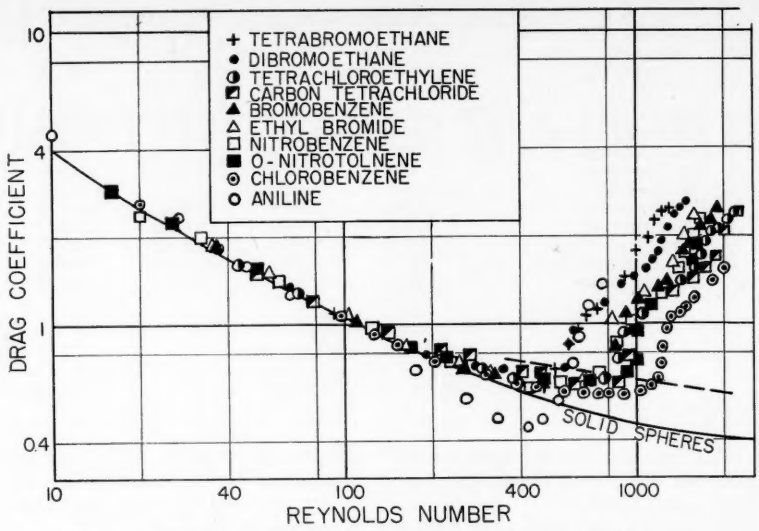

FIG. 1. VARIATION OF DRAG COEFFICIENT WITH REYNOLDS NUMBER.

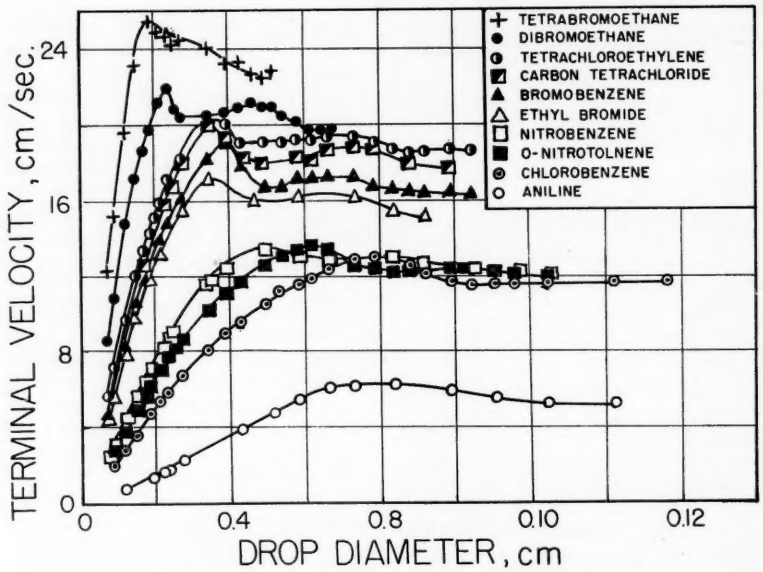

FIG. 2. VARIATION OF TERMINAL VELOCITY WITH DROP SIZE.

EXPERIMENTAL*

Ten technical-grade organic liquids, with densities greater than the density of water, were purchased from Mathieson Chemical Corp. for forming the drops. Before being used, each compound was saturated with distilled water by being shaken with it in a separatory funnel. Distilled water, to be used as the field liquid, was also saturated with the organic compound, the two being stirred with a small mixer in a storage tank.

The densities and viscosities of the two phases and the interfacial tension of each system were determined both before and after each run in order to make sure that no appreciable changes in these constants had taken place during the course of the run. Densities were determined by the conventional weighing method by means of a fine balance and a glass bob. An Ostwald viscometer was used for the viscosity measurements. The capillary method for surface-tension measurements was modified to determine the interfacial tension of the liquid-liquid-systems (*5*). Table 1 gives the average results.

Drops of from 1.6×10^{-4} ml. to 8.0×10^{-3} ml. volume were delivered directly from a capillary tube into the test tank for velocity measurements. The capillary was made from a thermometer stem with a tip drawn out at one end and a rubber bulb fitted on the other end. The capillary bore, calibrated with a mercury bead of known weight, was found to be 0.226 mm. in radius. With the tip immersed under the water surface in the test tank, the desired amount of organic liquid was squeezed out by slightly pressing the rubber bulb and shaking the drops off from the tip. Care was taken to see that the tiny droplet formed in this way did not stick back to the side of the tip or break up when coming off.

Drops from 10^{-2} to 2.000 ml. in size were delivered into small weighing bottles from a microburette graduated to 10^{-2} ml. The tip of the burette was always kept immersed in a basin partly filled with the water phase so that the organic liquid would never come into contact with any free water

*For Tables 5 to 14, giving the detailed diameter vs. velocity data, order document 4478 from American Documentation Institute, Photoduplication Service, Library of Congress, Washington 25, D.C., remitting $1.25 for microfilm or photoprints.

surface. This precaution prevented part of the drop liquid from floating on the water surface, thus rendering the volume measurement inaccurate. The receiving vessels were always kept clean in order to avoid any sticking of the drop to the vessel walls. Twenty-five weighing bottles were used to hold twenty-five drops of the same size. The weighing bottles were then transferred one at a time to the test tank and the drop was carefully poured out under the water surface for the terminal-velocity measurement.

The test tank was made by cementing four 1/4- by 12- by 48-in. glass plates onto a framework of 1 1/2-in. angle irons bolted together. Permanite cement, made by Maurice A. Knight Co., was used for cementing the glass and Pliobond cement, made by Goodyear Rubber Co., for sealing the leaks. The tank bottom was a 1/16-in. stainless steel sheet bolted to the framework with a rubber gasket in between. A storage tank was connected with 1-in. iron pipes to a 4-in. stainless steel funnel soldered to the center of the stainless steel bottom of the test tank. A centrifugal pump installed in the pipe line served to pump the water through a two-way valve connection from one tank to the other as desired.

A thermometer was kept hanging half way down one corner of the test tank to keep a close check on the water temperature, which was maintained constant within $\pm 0.5°C$.

The terminal velocities of the drops were measured by timing with an electric chronograph a distance of fall of 1 ft. between two marks near the bottom of the tank but sufficiently high to eliminate end effects. Twenty-five time measurements were made for each drop size, and the average was used for calculating the velocity.

In order to be certain that terminal velocity had been reached in all cases, the equations presented before were used to calculate the distance of fall required for attaining steady-state conditions, and the values obtained were found to be very much less than the actual distance of fall of about 70 cm. prior to the time measurements. Photographic measurements on three systems also substantiated the attainment of terminal velocity. Furthermore, these values check remarkably well with the results obtained by time measurements, indicating the timing equipment to be a reliable one.

The effects of rigid surface proximity on the motion of solid spheres in the Stokes'-law region have been studied rather exhaustively in the past (*14, 17, 19, 32*). For a solid sphere moving along the axis of a cylindrical container, the general form of the Stokes'-law correction factor is (*9*)

$$K_w = 1 + m\ (d/D)$$

where the constant m ranges from 2.1 to 2.4 according to different authors. Generalized correction for wall effects at higher Reynolds numbers has not yet been found possible (*18, 19*). Absence of wall effects in the test tank has been proved by comparing the data on three systems with those obtained in four glass cylinders with inside diameters of 2.14, 4.59, 6.99, and 9.46 cm. respectively after the method used by McNown, et al. (*19*).

OBSERVATIONS ON DROP MOTION

Although it has been speculated that any surface flow or internal circulation may cause a liquid drop to behave differently from a rigid sphere, yet the data obtained in the present work indicate that no such difference can be observed up to a *Re* of about 300. This fact is borne out by the coincidence of log C_D vs. log *Re* curves for the liquid drops with that for solid spheres below *Re* 300, as shown in Figure 1.

As the limiting *Re* range is passed, however, the log C_D vs. log *Re* curves for the liquid systems depart from the curve for solid spheres but still retain a similar general pattern. At first C_D decreases only very slightly with increasing *Re* for a rather large *Re* range, but when the *Re* reaches a certain value, C_D starts to increase rather abruptly within a narrow *Re* range. After the abrupt rise the curve proceeds at a more or less constant slope until the critical drop size is reached.

On plotting the terminal velocities against the equivalent drop diameters in rectangular coordinates for each system, as shown in Figure 2, one finds that there is a maximum or peak in each curve. This peak velocity occurs at correspondingly larger drop sizes and decreases in value as the density difference of the system becomes smaller. After the peak, the curve shows a dip and then flattens out, sometimes with a slight bump.

The general forms of the log C_D vs. log *Re* and U_o vs. d curves can be interpreted in the light of the change in behavior of the falling drops. It is observed that, as the

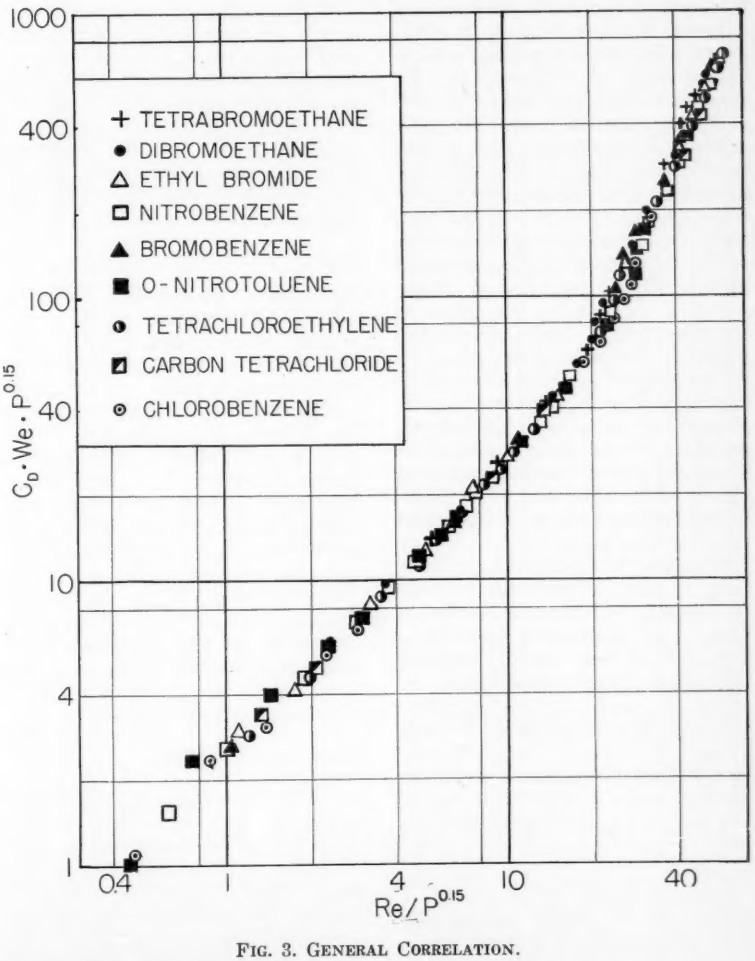

FIG. 3. GENERAL CORRELATION.

TABLE 2.—DATA AT PEAK TERMINAL VELOCITIES

$$\left(\frac{Re}{We}\right)_p = 0.816\,P^{0.238} \qquad (U_o)_p = 1.23\left(\frac{\sigma_i}{\mu}\right)P^{-0.238}$$

$$(We)_p = 3.58 \qquad (d)_p = 3.58\left(\frac{\sigma_i}{\rho}\right)\times\frac{1}{U_o^{\,2}}$$

	System	$(d)_{p\ obs}$, cm.	$(U_o)_{p\ obs}$ cm./sec.	$(Re)_p$	$(We)_p$	$\left(\frac{Re}{We}\right)_p$	P	$(d)_{p\ calc}$, cm.	Dev. d, %	$(U_o)_{p\ calc}$ cm./sec.	Dev. U_o, %
1	Aniline	0.726	6.2	474	10.3	46	1.41×10^{8}	0.600	—17.4	4.1	—33.9
2	TBE	0.200	25.9	576	3.73	155	3.73×10^{9}	0.190	— 5.0	26.0	+ 0.4
3	DBE	0.230	22.1	565	3.51	161	4.39×10^{9}	0.232	+ 0.9	22.2	+ 0.5
4	EB	0.345	17.4	679	3.47	195	1.01×10^{10}	3.356	+ 3.2	17.4	0
5	NB	0.485	13.5	741	3.66	202	1.18×10^{10}	0.475	— 2.1	13.5	0
6	BB	0.395	19.2	823	3.74	220	1.75×10^{10}	0.377	— 4.6	19.0	— 1.0
7	NT	0.630	13.7	957	4.45	215	1.80×10^{10}	0.554	—10.6	13.1	— 4.4
8	TCE	0.350	20.6	804	3.33	241	2.25×10^{10}	0.362	+ 3.4	21.0	+ 1.9
9	CT	0.350	20.2	903	3.50	258	3.14×10^{10}	0.354	+ 1.1	20.3	+ 0.5
10	CB	0.790	13.1	1142	3.68	310	7.30×10^{10}	0.792	+ 0.3	12.9	— 1.5

Aniline = aniline
TBE = tetrabromoethane
DBE = dibromoethane
EB = ethyl bromide
NB = nitrobenzene
BB = bromobenzene
NT = *o*-nitrotoluene
TCE = tetrachloroethylene
CT = carbon tetrachloride
CB = chlorobenzene

drop size gradually increases, the terminal velocity increases linearly with it. This part of the U_o vs. d curve is a straight line and the corresponding C_D values fall along the log C_D vs. log Re curve for solid spheres. Further increase in drop size brings about a zig-zag motion of the drops, and the apparent U_o measured is actually lower than the vectorial velocity value. This phenomenon may be the reason that the C_D stays practically constant and always higher than the C_D for solid spheres up to the abrupt rise. Correspondingly, the U_o vs. d plot starts to show a slight curvature as the peak is approached. When U_o vs. d is plotted on log-log paper for the curved part before the peak, it has been found that U_o varies as the 2/5 to 3/4 power of d, corresponding to the third region in Allen's analysis in which U_o varies as $d^{0.5}$. In other words, d/U_o^2 is approximately constant and thus C_D, being equal to $K(d/U_o^2)$, is almost independent of Re in this region.

The peak terminal velocity is a point of special interest in view of its direct bearing on practical liquid-liquid contacting operations. Data for the peak indicate that the following relationship exists:

$$(Re/We)_p = 0.816\,P^{0.238} \qquad (1)$$

On simplification,

$$(U_o)_p = 1.23\,(\frac{\sigma_i}{\mu})\,P^{-0.238} \qquad (2)$$

Equation (2) shows that the peak terminal velocity of a system is dependent only upon its physical properties. For a rain drop falling in air at 20°C. Equation (2) gives $(U_o)_p = 800$ cm./ sec., which checks closely with reported values (*16*). It is however impossible to find the corresponding drop size by means of Equation (2) alone, because all the d terms are cancelled.

It is interesting to note that the peak of the U_o vs. d curve corresponds to the nose of the log C_D vs. log Re plot, at which the abrupt rise starts. A straight line joining all the nose points indicates very little scattering of the data except for the aniline system, which seems to be out of line with the other nine systems. The equation of this line, shown by the broken line in Figure 1, is found to be

$$(C_D)_p = 1.973\,(R_e)_p^{-0.161} \qquad (3)$$

From this equation

$$(d)_p = (\frac{1.51\times10^{-3}}{\Delta\rho})^{0.861}\,\rho^{0.723}\,\mu^{0.139}\,U_o^{1.584} \qquad (4)$$

TABLE 3.—Re AND C_D AT PEAK TERMINAL VELOCITIES

$$(Re)_p = 2.92\,P^{0.238}$$

$$(C_D)_p = 1.66\,P^{-0.038}$$

	System	Re^*, calc.	Re^*, obs.	Dev., %	C_D, calc.	C_D, obs.	Dev., %
1	Tetrabromoethane.....	550	580	— 5	0.719	0.762	—5.6
2	Dibromoethane.....	580	570	+ 2	0.714	0.715	—0.1
3	Ethyl bromide.....	700	680	+ 3	0.692	0.672	+3.0
4	Nitrobenzene.....	730	740	— 1	0.688	0.689	—0.1
5	Bromobenzene.....	800	820	— 3	0.678	0.690	—1.7
6	*o*-Nitrotoluene.....	810	960	—16	0.677	0.706	—4.1
7	Tetrachloroethylene ...	850	800	+ 6	0.671	0.667	+0.6
8	Carbon tetrachloride...	920	900	+ 2	0.663	0.655	+1.2
9	Chlorobenzene.....	1125	1140	— 1	0.642	0.619	+3.7

*Values rounded off.

Equation (4), though capable of giving good results, is rather inconvenient to use because of the fractional powers involved. A much simpler method has been found by plotting log We vs. log Re. Parallel straight lines with a constant slope of about 1.4 were obtained; however, these straight lines started to level off within a small We range of 3.33 to 3.68. It was found that these We values also corresponded to the respective peaks and an average of 3.58 seemed to be a good representation for all the systems. Thus

$$(We)_p = 3.58 \qquad (5)$$

which agrees quite well with the value of 3.65 reported by Peebles and Garber (*23a*) for gas bubbles in liquids.

When $(d)_p$ is solved for,

$$(d)_p = 3.58\,(\frac{\sigma_i}{\rho})/(U_o^2)_p \qquad (6)$$

Values of $(U_o)_p$ and $(d)_p$ for all the systems, calculated by Equa-

TABLE 4.—CRITICAL DIAMETERS

$$d_c = \left[1.452 \times 10^{-2} \left(\frac{\sigma_i}{\Delta\rho}\right)\right]^{1/2}$$

	System	$\Delta\rho$	σ_i	$(d_c)_{calc}$, cm.	$(d_c)_{obs}$, cm.	Dev., %
1	Aniline	0.0197	2.8	1.436		
2	Tetrabromoethane	1.9501	35.9	0.517	0.511	+ 1.2
3	Dibromoethane	1.1575	31.9	0.633	0.674	— 6.1
4	Ethyl bromide	0.4501	30.0	0.984	0.914	+ 7.7
5	Nitrobenzene	0.1975	24.1	1.331	1.537	—13.4
6	Bromobenzene	0.4910	37.9	1.059	1.132	— 6.4
7	*o*-Nitrotoluene	0.1606	26.5	1.548		
8	Tetrachloroethylene	0.6173	44.4	1.022	1.040	— 1.7
9	Carbon tetrachloride	0.5813	40.6	1.007	1.040	— 3.6
10	Chlorobenzene	0.1026	37.4	2.301		
11*	Dirty water	0.980	48.0	0.70	0.84	+20.0
12*	Distilled water	0.980	70.6	1.00	1.02	+ 0.2
13*	Carbon tetrachloride	1.568	24.5	0.36	0.48	+33.3
14*	Methyl salicylate	1.303	34.3	0.65	0.62	— 4.6
15*	Methyl salicylate (thickened)	1.313	37.2	0.85	0.64	—24.7
16*	Glycerine+2% Water	1.186	63.7	0.90	0.88	— 2.2

*Data by Merrington and Richardson on liquid drops in air.

tions (2) and (6), are found in Table 2. However a more direct method of estimating the nose C_D and Re is by substituting Equation (5) into Equation (1) and eliminating Re from Equation (3). Thus,

$$(Re)_p = 2.92\ P^{0.238} \qquad (7)$$

$$(C_D)_p = 1.661\ P^{-0.038} \qquad (8)$$

Values of $(Re)_p$ and $(C_D)_p$ are found in Table 3.

The abrupt rise in the log C_D vs. log Re curve corresponds to the dip after the peak in the U_o vs. d plot. Vigorous oscillation has been observed in the falling drops, and the deformation in drop shape may or may not be noticeable, depending on the relative magnitudes of the interfacial tension and the density difference of the system concerned. This indicates that the oscillation induced by the peak velocity is the main reason for the rapid increase in C_D and the corresponding decrease in U_o within this short Re range. The effect of deformation seems to be only of secondary importance.

After the abrupt rise in the log C_D vs. log Re curve, deformation of the drops becomes more and more severe and the oscillation progressively erratic. This part of the curve has a fairly constant slope which later increases slightly owing to the excessive deformation of the drops; however, the family of curves for different systems exhibits a great extent of intercrossing with one another in this region, even though the same general pattern is retained. Different methods have been tried to disentangle the data and the best solution found after many trials is a log $C_D \cdot We\ P^{0.15}$ vs. log $(Re/P^{0.15})$ plot, which surprisingly enough is capable of bringing all the data into one single curve for the entire Re range covered in this study, the aniline system being again excluded. This generalized curve, shown in Figure 3, has a slight curvature in the low Re region and shows a distinct break at an Re region approximately corresponding to that where the peak terminal velocity occurs. When the pertinent physical properties of a system are known, this curve can be used directly to obtain the terminal velocity for any given drop size and hence the corresponding C_D, We, and Re are readily calculable, involving no trial-and-error solution at all.

That prediction of drop motion is not possible in the absence of such a generalized curve is obvious. In this event, the following two equations representing the generalized curve may be used to advantage:

$$Y = (4/3)\ X^{1.275} \quad \text{for } 2 < Y \leqq 70 \qquad (9)$$

$$Y = (0.045)\ X^{2.37} \quad \text{for } Y \leqq 70 \qquad (10)$$

where

$$Y = C_D\ We\ P^{0.15}$$

and

$$X = (Re/P^{0.15}) + 0.75$$

These two equations give errors usually well below 10%. Furthermore, at the break point of $Y = 70$ and $X = 22.25$, calculated values of drop size, Reynolds number, and terminal velocity are found to check with the observed peak quantities within 10% with the exception of four occasions. The break point can be therefore safely used to calculate the peak quantities in addition to methods outlined above.

It is interesting to note that the chlorobenzene system, with a low density difference coupled with a comparatively high interfacial tension, behaves almost ideally. Even large drops are only slightly deformed into a symmetrical, ellipsoidal shape and maintain a smooth motion with very little oscillation. On the other hand, the interfacial tension of the aniline system is so low that, despite its very low density difference, even a medium-sized drop will be badly deformed into a rather irregular shape being continually deformed into various queer shapes by the wake turbulence. Furthermore, the system itself is not stable against oxidation and discoloration. In view of these facts, it is not surprising to find the data for this system fall out of line with the rest.

It should be pointed out that the viscosity of the drop liquid seems to have no discernible effects on drop motion. The most that can be said is that, according to the analyses of previous workers (*13, 29*), this viscosity might exert a damping action on the oscillation of the drops. But this effect is difficult to isolate from the much greater effects of deformation and oscillation in gross-motion measurements.

The velocity measurements were discontinued when either the oscillation became too erratic or the deformation too severe, thus rendering the data meaningless. However, for certain systems the experiment had to be terminated at an early stage, long before any severe deformation or oscillation had taken place, because further increase in size would cause splitting of the drops. This phenomenon indicates that, for each system, there is a definite maximum drop size, or critical size, beyond which the falling drops cannot be preserved without being ruptured.

Similar phenomena have been observed in the past for the case of liquid drops falling in air. The analysis made by Hinze (*12*) on the data of Merrington and Richardson (*20*) on drops of six liquids falling in a tower over 125 ft. high suggests a critical We, based on the density of the liquids, as the criterion for the critical drop size. Although the We values so calculated vary from 7.7 to 14.9 for the six liquids, Hinze concludes that an average of 10 can be used for the characterization.

Applying the previous argument to the systems in which splitting has been observed in the present study, the critical We are found to vary from 10 to 22. Evidently We is not the only dimensionless group that characterizes the critical drop size. From both dimensional analysis and force balances, it has been found that (*12a*)

$$(WeC_D)_c = \text{constant}$$

From the data

$$d_c = \left[1.452 \times 10^{-2} \left(\frac{\sigma_i}{\Delta\rho}\right)\right]^{\frac{1}{2}} \quad (11)$$

Table 4 gives the calculated values of d_c for all the ten systems used in the present work as well as for some air-liquid systems reported in the literature (*20*).

SUMMARY

Terminal velocity measurements have been made on single drops of ten organic liquids falling in a stationary water field in a glass-walled tank 1 ft. square and 4 ft. high. The drop size ranged from 1.6×10^{-4} to 2.000 mm. in diameter, covering a range of Reynolds numbers from 10 to 2,200.

The aniline-water system has a very low interfacial tension and is very easily oxidized and discolored by contact with air. Results of the other nine systems, however, have been successfully correlated by means of a dimensionless parameter, P, composed of the pertinent physical properties of a system in the following manner:

$$P = \frac{\rho\sigma_i^3}{g\mu^4}\frac{\rho}{\Delta\rho} = \frac{3}{4}\frac{(Re)^4}{C_D\,(We)^3}$$

which is a constant for each system at constant temperature. It has been found that for the data on all the nine systems (excluding aniline-water) a plot of log $C_D We P^{0.15}$ against log $(Re\,P^{0.15})$ resulted in a single unique curve for the entire range of Reynolds numbers covered. Equations have been obtained for this generalized curve and either the equations or the curve can be used directly to obtain the terminal velocity, drag coefficient, and Reynolds and Weber numbers for any given drop size. The errors involved are generally less than 10%. The curve contains a break point which can be used to predict the peak terminal velocity and its related quantities. Alternate methods for predicting the peak quantities have also been presented.

The maximum, or critical, drop size of the systems is found to be dependent on the criterion

$(C_D We)_c$ = a constant

which leads to an equation for estimating the critical drop size from the density difference and interfacial tension of a system.

Work on systems of very low interfacial tension and on systems using field liquids other than water is in progress.

NOTATION

a = constant
c = constant
C_D = drag coefficient
d = diameter of a solid sphere or equivalent diameter of a drop
d_c = critical equivalent drop diameter for maximum drop size
d_p = equivalent drop diameter corresponding to peak terminal velocity
D = diameter of cylindrical container
F = resistance force to motion
Fr = Froude number, $\frac{U_o^2}{gd}$
g = gravitational acceleration, 980.3 cm./sec.^{2} for Chicago
i = constant
K_1 = correction factor for fluidity of moving body
K_w = wall effect correction factors
m, n = constants
M = M group, $\frac{g\mu^4}{\rho\sigma_i^3}$
P = physical property group, $\frac{\rho\sigma_i^3}{g\mu^4}\frac{\rho}{\Delta\rho}$
Re = Reynolds number, $\frac{dU_o\rho}{\mu}$
S = distance of fall required for reaching terminal velocity when starting from rest
t = time
T = temperature
u = velocity
U_o = terminal velocity with no wall effect
We = Weber number, $\frac{U_o^2 d\rho}{\sigma_i}$
μ_o, μ = viscosities of organic and water phase respectively
ν = kinematic viscosity
π = 3.1416
ρ_o, ρ = densities of organic and water phase respectively
$\Delta\rho$ = density difference of a system, $\rho_o - \rho$
σ_i = interfacial tension

LITERATURE CITED

1. Allawala, M. A., M.S. thesis, Illinois Inst. Technol. (1952).
2. Allen, H. S., *Phil. Mag.* (5), **50**, 323 (1900).
3. Arnold, H. D., *Phil. Mag.* (6), **22**, 755 (1911).
4. Ballard, J. H., and E. L. Piret, *Ind. Eng. Chem.*, 42, 1088 (1950).
5. Bartell, F. E., and F. L. Miller, *J. Am. Chem. Soc.*, **50**, 1961 (1928).
6. Basset, A. B. "Treatise on Hydrodynamics," Vol. II, Cambridge University Press (1890).
7. Bond, W. N., *Phil. Mag.* (7), **4**, 889 (1927).
8. Bond, W. N., and D. Newton, *Phil. Mag.* (7), **5**, 794 (1928).
9. Francis, A. W., *Physics*, **4**, 403 (1933).
10. Goldstein, S., "Modern Developments in Fluid Dynamics," Vol. I, p. 104, Oxford University Press (1938).
11. Hadamard, M. I., *Compt Rend.*, **152**, 1735 (1911).
12. Hinze, J. O., *Appl. Sci. Research, A1*, 273 (1948).

12a. Hu, S., Ph.D. thesis, Illinois Inst. of Technol. (1953).

13. Jones, O. G., *Phil Mag.* (5), **37**, 451 (1894).
14. Ladenberg, R., *Ann. Physik*, **23**, 447 (1908).
15. Lamb, H., "Hydrodynamics," 6 ed., Dover Publications, New York (1945).
16. Lapple, C. E., et al., "Fluid and Particle Mechanics," Univ. Del. Press, Wilmington, Del. (1951).
17. Lorentz, H. A. *Abhandl. uber theo. Phys.*, **1**, 23 (1907).
18. Lunnon, R. G., *Phil. Mag.* (6), **47**, 173 (1924); *Proc. Roy. Soc. (London), 110A*, 302 (1926).
19. McNown, H. M., et al., *State Univ. of Iowa Reprints in Engineering.* No. 81 (1948).
20. Merrington, A. C., and E. G. Richardson, *Proc. Phys. Soc., (London)*, **59**, 1 (1947).
21. Millikan, R. A., "Electrons," p. 95, Univ. Chicago Press (1935).
22. Miyagi, O., *Tôhoku Imp. Univ. Tech. Repts.* (5), No. 3, p. 1 (1925).
23. Morello, V. S., and N. Poffenberger, *Ind. Eng. Chem.*, **42**, 1021 (1950).

23a. Peebles, F. N., and H. J. Garber, *Chem Eng. Progr.*, **49**, 88 (1953).

24. Rayleigh, Lord, *Phil. Mag.* (4), **36**, 354 (1893); *Proc. Roy. Soc. (London)*, **24**, 71 (1879).
25. Rybcsynski, W., *Bull. acad. Sci. de Cracovie (A)*, **40** (1911).
26. Reynolds, O., *Phil. Trans.*, **174**, 935 (1883).
27. Rosenberg, B., *Report* 727, D. W. Taylor Model Basin, Navy Dept., Washington, D. C. (September 1950).
28. Smirnov, N. I., and V. L. Ruban, *J. Appl. Chem. (USSR)*, **22**, 1068 (1949); **22**, 1211 (1949); and **24**, 57 (1951).
29. Spilhaus, A. F., *J. Met.*, **5**, 108 (1948).
30. Stokes, G. G., "Mathematical and Physical Papers," Vol. 1, Cambridge University Press, London (1880).
31. Thompson, Sir W., "Papers," Vol. 3, 384 (1876).
32. Williams, W. E., *Phil. Mag.* (6), **29**, 526 (1915).

(Presented at A.I.Ch.E. Glenwood Springs meeting)

ABSORPTION OF ETHYLENE OXIDE in a PACKED COLUMN WITH VARIOUS SOLVENTS

C F. BONILLA and S. BARON

Data were obtained on the solubility of ethylene oxide gas in a number of aqueous and nonaqueous solvents at various temperatures and gas concentrations. Its absorption from high concentrations in air was studied in a packed column with a cooling jacket for removal of the heat evolved. The results can be correlated with adequate accuracy in terms of the conditions at the top or dilute end of the column. The values of $(H.T.U.)_G$ and $(H.T.U.)_L$ agree approximately with known values for other systems. For the solvents tested, the liquid-film resistance is controlling at room temperatures.

In this research the absorption of ethylene oxide has been studied under varying conditions of gas composition, temperature, and solvent; and the relationship between absorption rate and the significant variables has been investigated. Ethylene oxide is an organic gas which boils at 10.5°C. and is readily soluble in many organic and inorganic solvents. The absorption was not strictly kept under either isothermal or adiabatic conditions, but rather a cooling jacket with refrigerant flowing upward at a constant rate was employed. The immediate purpose was to investigate the practicability of recovering ethylene oxide by scrubbing the vent gases of a plant producing acetyl butyro lactone ($C_6H_8O_3$) from ethyl aceto acetate and ethylene oxide. An additional purpose was to check the suitability of present over-all methods of column design to absorption of concentrated soluble gases with heat evolution and cooling. Solvents employed included acetone, ethyl alcohol, water, 52% by volume ethyl alcohol, benzene, and ethyl aceto acetate. For each solvent the concentration of ethylene oxide in air at the inlet to the column was varied from 10 to 46 mole %. The solubility of ethylene oxide in the various solvents was also measured.

C. F. Bonilla is with Columbia University, New York, New York, and S. Baron with Burns and Roe, Inc.

This article is contribution 49 from the Chemical Engineering Laboratories, Engineering Center, Columbia University, New York, and is taken in part from the M. S. thesis written by Dr. Baron at the Johns Hopkins University in 1947.

GENERAL LITERATURE SURVEY AND ABSORPTION THEORY

Since the publication of the two-film theory (*18*) and the development of the diffusion theory (*17*), researchers have tried to correlate their absorption data on these bases. Early workers assumed that one film predominated and reported the film coefficient as a function of either the gas or liquid flow rate (*4, 8, 11*). Recent investigators have measured the resistances of both films and related them to the liquid and gas flow rates (*5, 7, 10, 14, 19*).

In terms of over-all height per transfer unit (*3*) $(H.T.U.)_{OG}$, the equation that expresses the addition of the individual gas and liquid resistances for an isothermal system following Henry's Law (so that m is constant) is

$$(H.T.U.)_{OG} = (H.T.U.)_G + (H.T.U.)_L \frac{mG}{L} \frac{(1-x)_f}{(1-y)_f} \quad (1)$$

When the experimentally determined values of $(H.T.U.)_{OG}$ vs. $\frac{mG}{L} \frac{(1-x)_f}{(1-y)_f}$ for each absorption run at some constant temperature for the same solvent are plotted, the slope of the straight line yields $(H.T.U.)_L$ and the intercept, at $\frac{mG}{L} \frac{(1-x)_f}{(1-y)_f}$ equal to zero, is $(H.T.U.)_G$. The values of the over-all and individual film H.T.U.'s are related to the over-all and individual mass transfer coefficients by

$$(\text{H.T.U.})_{OG} = \frac{G}{K_g a\ (1-y)} \quad (2)$$

$$(\text{H.T.U.})_{G} = \frac{G}{k_g a\ (1-y)_f} \quad (3)$$

$$(\text{H.T.U.})_{L} = \frac{L}{k_L a\ (1-x)_f} \quad (4)$$

If the separate film coefficients are proportional to the flow rate of the corresponding streams and the concentration of solute in the streams is low, the $(\text{H.T.U.})_{OG}$ would then be a linear function of $\frac{mG}{L}\ \frac{(1-x)_f}{(1-y)_f}$. Several investigators have studied systems obeying this relationship (*1, 2, 6, 8*).

Some work has been done to study the effect of temperature in isothermal absorption. The results have shown that the liquid-film coefficient is very sensitive to temperature whereas the gas-film coefficient is only slightly affected by temperature (*5, 8, 15*). However, no over-all analyses of concentrated systems involving a soluble gas have been located.

METHOD OF CALCULATION

The solubility data as tabulated in Table 1* show that at the determined temperatures Henry's Law holds, namely $y = mx$. When there is no solute in the entering solvent, Colburn (*3*) has shown that where (mG/L) is constant, the number of transfer units N_{OG} is determined by the equation:

$$N_{OG} = \frac{2.3}{\left(1 - \frac{mG}{L}\right)} \log\left[\left(1-\frac{mG}{L}\right)\frac{y_B}{y_T} + \frac{mG}{L}\right] \quad (5)$$

The dilute, and thus substantially isothermal, runs, in which the outlet solvent temperature was within ± 2°C. of its inlet temperature, were first analyzed.

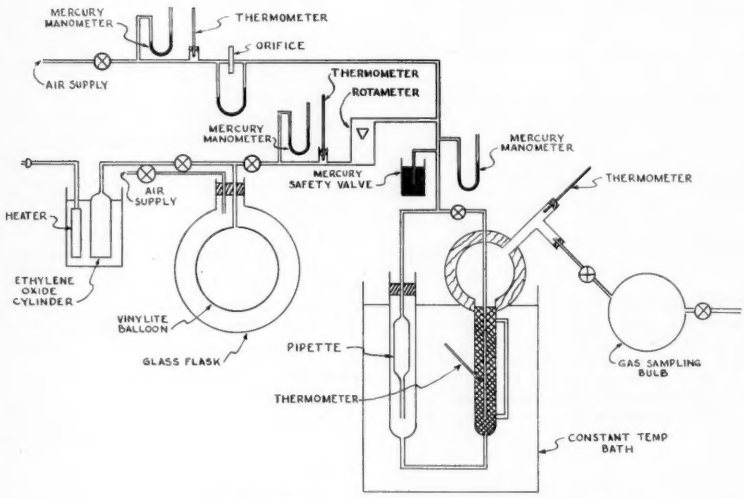

FIG. 1. SOLUBILITY APPARATUS.

For this case Equation (1) substantially equals

$$(\text{H.T.U.})_{OG} = (\text{H.T.U.})_{G} + (\text{H.T.U.})_{L}\ \frac{mG}{L}\ \frac{1}{(1-y_T)} \quad (6)$$

By a plot of $(\text{H.T.U.})_{OG}$ vs. $\frac{mG}{L}\ \frac{1}{(1-y_T)}$ for any given solvent at the same temperature, the values of H.T.U._G and H.T.U._L were determined.

When the solvent temperature changed by more than two degrees in each set of runs with a given solvent inlet and jacket temperatures, values of m corresponding to the range of solvent temperatures were used in calculating the over-all H.T.U. That value of m which gave best agreement in $(\text{H.T.U.})_{OG}$ between the isothermal and nonisothermal runs at the same average temperature was considered as representing the mean value for the column. As the calculated results in Table 3 indicate, the temperature corresponding to the mean m is in general approximately the same as the solvent temperature at the top of the column. This fact substantiates the approach of correlating the data with the conditions at the top or the dilute end of the column, as is recommended (*12*) by Perry for quick approximate solution in nonisothermal cases.

ANALYTICAL PROCEDURE AND SOLUBILITY APPARATUS

Ethylene oxide when absorbed in aqueous hydrochloric acid in the presence of calcium chloride reacts quantitatively with the hydrochloric acid to form ethyl chlorhydrin. The excess hydrochloric acid is back-titrated with sodium hydroxide; bromphenol blue is the indicator. Experiments run previously at the laboratory of U. S. Industrial Chemicals, Inc., showed immediate absorption of ethylene oxide by this method if the water is approximately saturated with calcium chloride and the normality of the hydrochloric acid is between 0.7 and 0.8. The calcium chloride is first dissolved in the water and the solution filtered to remove insoluble impurities, apparently from the calcium chloride. Concentrated hydrochloric acid is added to bring the solution to the correct normality. A stock solution containing 3.2 lb. of calcium chloride (anhydrous), 2,600 ml. of water, and 200 ml. of concentrated hydrochloric acid was used for all ethylene oxide determinations.

The solubility data were obtained by passing a mixture of ethylene oxide and air in a constant ratio through the solvent at a specific temperature until the liquid was saturated. The gas and liquid phases were then analyzed for ethylene oxide. The equipment is shown in Figure 1.

The saturator was a 1-liter flask used in an inverted position; to the neck of the flask was blown a 1 3/8-in. I.D., 1 1/2-ft.-long glass extension tube packed with 1/4-in. Raschig rings through which the gases were admitted into the absorber. A 1/8-in. glass return tube to the bottom of the packing gave good liquid recirculation. Sealed at the bottom of the packed tube was a 1/2-in. glass tube

*Tabular data are available as document 4474 from A. D. I. Auxiliary Publications Project, Photoduplication Service, Library of Congress, Washington 25, D.C., for $2.50 for photoprints or $1.75 for 35-mm. microfilm.

that held a rubber stopper and a pipette for sampling the liquid. The 1-liter flask was thermally insulated with asbestos cement 1/4 in. thick provided with peep holes. The exit-gas sampling bulb was a 2-liter flask of measured volume with rubber connections and screw clamps. When a sample was taken, the inlet connection was closed first and then the outlet connection.

The air was obtained from the regular laboratory compressed-air-supply system. The ethylene oxide was stored in liquid form in a 50-lb. cylinder which fed to a 5-lb. gas cylinder in a heated water bath to provide the necessary heat to vaporize the ethylene oxide. Owing to irregular boiling of the ethylene oxide in the cylinder, large fluctuations in the pressure occurred. A constant ethylene oxide gas pressure slightly above atmospheric pressure was accomplished by employing as a gas holder a Vinylite balloon, of the type used by the Army Weather Bureau, in a round 50-liter flask. An accurately controlled air pressure was connected to the space between the flask and the balloon. To inflate the balloon, its outlet connection was shut off, the space between the flask and balloon vented to the atmosphere, and the connection from the 5-lb. cylinder to the balloon opened. When the balloon completely filled the flask, the ethylene oxide was shut off and the air supply to the flask turned on. A constant air pressure on the balloon caused a steady stream of ethylene oxide gas to pass into the absorber.

The ethylene oxide flow rate was measured by means of a rotameter calibrated with air against two wet-test meters which agreed with each other. Correction to the specific gravity of ethylene oxide of 1.52 was made by the nomograph supplied by the manufacturer. The air-flow rate was measured by an orifice calibrated against the wet-test meters. The ratio of ethylene oxide to gas-flow indications was also directly checked by the analysis for ethylene oxide in the exit gas after saturation. Thermometers and manometers were always used, as required, in the air lines and during calibration tests, so that the flow rates might be corrected to standard conditions. All gas-line connections were sealed with cellulose nitrate solutions.

The saturator was thermostatted in a 20-gal. barrel with a coolant at the desired temperature. Below 0°C., ethanol cooled in a deep-freeze unit was circulated through the barrel by a centrifugal pump. The temperature was controlled by settings on the freezer and by the rate of flow of the ethanol. Above 0°C. the ethanol was also employed as the coolant.

The saturator was filled with the solvent to be tested to about 1 in. below the top of the packing and then immersed in the barrel to the top of the packing.

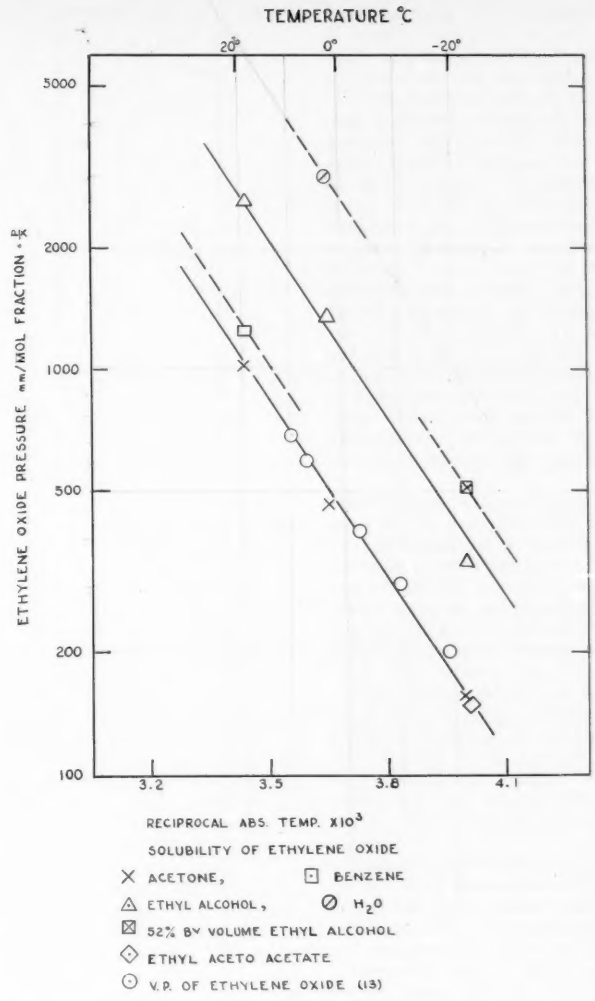

FIG. 2.

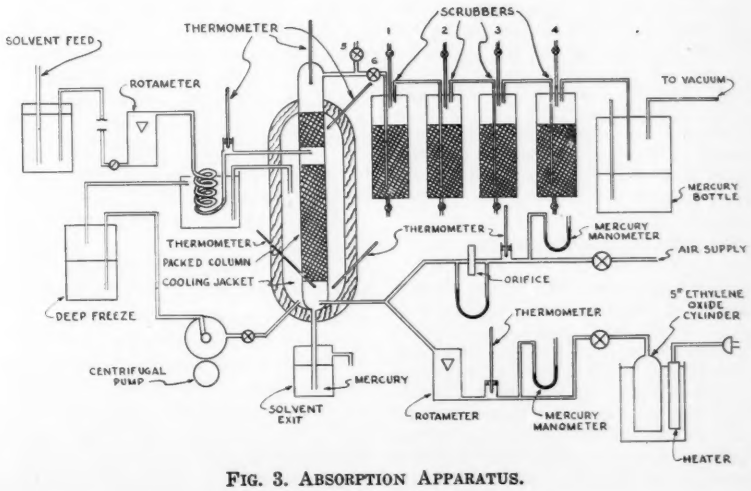

FIG. 3. ABSORPTION APPARATUS.

The ethylene oxide and air flow were started at the same time. A screw clamp at the saturation inlet was set so that the gas flow was divided about equally between the absorber and the pipette. Every 5 min. during a run the exit-gas sampling bulb was analyzed for ethylene oxide. When the ratio of ethylene oxide to air was the same in the bulb as on entering the absorber, then the liquid was considered saturated, and a sample of the liquid was withdrawn with the 5-ml. pipette and analyzed for ethylene oxide. It was found that the dilute gas mixtures would saturate the solvent in 10 min. and the more concentrated mixtures in 15 min. The saturation pressure was taken to be that at the gas inlet to the packing, which would be substantially correct from the location of the pipette.

Solubility runs were started with dilute gas mixtures, and the concentration increased after each run. At the end of a run the screw clamp before the gas bulb was closed, the gas releasing through the mercury valve. The gas flows were then shut off, and a liquid sample was immediately taken. Since the pipette was calibrated and the liquid density known, it was possible to analyze the liquid for ethylene oxide without weighing it. This method gave reproducible results and avoided the necessity of weighing the sample and the possibility of losing ethylene oxide in the process.

The gas sampling bulb, completely pinched off, was allowed to warm up to room temperature and the excess gas was released. A measured amount of the hydrochloric acid solution between 50 and 100 cc. was placed in a separatory funnel and about three fourths allowed to flow into the bulb. The bulb was shut off and the hydrochloric acid swirled for about 5 min. The remaining hydrochloric acid was admitted and again swirled and then drained out and the bulb washed twice with equal volumes of water. The washes were added to the hydrochloric acid and the sample was titrated, the results being plotted in Figure 2. It is evident that solutions in acetone and ethyl aceto acetate obey Raoult's Law, with increasing positive deviations both for less polar (benzene) and more polar (water) liquids. The equations of the five lines plotted are given in Table 2.

ABSORPTION APPARATUS

The apparatus used for the absorption-rate data is shown in Figure 3. An air-ethylene oxide mixture of known composition was passed up the absorption column, and a measured liquid flow rate passed down. Scrubbers on the gas-outlet line measured the amount of ethylene oxide leaving the column. The difference was the amount of ethylene oxide absorbed.

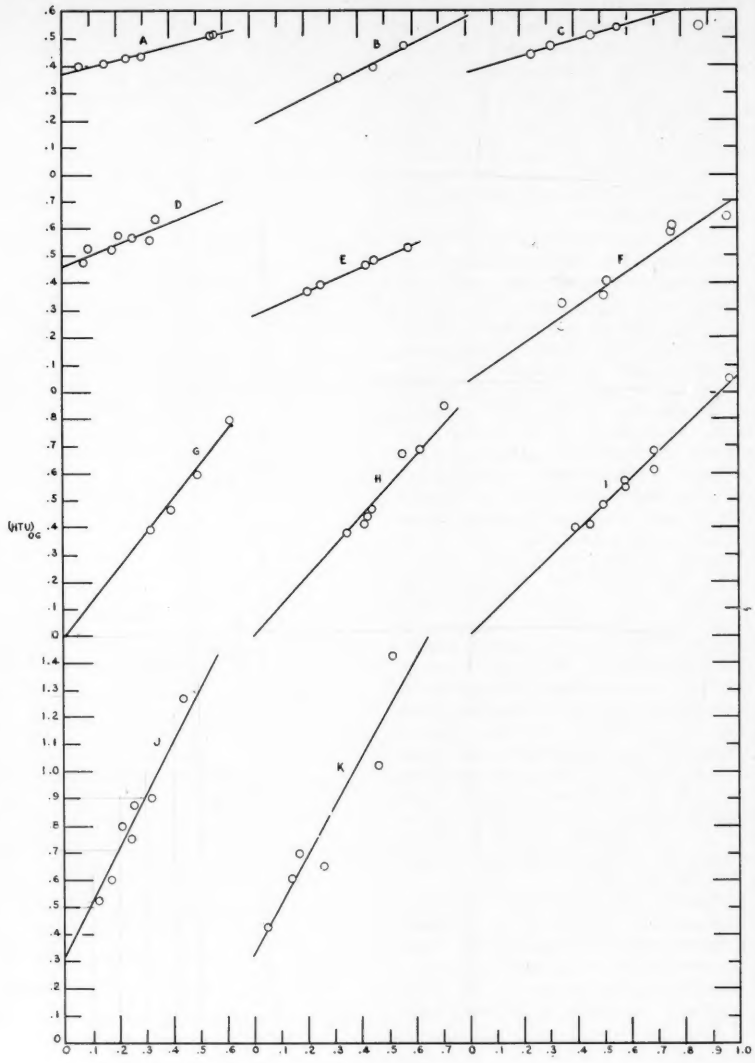

CURVE	SOLVENT	TEMPERATURE RANGE	$(HTU)_G$	$(HTU)_L$
A	ACETONE	+2 TO -12.5 °C	0.37	0.25
B	ACETONE	17 TO 19 °C	0.18	0.50
C	ACETONE	4.5 TO 8 °C	0.37	0.31
D	ETHYL ACETO ACETATE	-5 TO -10 °C	0.46	0.43
E	ETHYL ALCOHOL	-5 TO -10 °C	0.28	0.43
F	ETHYL ALCOHOL	13 TO 18 °C	0.04	0.69
G	ACETONE	22 TO 25 °C	0.00	1.26
H	BENZENE	22 TO 26.5 °C	0.00	1.10
I	ETHYL ALCOHOL	24 TO 27 °C	0.00	0.97
J	WATER	6 TO 14 °C	0.33	1.80
K	52% ETHYL ALCOHOL	-3 TO -10 °C	0.32	1.82

FIG. 4. COLBURN PLOT FOR ETHYLENE OXIDE ABSORPTION BASED ON TOP (PINCH) CONDITIONS.

The absorption column measured 1.1 in. I.D. and 45 in. high. The liquid level in the bottom of the column was maintained constant and gas leakage was prevented by a mercury seal on the outlet tube. The gas inlet and bottom of the packing were just above the liquid level.

The column was packed randomly with a thorough mixture of three sizes of glass Raschig rings to a height of 30.5 in. One-third of the total number was 21/64 in. O.D., 13/64 in. I.D., and 21/64 in. long; 1/3 was 9/32 in. O.D., 5/32 in. I.D., and 21/64 in. long; and 1/3 was 8/32 in. O.D., 4/32 in. I.D., and 9/32 in. long. The calculated surface is 215 sq. ft./cu. ft. Above the liquid inlet there was a 3-in. entrainment-removing section. A cooling jacket surrounded the packed column, which contained thermometers in the liquid at the bottom, in the exit gas stream at the top, and in the inlet and outlet streams of the coolant. The column was completely insulated with asbestos 0.85 in. thick.

The outlet gases bubbled through four glass-Raschig-ring-packed scrubbers 1 ft. high in series. The first and third scrubbers contained the hydrochloric acid– and calcium chloride–absorbing solution and the others contained water to catch any entrained or vaporized hydrochloric acid. The gas line from the last absorber, as well as a line through which the gas was allowed to by-pass the absorbers at the start of the run, led to a mercury bottle and air tube connected to a vacuum pump. By adjusting the submergence of the air tube it was possible to maintain enough vacuum in the air bottle just to counteract the liquid head in the four scrubbers and maintain atmospheric pressure in the absorption column.

The cooling system consisted of the deep-freeze unit filled with 30 gal. of alcohol, which was circulated at 1.3 liters/min. by a small centrifugal pump through the column cooling jacket and next through a Dewar flask that precooled the liquid feed stream and then was returned to the deep freeze.

The solvent for the absorption was fed from a 2-liter constant-head bottle stationed about 10 ft. above the column. The liquid flowed through a rotameter calibrated with the same solvent through three turns of 1/8-in. copper tubing 3 in. in diam., in the Dewar bottle, and then into the column.

The air came from the previously mentioned air system and orifice meter. At the higher flow rates used in the absorption tests the boiling of the ethylene oxide was much steadier and the plastic bag was unnecessary; otherwise the system was as before. The gases mixed in a 1-ft.-long tube before entering the column.

In starting a run the coolant alcohol was cooled to the desired temperature and circulated through the column for 1/2 hr. Then the solvent and gases were started through the column for 15 min., the gases bypassing the scrubbers. Stopcock 5 was closed and 6 opened, and timing started with a stopwatch. Absorption was continued from 10 to 20 min., but not to exceed the capacity of the first scrubber. All temperatures, pressures, and flow rates were recorded every 5 min. At the end of the run the streams were stopped, and the hydrochloric acid scrubbers drained, washed, and analyzed. The first scrubber was found always to have caught all the ethylene oxide.

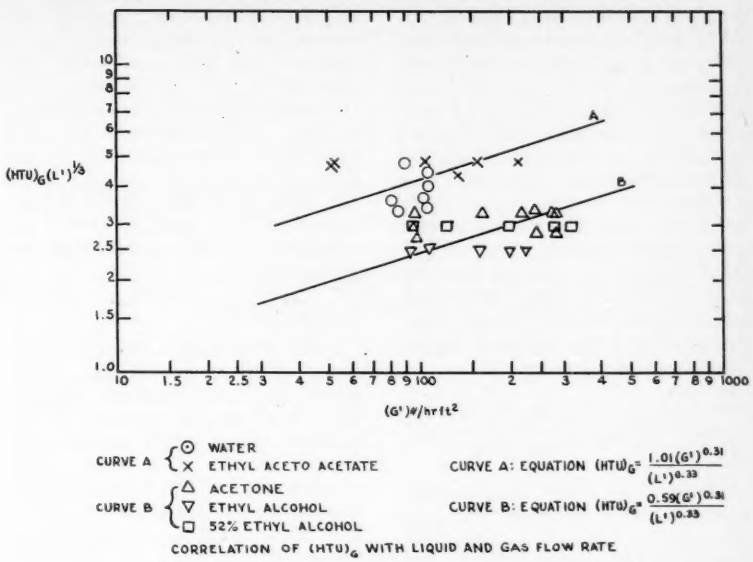

FIG. 5.

RESULTS

For each run first the number of transfer units, N_{OG}, was computed by Equation (5) by use of (mG/L) at the top of the column, then $(H.T.U.)_{OG}$ was computed by (H/N_{OG}). On analysis of the data it was found that $(H.T.U.)_{OG}$ correlated better with the function $\frac{mG}{L}\frac{1}{(1-y_T)}$ than with any fractional powers of gas or liquid flow rates, where (mG/L) again was for the top of the column (Figure 4).

When the temperature is approximately constant, this method should be reliable since the operating and equilibrium lines diverge in going from the top to the bottom of the column, most of the transfer units being at the dilute end. When the temperature rises in passing down the column, the equilibrium line approaches the operating line, and the concentrated end, or bottom, of the column has an increasing number of transfer units. The effective mean temperature for the column would then be intermediate between those at the top and bottom of the column.

Four of the runs (*AL*, *AM*, *AN*, and *AO*), however (Table 4), determine a mean temperature as described above which is higher than both the inlet and outlet solvent temperatures. No explanation is evident, for it does not seem reasonable that absorption was faster in the middle or the top of the column than in the bottom and so overheated the liquor in the middle.

At mean temperatures above 20°C. with the solvents ethyl alcohol, acetone, and benzene, the liquid film showed as the only resistance to mass transfer. With water in the temperature range from 6° to 14°C., $(H.T.U.)_L$ is five times greater than $(H.T.U.)_G$. The 52% ethyl alcohol at —3° to —10°C. yielded $(H.T.U.)_L$ six times greater than $(H.T.U.)_G$. At temperatures below 0°C., ethyl alcohol, acetone, and ethyl aceto acetate have $(H.T.U.)_L$ and $(H.T.U.)_G$ of the same order of magnitude.

Within the range of accuracy of the experimental results, ethyl alcohol, acetone, benzene, and ethyl aceto acetate have approximately the same value of $(H.T.U.)_L$ at the same solvent temperature. With water and 52% ethyl alcohol as solvents, the value of $(H.T.U.)_L$ is

about four times as great as for the other above-mentioned solvents.

Figure 5 is a comparison of the experimental results of $(H.T.U.)_G$ with the equation (curve A) proposed by Sherwood and Pigford (*16*) based on absorption data for ammonia, sulfur dioxide, and chlorine with water. The solvents water and ethyl aceto acetate seem to fall reasonably close to the proposed curve. The solvents acetone, ethyl alcohol, and 52% ethyl alcohol average some 40% lower, clustering around the curve B represented by the equation

$$(H.T\ U.)_G = \frac{0.59\ (G')^{0.31}}{(L')^{0.33}} \qquad (7)$$

Considering only the results herein reported, however, the first two solvents fall closer to the line A', or $(H.T.U.)_G(L')^{1/3} = 4.5$, and the other three to line B', or $(H.T.U.)_G(L')^{1/3} = 2.9$. The relative

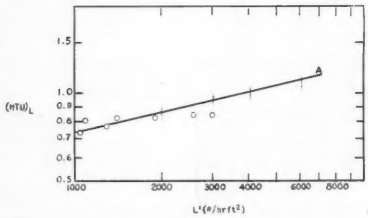

FIG. 6. CORRELATION OF $(H.T.U.)_L$ WITH LIQUID-FLOW RATE. CURVE A = 1-IN. CERAMIC RINGS, DESORPTION OF O_2 FROM H_2O AT 25° C. (*15*); O = ETHYLENE OXIDE — WATER SYSTEM CORRECTED TO OXYGEN-WATER SYSTEM AT 25°C.

variation in $(H.T.U.)_G(L')^{1/3}$ does not match the variation in solubility shown in Figure 2, but there is a partial correlation with surface tension of the solvent, since water and ethyl aceto acetate have higher surface tensions than have the other solvents.

Figure 6 compares the experimental results of $(H.T.U.)_L$ for the ethylene oxide–water system with the data obtained by Sherwood and Holloway (*15*) for the desorption of oxygen from water. The test results were first corrected to 25°C. by use of Sherwood and Holloway's recommended corrections for temperature variation. Then, based on the diffusivity of the ethylene oxide–water system the test values of $(H.T.U.)_L$ were converted to the oxygen-water basis, as at the same solvent flow rate $(H.T.U.)_L$ is inversely proportional to the one-half power of diffusivity. The diffusivity of the ethylene oxide–water system was estimated to be equal to the known value of the glycerine–water system (0.72×10^{-5} sq. cm./sec. at 20° C.) since ethylene oxide converts to a glycol upon hydrolysis. The test results lie reasonably close to the data of Sherwood and Holloway for 1-in. rings of curve A. The other solvent systems were not compared as their diffusivities are not known.

CONCLUSIONS

1. It is feasible to recover ethylene oxide from process waste gases by countercurrent absorption in a packed column. Of the solvents tested, ethyl alcohol, acetone, benzene, and ethyl aceto acetate require the lowest column height for a particular temperature and change in gas and liquor concentrations.

2. At room temperature the liquid-film resistance is controlling under practical conditions. At solvent temperatures below 0°C. the gas- and liquid-film resistances become comparable in magnitude.

3. The absorption of ethylene oxide gas in the high concentration range (10 to 46 mole %) can be correlated with adequate accuracy for most design purposes in terms of the conditions at the dilute end of the column.

4. The values of $(H.T.U.)_G$ and $(H.T.U.)_L$ for the ethylene oxide–water system agree generally with the known values for other systems. The $(H.T.U.)_L$ of the other solvents were not compared because of inadequate diffusivity data and insufficient published results on nonaqueous systems.

NOTATION

G = gas exit flow rate, lb. moles (hr.$^{-1}$) (ft.$^{-2}$)

G' = gas exit flow rate, lb./(hr.$^{-1}$) (ft.$^{-2}$)

H = absorption (packed) height of column, ft.

$(H.T.U.)_{OG}$ = height of over-all transfer unit, ft.

$(H.T.U.)_G$ = height of gas-film transfer unit, ft.

$(H.T.U.)_L$ = height of liquid-film transfer unit, ft.

K_Ga = over-all mass transfer coefficient, lb. moles/(hr.$^{-1}$) (ft.$^{-3}$) (atm.$^{-1}$)

L = solvent inlet flow rate, lb. moles/(hr.$^{-1}$) (ft.$^{-2}$)

L' = solvent inlet flow rate, lb./(hr.$^{-1}$) (ft.$^{-2}$)

N_{OG} = number of transfer units

a = interfacial area, ft.^{2}/ft.^{3}

k_Ga = gas film coefficient, lb. moles/(hr.$^{-1}$) (ft.$^{-3}$) (atm.$^{-1}$)

k_La = liquid film coefficient, lb. moles/(hr.$^{-1}$) (ft.$^{-3}$) lb. moles/ft.$^{-3}$)

m = slope of the equilibrium line on x-y coordinates

p = partial pressure of ethylene oxide in air, mm.

t = temperature, °C.

t_m = mean temperature, °C.

x = mole fraction of solute in body of liquid phase

y = mole fraction of solute in body of gas phase

$(1-x)_f$ = logarithmic mean of $1-x$ and $(1-x)$ at equil.

$(1-y)_f$ = logarithmic mean of $1-x$ and $(1-x)$ at equil.

Subscripts

B = bottom of the column

T = top of the column

LITERATURE CITED

1. Adams, F. W., *Trans. Am. Inst. Chem. Engrs.*, 25, 424 (1933).
2. Adams, F. W., and R. G. Edmonds, *Ind. Eng. Chem.*, 29, 447 (1937).
3. Colburn, A. P., *Trans. Am. Inst. Chem. Engrs.*, 35, 211 (1939).
4. Comstock, C. S., and B. F. Dodge, *Ind. Eng. Chem.*, 29, 520 (1937).
5. Dwyer, E., and B. F. Dodge, *Ind. Eng. Chem.*, 33, 485 (1941).
6. Haslam, R. T., W. P. Ryan, and H. C. Weber, *Trans. Am. Inst. Chem. Engrs.*, 15, 177 (1923).
7. Hutchings, L. E., L. F. Stutzman, and H. A. Koch, *Chem. Eng. Progr.*, 45, 253 (1949).
8. Kowlke, O. L., O. A. Hougen, and K. M. Watson, *Bull. Univ. Wis. Eng. Exp. Station, Ser.* 68, (1925).
9. Maxwell, J. C., *Phil. Mag.*, 20, 21 (1860).
10. Molstad, M. C., and L. F. Parsly, Jr., *Chem. Eng. Progr.*, 46, 20 (1950).
11. Osborne, H. B., and C. W. Simmons, *Ind. Eng. Chem.*, 31, 1105 (1939).
12. Perry, J. H., "Chemical Engineers' Handbook," p. 1151, McGraw-Hill Book Company, Inc., New York (1941).
13. *Ibid*, p. 379.
14. Scheibel, E. G., and D. F. Othmer, *Trans. Am. Inst. Chem. Engrs.*, 40, 611 (1944).
15. Sherwood, T. K., and F. A. Holloway, *Trans. Am. Inst. Chem. Engrs.*, 36, 39 (1940).
16. Sherwood, T. K., and R. L. Pigford, "Absorption and Extraction," p. 285, McGraw-Hill Book Co., Inc., New York (1952).
17. Stefan, J. *Ber. deut. Chem. Ges.*, 68, 385 (1873).
18. Whitman, W. G., *Chem. & Met. Eng.*, 29, 147 (1923).
19. Whitney, R. P., and J. R. Vivian, *Chem. Eng. Progr.*, 45, 323 (1949).

TRANSPORT OF MOMENTUM AND ENERGY IN A DUCTED JET

L. G. ALEXANDER, ARNOLD KIVNICK, E. W. COMINGS, and E. D. Henze
Engineering Experiment Station, University of Illinois, Urbana, Illinois

I. Experimental Study of a Nonisothermal Jet of Air Discharging into a Duct

A heated jet of air from an 0.898-in. standard A.S.M.E. nozzle was discharged into a 4-in. steel duct, well insulated over its entire 10-ft. length. Air from the region surrounding the nozzle was entrained into the duct. At a number of points along the duct, radial profiles of air velocity and temperature were obtained by means of a probe which combined an impact tube and a thermocouple. The temperature at each of several points along the duct wall was indicated by thermocouples imbedded in the wall.

In the experiments reported here the velocity at the jet was 585 ft./sec.; the temperature of the jet was about 220°F. and that of the entrained air was about 88°F. The total air flow rate through the duct was 0.67 lb./sec. and the heat flux was 4.9 B.t.u./sec., with the temperature of the entrained air taken as the datum.

The radial and axial profiles of velocity and temperature are compared and discussed; the temperatures of the stream near the duct wall and of the duct wall itself are given. Conservation of mass and heat was checked by graphical integration of the radial profiles.

The mixing of high-velocity gas streams is a problem of numerous facets, many of which have industrial importance. This study deals with gas mixers, jet-pumps, and ejectors—all examples of a jet discharging into a duct and entraining with it fluid from outside the duct entrance.

L. G. Alexander is at present at Oak Ridge National Laboratory, Oak Ridge Tennessee, Arnold Kivnick is with the Pennsylvania Salt Mfg. Co., Wyndmoor, Pennsylvania, E. W. Comings with Purdue University, Lafayette, Indiana, and E. D. Henz is at the Army Chemical Center, Maryland.

APPARATUS

The equipment used to supply the air, to heat it, and to control and meter its rate of flow, has been described previously (*1*). The experimental flow section used consisted of an approach section, a flow nozzle, a duct, and a probe. Figure 1 shows the details of the duct assembly. The approach section was fitted with five screens, to eliminate abnormal flow distribution upstream of the nozzle; with a thermocouple; and with a static pressure tap. The flow nozzle was a standard A.S.M.E. long-radius nozzle, approximately 0.9 in. diam. The duct was a 10-ft. length of 4-in. O.D. steel tubing, with thermocouples soldered into the wall at intervals. The axes of the duct and the flow

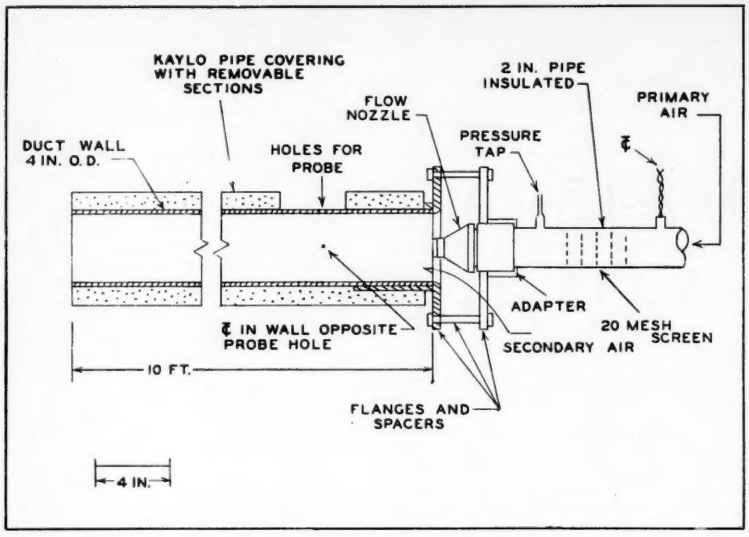

FIG. 1. DETAILS OF DUCT ASSEMBLY.

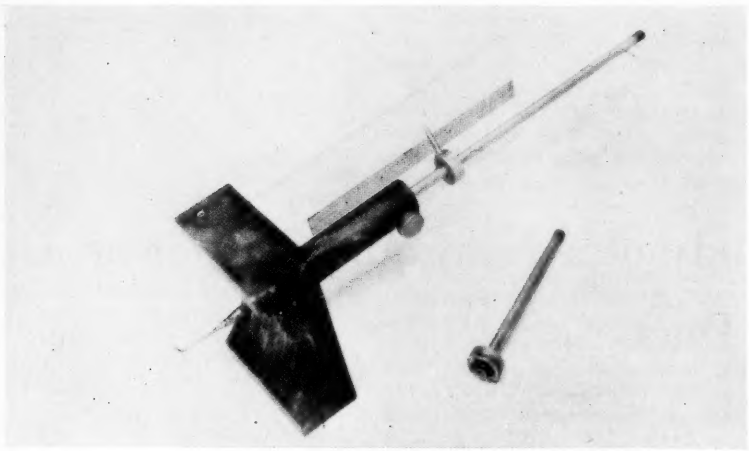

FIG. 2. TEMPERATURE-IMPACT PROBE.

nozzle were aligned by means of the flanges and spacers shown in Figure 2.

The duct was insulated with a 1-in. Kaylo pipe covering to prevent heat loss. An insulating material of high structural stability was required, for it was necessary to remove sections of the insulation repeatedly in order to place the probe holder.

The probe drawn in Figure 2 was made by bending a length of 0.065-in. O.D. hypodermic tubing to form a right angle. One side of the angle was 1.0 in. long with the open end carefully machined to the proportions recommended for sharp-edged Pitot tubes (2); the other side of the angle was soldered to a length of brass tube. Beyond the brass tube the thermocouple wires were cemented to the impact tube and were wound with thread to keep them in place. The wires were joined in a short twisted and soldered junction, placed just beneath the mouth of the impact tube. The positioning device on which the temperature - velocity probe was mounted was machined to fit on the outside surface of the duct; a scale was attached to the positioning device. A pointer was attached to the probe so that when the pointer was placed at the edge of the scale on the positioning device, the axis of the impact tube was oriented parallel with the axis of the duct, and the scale indicated the radial position of the impact tube. The probe was inserted into the duct through holes drilled at intervals in the duct wall. Static pressure readings were made through the same holes by means of a tube, the end of which had been machined so as to conform closely with the inner surface of the duct.

Pressures were measured by means of a manometer system which included a mercury manometer, a water manometer, and a Meriam draft gauge. Temperature readings were obtained by means of a potentiometer and copper-constantan thermocouples.

PROCEDURE

Before any experiments were made, the apparatus was checked to assure correct alignment of duct and nozzle, and of probe and positioning scale. Such checks were also made at intervals to assure the reliability of the measurements. The holes in the duct through which the probe might be inserted were spaced fixed distances apart; the distance from these holes to the nozzle was determined to the nearest 1/16 in.

All the data reported here were obtained at an air flow rate of 2.07 std. cu. ft./sec. The flow rate was indicated by the temperature and pressure upstream of the critical orifice meter. The metered air passed through heat exchangers where it was heated to 222° to 225°F. measured upstream of the flow nozzle.

One run was made to establish each profile. Several times during each run the pressure and temperature upstream of the critical orifice, the pressure and temperature upstream of the flow nozzle, the room temperature, and the barometric pressure were all checked to discover variation from the desired mean values. At the beginning and end of each run the static pressure probe was used to measure the static pressure at the duct wall. It was assumed that the static pressure was invariant across the duct. Since the axial positions at which static pressure was measured did not coincide with the positions of the profiles, the static pressures at various points along the wall were plotted vs. distance from the nozzle, and the pressure corresponding to the position at which the profile was determined was selected from a smoothed curve through the measured values. The wall temperature, T_w, was observed several times in each run.

A traverse was performed as follows. The probe was inserted into the desired hole in the duct and raised to its highest position at the top of the duct; then its position on the scale was noted. Next it was lowered to the bottom of the duct and that position noted. The axis position was assumed to be midway between the two extremes. In the course of preliminary runs this procedure was checked against the pressure profiles obtained, and in each case the geometrical centers coincided. Because of undue disturbance of the flow pattern by the brass tube supporting the impact tube when the probe was located below the center line of the duct and because of the symmetry of the duct, the profiles were observed only from the duct axis upward to the top of the duct.

INSTRUMENTATION

Velocity was measured by means of the modified impact tube, with the effect of turbulence upon the impact tube being ignored. Since the presence of the thermocouple immediately beneath the opening of the impact tube was thought likely to disturb the behavior of the instrument, the modified impact tube was checked by calibration against an ordinary impact tube. The presence of the thermocouple was found to have no noticeable effect. Hence, the velocity was calculated from the difference between the observed impact and static heads by the use of the calculated impact tube coefficients given by Taylor, Grimmett, and Comings(*10*).

The thermocouples soldered to the duct wall were checked against each other and against the probe thermocouple at three temperatures, and at no time did they show a difference greater than 1°F.

There was some question as to the significance of the temperature indicated by the probe thermocouple. At low velocities the indicated temperature, T_{in}, should approximate the free-stream temperature; at higher velocities the temperature should be between the stagnation temperature, T_s, and the free-stream temperature, T_f. Hottel and Kalitinsky(*7*) indicate that for twisted thermocouples the recovery factor should be between 0.79 and 0.83; that is,

$$\frac{T_{in} - T_f}{T_s - T_f} = R, 0.79 < R < 0.83 \quad (1)$$

The flow nozzle used in these experiments was designed to permit isentropic flow, and so the stagnation temperature downstream of the nozzle should be equal to the gas temperature upstream of the nozzle. Because the temperature upstream of the nozzle, and hence the stagnation temperature immediately downstream, were known, it was possible to determine the recovery factor experimentally. In one case the upstream temperature was 221°F., the temperature indicated by the thermocouple was 216°F., and the gas velocity was 585 ft./sec. The relationship among stagnation temperature, free-stream temperature, and velocity was based on the assumption that the stagnation temperature is obtained when all the kinetic energy of the flowing gas is converted to heat; that is,

$$T_s = T_f + \frac{\bar{u}^2}{2\,g_c \cdot 778 \cdot C_p}$$

where 778 ft. lb. force/B.t.u. is the mechanical equivalent of heat. By taking the specific heat of air to be 0.237 B.t.u./(lb. mass)(°F.), one obtains from this equation

$$T_s = T_f + \frac{\bar{u}^2}{11{,}900}$$

where the temperatures are in °F., and the velocity is in ft./sec.

For this case, then, the calculated free-stream temperature is

$T_f = 221 - (585)^2/11{,}900$
$= 193$°F., and $R = 0.82$.

CALCULATIONS

The results were computed by means of the following equations:

$$\overline{\rho u^2} = 2 g_c C_v^2 (5.2) \left[\Delta P + P_{atm} - \overline{P}\right] \quad (2)$$

$$\bar{u}^2 \cong \frac{\overline{(\rho u^2)}}{\rho} \quad (3)$$

$$\rho = \frac{(13.5\,P_{atm} + \overline{P})\,5.2}{53.35\,(T_f + 460)} \quad (4)$$

$$T_f = T_{in} - (0.82)\frac{\bar{u}^2}{11{,}900} \quad (5)$$

$$T_s = T_f + \frac{\bar{u}^2}{11{,}900} \quad (6)$$

$$W = 2\pi \int_0^{D/2} \rho \bar{u}\, r\, dr \quad (7)$$

$$\Delta T = T_s - T_i \quad (8)$$

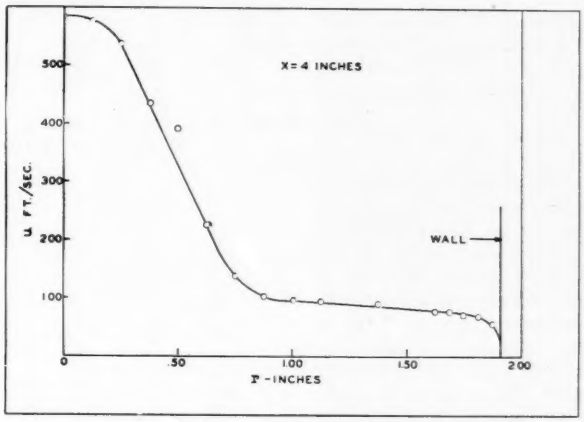

FIG. 3. TYPICAL VELOCITY PROFILE.

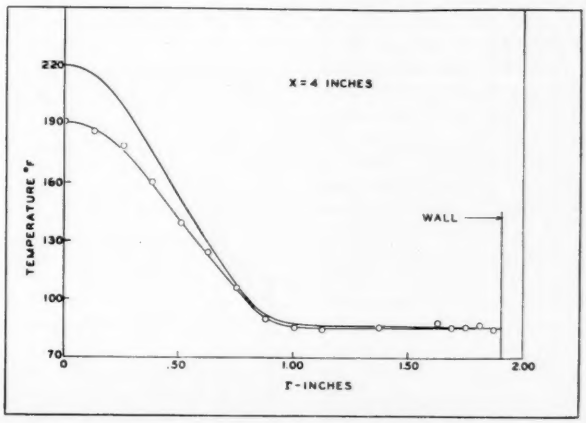

FIG. 4. TYPICAL PROFILE OF STREAM (LOWER CURVE) AND STAGNATION (UPPER CURVE) TEMPERATURE.

$$H = 2C_p\pi \int_0^{D/2} \rho\bar{u}\,\Delta T\, r\, ar \quad (9)$$

A trial and error procedure was necessary to solve for ρ, $\bar{u}$ and T_f. First C_f was assumed to be 1. Then $\overline{\rho u^2}$ was found from Equation (2). If T_f was assumed equal to T_{in} then ρ could be calculated from Equation (4). Then $\overline{u^2}$ was obtained by Equation (3). By the use of that value of $\overline{u^2}$, C_f was obtained(*10*), and T_f was found from Equation (5). Final values were obtained by iteration.

At each value of x the velocity was plotted as a function of r and a faired curve was drawn. Similar plots were made for T_f and T_s. In subsequent calculations the values of $\bar{u}$, T_f, and T_s were taken from the faired curve. Figures 5 and 6 are examples of such plots.

RESULTS

The experimental data are listed in Tables 1 through 4*. Profiles of temperature and velocity have been plotted in Figures 5 through 8. Those parts of the velocity profiles near the center of the duct resemble free-jet profiles (Figures 5 and 6). This resemblance persists down the duct until the jet spreads far enough to be affected by the presence of the duct wall. If the radial jet boundary is defined as the point at which the jet property being considered appears first to have been imparted to the entrained air stream, the jet boundary reached the wall at a point between 10 and 16 in. from the nozzle. The potential cone extended about 5 in. from the nozzle.

The temperature profiles are similar to the velocity profiles in the region near the duct axis, as seen from Figures 7 and 8. It is apparent that the jet boundaries defined in terms of stagnation temperature reach the duct wall sooner than the boundaries defined for velocity. The potential cone is shorter for the temperature case than for velocity. These phenomena are expected, in view of the experimentally observed fact that heat is transported more readily in turbulent systems than is momentum. The temperature profile across the nozzle is not nearly so flat as the velocity profile. This may be attributed to the impossibility of adequately insulating the nozzle to prevent heat flow through it. A similar phenomenon has been reported by Landis and Shapiro(*8*).

*Tables 1 through 4 (I A-D) are on file with the American Documentation Institute, Auxiliary Publications, Library of Congress, Washington 25, D. C., and may be ordered as document 4485 for $1.75 for microfilm and $2.50 for photoprints.

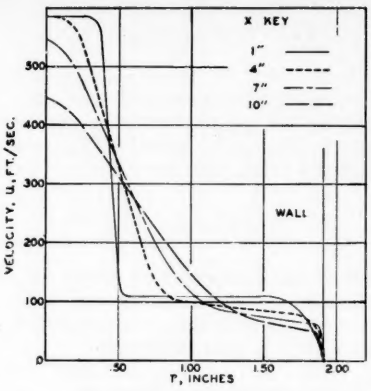

FIG. 5. VELOCITY-RADIAL PROFILE CLOSE TO NOZZLE.

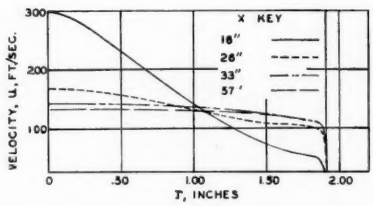

FIG. 6. VELOCITY-RADIAL PROFILES BEYOND $x = 10$ IN.

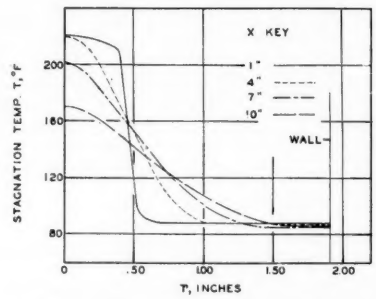

FIG. 7. TEMPERATURE-RADIAL PROFILES CLOSE TO NOZZLE.

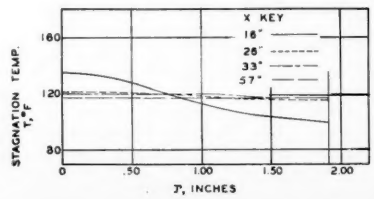

FIG. 8. TEMPERATURE-RADIAL PROFILES BEYOND $x = 10$ IN.

The axial profiles of velocity and temperature are compared in Figure 9. It is evident that the temperature begins to fall off before the velocity and that the rate of fall is greater.

In Figure 10 the stagnation temperature of air near the duct wall is compared with the duct wall temperature at various points. At 33 in. the air temperature rises smoothly to its maximum, the temperature of the fully mixed stream. The duct temperature is constant immediately downstream from the nozzle, rises to a maximum, then decreases to a minimum, and finally levels off at about 30 in.

The mass flux was determined at several values of x by plotting $\rho\bar{u}$ vs. r^2 and integrating under the curve. Figure 11 shows three such plots. Figure 12 indicates that the average mass flux was 0.67 lb./sec. and the most of the points deviate only slightly from the average. Heat flux was determined in a similar manner by plotting $\rho\bar{u}\ \Delta T$ against r^2 and integrating under the curve (Figure 13). The average heat flux was 4.9 B.t.u./sec. (Figure 14). The points scatter rather more than do those for mass flux.

DISCUSSION

The initial velocity profiles are similar to those of a free jet in a moving gas stream; however a significant difference occurs near the duct wall. The abrupt decrease in the velocity of the entrained air close to the wall cannot be attributed to wall friction at points near the duct entrance since the boundary layer at the wall should not yet have been built up; moreover, the wall friction should increase down the duct. Since the velocity gradient for the profile farthest down the duct is less sharp than for all profiles at distances less than 20 in., friction cannot explain the sharp velocity gradient near the duct wall.

For this phenomenon, previously discussed by Alexander et al.(*1*), several possible explanations can be presented. It may be due to choking, which occurs when the jet cannot discharge from the duct all the fluid induced by it. It may be due to a combination of static and impact tube effects in a region of entrainment and eddies. It may

also be a consequence of the relatively sharp duct entrance past which the entrained air flowed. In experiments subsequent to those described here, Danielson(*4*), duplicating this study, used an apparatus differing from the one employed here only in that the entry section was faired, as in a subsonic induction wind tunnel. The abrupt velocity decrease was eliminated.

The temperature profiles have the expected form (Figures 7 and 8). They support the contention that heat is more rapidly transported in turbulent systems than is momentum. This has been observed experimentally by several independent investigators(*5, 6*). The vorticity-transport theory of G. I. Taylor(*9*) was designed to present a phenomenological basis for these observations. This anomalous behavior can be allowed for readily in the mathematical treatment of free jets(*3*) by changing the value of an empirical constant in the equations for momentum and heat transport. Inasmuch as no fundamental mechanism of turbulence has yet been brought forward, the unequal rates of heat and momentum transport cannot be explained adequately.

An important difference exists between the velocity and temperature profiles. The velocity profiles indicate unusual gradients near the duct wall. However, no temperature gradients were observed at the duct wall at any cross section. The duct was insulated, and, since there was no heat flow through the wall, there should have been no temperature gradient at the wall. No reverse flow occurred; such a flow would have been from a region of high temperature to one of low temperature. Instead, the temperatures near the wall appeared to fall off slightly immediately downstream of the nozzle, before they rose because of mixing with the heated jet. This decrease in temperature might be explained as follows. The temperatures plotted on Figures 7 and 8 are stagnation temperatures, which include the effect of kinetic energy carried by the mean component of the axial stream velocity. No account has been taken of the energy carried by the turbulent velocity components, which are unquestionably large in the region being considered because of the sharp-cornered entry. If the energy involved in these fluctuating velocities could be taken into account, it is likely that the stagnation temperatures near the wall would be approximately constant until the jet boundaries reach the wall, where they should begin to rise. The only effect to be expected from the tendency for back-flow in the absence of actual reverse flow should be a change in the rate of rise of temperature. Since no data are available for the case without tendency for backflow, it is not possible to detect this tendency by comparison.

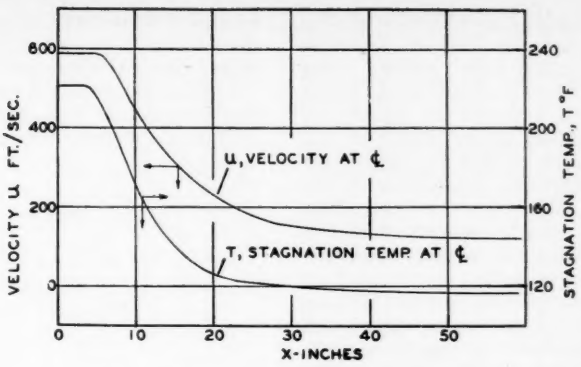

FIG. 9. AXIAL PROFILES—VELOCITY AND TEMPERATURE.

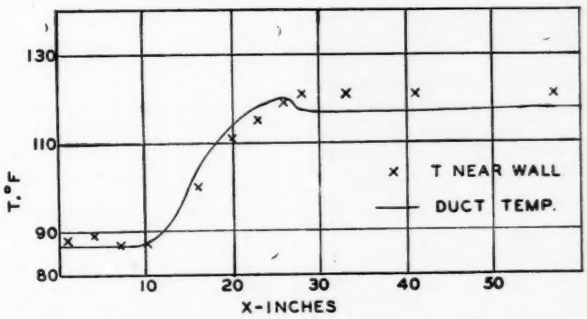

FIG. 10. TEMPERATURES OF DUCT AND AIR NEAR DUCT.

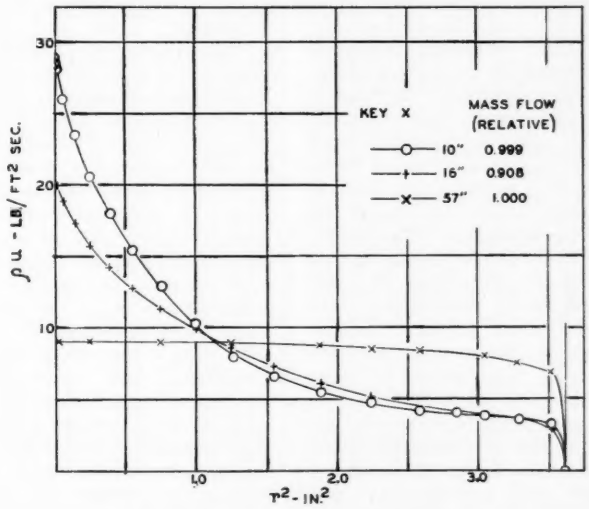

FIG. 11. TYPICAL MASS-FLUX PLOTS.

The unusual pattern of wall temperatures is puzzling. As shown in Figure 15, this pattern was checked at various air rates. In all cases the temperature reached a maximum at 26 in. At 28 in. the temperature either leveled off or passed through a minimum in the case of higher jet velocities. This unusual behavior was not caused by erroneous thermocouple readings: the thermocouples were checked when hot air was passed through the duct, the duct was plugged, and the indicated temperatures were observed as a function of time. The temperatures were high at the downstream end of the duct and lower at the upstream end because of heat loss from the duct through the flange at the upstream end to the ambient air. But the progression of temperatures was a smooth one, indicating no erratic thermocouples. Nor was the behavior attributable to heat conduction from the duct to its supports. There were no supports in the region from 10 to 36 in. downstream of the nozzle.

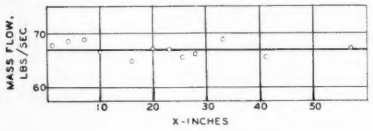

FIG. 12. MASS-FLUX VARIATION WITH x.

The following speculative mechanism may explain the wall temperatures. The wall was alternately heated by hot eddies and cooled by cold ones, and the resulting wall temperature depended more upon the maximum temperature, that of the hottest eddies, than upon the mean air temperature. This mechanism existed in the region immediately downstream from the jet, as far as 26 in. downstream. At another region of the duct the gas was mixed sufficiently so that its temperature was relatively constant, subject to minor fluctuations. In this region heat transfer to the wall from the air stream was a function of the mean temperature, and the wall temperature approached the temperature of the mixed gases. Heating by distinct eddies occurred near the nozzle; heating by the mean fluid stream occurred after the jet boundaries had spread as far as the wall. The transition between the two modes of transfer was sharp; hence the wall temperature fell sharply when the heat transfer changed from dependence upon hot, turbulent eddies to dependence on a moderately warm, low-turbulent stream.

If this explanation is correct, one would expect to find that at high velocities under conditions of greater turbulence, the effect of hot eddies would be enhanced since the heat transfer rate is increased by high turbulence. Further, the transition between the two modes of heat transfer would be more pronounced. Figure 15 indicates this to be true.

The stagnation temperature of the air close to the duct wall also presents an unusual problem. Since the wall must be heated by the air, the second law of thermodynamics would preclude the wall temperature from being higher than that of the air, as is apparently the case between 10 in. and 28 in. as indicated in Figure 10. There are several possible explanations for this phenomenon. First, because of the high turbulence present in the region close to the wall in the vicinity mentioned, the stagnation temperatures computed might not be correct, since under conditions of high turbulence the turbulent velocity components might bear a substantial portion of the total kinetic energy; the stagnation temperatures might therefore be appreciably higher than those calculated from mean velocity measurements. Second the effect of alternate hot and cold eddies on a thermocouple is not necessarily the same as the effect of those eddies on a solid wall. In either case, the calculated values would be in error.

At positions beyond $x = 28$ in. the stagnation temperature near the wall is constant at a value higher than the duct wall temperature; the stream temperature, however, is equal to that of the duct wall, as expected for an insulated wall.

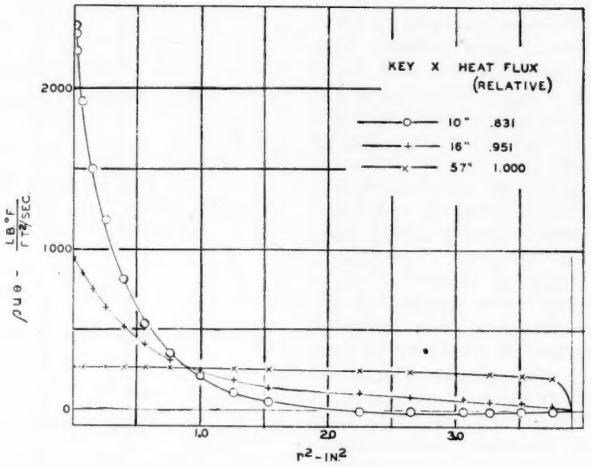

FIG. 13. TYPICAL HEAT-FLUX PLOTS.

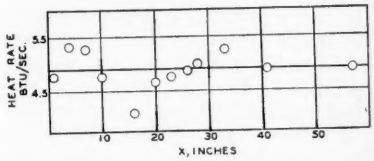

FIG. 14. HEAT-FLUX VARIATION WITH x.

The mass balance along the duct is satisfactory, Figure 12. If the value at 16 in. is disregarded, the mean deviation from the average mass flux is 1.4%, and the maximum deviation is 2.4%. the heat balance, since it must reflect the errors in temperature measurement as well as those in velocity measurement, is less precise, Figure 14. The mean deviation from the average heat flux is 4.1%; the maximum deviation is 8.6%; again, the profile at 16 in. has been disregarded.

SUMMARY

Profiles of temperature and velocity were measured for the case of a jet of air at 585 ft./sec. and 222°F. discharging into an insulated duct and entraining air at 88°F. The temperature of the wall at several points along its length was also measured. From these measurements heat and mass fluxes

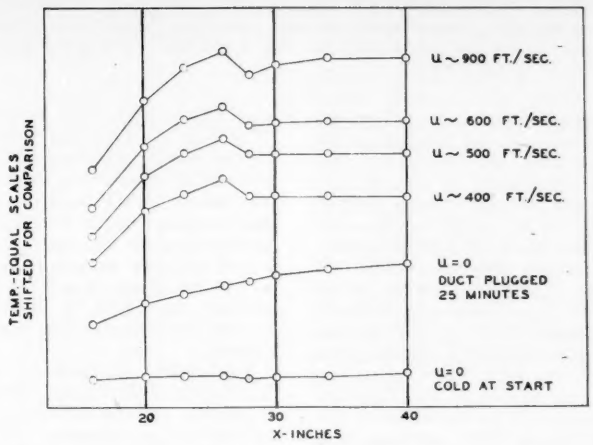

FIG. 15. VARIATION OF WALL TEMPERATURES WITH AIR RATE.

were computed at several points along the duct. The deviation of the measured values of mass flux from the mean value was small; the corresponding deviation in the case of heat flux was appreciably larger.

ACKNOWLEDGMENT

This work was performed as a part of a research program in the Engineering Experiment Station of the University of Illinois on the mixing of high-velocity gas streams. The main investigation was begun in 1946 under Contract N6-ori-71 Task XI with the Office of Naval Research. It was supported during the period from October 1, 1950, to December 31, 1951 under Contract DA-18-064-CML-445 with the Army Chemical Corps.

NOTATION

C_f = impact tube coefficient
C_p = specific heat at constant pressure
c = momentum-spreading coefficient, empirical constant in Equation (19)
g_c = 32.2 ft. lb. (mass)/lb. (force) sec.^{2}
H = energy flux at any section. B.t.u./sec.
P = static pressure in duct
P_{atm} = static pressure in atmosphere
ΔP = pressure indicated by manometer, one end connected to a total head impact tube in a duct and the other open to the atmosphere
R = thermocouple recovery factor, Equation (1)
r = radial coordinate, distance from axis of duct
T = temperature
ΔT = temperature difference, Equation (8)
u = x-directed component of velocity
W = mass flux at any section, lb./sec.
x = axial coordinate, distance along axis of duct from nozzle
ρ = density of fluid

Subscripts

atm = atmosphere
f = free stream or static condition
i = induced stream conditions in plane of nozzle
in = indicated by thermocouple
n = upstream from flow nozzle
or = upstream at orifice
s = stagnation
w = condition in duct wall

LITERATURE CITED

1. Alexander, L. G., E. W. Comings, H. Grimmett, and E. W. White, *Chem. Eng. Progr. Symposium Series No. 10*, **50**, 93 (1954).
2. "Fluid Meters, Their Theory and Application," 4th ed., Am. Soc. Mech. Engrs. (1937).
3. Baron, T., and L. G. Alexander, *Chem. Eng. Progr.*, **47**, 181 (1951).
4. Danielson, R. D., M. S. Thesis, Univ. Illinois (1953).
5. Forstall, W., and A. H. Shapiro, *J. Appl. Mechanics*, **17**, 399 (1950).
6. Hinze, J. O., and B. G. van der Hegge Zignen, *Appl. Sci. Research*, A-1, 435 (1949).
7. Hottel, H. C., and A. Kalitinsky, *J. Appl. Mechanics*, **12**, 25 (1945).
8. Landis, F., and A. H. Shapiro, Preprints of papers presented at the Heat Transfer and Fluid Mechanics Institute (1951).
9. Taylor, G. I., *Proc. Roy. Soc. (London)*, **135A**, 685 (1932).
10. Taylor, J. F., H. L. Grimmett, and E. W. Comings, *Chem. Eng. Progr.*, **47**, 175 (1951).

II. Theoretical Study of Turbulent Transport of Momentum, Energy, and Matter in Ducted Coaxial Streams

This paper concerns the kinetics of the processes that take place when a high-velocity jet of fluid mixes turbulently with a low-velocity, induced stream of the same fluid in a duct of uniform diameter. Semi-two-dimensional solutions of the equations of transport involving two empirical coefficients were obtained by application of Reichardt's hypothesis and three assumptions: (*a*) a negligible fraction of the flow entity (energy, mass, or momentum) is lost at the wall and the presence of the boundary layer may be ignored, (*b*) the static pressure is uniform over a section of the duct, and (*c*) the turbulence pattern is similar to

that in free jets except that the duct wall limits the growth of the scale of the turbulence. A mixing index, which is a measure of the degree to which the jet stream remains unmixed with the induced stream at any point, was defined and related to the geometry of the system and the flow parameters by means of the theoretical equation, and a method of evaluating the empirical coefficients for a typical case of momentum transport was described.

The physics of the exchange of energy, mass, and momentum between fluid streams is of theoretical and practical importance. Examples of application are jet pumps, Venturi atomizers, spray driers, combustion chambers, and gas burners.

Fluid-mixing processes fall into two general categories: the isobaric, as in free jets, and the nonisobaric, as in the jet ejector. An idealized example of the latter consists of a circular nozzle discharging an incompressible fluid into a cylindrical duct open at both ends to a second fluid. If the momentum losses can be estimated or neglected, the flow rates may be determined from jet- and induced-stream stagnation pressures and temperatures, flow areas, and discharge pressure by well known methods of thermodynamics.

Qualitatively the mixing of the streams is conceived to proceed as follows. The high-velocity jet stream imparts momentum to the fluid in the duct, causing it to flow toward the discharge. This lowers the pressure at the inlet, whereupon exterior secondary fluid begins to flow into the duct. Eventually a steady state is reached. In the induced stream the static pressure falls between the inlet and the plane of the jet nozzle, where the mixing process begins. The momentum, mass, and energy of the jet stream spread by turbulent convection into the secondary stream, and the static pressure rises toward the discharge pressure. If the mixing tube is long, so that mixing is nearly complete in, for example, one third of the length, then the static pressure must rise above the discharge pressure by an amount sufficient to overcome the resistance to flow of the remaining two thirds of length.

The purpose of this research was to set forth quantitatively the kinetics of the mixing process in such systems.

HISTORY

General. The literature on the mixing of fluid streams in a duct is too extensive to be reviewed in detail here. The greater part of the work deals with the over-all dynamics of jet ejectors. The thermodynamic theories appear to be satisfactory, and predictions of the optimum design of ejectors have been reasonably well verified by numerous experiments.

In contrast, theoretical and experimental studies of the kinetics of the mixing process are relatively few. Some investigations of the over-all performance included limited tests to ascertain that the lengths of the mixing sections were at least adequate. The conclusions have been of an approximate nature and are not all in agreement. It is generally thought that the length of the mixing section should be from four to eleven times the diameter, with seven diameters probably optimum (*8, 10, 12*). Opinions differ concerning the variation of this optimum length with entrance and exit geometry and pressures and with the velocities of the jet and induced streams (*8, 11, 12*). Of the experimental investigations of the mixing process, those of Forstall and Shapiro (*7*), Ledgett (*11*), Ferguson (*5*), Reid (*14*), and Viktoren (*15*) are significant. These authors measured impact pressures at various points in the zone of mixing. Ledgett and Viktoren also measured static pressures throughout this zone, and their results agree qualitatively with the description given in this introduction.

Flugel's (*6*) analysis involves the crude assumption that at any cross section individual average velocities may be assigned to the high-velocity core and the low-velocity flow surrounding it. The drag force between the two streams is then equated to the product of the square of the difference between their velocities and an empirical drag coefficient. His equations satisfy the momentum balance but have little relation to the mechanics of the mixing process.

Viktoren (*15*) obtained a solution that approximates the flow pattern in the limited region of mixing where the distance from the nozzle is sufficiently great that the jet may be regarded as a point source of mass and momentum and yet sufficiently close to the nozzle that the spreading of the jet is not affected by the presence of the wall. His assumptions were that (*a*) the pressure is uniform throughout the mixing tube, (*b*) the mixing processes in cross sections at various distances from the nozzle are geometrically and mechanically similar, and (*c*) the Prandtl mixing length lp is uniform over a cross section and, moreover, proportional to the width of the mixing zone. These assumptions seriously limit the value of his solution. In some cases, as with jet pumps, the pressure rise in the mixing tube is the most important effect. It is clear that the flow profiles and mixing processes cannot be similar, as supposed by Viktoren, except in a limited region which may not exist at all unless the jet nozzle is very small compared with the duct. That is, for a point-source jet the successive flow profiles will be similar as in a free jet until the spread of jet momentum is inhibited by the wall. But it is precisely a knowledge of the effect of the wall on the mixing process that is desired. A solution limited to the region in a duct where the flow approximates that in a free jet gives no information concerning the length of duct required to mix the two streams to any given degree.

Reichardt's Hypothesis. Herman Reichardt, of Göttingen, has proposed a formula for the turbulent shearing stress (*13*). In previous publications from this laboratory (*1*) the singular success of Reichardt's hypothesis and the principle of superposition deduced from it by Baron and Alexander (*3*) in correlating measurements in free jets was demonstrated. The flow pattern in the region adjacent to the nozzle was predicted with reasonable success. The treatment also was applied in the region of confluence of twin parallel jets and in the region of flow of a free jet parallel to a plane surface (*1*). Reichardt's hypothesis has been generalized to include the transport of heat and mass in a free turbulent jet (*3*).

The hypothesis relates the turbulent shearing stress to the gradient of the momentum flux density.

$$\rho \overline{uv} = -\Lambda \frac{\delta \overline{\rho u^2}}{\delta r} \qquad (1)$$

where Λ is a scale factor somewhat analogous to Prandtl's mixing length and is to be related to the boundary conditions. Setting Λ equal to $\frac{c^2 x}{2}$ leads to the well known distribution of momentum flux in a free jet (*1*) where c is reasonably invariant. There appear to be some second-order variations in c with changes in boundary conditions, but these have not been delimited (*1*).

KINETICS OF MIXING IN THE DUCTED JET

General Solution. When viscous and body forces may be neglected, the equation of motion for axially symmetrical turbulent flow becomes (*1*)

$$\frac{\delta \overline{P}}{\delta x} + \frac{\delta \overline{\rho u^2}}{\delta x} + \frac{1}{r}\frac{\delta}{\delta r}\left[r \overline{\rho uv}\right] = 0 \qquad (2)$$

where x and r are axial and radial coodinates, u and v are axial and radial components of velocity, P is the static pressure, and ρ is the density. The bar denotes time average values:

$$\overline{P} = \lim_{\theta \to \infty} \frac{1}{\theta} \int_{\theta_o}^{\theta_o + \theta} P \, d\theta \qquad (3)$$

where θ is the time of observation.

Application of Reichardt's hypothesis with certain approximations leads to a semi-two-dimensional solution of the axial flow in a tube with mixing induced by a jet. Substitution of Equation (1) into Equation (2) gives

$$\frac{\delta \overline{P}}{\delta x} + \frac{\delta \overline{\rho u^2}}{\delta x} - \frac{1}{r} \frac{\delta}{\delta r} \left[r \Lambda \frac{\delta \overline{\rho u^2}}{\delta r} \right] = 0 \qquad (4)$$

The sum $\overline{P} + \overline{\rho u^2}$ is recognized as the total momentum. If it is assumed that the static pressure is uniform over a cross section, then

$$\frac{\delta \overline{P}}{\delta r} \cong 0 \qquad (5)$$

Equation (5) is almost certainly untrue in detail. Measurements of the static-pressure distribution reported in the literature are meager and equivocal. Viktoren(*15*), studying a system employing water for both jet and induced fluids, found large apparent variations across the duct near the jet nozzle and concluded that static-pressure measurements in such regions are not reliable. Ledgett(*11*), however, using air, studied a system very similar to that treated here and found the variations to be less than 10% of the dynamic head in the same region. Hence Equation (5) is probably a reasonably good first approximation. Equation (4) may be written

$$\frac{\delta}{\delta x} (\overline{P} + \rho \overline{u^2}) - \frac{1}{r} \frac{\delta}{\delta r} \left[r \Lambda \frac{\delta}{\delta r} (\overline{P} + \rho \overline{u^2}) \right] = 0 \qquad (6)$$

This equation is linear in $\overline{P} + \rho \overline{u^2}$ and a solution may be obtained in orthogonal functions.

To simplify the boundary conditions, a variable, M, is introduced such that

$$M = \frac{m - m_\infty}{m_{j,\,avg} - m_{i,\,avg}} \qquad (7)$$

and

$$m = \overline{P} + \rho \overline{u^2} \qquad (8)$$

where the subscript j denotes the initial jet stream; i, the initial induced stream; ∞, the final, completely mixed stream. In the definition of m_x, it is assumed that friction drag at the walls may be neglected and that the final distribution of momentum flux is uniform over a cross section. To simplify the mathematics, only the case where m_j and m_i are uniformly distributed in the plane of the nozzle discharge will be treated; however, any arbitrary distribution can be treated. The variable M satisfies Equation (6), which may be written

$$\frac{\delta M}{\delta x} - \frac{4}{r_* D^2} \frac{\delta}{\delta r_*} \left[r_* \Lambda \frac{\delta M}{\delta r_*} \right] = 0 \qquad (9)$$

where D is the diameter of the duct, and r_* is a normalized radial coordinate such that

$$r_* = \frac{2r}{D} \qquad (10)$$

If it is assumed that λ is a function of x only, a solution is readily obtained by separating the variables.

$$M = \left[A J_o (K r_*) + B Y_o (K r_*) \right] exp - \int_o^x \frac{4K^2 \Lambda}{D^2} dx \qquad (11)$$

Differentiation with respect to r_* gives

$$\frac{\delta M}{\delta r_*} = \left[AK J_1 (K r_*) + BK Y_1 (K r_*) \right] exp - \int_o^x \frac{4K^2 \Lambda}{D^2} dx \qquad (12)$$

The boundary condition that

$$\frac{\delta M}{\delta r_*} = 0; \; r_* = 0 \qquad (13)$$

requires that both terms in the bracket vanish on the axis. Then

$$J_1 (0) = 0 \qquad (14)$$

as required, but

$$Y_1 (0) = - \infty \qquad (15)$$

hence

$$B = 0 \qquad (16)$$

Neglecting friction requires that no momentum be lost at the wall; hence

$$\frac{\delta M}{\delta r_*} \cong 0; r_* = 1 \qquad (17)$$

This condition is satisfied by Equation (12) provided K is a root of J_1.

The particular solutions may now be combined:

$$M = \sum_1^\infty A_n J_o (a_n r_*) exp - \int_o^x \frac{4 a_n^2 \Lambda}{D^2} ax \qquad (18)$$

where a_n is the n-th root of J_1.

The quantity Λ is probably related to the scale and intensity of the turbulence. In the vicinity of the nozzle the turbulence pattern should be similar to that in the corresponding region in a free jet. Far from the nozzle, the duct wall modifies the flow in at least two ways: it (*a*) confines the flow of momentum and (*b*) modifies the turbulence pattern in that the turbulence in the vicinity of the wall is damped. This latter phenomenon is associated with the transfer of momentum to the wall by a boundary layer. Since friction at the wall has been neglected throughout, the only mathematically expressible property of the wall left is that of being a geometric boundary, and its action is represented by Equation (17). The corollary assumption regarding Λ, then, is that it is constant across a section and is a function only of x.

Implicit in these assumptions is the prediction that because of the high level of turbulence generated by the jet, the velocity profile will become substantially uniform over the duct before the boundary layer has time to develop significantly.

In fully developed turbulent flow in a pipe the turbulence level is only about 3%. In free jets the level reaches 20% and higher(*4*). With a jet mixing in a duct, the turbulence level will decrease from that of a free jet to that of normal pipe flow. On the other hand, the

scale of turbulence, as measured by Λ, cannot grow indefinitely in a duct, as it does in a free jet, and the relation between Λ and x must take this into account. A purely arbitrary function that reduces to the free-jet relation in the vicinity of the nozzle, but which imposes on Λ an upper limit which is a function of the duct diameter, is

$$\Lambda = \frac{c^2 x}{2\left[1 + \frac{bx}{D}\right]} \tag{19}$$

where b and c are empirical coefficients. Substitution of this into Equation (18) followed by integration gives

$$M = \sum_1^\infty A_n J_o(a_n r_*)\, exp\left\{ - \frac{2a_n^2 C^2}{b^2}\left[\frac{bx}{D} - \ln\left(1 + \frac{bx}{D}\right)\right]\right\} \tag{20}$$

For the case where b is zero, this reduces to

$$M = \sum_1^\infty A_n J_o(a_n r_*)\, exp\left[-a_n^2\left(\frac{cx^2}{D}\right)\right] \tag{21}$$

The remaining boundary conditions are

$$M \longrightarrow 0 \text{ as } x \longrightarrow \infty$$

and

$$M_o = f(r_*)$$

where the subscript o denotes the plane of the jet nozzle. The first condition results from the fact that m approaches m_∞ and is satisfied by the exponential term, which tends toward zero as x increases without limit. The second condition is imposed on the A_n by use of the Bessel series.

$$A_n = \frac{2}{J_o^2(a_n)} \int_o^1 r_* M_o J_o(a_n r_*)\, dr_* \tag{22}$$

Although any arbitrary initial profile of total momentum can be imposed on the A_n, the only case developed here will be that where the jet velocity is uniform over the plane of the nozzle and the velocity of the induced stream is uniform in the same plane. It follows that

$$M_j = \frac{m_j - m_\infty}{m_j - m_i};\ 0 < r_* < \frac{d}{D} \tag{23}$$

where d is the diameter of the jet nozzle and

$$M_i = \frac{m_i - m_\infty}{m_j - m_i};\ \frac{d}{D} < r_* < 1 \tag{24}$$

Substitution in Equation (22) and integration results in

$$A_n = \frac{2\frac{d}{D} J_1\left(a_n \frac{d}{D}\right)}{a_n J_o^2(a_n)} \tag{25}$$

Thus the definition of M chosen in Equation (18) renders the A_n dependent only on the ratio d/D and independent of the initial velocities for the case under consideration.

The quantity m_∞ may be evaluated from the fact that the total momentum, with friction neglected, is conserved. Thus

$$\int_o^1 M 2\pi r_*\, dr_* = \text{const}\ (=0) \tag{26}$$

Since M tends toward zero with increasing x, the constant must be zero. Substitution of Equations (23) and (24) into Equation (26) followed by integration and solution for m_∞ gives

$$m_\infty = m_j\left(\frac{d}{D}\right)^2 + m_i\left[1 - \left(\frac{d}{D}\right)^2\right] \tag{27}$$

The principal defect of the treatment given here is that a knowledge of M does not immediately yield information concerning the distribution of the static pressure, $\overline{P}$, nor of the flow momentum, $\overline{\rho u^2}$. A knowledge of the distribution of the turbulence intensity is required. It is thus desirable to expand the flow variables in mean and fluctuating components, as follows:

$$\begin{aligned} u &= \bar{u} + u' \\ v &= \bar{v} + v' \\ \boldsymbol{P} &= \overline{P} + P' \end{aligned} \tag{28}$$

where the mean value is denoted by the bar and the primed quantity is the fluctuating component. By definition

$$\begin{aligned} \overline{u'} &= 0 \\ \overline{v'} &= 0 \\ \overline{P'} &= 0 \end{aligned} \tag{29}$$

Combining Equation (8) and (28) gives

$$\rho\bar{u} = \sqrt{\rho\,(m - \overline{P} - \rho\overline{u'^2})} \tag{30}$$

whence the total flux of mass is obtained by integrating $\overline{\rho u}$ over a cross section.

$$\int_o^1 \frac{D^2}{2}\sqrt{\rho\left(m - \overline{P} - \rho\overline{u'^2}\right)}\pi r_* dr_* = \text{mass flux} \tag{31}$$

The distribution of m may be obtained from that of M. To evaluate $\overline{P}$ and obtain the distribution of $\overline{\rho u^2}$ at any cross section, it is necessary to choose values of $\overline{P}$, perform the integration numerically, and compare the result with the integral mass flux until agreement is obtained. However, there is no satisfactory way of estimating $\overline{u'^2}$ and experimental data are nonexistent. Possibly the best course at present is to assign to $\overline{u'^2}$ an average value, based on Corrsin's free-jet data (*4*), of 0.04 $\overline{u^2}$.

The tedious procedure outlined above is neither necessary nor desirable for comparing Equations (20) and (21) with measured values. If the turbulence components are to be neglected or approximate values used, it is better to do so in connection with the quantity m.

In experimental work the flow is conveniently explored with a total-head impact tube connected to a manometer having one arm open to the atmosphere. Unfortunately impact-tube measurements do not immediately yield a knowledge of $\overline{\rho u^2}$ (*1*). So far as turbulence is con-

cerned, impact tubes should respond in (locally) incompressible flow according to the equation

$$\Delta P = \overline{P} + \frac{\rho\overline{u^2} + \rho(\overline{v'^2} + \overline{w'^2})}{2g_c C_f^2} - P_{atm}$$

To obtain $\rho\overline{u^2}$, a knowledge of $\overline{v'^2}$ and $\overline{w'^2}$ is required. Since this is, in general, not available, these terms must be neglected, and approximately

$$m \cong 2g_c C_f^2 (\Delta P + P_{atm} - \overline{P}) + g_c\overline{P} \qquad (32)$$

where ΔP is the manometer pressure reading in consistent units, C_f is an impact-tube coefficient, and P_{atm} is the atmospheric pressure.

The Mixing Index. There is as yet no way of predicting the values of the constants b and c, in Equation (19). In free jets discharging into a stagnant atmosphere, c ranges from 0.07 to 0.08 with a small variation with position in the jet, nozzle geometry, and discharge velocity(*1*). Calculations based on the data of Forstall and Shapiro(*7*) for a free jet discharging into a moving secondary stream give values of c down to 0.01 as the velocity of the secondary stream approaches the jet velocity(*9*).

Point-by-point application of Equations (20) and (21) is not a satisfactory means of evaluating b and c from experimental data. It is preferable that these be determined from a plot of the axial distribution of some function integral in r. Linear plots are to be desired but are not always obtainable. If wall friction is neglected, the total momentum flux is conserved, and the axial distribution of the left-hand member of Equation (26) gives no information concerning c and b. However, the integral of the square of the momentum flux density is not conserved and may be used to define a mixing index in terms of the deviation of the square of the momentum-flux density from the average value; thus

$$\gamma = \int_0^1 (M - M_{avg})^2 \, 2\pi r_* dr_* \qquad (33)$$

where

$$M_{avg} = \int_0^1 M d(r_*^2) \qquad (34)$$

But the latter integral has already been shown to be zero. Hence M_{avg} is zero. Substitution now from Equations (20) and (25) into Equation (33) gives

$$\gamma = \int_0^1 \left\{ \sum_1^\infty \frac{2\frac{d}{D} J_1\left(a_n \frac{d}{D}\right)}{a_n J_o^2(a_n)} J_o (a_n r_*) \exp - \frac{2a_n^2 c^2}{b^2}\left[\left(\frac{bx}{D}\right) - \ln\left(1 + \frac{bx}{D}\right)\right]\right\}^2 2\pi r_* dr_* \qquad (35)$$

From the orthogonality of the series,

$$\int_0^1 r_* J_o(a_k r_*) J_o(a_n r_*) dr_* = 0 \qquad (36)$$

for $k \neq n$, whereas

$$\int_0^1 r_* J_o^2 (a_n r_*) dr_* = \frac{1}{2}\left[J_o^2(a_n) + J_1^2(a_n)\right] \qquad (37)$$

Hence, integration of Equation (35) leads to the equation

$$\gamma = 4\pi\left(\frac{d}{D}\right)^2 \sum_1^\infty \frac{J_1^2\left(a_n \frac{d}{D}\right)}{a_n^2 J_o^2(a_n)} \exp - \frac{4a_n^2 c^2}{b^2}\left[\left(\frac{bx}{D}\right) - \ln\left(1 + \frac{bx}{D}\right)\right] \qquad (38)$$

which converges rapidly except for small values of x. For the case where b is zero, Equation (38) reduces to

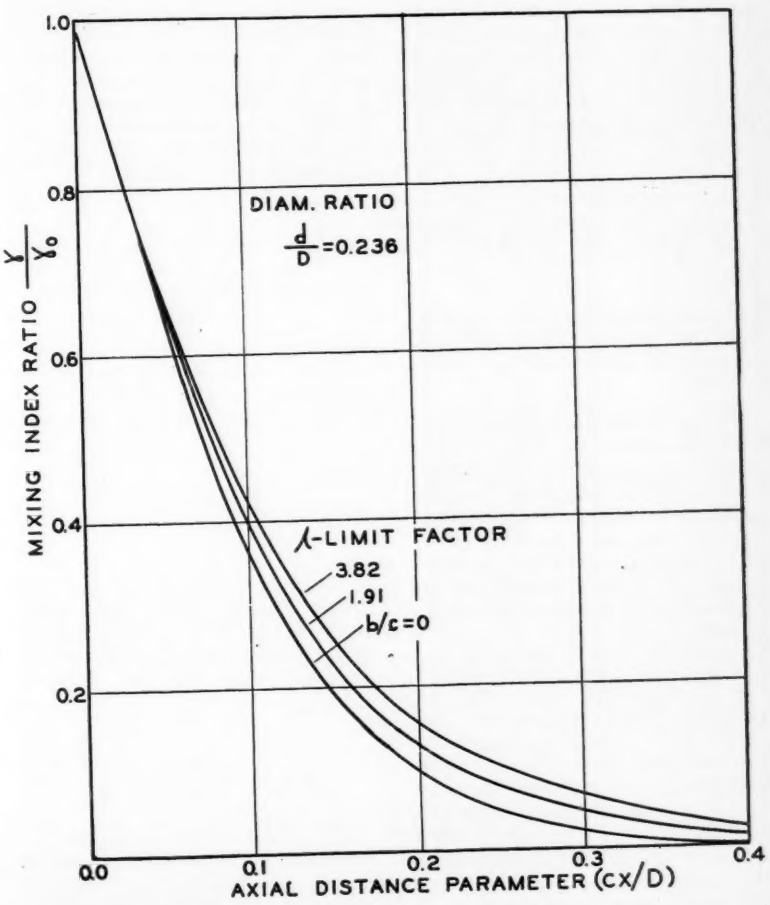

FIG. 1.

$$\gamma = 4\pi\left(\frac{d}{D}\right)^2 \sum_1^\infty \frac{J_1^2(a_n \frac{d}{D})}{a_n^2 J_o^2(a_n)} exp - 2a_n^2\left(\frac{cx}{D}\right)^2 \quad (39)$$

TABLE 1.—THE MIXING INDEX

Calculated from Equations (38) and (39) with $d/D = 0.23\gamma$

Axial distance parameter, cx/D	Λ-Limit factor, b/c		
	0	1.91	3.81
	Mixing index, γ		
0.00	0.1650	0.1650	0.1650
0.02	0.1408	0.1408	0.1408
0.04	0.1155	0.1200	0.1205
0.06	0.0975	0.0996	0.1018
0.08	0.0771	0.0779	0.0837
0.10	0.0606	0.0649	0.0683
0.15	0.0313	0.0371	0.0413
0.20	0.0163	0.0215	0.0258
0.30	0.0035	0.0076	0.0109
0.40	0.0005	0.0020	0.0045

Inspection of Equation (38) shows that γ approaches zero as x increases and that the initial value, γ_o, is dependent only on the diameter ratio, d/D. It may be evaluated by substitution from Equations (23) and (24) into Equation (33) followed by integration, whence

$$\gamma_o = \pi\left(\frac{d}{D}\right)^2\left[1 - \left(\frac{d}{D}\right)^2\right] \quad (40)$$

The mixing index, γ, may also be evaluated from experimental data by graphical integration of Equation (33).

Values of the mixing index have been calculated. In order to generalize the calculations, they were carried out by assigning various values to an axial distance parameter cx/D and to a Λ-limit factor, b/c. The results are listed in Table 1 and are shown graphically in Figure 1 for a diameter ratio, d/D, of 0.236.

For given values of x, b, and c, the corresponding value may be found readily by interpolation. The values of b/c chosen correspond to the condition that if c is 0.075, then Λ will have increased in seven duct diameters to the fractions 0, 1/2, and 2/3 of its maximum value respectively. It is seen that limiting the growth of Λ does not affect the decay of γ greatly except at small values of γ/γ_o.

Experimental data will show some loss of momentum through friction at the wall. This nonconservation of the experimentally determined flux of total momentum presents a difficulty in calculating the mixing index, γ, from the data. If m_x is calculated from Equation (27), Equation (26) is not borne out by the experimental measurements. It is important that the data satisfy both Equations (26) and (27). Accordingly, a variable $m_{x,x}$ was defined which is to be evaluated at each cross section:

$$m_{\infty,x} = \int_o^1 m dr_*^2 \quad (41)$$

That is, m_x at x is taken as the average value of m over the cross section at x.

The spreading coefficient is evaluated by assigning to it the value which gives the best fit between Equation (39) (if b is zero), normalized with respect to γ_o, and the experimental data points calculated from Equation (33), also normalized. The method of least squares may be applied conveniently. Let Δ be the deviation between theoretical and experimental values of γ/γ_o for a value of c that gives a reasonably good visual fit:

$$\Delta = \left(\frac{\gamma}{\gamma_o}\right)_e - \left(\frac{\gamma}{\gamma_o}\right)_t \quad (42)$$

From statistical theory, the most probable value of c is that which minimizes the sum of the squares of the deviations for all the data:

$$\frac{\delta(\Sigma\Delta^2)}{\delta c} = 0 \quad (43)$$

If the probable value, c_P, does not differ greatly from the value chosen visually, c_V, derivatives of orders higher than the first may be neglected, and in the interval $c_P - c_V$,

$$\Delta = \Delta_V + \frac{\delta\Delta}{\delta c}(c - c_V) \quad (44)$$

where Δ_V is the deviation obtained by visual matching. Substitution in Equation (43) followed by solution for c_P gives

$$c_P = c_V - \frac{\sum\left(\Delta_V \frac{\delta\Delta}{\delta c}\right)}{\sum\left(\frac{\delta\Delta}{\delta c}\right)^2} \quad (45)$$

But by Equation (42)

$$\frac{\delta\Delta}{\delta c} = -\frac{1}{c}\left(\frac{cx}{D}\right)\frac{\delta\left(\frac{\gamma}{\gamma_o}\right)_t}{\delta\left(\frac{cx}{D}\right)} \quad (46)$$

The differential is readily evaluated by differentiating Equation (39) after normalizing; whence

$$\frac{\delta\Delta}{\delta c} = \frac{\frac{4}{c}\left(\frac{cx}{D}\right)\sum_1^\infty \frac{J_1^2(a_n\frac{d}{D})}{J_o^2(a_n)} exp[-2a_n^2(\frac{cx}{D})^2]}{\sum_1^\infty \frac{J_1^2(a_n\frac{d}{D})}{a_n^2 J_o^2(a_n)}} \quad (47)$$

Now let there be defined a function $\varphi\left(\frac{cx}{D}\right)$ such that

$$\varphi\left(\frac{cx}{D}\right) = c\frac{\delta\Delta}{\delta c} \quad (48)$$

Substitution of Equations (46) and (48) into (45) gives

$$c_P \cong c_V\left[1 - \frac{\Sigma(\varphi_{\Delta V})}{\Sigma(\varphi^2)}\right] \quad (49)$$

Values of φ for various selected values of (cx/D) are listed in Table 2.

TABLE 2.—THE FUNCTION $\varphi\left(\frac{cx}{D}\right)$

For evaluating c from the gamma correlation

(cx/D)	φ
0.00	0.000
0.02	0.152
0.04	0.297
0.06	0.407
0.08	0.468
0.10	0.484
0.15	0.417
0.20	0.232
0.25	0.155
0.30	0.093
0.40	0.021

This method of evaluating c weights heavily those data corresponding to middle values of cx/D. These are the most accurate data

because near the nozzle turbulence interferes, and far down the duct, where γ is small, the boundary layer contributes significantly to the shape of the profile.

TRANSPORT OF ENERGY IN A DUCTED JET

If molecular transport and generation terms may be neglected, the equation for the turbulent transport of energy may be put in the form(*1*)

$$\nabla \cdot \rho C_p \overline{VT_s} = 0 \qquad (50)$$

which, in cylindrical coordinates for axially symmetrical flow, takes the form

$$\frac{\delta}{\delta x}(\rho C_p \overline{T_s u}) + \frac{1}{r}\frac{\delta}{\delta r}(r\rho C_p \overline{T_s v}) = 0 \qquad (51)$$

Here T_s denotes the total or stagnation temperature:

$$\rho C_p T_s = \rho C_p T_f + \frac{J\rho \overline{V^2}}{2g} \qquad (52)$$

where T_f is the free-stream temperature. Substituting and regrouping give

$$\delta \frac{(\rho C_p \overline{T_f u})}{\delta x} + \frac{1}{r}\frac{\delta}{\delta r}(r\rho C_p \overline{T_f v}) + \frac{\delta}{\delta x}\left(\frac{\overline{J\rho V^2 u}}{2g_c}\right) + \frac{1}{r}\frac{\delta}{\delta r}\left(\frac{r\overline{J\rho V^2 v}}{2g_c}\right) = 0 \qquad (53)$$

Assume now that similarity exists between the transport of heat and momentum in free turbulence. The equation analogous to Reichardt's formula for shearing stress is(*1*)

$$\overline{T_f v} = -\Lambda_T \frac{\delta \overline{T_f u}}{\delta r} \qquad (54)$$

1. *Case of Negligible Kinetic Energy*

For this case the last two terms in Equation (53) drop out, and application of Equation (54) gives

$$\frac{\delta(\rho C_p \overline{T_f u})}{\delta x} - \frac{\Lambda_T}{r}\frac{\delta}{\delta r}\left(r\frac{\delta \rho C_p \overline{T_f u}}{\delta r}\right) = 0 \qquad (55)$$

which is linear in $\overline{T_f u}$. If one defines

$$m_T = \rho C_p \overline{T_f u} \qquad (56)$$

and substitutes Equations (7) and (10) into Equation (55), it becomes identical with Equation (9) except for subscripts. Therefore Equation (18) is a solution of Equation (55), and a mixing index for heat transport may be defined in the same way as that for momentum, by Equation (38) or (39).

2. *Case of Appreciable Kinetic Energy*

For Equation (53) to be linearized completely, it is necessary that the lateral transport of kinetic energy be governed by an equation similar to Equation (54) with the same value of Λ_T. But this law must also be consistent with the law governing the lateral transport of momentum. The approximations involved in assuming such a law for transport of kinetic energy to be valid will be investigated.

Expanding the velocity in mean and fluctuating components,

$$\overline{V^2 v} = 2\bar{u}\,\overline{u'v'} = 2\bar{u}\,\overline{uv} \qquad (57)$$

for axially symmetrical flow where $\bar{v} = \overline{w} = 0$.

Application of Equation (1) now gives

$$\overline{V^2 v} = -2\Lambda\,\bar{u}\frac{\delta \overline{u^2}}{\delta r} \qquad (58)$$

On the other hand,

$$\overline{V^2 u} = \bar{u}^3 + \bar{u}(3\overline{u'^2} + \overline{v'^2} + \overline{w'^2}) \qquad (59)$$

Now assuming that, to a first degree of approximation,

$$\overline{u'^2} \cong \overline{v'^2} \cong \overline{w'^2} \qquad (60)$$

whence

$$\overline{V^2 u} = \bar{u}^3 + 5\,\bar{u}\,\overline{u'^2} \qquad (61)$$

Differentiation with respect to r gives

$$\frac{\delta \overline{V^2 u}}{\delta r} = \frac{3}{2}\bar{u}\frac{\delta \overline{u^2}}{\delta r} + 5\bar{u}\frac{\delta \overline{u'^2}}{\delta r} + 5\overline{u'^2}\frac{\delta \bar{u}}{\delta r} \qquad (62)$$

Recombining terms gives

$$\frac{\delta \overline{V^2 u}}{\delta r} = \frac{3}{2}\bar{u}\frac{\delta \overline{u^2}}{\delta r} + \frac{7}{2}\bar{u}\frac{\delta \overline{u'^2}}{\delta r} + 5\overline{u'^2}\frac{\delta \bar{u}}{\delta r} \qquad (63)$$

If the last two terms may be neglected (they are small throughout most of the flow field of a free jet),

$$\frac{\delta \overline{V^2 u}}{\delta r} \cong \frac{3}{2}\bar{u}\frac{\delta \overline{u^2}}{\delta r} \qquad (64)$$

The equation for kinetic energy transfer analogous to Equation (54) is

$$\overline{V^2 v} = -\Lambda_E \frac{\delta \overline{V^2 u}}{\delta r} \qquad (65)$$

Combining Equations (58), (64), and (65) and solving for Λ_E gives

$$\Lambda_E \cong \frac{4}{3}\Lambda \qquad (66)$$

It has been observed repeatedly that heat is dissipated more rapidly than momentum in turbulent flow, and the ratio of the relative rate factors has been given as approximately 4/3 in free jet(*8*). Therefore

$$\Lambda_T \cong \frac{4}{3}\Lambda$$

and consequently

$$\Lambda_E \cong \Lambda_T \qquad (67)$$

When this result together with Equations (52) and (54) is applied to Equation (53), there results

$$\frac{\delta}{\delta x}(\rho C_p \overline{T_s u}) - \frac{\Lambda_T}{r}\frac{\delta}{\delta r}\left[r\frac{\delta}{\delta r}(\rho C_p \overline{T_s u})\right] = 0 \qquad (68)$$

which is linear in $\overline{T_s u}$. By defining

$$m_s = \rho C_p \overline{T_s u} \qquad (69)$$

and using Equations (7) and (10), Equation (68) becomes identical with Equation (9) except for subscripts. Equation (18) is therefore a solution of Equation (68), and Equation (38) or (39) may be applied to the correlation of the stagnation temperature.

TRANSPORT OF MASS IN A DUCTED JET

For the transport of mass when there are no sources or sinks present and chemical interconversion is negligible:

$$\frac{\delta \rho \overline{gu}}{\delta x} + \frac{1}{r}\frac{\delta}{\delta r}\left[r\,\rho \overline{gr}\right] = 0 \quad (70)$$

where g is the mass fraction of jet-stream fluid in the mixture. If similarity to momentum transport exists, then

$$\overline{gv} = -\Lambda_g \frac{\delta \overline{gu}}{\delta r} \quad (71)$$

when

$$m_g = \rho \overline{gu}$$

Equation (70) is transformed into Equation (9), and the solution follows as before.

Of course, in order to solve Equation (21) for the distribution of energy or mass, the velocity profile must be known. A difficulty enters here in that the products $\overline{Tu}$ and $\overline{gu}$ involve cross products of the fluctuating components:

$$\overline{Tu} = \overline{T}\,\overline{u} + \overline{T'u'}$$

$$\overline{gu} = \overline{g}\,\overline{u} + \overline{g'u'}$$

$$\overline{u^2} = \overline{u}^2 + \overline{u'^2}$$

Presumably $\overline{T}$ can be measured with a thermocouple and $\overline{g}$ by chemical analysis, but the situation is equivocal. The mean products of the fluctuating components can be measured, in theory, with a suitable type of hot-wire anemometer (*4*), but such measurements are not easy. There is evidence (*1*) that neglect of these fluctuating components introduces errors of 30% or more into the correlations of energy and mass transport in free jets.

SUMMARY

It has been shown that (*a*) if Reichardt's formula applies to the turbulent transport of energy, mass, and momentum in ducted jets, (*b*) if molecular transport and boundary layer formation may be neglected, and (*c*) if radial pressure gradients and heat losses at the wall may be neglected, then the transport equations are linearized in the corresponding fluxes, and solutions may be obtained in orthogonal functions. This was done. In order to permit evaluation of the empirical constants appearing in the solutions, a function γ, the mixing index, was devised. It is a measure of the degree to which the two streams remain unmixed at any point, and it approaches zero as the mixing proceeds. Methods of correlating experimental data in terms of γ were given.

ACKNOWLEDGMENT

The comments and suggestions of E. W. Comings, Clarke L. Coldren, Arnold Kivnick, and E. D. Henze are gratefully acknowledged. This paper contains a part of the results obtained in an investigation in the Engineering Experiment Station of the University of Illinois on a contract with the Office of Naval Research, N6-ori-71, T.O. XI.

NOTATION

A = cross-sectional area of mixing duct

A_n = arbitrary coefficient of nth term in a series of J_o

a_n = nth root of J_1

B_n = arbitrary coefficient of nth term in series of Y_o

b = empirical constant in Equation (19)—a measure of the action of the duct wall in inhibiting the growth of the scale of the turbulence

C_f = impact-tube coefficient

C_p = specific heat at constant pressure

c = momentum spreading coefficient, empirical constant in Equation (19)

D = diameter of mixing duct

d = diameter of jet nozzle

g = fraction by weight of jet fluid in mixture

J_o = zero-order Bessel function of the first kind

J_1 = first-order Bessel function of the first kind

K = constant of integration in Equation (11); the boundary conditions require that K be a root of J_1

M = variable defined by Equation (7); M is proportional to the flux density of total momentum, energy, or mass

m = flux density of total momentum, energy, or mass, Equation (8)

P = static pressure in duct

P_{atm} = static pressure in atmosphere

ΔP = pressure indicated by manometer one end of which is connected to a total-head impact tube in a duct and the other open to the atmosphere

r = radial coordinate, distance from axis of duct

r_* = normalized radial coordinate, Equation (10)

T = temperature

u = x-directed component of velocity

v = r-directed component of velocity

x = axial coordinate, distance along axis of duct from nozzle

Y_o = zero-order Bessel function of second kind

Y_1 = first-order Bessel function of second kind

Greek

γ = mixing index, Equation (33)

Λ = proportionality function in Reichardt's shearing-stress equation, function of x and r, Equation (1)

ρ = density of fluid

θ = time

Subscripts

avg = average

atm = atmosphere

E = transport of energy

f = free stream

g = transport of mass

i = induced stream conditions in plane of nozzle

j = jet-stream conditions in plane of nozzle

k = kth term in series of J_o

s = stagnation

T = transport of heat

x = conditions in cross section of flow at distance x from nozzle

o = conditions in plane of jet nozzle

∞ = condition that would be obtained by complete mixing of the flow at any section with no further loss of momentum or energy

LITERATURE CITED

1. Alexander, L. G., T. Baron, and E. W. Comings, *Univ. Illinois, Eng. Expt. Sta. Bull.* 405 (1952)
2. Alexander, L. G., E. W. Comings, H. L. Grimmett, and E. A. White, *Chem. Eng. Progr., Symposium Series No. 10*, **50**, 93 (1954).
3. Baron, T., and L. G. Alexander, *Chem. Eng. Progr.*, **47**, 181 (1951).
4. Corrsin, S., and M. S. Uberoi, *Natl. Advisory Comm. Aeronaut. Tech. Note* 1865 (1949).
5. Ferguson, C. K., 1949 Fluid Mechanics and Heat Transfer Institute, Berkeley, Calif. (1949).

6. Flugel, G., *Forsch. Gebiete Ingenieurw., Forschungsheft,* 395 (1939); *Natl. Advisory Comm. Aeronaut. Tech. Mem* 982 (1941).
7. Forstall, W., and A. H. Shapiro, *J. App. Mech.*, 17, 399 (1950).
8. Keenan, J. H., et al., *J. App. Mech.*, 17, 299 (1950).
9. Kivnick, A., *Eng. Expt. Sta. Univ. Illinois Tech. Rept.* 2, DA-18-064-CML-445 (1952).
10. Kroll, H. E., *Chem. Eng. Progr.*, 43, 21 (1947).
11. Ledgett, L. A., Preprint, Am. Soc. Mech. Engrs., Summer Meeting (1934), George Reproduction Co. (1934).
12. McElroy, G. E., *U. S. Bur. Mines Tech. Paper* 678 (1945).
13. Reichardt, H., *Z. Math. u. Mech.*, 21, 257 (1941).
14. Reid, E. G., *Natl Advisory Comm. Aero Tech. Note* 1949 (1949).
15. Viktoren, K., *Forsch. Gebiete Ingenieurw.* 12, 1, 16 (1941); *Natl. Advisory Comm. Aeronaut. Tech. Mem.* 1096 (1946).

III. Correlation of Profiles of Total Momentum and Energy Flux in a Nonisothermal Jet Discharging into a Duct

The data in the first paper of this series on the distribution of momentum and energy in nonisothermal air streams mixing in a straight duct were correlated by the methods described in the second paper. Mixing indexes were evaluated and used to correlate profiles of total momentum and stagnation temperature at various sections of the duct.

The understanding and prediction of the processes that take place when a fluid stream mixes turbulently with another of different velocity, composition, or temperature is becoming of ever greater technological importance. This paper studies the mixing of a round jet of heated air, discharged into a straight, cylindrical duct, with a freely induced ambient air stream. The *mixing index*, a quantity which is a measure of the degree to which the two streams remain unmixed at any given section of flow, was computed from the experimental data presented in the first paper of this series and was correlated theoretically by methods described in the second. From this correlation, empirical spreading coefficients were evaluated, and these were used to predict distribution of energy and momentum flux (temperature and velocity distribution) at various sections.

APPARATUS AND PROCEDURE

The aparatus and procedure employed in the experimental work, the results of which are correlated here, have been described in detail in Part I of this series. All the data were obtained at an air-flow rate of 2.07 std. cu. ft./sec., as metered through a calibrated orifice. The air was heated to 222° to 225°F. as measured upstream from the flow nozzle.

RESULTS

Correlation of the Mixing Index for Momentum Transport. On approach to the problem of correlating the momentum data it was clear that account would have to be taken of the scatter in the integral mass flux noted in connection with Figure 14 of Part I. This scatter is amplified in momentum-flux calculations, where the velocity enters as the square, and to an even greater extent in mixing-index calculations, where the velocity enters as the fourth power. It was noticed that the individual points on the velocity profiles did not show much scatter relative to one another and that the continuous curves appeared to be reasonably well defined. It seemed to be more likely that the scatter in the integral mass flux resulted from random changes of 5 to 10% in the flow pattern and induction ratio between successive profile measurements. This effect has been noticed by others(*3*) and is thought to reflect a true physical instability in the system.

It was postulated, however, that the relative shape of a momentum-flux profile, rather than its relative position, is the true measure of the degree of mixing of the two streams, and it seemed reasonable that some method of normalizing the profiles might eliminate the scatter and yield reliable values of the mixing index. Implicit in this is the hypothesis that the mixing is a function only of the geometry of the system and independent of the relative velocities of the initial streams. The manner in which the generalized flux function M was constructed [Equation (7)*] accomplishes the desired normalization as shown by the fact that it leads to an analytical solution [Equations (20) and (25) and discussion] that is independent of the relative velocities, provided the spreading coefficient c is independent also. Although this in general is probably not the case(*2*), minor variations in the flow ratio, as encountered here, should result in only second-order variations in c.

In Part II the necessity of evaluating m_∞ at each cross section because of the unavoidable loss of momentum at the wall of the duct was discussed [Equation (41)]. The

*All equations referred to appear in Part II.

present scatter is an effect of the same kind but of a larger order of magnitude and may be treated in the same way.

The following procedure was used in assigning values to $m_{j,avg}$ and $m_{i,avg}$ appearing in Equation (7). The first profile was taken at 1 in. from the nozzle. It was assumed that the velocity on the axis of flow here was the same as at the nozzle discharge. A value of 20,500 ft.-lb./(sec.) (sq.ft.)/sec. was calculated for $m_{j,avg}$ from the impact and static pressure data for this profile, as it was assumed that this value fairly represented the average momentum flux density over the nozzle discharge. It is possible by use of this value of $m_{j,avg}$ and $m_{x,x}$ as defined by Equation (41) to calculate by difference an apparent $m_{i,avg}$ at each cross section by use of Equation (27). The results are shown in Table 1.

TABLE 1

x, distance from nozzle, in.	$m_{i\ avg.}$, ft. lb./(sec.) (sq. ft.) sec.
1	396
4	95
7	480
10	291
16	—98
20	131
23	171
26	96

It is seen that there is considerable variation, and in one instance a negative value occurred. Reference to Equation (33) shows that the stream momenta enter into the calculation of the mixing index as the term $(m_{j,avg}-m_{i,avg})^2$. Although $m_{i,avg}$ is small compared with $m_{j,avg}$, nevertheless, when the difference is squared, the variations in $m_{i,avg}$ introduce fluctuations into the gamma values. But it is these fluctuations which it is desired to eliminate by the normalization procedure.

The quantity $m_{i,avg}$ may be estimated in another way. The static pressure at the first profile was —2.6 in. of water relative to the atmosphere. If the inlet section of the duct is treated as an ideal-flow nozzle, it is readily calculated that the flow momentum, $\overline{\rho u^2}$, is 896 ft. lb./(sec.)/(sq.ft.)/sec. Conversion of the static pressure to momentum units gives P_g equal to —436. The sum, which is the total momentum of the induced stream, m_i, is 433, which is in fair agreement with the value listed in Table 1 for the first profile. Since there was undoubtedly some irreversibility in the flow in the inlet section of the duct, it was decided to use a compromise value of 400 for $m_{i,avg}$ throughout the calculations.

The mixing index γ was evaluated at the various cross sections by graphical integration of Equation (33). The values listed in Table 2 when plotted vs. x defined a smooth curve which appeared to extrapolate with reasonable probability to a gamma of 0.165. This is the theoretical value at x equal to zero for the system studied as calculated from Equation (40) with nozzle diameter d of 0.898 in. and duct diameter D of 3.81 in. The spreading coefficient c was then evaluated by the method discussed in Part II [Equation (49)] and found to be 0.0480. Values of the mixing-index ratio γ/γ_o are listed in Table 2 and are shown plotted in Figure 1. The solid curve represents Equation (39) with b taken as zero. This value of b correlates the data better than any positive value. In fact, the three points at highest cx/D lie below the curve, implying that the mixing here is proceeding more rapidly than corresponds to b equal to zero. The correlation could be improved by increasing the mixing coefficient c and taking negative values of b. Physically this situation would correspond to the condition where the presence of the duct wall increases the rate of growth of Λ over that occurring in free jets. Such a possibility cannot be excluded because the boundary layer at the wall does generate turbulence; however, as discussed in Part II, the correlation is not sensitive to variations in b, and the scatter in the present data prevents a precise evaluation of b. For this reason, the data were provisionally correlated with b taken as zero.

The correlation in Figure 1 is reasonably good. A correlation of momentum data obtained with an isothermal jet in the same apparatus used in this study has been published elsewhere(*1*). In that case, c was found to be 0.0445. It appears that heating the jet to 225°F. may have increased the rate of mixing of the two streams compared with the isothermal case. However, sufficient data have not been accumulated to permit estimating the precision of these values of c, and it would be premature to conclude that heating the jet affected the mixing significantly.

Correlation of the Mixing Index for Energy Transport. Mixing indexes were calculated from the temperature and momentum data of Part I by means of Equations (56), (7), and (33). It was observed that the temperature profile taken nearest the discharge of the nozzle did not have a central region of uniform temperature corresponding to the core of uniform velocity observed in the momentum measurements. Although no temperature profile in the nozzle discharge was obtained, it is readily apparent that it could not have been uniform because of heat losses to the nozzle and antecedent piping. However the relative nonuniformity was certainly not great—at most 5° or 6°F. It was believed that the equations devel-

TABLE 2.—EXPERIMENTAL VALUES OF MIXING INDEX FOR MOMENTUM TRANSPORT

$\frac{x}{D}$	$\frac{x}{d}$	γ	γ/γ_o	$\frac{cx}{D}$ ($c=0.0480$)
0.00	0.00	(0.165)	(1.000)	0.000
0.26	1.11	0.140	0.849	0.013
1.05	4.45	0.102	0.618	0.050
1.84	7.80	0.0754	0.457	0.088
2.62	11.1	0.0470	0.285	0.126
4.20	17.8	0.0126	0.076	0.202
5.25	22.3	0.0056	0.034	0.252
6.03	25.6	0.0021	0.013	0.290
6.83	29.0	0.0007	0.004	0.328

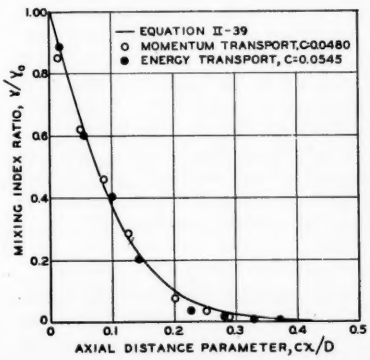

FIG. 1. CORRELATION OF MIXING-INDEX RATIO FOR MOMENTUM AND ENERGY TRANSPORT.

oped in Part II on the basis of an assumed uniformity of initial jet temperature could be used with reasonable success in correlating the data and that marked discrepancies would appear only adjacent to the nozzle. The mean energy flux, $m_{x,x}$, was calculated from Equation (41), and the results are listed in Table 3.

TABLE 3.—EXPERIMENTAL VALUES OF MIXING INDEX FOR ENERGY TRANSPORT

$\frac{x}{D}$	$\frac{x}{d}$	$m_{\infty,x}$	γ	γ/γ_o	$\frac{cx}{D}$ $(c=0.0545)$
0.00	0.00	...	(0.165)	(1.000)	0.000
0.26	1.11	240	0.1459	0.884	0.014
1.05	4.45	269	0.0991	0.601	0.057
1.84	7.80	267	0.0663	0.402	0.100
2.62	11.1	240	0.0330	0.200	0.143
4.20	17.8	206	0.0060	0.036	0.229
5.26	22.3	235	0.0026	0.016	0.286
6.03	25.6	240	0.0010	0.006	0.329
6.83	29.0	246	0.0005	0.003	0.372

Considerable scatter is observed in the values of $m_{x,x}$. These should show only a monotonic decrease with increasing x owing to loss of heat at the wall. The average of these values gave 4,460 for $m_{j,avg}$ when substituted into Equation (27). This value was used throughout the calculations. The resulting values of γ when plotted vs. x defined a smooth curve which could be extrapolated with reasonable probability to 0.165. The gammas were then normalized with respect to $\gamma_o = 0.165$ and the spreading coefficient c was evaluated by Equation (49). A value of 0.0545 was obtained. The mixing-index ratios γ/γ_o are listed in Table 3 and are plotted in Figure 1. The scatter appears to be of the same order as that for the momentum transfer data, and the same trend to values less than theoretical with increase in cx/D is observed.

As the spreading function Λ is proportional to c^2, the ratio of the lambdas for energy and momentum transport may be evaluated:

$$\frac{\Lambda_E}{\Lambda} = \frac{C_E^{\,2}}{c^2} = \left(\frac{0.0545}{0.0480}\right)^2 \cong 4/3 \qquad (1)$$

which is in agreement with the hypothesis introduced in Part II.

Prediction of Energy- and Momentum-Flux Profiles in the Ducted Jet. Theoretical values of M, which may represent either momentum- or energy-flux density in the theory used here, were calculated from Equation (21) with d/D equal to 0.236. They are listed in Table 4† as a function of r_* with cx/D as the parameter and are plotted in Figure 2 vs. cx/D with r_* as parameter. Profiles of M at any cx/D may be obtained from that figure.

† For Tables 4, 5, and 6 (III D-F) order document 4485 from American Documentation Institute, Auxiliary Publications Service, Library of Congress, Washington 25, D. C., remitting $1.75 for microfilm or $2.50 for photoprints.

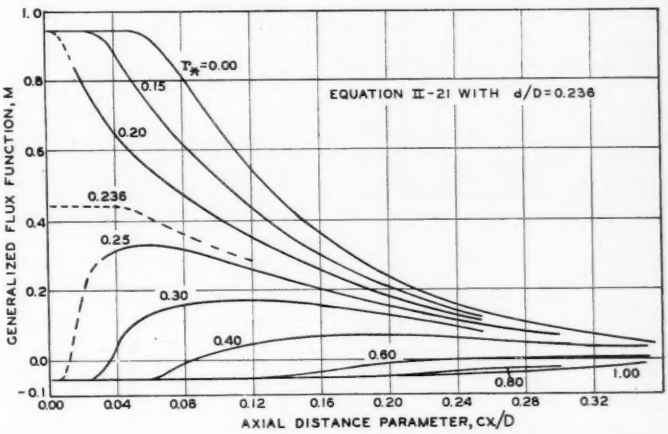

FIG. 2. GENERALIZED FLUX FUNCTION.

Only twenty terms of the series in Equation (21) were used. The series converges very slowly for r equal to d/D. Scatter was observed in calculated M at r_* values of 0.20 and 0.25, being greater in the latter case. However, it is believed that the best smooth curve through the points is sufficiently reliable for present purposes and that the uncertainty involved is within the probable error in the experimental data.

Correlation of the Generalized Flux Function M for Simultaneous Transport of Energy and Momentum. The function M of Equation (7) was calculated from the momentum-flux data. The same values of m_j and m_i were used as in the calculation of the mixing indexes. The results are listed in Table 5† and are plotted in Figure 3. Also shown as solid lines are curves taken from Figure 2 at the appropriate values of x/D, and with c equal to 0.0480 as evaluated from the mixing-index correlation. It is seen that the agreement is within the precision required for engineering calculations. The curve at x/D of 0.26 shows the data to fall off as r_* approaches unity. This is believed to be indicative of a tendency toward separation of the flow in the vicinity of the sharply rounded entrance plate. In subsequent curves only the point nearest the wall shows appreciable diminution; this is thought to signify the presence of a thin boundary layer.

As expected from the trend exhibited by the gamma correlation, the M correlation shows the points along the center line to lie above the theoretical curve close to the nozzle and below the curve farther away.

In a similar way, the data on the distribution of energy were correlated. The M values are listed in Table 6† and are plotted in Figure 4, together with solid curves cross-plotted from Figure 2. The initial temperature profile in the jet stream was not uniform because of experimental difficulties. As a result, the central points on the curve at x/D of 0.262 lie above the theoretical curve, as expected. On

the other hand, it is unlikely that the nonuniformity of the initial jet temperature can account for the excessive magnitudes of the M values near the center of the profile at x/D of 1.84 and 2.62. This is more probably the same effect noted in the momentum-flux correlation and represents a fundamental defect in the theory.

under one set of operating conditions, and it is not known how the spreading coefficients vary with the ratios of velocities, diameters, and temperatures of the jet and induced streams. The transport variables were defined in such a way that, if the theory is correct, the spreading coefficient should be independent of diameter and temperature ratio. The theory provides no clue concerning the dependence of the spreading coefficient on the velocity ratio. The system used in these experiments is intermediate between the extremes of a free jet discharging into a stagnant fluid and a jet discharging into a stream having nearly the same velocity. The evidence is that the spreading coefficient varies from 0.075 for free jets down to zero as the velocity ratio approaches unity (*2*).

SUMMARY AND CONCLUSIONS

The data on turbulent transport of momentum and energy presented in Part I may be successfully correlated by the method developed in Part II. The correlation depends upon the evaluation of two empirical coefficients, c and b. However it is insensitive to variations in b, which is a measure of the limitation imposed by the duct on the growth of the scale of the turbulence. A value of zero for b was found to be not inconsistent with the data. Thus momentum- and energy-flux profiles were correlated in effect by the single (spreading) coefficient c, the value of which was 0.0480 for momentum transport and 0.0545 for energy transport. The theory neglected radial static pressure gradients as well as momentum and heat losses at the wall of the duct; neverthe-

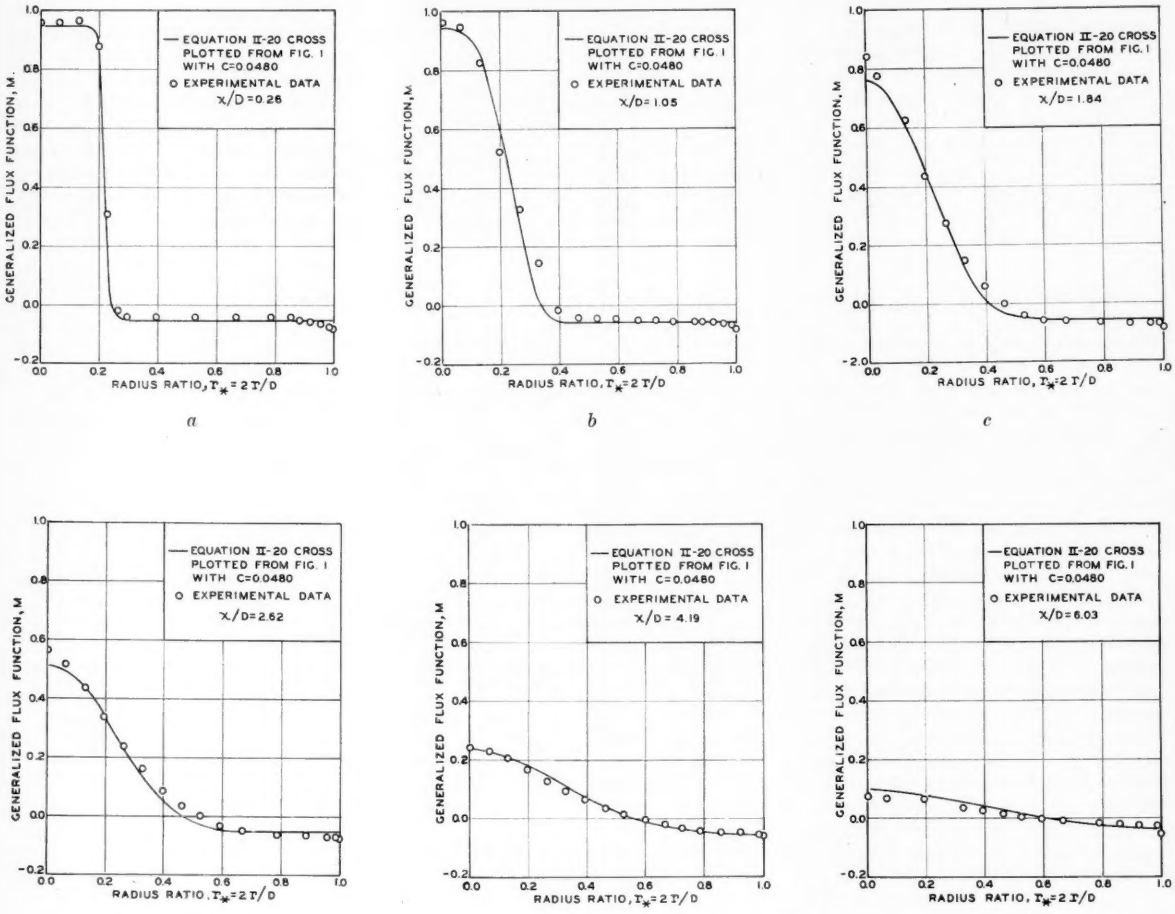

FIG. 3. CORRELATION OF GENERALIZED FLUX FUNCTION M FOR MOMENTUM TRANSPORT.

As before, at increasing x/D, the experimental points tend to fall below the theoretical curves, whether because of neglect of heat loss at the wall or of some other defect in the theory is uncertain. The M curves could all be rectified by progressive diminution of the corresponding m_j's. However very precise data yielding values of m with negligible scatter would be required for such a procedure to be feasible.

The experiments were performed

less these values of c suffice to describe satisfactorily the entire flow field.

ACKNOWLEDGMENT

The comments and suggestions of H. F. Johnstone, E. W. Comings, and Clarke Coldren are gratefully acknowledged. This study was performed as a part of a program of the Engineering Experiment Station, University of Illinois, under Contract N6-ori-71, T. O. XI, sponsored jointly by the Office of Naval Research and Flight Research Laboratory.

NOTATION

b = empirical coefficient in Equation (19), a measure of the effect of the duct wall on the growth of the scale of the turbulence

c = momentum spreading coefficient, empirical coefficient in Equation (19)

D = diameter of mixing duct

d = diameter of jet nozzle

M = variable defined by Equation (7); M is proportional to the flux density of total momentum or of energy as the case may be

m = flux density of total momentum or of energy, Equation (8), Equation (69)

P_g = gauge static pressure in duct. $\overline{P} - P_{atm}$.

r_* = normalized radial coordinate, $r_* = 2r/D$

u = x-directed component of velocity

x = axial coordinate, distance along axis of duct from nozzle

Greek

γ = mixing index, Equation (33)

Λ = proportionality function in Reichardt's shearing-stress formula, function of x and r in general, Equation (1), Part II

ρ = density of fluid in duct

Subscripts

avg = average

E = transport of energy

i = induced stream conditions in plane of nozzle

j = jet-stream conditions in plane of nozzle

x = conditions in cross section of flow at distance x from nozzle

o = conditions in plane of jet nozzle

∞ = condition that would be obtained by complete mixing of the flow at any section with no further loss of momentum or energy

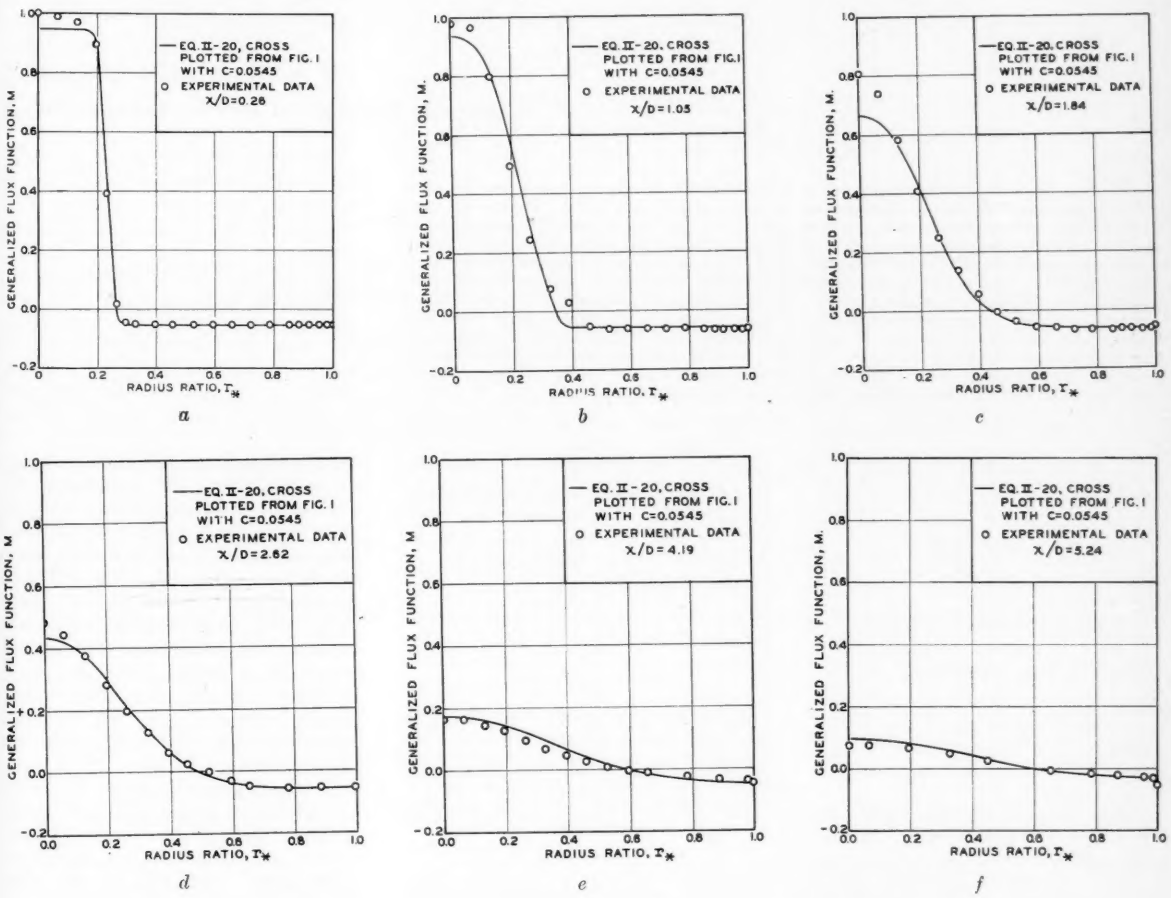

FIG. 4. CORRELATION OF GENERALIZED FLUX FUNCTION M FOR TRANSPORT OF ENERGY.

LITERATURE CITED

1. Alexander, L. G., E. W. Comings, H. L. Grimmett, and E. A. White, *Chem. Eng. Progr. Symposium Series* No. 10, 50, 93 (1954).
2. Kivnick, A., Univ. Illinois Eng. Exp. Sta. Tech. Rept. 2, DA-18-064-CML-445 (1952).
3. Wagner, F., Rept. ZWB/UM/Re /7602, Arado Aircraft Co., Brandenburg, Germany; C.A.D.O. Translation A.T.I.-20255, A.M.C. Trans. F-TS-2559-Re, Wright Field, Dayton, Ohio (1944).

(Presented at the A.I.Ch.E. Biloxi meeting)

Laws of Corresponding States

L. NELSON and E. F. OBERT

Northwestern Technological Institute, Evanston, Illinois

Various laws of corresponding states are examined briefly in this paper to show the corrections that are in common use to increase the accuracy of forecasting compressibility factors. Two trends are noticeable: (1) the use of specific compressibility charts with the results generalized for all gases either by corrections related to z_c (the compressibility factor at the critical point) or by the use of pseudocritical properties and (2) the use of a true generalized chart based upon averaged data. It is shown that the selection of the plot parameters affects the accuracy of the generalized chart. In recent years reduced parameters based upon kinetic theory have been proposed but for a restricted class of gases (nonpolar gases with spherically symmetrical molecules and negligible quantum effects). It is shown that the kinetic parameters are directly related to the critical constants and also that the kinetic parameter charts can be used for all gases without serious loss of accuracy.

The compressibility factor z is defined:

$$z = \frac{pv}{RT} \qquad (1)$$

In terms of reduced properties relative to the critical constants, Equation (1) is equivalent to

$$z = \frac{p_r v_r}{T_r} z_c \qquad (2)$$

where z_c is the compressibility factor at the critical point. A compressibility chart can be constructed to correlate z with two selected reduced properties, such as T_r and p_r, with acceptable accuracy for most gases. As an approximation therefore

$$z = f(T_r, p_r)_{\text{all gases}} \qquad (3)$$

The implications of Equation (3) and other laws of corresponding states have been discussed many times [(*1* and *2*) for examples], but several aspects of the generalized laws are not usually recognized. It may be considered that for any one gas, as z is a state property, an exact functional relationship exists between z and any two of the independent properties p, v, and T. If p and T are selected so that for several gases $T_{ra} = T_{rb} = T_{ri}$ and $p_{ra} = p_{rb} = p_{ri}$, then by Equation (2), which is also an exact equation,

$$\frac{z_a}{z_b} = \frac{v_{ra}}{v_{rb}} \frac{z_{ca}}{z_{cb}} \qquad (4)$$

Equation (4) shows that the generalization of Equation (3) is successful for gases having essentially the same z_c values because the van der Waals law of corresponding states,

$$v_r = f(T_r, p_r) \qquad (5)$$

holds with adequate precision; the generalization is successful for gases having different (or the same) z_c values because the modified law of corresponding states proposed by Su(*3*),

$$v_{r'} = v_r z_c = f(T_r, p_r) \qquad (6)$$

holds with adequate precision. It is emphasized that where z_c values are essentially constant, the regions of the generalized chart where correlation is exceptional can be found only by trial. Similarly, when gases have different z_c values, obviously from Equation (2) correlation at or near the critical point will be poor, but this is no assurance that correlation will continue to be poor in regions other than the critical. In other words a compensating effect for z_c is the failure of Equation (5) to hold exactly for all gases. Thus gases with the same z_c value usually correlate closely on the chart, but this happens because the molecular structures are closely related. When the structures or molecular laws of force are different, gases will not correlate well no matter whether the z_c values are equal or not (and an additional parameter becomes necessary: a quantum parameter for the light gases such as helium and hydrogen; a dipole-moment parameter for polar gases, such as the freons, water, and ammonia; and size or shape parameters for the complex organic gases).

z_c CORRECTION FACTORS

Meissner and Seferian (*2*) have published correction charts to account for deviations in z_c between gases. These charts are useful when z values below 0.6 are indicated and *when the molecular structures are closely related.* The law of corresponding states for their work has the form

$$z = f(T_r, p_r, z_c) \qquad (7)$$

The corrections can be ignored however for regions above $T_r = 1.3$ and also for all similar gases with values of z_c between 0.25 and 0.28. In the latter case a difference of over 10% exists in z_c; yet correlation on the compressibility chart is well within 2 1/2% for most gases.

A fundamentally correct method for modifying the generalized z values to account for the deviations of polar gases has been recently proposed by Hall and Ibele(*13*). Their work is based upon a law of corresponding states of the form

$$z = f(T_r, v_r', \mu_r) \qquad (7b)$$

where μ_r is a reduced dipole moment. The corrections of Hall and Ibele enable z values for the polar gases to be obtained with surprising accuracy from a generalized compressibility chart (such as Figure 1). However, the important by-product of their work is the added reliance that can now be given to generalized property charts when allowances are made for the type of molecular structure.

CHANGE IN INDEPENDENT VARIABLE

The inconsistency between Equations (2) and (5) was first recognized by Onnes(*4*), who proposed combining z_c and v_r because in those days critical volumes were open to serious question. The Onnes transformation yields the Su law of corresponding states, Equation (6), which is equivalent to Equation (3), as

$$v_r' = z\frac{T_r}{p_r} = \frac{v}{RT_c/p_c} \qquad (8)$$

For that matter, the variable z_c could have been combined with either T_r or p_r, rather than v_r, to yield a pseudoreduced temperature and a pseudoreduced pressure:

$$p_r' = \frac{p}{RT_c/v_c} \qquad T_r' = \frac{T}{p_c v_c/R} \qquad (9)$$

The laws of corresponding states for these two cases are of the form

$$f(z, T_r, v_r) = 0 \qquad (10)$$

The correlations implied by Equations (3), (10), and (11) are not equivalent because none of the

$$f(z, p_r, v_r) = 0 \qquad (11)$$

"laws" are exactly true. No one to the authors' knowledge has investigated which of the three equations would best serve for a generalized compressibility chart, probably because the critical volume has in the past been either unknown or else a variable of some disrepute. For this reason a study was made of twelve gases (CH_4, C_2H_4, N_2, NH_3, H_2, CO_2, CO, Ne, C_3H_8, Xe, A, and air), which indicated that a chart based upon one equation would yield regions of improved correlation relative to charts based upon the other two equations, and of course the opposite trend was also true for other regions. For one example the following data for water ($z_c = 0.232$) and methane ($z_c = 0.289$) at reduced pressures less than $p_r = 1.5$ may be considered:

MAXIMUM DEVIATIONS IN z_{exp}

Chart of	$T_r = 1.1$	$T_r = 1.3$	$T_r = 1.8$
$z = f(T_r, p_r)$	0.05	0.038	0.015
$z = f(T_r, p_{r'})$	0.06	0.015	0.004

Thus for these two gases correlation has been improved in the higher T_r regions with some loss of accuracy near the critical. It is suggested that further work along this line may prove profitable.

EMPIRICAL PSEUDOCRITICAL CONSTANTS

To improve the correlation of data, corrections can be applied to the critical constants. Such corrections can be found by either graphical or analytical methods but in both methods a solution by trial is required. Empirical corrections have been proposed by Morgan and Childs(*5*) and by Maslan and Littman(*6*), among others. A study of certain of these corrections shows that the correction does no more than to shift the region of deviation, and unsuspected errors may arise; for example, the so-called Newton corrections for H_2 and He ($T_c + 8, p_c + 8$) when used in regions below the Boyle-point isotherm have been reported by several investigators(*2, 7*) to cause errors as much as 40% in z although improving considerably the correlation at higher temperatures. It seems reasonable to conclude that the selection of correction factors by trial, because of the labor involved, is practically an impossibility.

THEORETICAL PSEUDOCRITICAL CONSTANTS

A means for obtaining the variable correction factors for a selected group of fluids without undue labor is now available by a method derived from statistical mechanics theory. Hirschfelder, Bird, and Spotz(*8, 9*) have developed a virial equation of state based upon the Lennard-Jones force potential. Their work is limited however to the semisymmetrical nonpolar gases, and the analytical results include only the effects of the first three virial coefficients. From the underlying theory, reduced quantities, first proposed by deBoer(*10*), can be defined:

Reduced density

$$\rho_r' = b_o\rho \qquad (12)$$

Reduced temperature

$$\tau = \frac{T}{\epsilon/k} \qquad (13)$$

Reduced pressure

$$p_r' = \frac{p}{R(\epsilon/kb_o)} \qquad (14)$$

The kinetic constants b_o and ϵ (and the gas constants k and R) will not be discussed here since several papers on them are available in the literature (*10, 11, 12*). The important point is that this analytical work rests upon a law of corresponding states of the form

$$f(\rho_r', \tau, p_r') = 0 \qquad (15)$$

which is equivalent, for one example, to

$$f(z, \tau, p_r') = 0 \qquad (16)$$

The Hirschfelder-Bird-Spotz tables (*9*) are limited to the low-density region (up to 40% of the critical density) since evaluations of the fourth and higher virials were not made. But if values of the reduced parameters are plotted as in Figure 1 from experimental data [details of construction in (*7*)], the resulting plot represents a virial equation with an infinite number of terms*. In other words, Figure 1 extends by graphical means the Hirschfelder-Bird-Spotz tables to regions of high density.

Once the kinetic parameters are determined, pseudocritical constants can be directly calculated from the following equations and Equations (12), (13), and (14):

*A series of various compressibility charts can be obtained by writing to the authors.

$$\tau = \frac{T}{C_1 T_c} \qquad (17)$$

$$p_r' = \frac{p}{C_2 p_c} \qquad (18)$$

$$\rho_r' = \frac{\rho}{C_3\ \rho_c} \qquad (19)$$

with values for various gases as shown in Table 1.

Example 1. Find the compressibility factor for methane at 251.5°K. and 131.3 atm.

Table 2 has been constructed to show the agreement of the chart with experimental data and with values obtained from existing charts. The data were selected not for high z values, but to agree essentially with Table 2 of Maslan and Littman (*6*). Figure 1 does not include the critical region [where the method and corrections of Meissner and Seferian (*2*) may be preferable].

As an aside comment on the use of Figure 1, it should be noted that the isotherms for nitrogen correlate other gases either on a chart based on critical constants or on a chart such as Figure 1. This fact allows the Bird-Spotz tables and Figure 1 to be extended to include all gases with a fair degree of accuracy (at z values above 0.6). Equations (12), (13), and (14) can be generalized by substituting reduced and critical values of nitrogen for ρ, T and p, for example,

$$\tau = \frac{T}{\epsilon/k} = \frac{T_r T_{c_{N_2}}}{(\epsilon/k)_{N_2}} = T_r \left[\frac{126.3}{95.4}\right] = 1.325\ T_r \qquad (20)$$

$$Rp_r' = \frac{p}{(\epsilon/k\ b_o)} = \frac{p_r\ p_{c_N}{}^2\ b_o}{\epsilon/k} = p_r \left[\frac{33.5\ (64.1)}{95.4}\right] = 22.52\ p_r \qquad (21)$$

In the same manner, pseudoforce constants can be determined:

$$\epsilon'/k = 0.756\ T_c \qquad (22)$$

$$b_o' = 17 \frac{T_c}{p_c} \qquad (23)$$

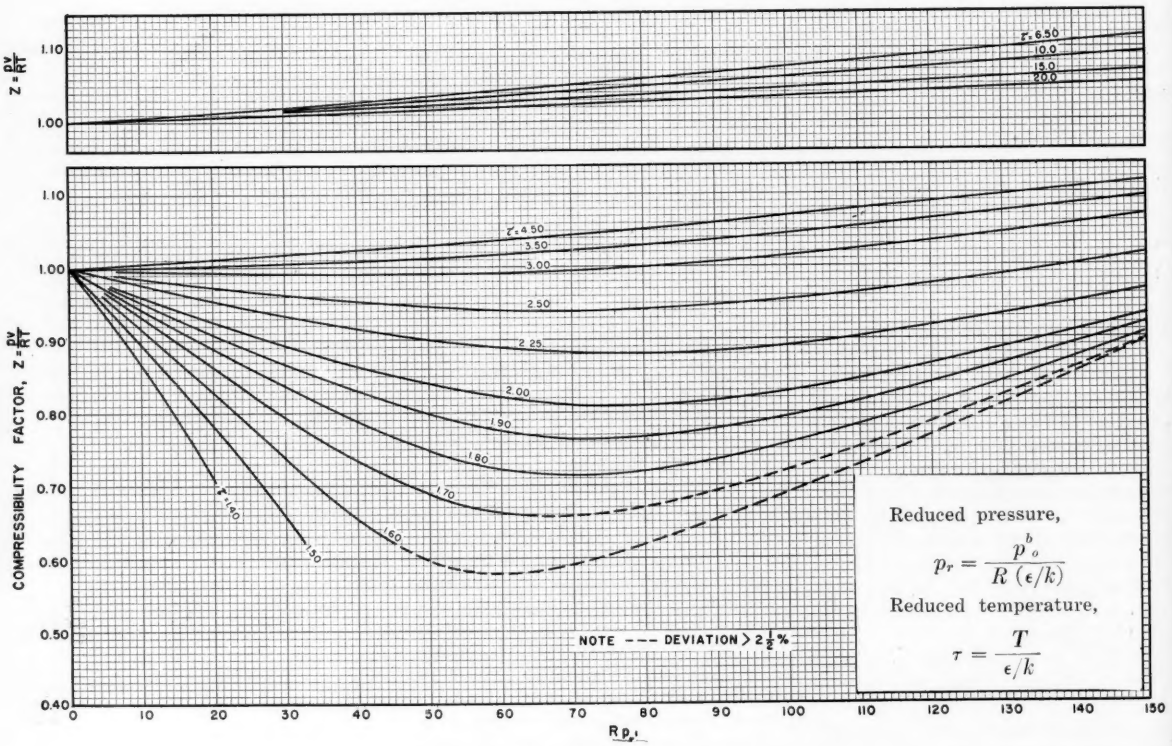

FIG. 1. GENERALIZED COMPRESSIBILITY CHART.

Solution

From Table 1,

$$\tau = \frac{T}{C_1 T_c} = \frac{251.5}{0.775\ (191)} = 1.70$$

$$Rp_r' = \frac{Rp}{C_2 p_c} = \frac{82.06\ (131.3)}{3.79\ (45.8)} = 62.1$$

$$\left(\text{Note } R = 82.06 \frac{\text{cc. atm}}{\text{mole °K}}\right)$$

From Figure 1, $z = 0.66$
($z_{exp} = 0.659$)

Example 2. Find the compressibility factor for ethylene at 425°K. and 126 atm.

Solution

$$p_r = \frac{p}{p_c} = \frac{126}{50.5} = 2.5$$

$$T_r = \frac{T}{T_c} = \frac{425}{283.1} = 1.5$$

With Equations (20) and 21),

$\tau = 1.325\ T_r = 1.325\ (1.5) = 1.99$

$Rp_r' = 22.52 p_r = 22.52\ \ (2.5) = 56.3$

Figure 1 for these values yields

$$z = 0.822$$

which is also the experimental value.

C_1 = kinetic critical-temperature constant = $\dfrac{\varepsilon/k}{T_c}$

C_2 = kinetic critical-pressure constant = $\dfrac{R(\varepsilon/k)}{b_o p_c}$

C_3 = kinetic critical-density constant = b_o/ϱ_c

ε' = pseudoforce constant = $0.756\ T_c k$

ϱ_r = kinetic reduced density = ϱb_o

τ = kinetic reduced temperature = $T\ k/\varepsilon = T/C_1 T_c$

μ = molecular dipole moment

μ_r = reduced dipole moment = $\mu^2/(RT_c)\ (v_c/N)$

TABLE 1.—A COMPARISON OF THE CRITICAL CONSTANTS AND THE KINETIC CONSTANTS FOR SOME SEMISPHERICAL NONPOLAR GASES

Substance	T_c°K.	p_c atm.	v_c cc./mole	ϵ/k °K.	b_o cc./mole	C_1	C_2	C_3
N_2	126.3	33.3	79.8	95.4	64.1	0.752	3.65	1.24
O_2	154.8	50.1	74.4	117.0	54.4	0.758	3.53	1.36
Air	132.5	37.2	82.9	102.0	60.3	0.769	3.73	1.33
Ne	44.4	26.9	41.7	34.9	27.1	0.788	3.94	1.54
CO	132.9	34.5	90.0	100.2	67.2	0.752	3.55	1.34
CH_4	191.0	45.8	98.7	148.2	70.2	0.775	3.79	1.41
A	150.7	48.0	75.2	119.8	49.8	0.794	4.29	1.51
Xe	289.8	57.9	113.7	221	86.9	0.764	3.60	1.31
Kr	209.4	54.2	107.3	117	58.9	0.820	4.38	1.83
H_2	33.2	12.8	65.0	29.2	29.8	0.877	6.25	2.18
				Average (except H_2)		0.770	3.82	1.43

TABLE 2.—COMPARISON OF EXPERIMENTAL DATA FOR SOME NONPOLAR GASES WITH THE GENERALIZED COMPRESSIBILITY CHARTS

	Temp. °K.	Pressure atm.	Exp., z	Maslan & Littman Chart z	Morgan & Childs Chart z	Nelson & Obert Chart z
Neon	60.04	59.77	0.712	0.730	0.680	0.715
	90.5	41.37	0.964	0.950	0.950	0.967
	293.1	61.7	1.040	1.030	1.020	1.043
Argon	157.26	41.9	0.673	0.700	0.675	0.705
	215.4	35.1	0.925	0.917	0.920	0.921
	293.5	61.7	0.970	0.956	0.962	0.964
	373.2	188.0	1.015	0.980	1.020	1.006
CO	273.2	150	0.989	.....	0.962	0.987
	323.2	200	1.061	.....	1.054	1.064
	473.2	200	1.101	.....	1.095	1.103
CH_4	248.2	200	0.697	.....	0.710	0.700
	323.2	200	0.881	.....	0.900	0.874
	473.2	300	1.070	.....	1.085	1.073

If the Bird-Spotz tables are to be used, Equations (22) and (23) will yield the correct pseudoconstants for the Bird-Spotz equations. If the real-force constants listed by Bird-Spotz for ethylene were to be used, the z value would be greatly in error as ethylene does not have the spherical symmetry of the gases listed in Table 1.

It should be emphasized however that the method shown in Example 2 can yield no better results than a good compressibility chart based upon critical constants. The advantage of the proposed method lies in the derivatives of the Bird-Spotz tables, which allow thermodynamic properties to be readily calculated (rather than to find compressibility factors). Since the computations for property values are tedious, no example is given here; the foregoing discussion and Equations (20) to (23) outline sufficiently the proposed method.

NOTATION

b_o = kinetic constant = $2/3\pi N r_o^3$

b_o' = pseudokinetic constant = $17\ T_c/p_c$

k = Boltzmann constant

N = Avogadro's number

p = pressure, atm.

p_c = critical pressure

p_r = reduced pressure = p/p_c

p_r' = pseudoreduced pressure = $p\ v_c/RT_c$ also, kinetic reduced pressure = $p\ k\ b_o/R\varepsilon = p/c_2 p_c$

R = universal gas constant = 82.06 cc.atm./mole °K.

r_o = collision diameter between two molecules with negligible kinetic energy

T = absolute temperature, °K.

T_c = critical temperature

T_r = reduced temperature = T/T_c

T_r' = pseudoreduced temperature = $RT/p_c v_c$

v = specific volume = cc./mole

v_c = critical volume

v_r = reduced volume = v/v_c

v_r' = pseudoreduced volume = $p_c v/RT_c$

z = compressibility factor = pv/RT

z_c = compressibility factor at the critical point = $p_c v_c/RT_c$

Greek Letters

ε = kinetic force constant or maximum energy of attraction between two molecules

LITERATURE CITED

1. Joffe, J., *Chem. Eng. Progr.*, **45**, 160 (1949).
2. Meissner, H. P., and R. Seferian, *Chem. Eng. Progr.*, **47**, 579 (1951).
3. Su, G. J., *Ind. Eng. Chem.*, **38**, 803 (1946).
4. Kammerlingh Onnes, H., *Commun. Phys. Lab. Univ. Leiden*, **11**, *Suppl.* 23, 115 (1912).
5. Morgan, R. A., and J. H. Childs, *Ind. Eng. Chem.*, **37**, 669 (1945).
6. Maslan, F. D., and T. M. Littman, *Ind. Eng. Chem.*, **45**, 1566 (1953).
7. Nelson, L. C., and E. F. Obert, *Trans. Am. Soc. Mech. Engrs.*, **76**, 1057 (October, 1954).
8. Hirschfelder, J. O., R. B. Bird, and E. L. Spotz, *Trans. Am. Soc. Mech. Engrs.*, **71**, 921 (1949).
9. Bird, R. B., and E. L. Spotz, *Univ. Wisconsin, CM-599* (May, 1950).
10. DeBoer, J., and A. Michaels, *Physica*, **6**, 97 (1939).
11. Hirschfelder, J. O., R. B. Bird, and E. L. Spotz, *Chem. Revs.*, **44**, 205 (1949).
12. Lennard-Jones, J. E., *Proc. Roy. Soc. (London)*, **A106**, 463 (1924).
13. Hall, N. A., and W. Ibele, Preprint Paper 54-A-140, Am. Soc. Mech. Engrs. (Dec. 3, 1954).

Upward Cocurrent Annular Flow of Air and Water in Smooth Tubes

SEYMOUR CALVERT AND BRYMER WILLIAMS
University of Michigan, Ann Arbor, Michigan

Two-phase fluid flow is distinguished from single-phase flow in two respects: (1) the cross section for flow of either fluid is not defined by the conduit alone and (2) not only the extent but the manner of frictional energy exchange for each fluid depends on the individual rates of flow for both fluids. It was believed therefore that an empirical approach would not adequately describe the various situations encountered in two-phase flow, and so study was undertaken to obtain some understanding of the mechanisms of the flow of liquid with a free surface and the momentum exchange between fluids at that surface. It resulted in the development of a method of predicting liquid holdup and pressure drop for flowing systems in which the liquid, lifted by the gas flowing as a central core, moves upward as an annular film along the pipe wall.

In order to clarify the relationship of annular flow to the entire range of vertical two-phase flow modes, a discussion of vertical two-phase flow is presented, followed by an analysis of the special case of vertical, upward, annular flow; a description of the experimental work; and a comparison of experimental data with predictions.

The possible modes of vertical, two-phase flow are illustrated in the sketches in Figure 1, the conditions of liquid and gas flow under which the modes occur being indicated by the positions of the letters on the plot of pressure drop vs. air rate, shown as the bottom part of the figure. This pressure drop was drawn from experimental data (*22*) for the upward flow of air and 175 lb./hr. of water in a 1-in. I.D. plastic tube. At zero air rate the pressure drop is 12 in. of water/ft. of tube plus a small frictional loss. When a small amount of air is introduced continuously, it is dispersed and the pressure drop with increasing air rate approaches a minimum as the density of the mixture in the tube decreases. This is the mode of flow in ordinary gas lift. At about this minimum the flow mechanism changes from aerated, in which the air flows as small bubbles, to piston flow, in which the air flows as large, bullet-shaped bubbles. As the air rate is further increased, the pistons become unstable and the flow mechanism passes through the regimes of churn and of wave entrainment. These regimes may be thought of as merely the transition region between piston and annular flow since the violent, patternless agitation of churn flow gives way to the more placid, but still erratic, movement of waves superimposed on a film of water and finally to the uniform motion of annular flow. At some higher air rate drops of water will be pulled from the crests of the small waves on the annular film and entrained.

Thus annular flow is bounded by the regimes of wave and drop entrainment. The lower limit of annular flow is at the second minimum pressure drop (at about 18 cu.ft./min. in Figure 1). The upper limit has not been observed within the range of experimental data

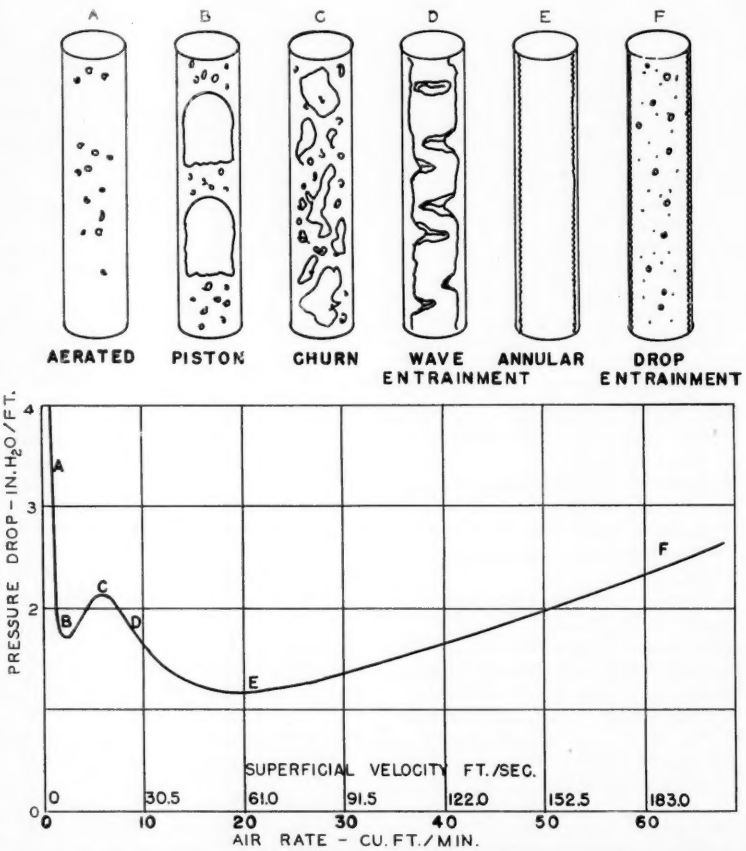

FIG. 1. FLOW PATTERNS IN UPWARD TWO-PHASE FLOW AND A PLOT OF PRESSURE DROP VS. AIR RATE IN A 1-IN. I. D. TUBE.

available (the position of point F in Figure 1 is merely illustrative).

The regime of upward, cocurrent annular flow is defined as that in which the liquid flows as a uniform annular film on the pipe wall while the gas flows as a central core inside the liquid annulus. Two simultaneous processes take place in annular flow: the liquid film flows as a result of the drag exerted on it by the gas and the flowing gas loses a quantity of energy which is dictated by the amount of liquid flowing. A mathematical description of the flow of the liquid film is derived here through an analytical procedure based on the Prandtl and Von Karman (*17*) theories of turbulent flow, and the result is a general expression which is valid for any liquid film. This special derivation is necessitated by the significant effect of gravity on the vertical flow of the liquid and by special consideration which must be given to the effect of the solid boundary, which is of more importance in film flow than in a full-running pipe.

Gas loses momentum to the liquid in annular flow in what may be considered two separate mechanisms. One is the loss by "skin friction," where the gas directly in contact with the boundary is moving slowly and the retarding effect is exerted gradually into the main stream. The other mechanism is that of "profile drag," where gas of high velocity impinges on a projecting object and loses a part of its kinetic energy. The obstacles in the path of the gas are the liquid waves. Their projected areas determine the drag area and their shapes and spacing determine the drag coefficient, which represents the fraction of the kinetic energy of impingement lost.

Skin friction can be determined in the usual manner of predicting pressure drop for single-phase flow through smooth pipes by employing the friction factor. The determination of profile drag requires a knowledge of the velocity of the gas striking the projections, the area of the projections, and the drag coefficient. The combined effect of these quantities on profile drag had to be determined experimentally.

Derivations of equations describing the liquid film and the determination of profile drag from experimental data will be given in the following pages. The rate of the liquid film can be defined in terms of the pressure drop and the thickness of the film. The pressure drop is also related to the air velocity and the liquid-film thickness. A combination of these two relationships will yield one equation with three variables: air rate, water rate, and pressure drop.

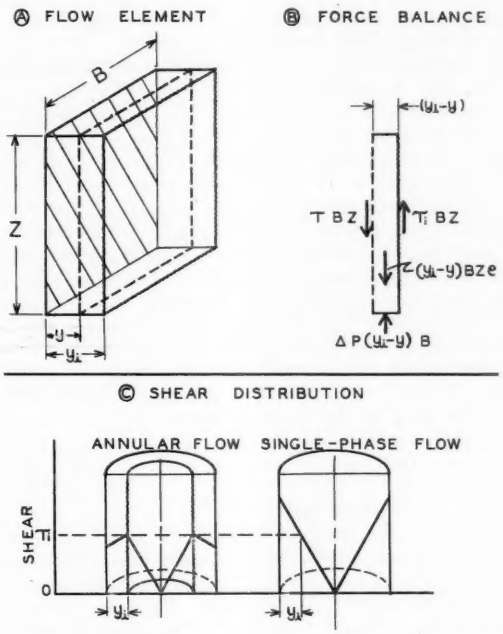

FIG 2. FLOW ELEMENT AND ILLUSTRATIONS OF FORCE AND SHEAR DISTRIBUTIONS.

LIQUID FILM

As every application of force is opposed by an equal reaction, the force distribution in a vertical annular film can be described in general terms by making free-body force balances over successive slices of the film as illustrated in Figure 2. By this means the pressure drop can be related to the local shear stress, which is the force acting in the direction of flow over a unit of area in a plane parallel to the flow.

The general expression for the shear distribution in a verticle film is

$$\tau(BZ) = \tau_i(BZ) + \Delta P(y_i - y)B - (y_i - y)\,BZ\rho_L \qquad (1)$$

where

τ = shear (force per unit area — BZ) at any position y in the film, lb./sq.ft.
τ_i = shear at the air-water interface, lb./sq.ft.
y = distance from the solid boundary, ft.
y_i = film thickness, ft.
B = width of the film, ft.
Z = height of the film
ΔP = pressure drop in the direction of Z, lb./sq.ft.
ρ_L = density of the liquid, lb./cu.ft.

Figure 2*a* is a sketch of an elemental section of the annular flow system, and Figure 2*b* illustrates the force balance over a slice of this element. It should be noted that the model element is simplified by being considered a flat plane rather than a cylinder. Figure 2*c* represents possible shear distributions in both vertical, upward, annular flow and single-phase flow in tubes. The shear distribution in both cases is given by a force balance; that for single-phase vertical flow is

$$\tau = \Delta P \frac{\pi r^2}{2\pi r Z} - \frac{\pi r^2 Z \rho}{2\pi r Z} \qquad (2)$$

or

$$\tau = \frac{r}{2}\left(\frac{\Delta P}{Z} - \rho\right) \qquad (3)$$

where r is the radius.

Equation (1) has been derived for annular film flow, and as τ_i can be related to $\frac{\Delta P}{Z}$ by Equation (2),

the shear distribution for a film can be written as

$$\tau = \left(\frac{\Delta P}{Z} - \rho_G\right)\left(\frac{r_o - y_i}{2}\right) + \left(y_i - y\right)\left(\frac{\Delta P}{Z} - \rho_L\right) \quad (4)$$

To clarify the disconcerting experimental observation that a water film can flow up a tube with a pressure drop of much less than 1 ft. of water/ft. of height (*see* Figure 1), one may compare the shear distributions for single- and two-phase flow.

If the fluid in the single-phase case has the same density as that flowing in the film, and the shear at a distance y_i from the wall is the same in both cases, as shown in Figure 2*c*, the pressure drops in the two cases are related by Equation (5):

$$\frac{\Delta P_A}{Z} - \rho_G = \frac{\Delta P_S}{Z} - \rho_L \quad (5)$$

where

ΔP_A = pressure drop for annular flow, lb./sq.ft.
ΔP_S = pressure drop for single-phase flow, lb./sq.ft.
ρ_G = density of gas phase, lb./cu.ft.

If the two fluids in question are air and water at atmospheric pressure, ρ_G is negligible. The pressure drop required to produce a given τ_i is lower for annular flow than for single-phase flow. It is seen that the shear distribution within the annular film is not the same as it would be for the same film in single-phase flow of the same fluid; therefore equations which describe single-phase flow will not describe vertical annular-film flow. The two cases will approach each other when the pressure drop is so high that it overshadows the effect of liquid density upon the shear distribution.

With the shear distribution defined, the next problem is to describe the manner in which the fluid will act to implement this distribution of forces. One element of a fluid body can exert a force on an adjacent element only if there is a difference in velocity between them. Consequently the ultimate goal of this next analysis is the determination of a velocity pattern that will sustain the annular-flow shear distribution.

One can predict whether the flow pattern will be laminar or turbulent in single-phase flow by the use of the Reynolds criterion of turbulence. Unfortunately this criterion becomes meaningless when it is applied to two-phase flow, because of the absence of a term which considers the phase-to-phase energy transfer. A more general criterion which has been developed here and will be discussed in a later section indicates that turbulent flow is the predominant type encountered in vertical, annular water-film flow. All further attention is, then, given to the turbulent flow of liquid films.

TURBULENT-FLOW CONCEPTS: ANNULAR FLOW

The application of the Prandtl theory to single-phase flow has been well discussed(*1*). Several simplifying assumptions which are made in that treatment, however, are not sufficiently accurate to justify its adoption for liquid-film flow. The fact that the bulk of the fluid in single-phase flow moves in the central turbulent core masks errors in the consideration of the fluid close to the boundary. In annular flow the liquid is so greatly influenced by the solid boundary that one must be especially concerned with fluid behavior in this region and the assumptions must be evaluated for this special case.

First, it may be assumed that the motion of the fluid at any point is dependent upon the local shear stress. With this concept Von Karman(*1*) arrived at a definition of turbulent flow which is almost identical with Prandtl's. Both definitions are valid for single-phase flow, as is shown by their use in correlating experimentally determined velocity profiles.

Next there are assumptions which are implied by the first condition. If the local velocity gradient is dependent on the local shear alone, then the mixing-length distribution in a film of liquid must be the same as that in a pipe running full of liquid. Likewise the thickness, δ of the laminar layer must depend on the shear at the laminar layer.

The first of these implications is quite sound as the mixing length is a function of distance from the wall and not of the flow conditions. The second assumption is more difficult to justify as the point conditions which determine thickness of the laminar layer δ are not known. The only definite information available is the empirical relationship giving δ as a function of kinematic viscosity and shear at the wall for single-phase flow.

$$\frac{\delta}{D} = \frac{N}{Re}\sqrt{\frac{8}{f}} = N\frac{\mu}{\rho\sqrt{\frac{\tau_o g}{\rho}}} \quad (6)$$

where

δ = thickness of the laminar layer
D = pipe diameter.
N = a constant for all fluids
Re = Reynolds number
f = friction factor
τ_o = shear at pipe wall
μ = absolute viscosity

This relationship must be modified and utilized to define δ for annular flow although it is not yet directly applicable. It was shown earlier (*see* Figure 2) that while the shear at the wall defines a unique shear distribution for single-phase flow, it does not for annular flow. Consequently, it is assumed that the shear stress at δ in an annular film bears the same relationship to δ that wall shear does in single-phase flow.

DERIVATION OF FILM-FLOW EQUATIONS

The mathematical description of film flow is attained in two steps. First the differential equations expressing velocity gradient are integrated to give a description of velocity distribution. Once the velocity distribution is known, the rate of flow can be determined by another integration process. This is done first for the turbulent layer and next for the laminar layer.

The shear is related to the velocity gradient which it produces by

$$\tau = \frac{\rho}{g} l^2 \left(\frac{du}{dy}\right)^2 \quad (7)$$

where l is the Prandtl mixing length and u is the velocity in the axial direction at a distance y from the wall.

The shear τ may be eliminated by combining Equations (4) and (7):

$$\frac{\rho_L}{g} l^2 \left(\frac{du}{dy}\right)^2 = \left(\frac{\Delta P}{Z} - \rho_G\right)\left(\frac{r_o - y_i}{2}\right) + \left(\frac{\Delta P}{Z} - \rho_L\right)\left(y_i - y\right) \quad (8)$$

The velocity distribution is found by integration of Equation (8), which states the relationship between local velocity gradient and local shear. To do this it is assumed that $(r_o - y_i) \approx r_o$ and that $(y_i - y)\frac{\Delta P}{Z}$ is negligible. This

amounts to taking an average value for the shear due to $\frac{\Delta P}{Z}$:

$$\frac{r_o}{2}\left(\frac{\Delta P}{Z}\right)-\left(y_i-y\right)\rho = \frac{\rho}{g}l^2\left(\frac{du}{dy}\right)^2 \quad (9)$$

The mixing length $l = 0.4y$, as evaluated by Nikuradse (*1*).

$$\frac{r_o}{2}\left(\frac{\Delta P}{Z}\right)-\left(y_i-y\right)\rho = \frac{\rho}{g}\left(0.4y\right)^2\left(\frac{du}{dy}\right)^2 \quad (10)$$

Next, if the equation is rearranged and the square root taken

$$\frac{du}{dy}=\frac{\sqrt{g}\left[\frac{r_o}{2\rho}\frac{\Delta P}{Z}+\left(y_i-y\right)\right]^{\frac{1}{2}}}{0.4y};$$

let

$$A=\frac{r_o}{2\rho}\frac{\Delta P}{Z} \quad (11)$$

To obtain a simple form after this equation is integrated, the term in the brackets is expanded according to the binomial theorem:

$$\frac{du}{dy}=\frac{\sqrt{Ag}}{0.4y}+\frac{\sqrt{g}}{2(0.4y)}\frac{(y-y_i)}{\sqrt{A}} - \frac{\sqrt{g}}{8(0.4y)A^{3/2}}\frac{(y-y_i)^2}{}+\cdots \quad (12)$$

with the condition for convergence that

$$\left[\frac{(y-y_i)}{\frac{r_o}{2\rho}\frac{\Delta P}{Z}}\right]^2 \leqq 1 \quad (13)$$

The significance of this condition may be more readily seen after rearrangement of (17) to give

$$\left|(y-y_i)\rho\right| \leqq \left|\frac{r_o}{2}\frac{\Delta P}{Z}\right| \leqq \left|\tau_i\right| \quad (14)$$

This means that the series will not converge for the values of $\tau_o = 0$ which would occur if the gravity terms were equal to the interfacial shear. The necessary condition is obtained in vertical, upward, annular flow, and so the series is convergent for the case.

Equation (12) may be integrated to give

$$u=\frac{\sqrt{Ag}}{0.4}\ln y+\frac{\sqrt{g}}{2(0.4)\sqrt{A}}(y-y_i\ln y)-\frac{\sqrt{g}}{2(0.4)A^{3/2}}\left(\frac{y_2}{2}+2yy_i+y_i\ln y\right)+\ldots+C \quad (15)^*$$

The velocity distribution in the turbulent region is thus given by

$$[u]_\delta^y=\left[\frac{\left(\sqrt{\frac{r_o}{2\rho}\frac{\Delta P}{Z}g}\right)}{0.4}\ln y+\frac{\sqrt{g}}{0.8\sqrt{\frac{r_o}{2\delta}\frac{\Delta P}{Z}}}(y-y_i\ln y)\right]_\delta^y \quad (16)$$

To simplify, if

$$\frac{\sqrt{\frac{r_o}{2\delta}\frac{\Delta P}{Z}g}}{0.4}=X;$$

$$\frac{\sqrt{g}}{0.8\sqrt{\frac{r_o}{2\delta}\frac{\Delta P}{Z}}}=Y$$

then

$$u-u_\delta=X\ln\frac{y}{8}+Y\left[(y-y_i\ln y)-\delta+y_i\ln\delta\right] \quad (17)$$

Equation (17) describes the velocity distribution in the turbulent region in terms of a base velocity, $u\delta$, which can be determined by application of laminar-flow equations in the region from the wall to δ. The quantity of liquid flowing through the film can be computed by integrating an equation giving the product of velocity and the differential area for flow; that is,

$$L=2\pi r\int_o^{y_i}u\,dy \quad (18)$$

The volume rate of flow, L, is defined as

$$L=2\pi r_o\left[\int_o^\delta u\,dy+\int_\delta^{y_i}u_\delta dy+\int_\delta^{y_i}(u-u_\delta)\,dy\right] \quad (19)$$

The first two terms in the brackets in Equation (19) depend on the laminar-flow mechanism and δ so they are called the *laminar terms.* As the third term involves the turbulent-flow mechanism, it is called the *turbulent term.*

The laminar terms may be approximated as

$$L_{lam}=2\pi r_o\left[u_\delta\left(y_i-\frac{\delta}{2}\right)\right] \quad (20)$$

In the derivation of the foregoing equation it was assumed that the laminar velocity gradient may be considered constant for the calculation of L_{lam} although it cannot be so assumed for the calculation of u

The volume rate of flow in the turbulent term is

$$L_t=2\pi r_o\int_\delta^{y_i}(u-u_\delta)dy=2\pi r_o\int_\delta^{y_i}\left[X\ln\frac{y}{\delta}+Y(y-\delta-y_i)\ln\frac{y}{\delta}\right]\ln y \quad (21)$$

Integration of Equation (21) gives Equation (22):

$$\frac{L_t}{2\pi r_o}=\ln\frac{y_i}{\delta}\left(Xy_i-Yy_i^2\right)-\left(1-\frac{\delta}{y_i}\right)\left(Xy_i\right)+\left(Yy_i^2\right)\left(1-\frac{\delta}{y_i}\right)\left(\frac{3-\delta/y_i}{2}\right) \quad (22)$$

and since $\delta/y_i \ll 3$

$$\frac{L_t}{2\pi r_o}=\ln\frac{y_i}{\delta}\left(Xy_i-Yy_i^2\right)-\left(1-\frac{\delta}{y_i}\right)\left(Xy_i-\frac{3}{2}Yy_i^2\right) \quad (23)$$

*It is interesting to note that this is in the form of the Prandtl velocity distribution for full pipes where

$$u=\frac{u^*}{k}\ln y+C$$

and in the same symbols, for Equation (15),

$$u=\frac{u^*}{k}\ln y+\frac{g}{2k\,u^*}(y-y_i\ln y)+\ldots+C$$

where

$$u^*=\sqrt{\frac{r_o g}{\rho}} \text{ and } k=\frac{l}{y}=0.4 \quad (15a)$$

In Equation (15a) the terms after the first on the right side account for the gravity effect. Without these terms Equation (15a) would be identical with Prandtl's. The first two terms on the right side of (15) are sufficient to represent the series with reasonable accuracy, and accordingly the remaining terms are neglected.

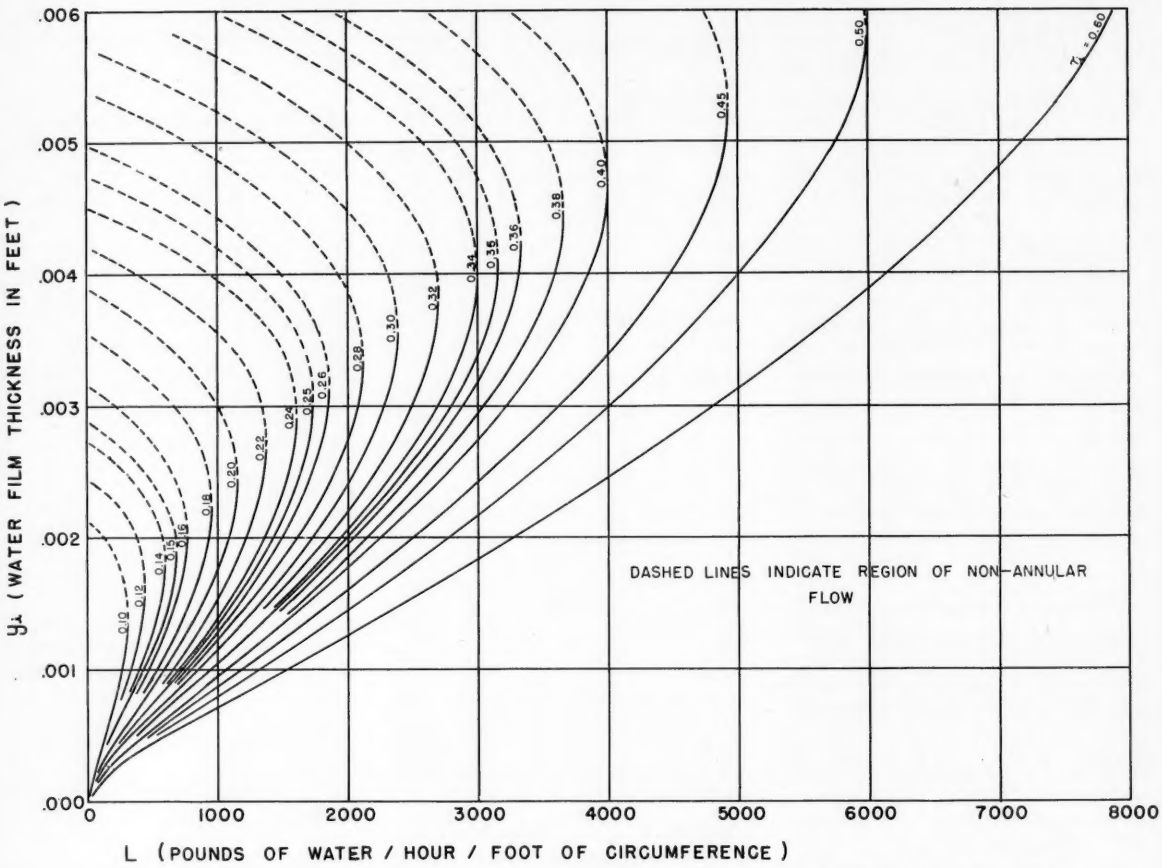

FIG. 3. PREDICTED FILM THICKNESS VS. WATER RATE WITH INTERFACIAL SHEAR AS THE PARAMETER.

The final form of the volume rate of flow equation is the sum of L_{lam} and L_t as given below:

$$\frac{L}{2\pi r_o} = \left[u\left(y_i - \frac{\delta}{2}\right) + \ln\frac{y_i}{\delta}\left(Xy_i - Yy_i^2\right) - \left(1-\frac{\delta}{y_i}\right)\left(Xy_i - \frac{3}{2}\,Yy_i^2\right)\right] \quad (24)$$

The remaining task is to evaluate u_δ and δ in terms of $\frac{\Delta P}{Z}$ and y_i. If δ is determined by τ_δ, one can evaluate δ by solving Equations (25) and (26) below:

$$\delta = \frac{N\mu}{\rho u_\delta} = 11.6\,\frac{\mu}{\rho\sqrt{\frac{\tau_\delta g}{\rho}}} \quad (25)$$

and

$$\tau_\delta = \tau_i - (y_i - \delta)\,\rho \quad (26)$$

The value of 11.6 has been taken for the value of the constant N; this is an assumption since there is some dispute as to the exact value of N although 11.6 appears to be good average (*1*).

Next u_δ can be determined by solving Equation (27), which is the definition of viscosity

$$\int_o^{u_\delta} du = \frac{g}{\mu}\int_o^{\delta} [\tau_i - \rho\,(y_i - y)]\,dy \quad (27)$$

which gives upon integration

$$u_\delta = \frac{g\rho}{\mu}\left[\left(\frac{\tau_i}{\rho} - y_i\right)\delta + \frac{\delta^2}{2}\right] \quad (28)$$

SUMMARY OF LIQUID-FILM FLOW MEASUREMENTS

To summarize the preceding development, one may set up a procedure for determining the volume rate of flow, L, if y_i, μ, ρ, r_o and τ_o are known. The following stages are involved:

1. Determination of δ with Equations (25) and (26).
2. Determination of μ_δ with Equation (28).
3. Determination of L_{lam} with Equation (20).
4. Determination of L_t with Equation (23).
5. Addition of L_{lam} and L_t to give L.

The results of a series of computations under the foregoing procedure can be tabulated graphically in a plot of y_i vs. L with τ_i as a parameter. Figure 3 is such a plot for the upward flow of water films. The lines of constant shear are dotted in the region in which annular flow does not exist.

THE CRITERION OF TURBULENCE

The Reynolds criterion has been applied to two-phase flow by various workers who used a hydraulic diameter as the significant length.

The success of such an approach is limited to special cases in which the interphase momentum exchange is either negligible or constant.

An example of this approach is the work of Friedman and Miller (*7*) on falling annular films in vertical pipes. They indicate that liquid films running downward while a stationary core of air fills the center of the pipe become turbulent at a Reynolds number of 1,000. Fallah, Hunter, and Nash (*6*) show that when another fluid, denser than air but lighter than water, is employed as the central core the critical Reynolds number is much less than 1,000, even as low as 15. Obviously, the flow rate of the film, its fluid properties, and the pipe diameter alone are not sufficient to define its state of motion.

In order completely to define the flow of each fluid in two-phase flow it is necessary to include the effect of momentum transfer between phases in the criterion of turbulence. One familiar quantity has this property although it is deficient in a significant length term: the thickness of the laminar layer δ set by the kinematic viscosity of and the shear in the fluid. The ratio of δ to pipe diameter for single-phase flow is a function of the Reynolds number and the friction factor only (*1*). Since the friction factor becomes a function of Reynolds number alone rather than of Reynolds number and relative roughness as the Reynolds number decreases to values of about 2,100, the ratio of δ to diameter has a single critical value corresponding to $Re = 2{,}100$.

By analogy, the ratio of δ/y_i is taken as the criterion of turbulence for film flow. Film thickness replaces pipe diameter as the significant length in the ratio. A critical value of this ratio, determined from the data presented by Friedman and Miller by evaluating δ/y_i at $Re = 1{,}000$, is

$$\left(\frac{\delta}{y_i}\right)_c = \frac{11.6}{2.85\sqrt{2.85g}} = 0.425 \quad (29)$$

This critical ratio marks the point of abrupt change from turbulent to laminar flow. If it is larger than 0.425 the flow pattern will be laminar. It is interesting to note that this criterion indicates that the film will become entirely laminar in character at a point where roughly half its thickness would flow by the laminar mechanism even if the flow were turbulent. This criterion was applied to the case of vertical upward annular flow of water, and the indication was that the flow is turbulent throughout the regime.

TABLE 1.—RANGE OF EXPERIMENTAL INVESTIGATION

Tube diameters, in.	1.98	1.112	1.0
Tube lengths, ft.	7	8	20 and 10
Water rate, lb./hr.	0-2000	0-300	0-300
Air rate, cu. ft./min. at test conditions	55-112	10-74	10-74

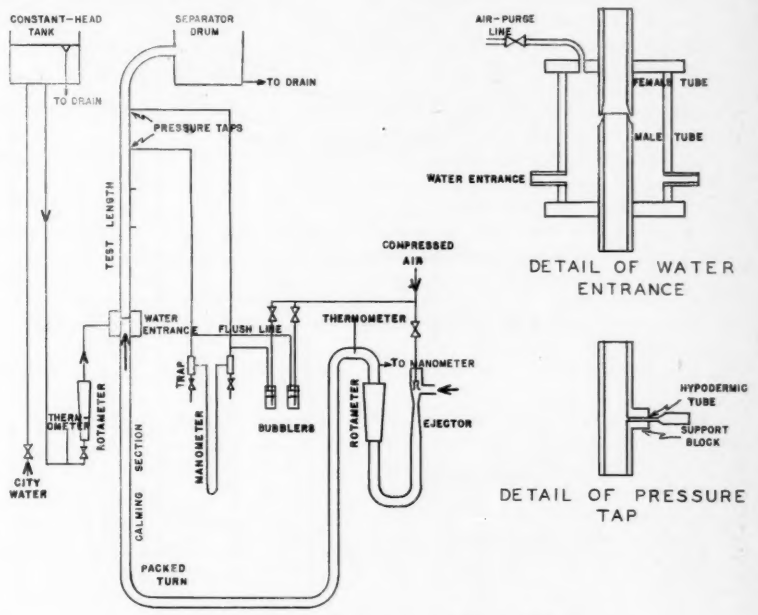

FIG. 4. DIAGRAMS OF EXPERIMENTAL APPARATUS.

EXPERIMENTAL

Theoretical considerations of the modes of flow predict the momentum transfer and pressure drop between the phases. It was necessary to obtain experimental data to establish the validity of these equations which define film flow and to evaluate certain coefficients. Data of B. H. Radford (*18*) for the upward flow of air and water in a 1-in. tube provided water-holdup information which was used to estimate liquid-film thickness. The present investigation provided pressure-drop data for the various tubes and flow conditions given in Table 1.

The system is shown in Figure 4. The equipment provides for metered air to enter the test pipe from a straightening section and metered water to enter through a circumferential slot in the bottom of the test section. Pressure drops were measured over 2- or 3-ft. intervals along the tube with manometers connected with air-flushed pressure taps. This arrangement provided for measurement of entrance and exit effects, if any. Various entrance devices were tried, and as the annular ring shown in Figure 4 proved to be the most stable, results reported are for its use. Typical data are shown in Figure 5.

EQUATION FOR PROFILE DRAG

One can describe the profile-drag process mathematically by writing first that the shear produced is equal to a fraction of the stagnation pressure of the gas stream times the area of stagnation, as

$$F = C_D(\Delta P_S A_D)\, Z\, 2\pi r_o \quad (30)$$

where

F = drag force, lb.

Z = length of pipe, ft.

C_D = drag coefficient

ΔP_S = stagnation pressure, lb./sq.ft.

A_D = projected area for drag, sq.ft. /sq.ft. inside pipe area.

r_o = pipe radius, ft.

The stagnation pressure is obtained from Bernoulli's equation as

$$\frac{u_A^2}{2g} = \frac{\Delta P_s}{\rho} \quad (31)$$

Thus

$$F = C_D\left(\frac{u_A^2 \rho_G A_D}{2g}\right) Z\, 2\pi r_o \quad (32)$$

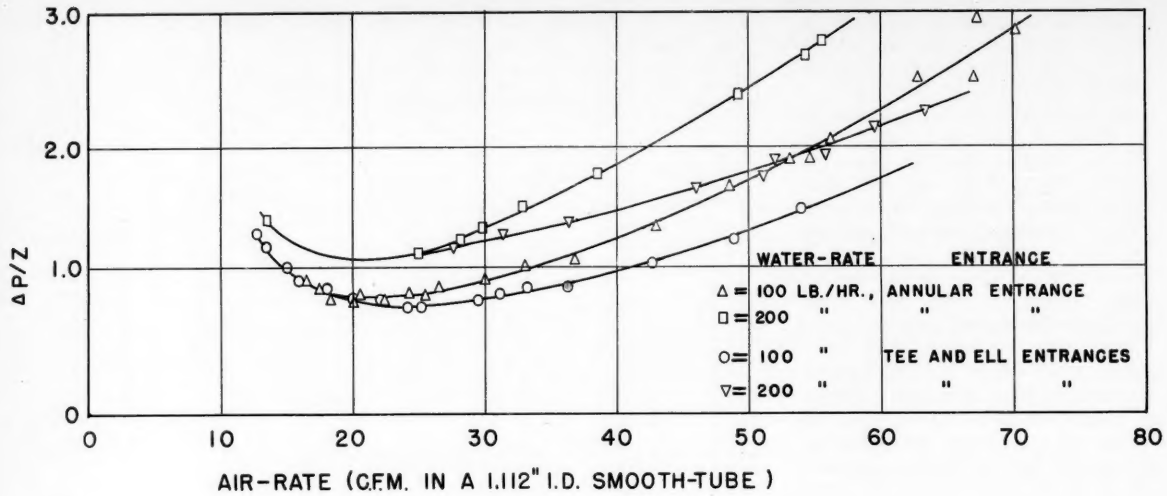

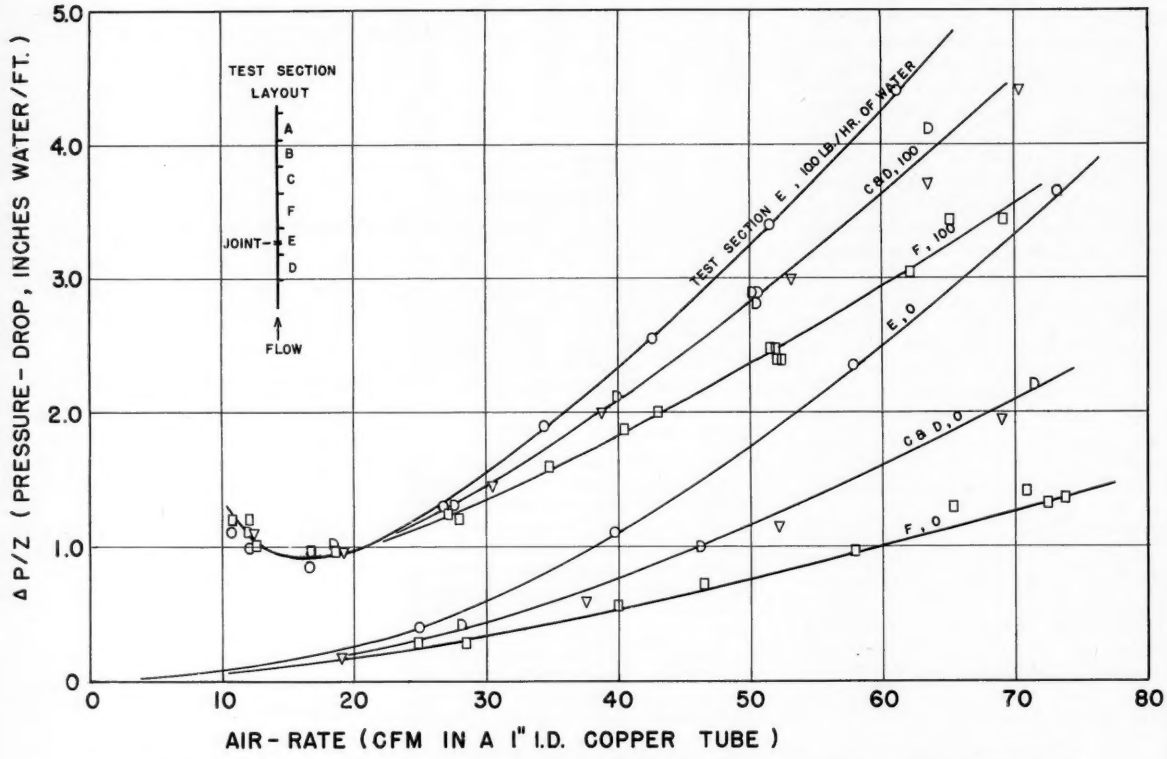

FIG. 5. PRESSURE-DROP VS. AIR-RATE PLOTS FOR VARIOUS WATER ENTRANCES AND FOR TUBE ROUGHNESS.

and also

$$\Delta P_E = C_D \left(\frac{u_A^2 \rho_G A_D}{2g} \right) Z \left(\frac{2\pi r_o}{\pi r_o^2} \right) \quad (33)$$

and

$$\tau_E = \frac{\Delta P_E}{Z} \left(\frac{r_o}{2} \right) \quad (34)$$

where

ΔP_E = pressure drop due to profile drag, lb./sq.ft.

τ_E = shear due to profile drag, lb./sq.ft.

ρ_G = gas density, lb./ cu.ft.

μ_{avg} = average velocity of gas stream based on superficial area, ft./sec.

Equation (33) is in a form which would permit one to predict profile-drag loss if the terms on the right-hand side are known. By adding profile drag to the skin friction the total pressure drop is obtained.

$$\Delta P_W = \Delta P_E + \Delta P_D \quad (35)$$

where

ΔP_W = total pressure drop (wet), lb./sq.ft.

ΔP_D = pressure drop for dry tube, lb./sq.ft.

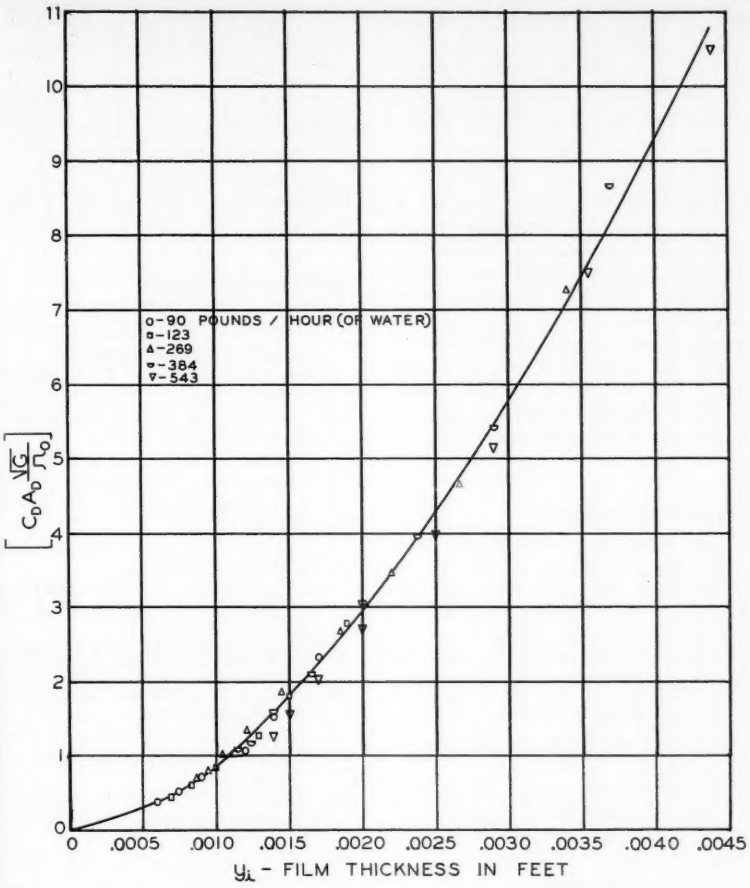

FIG. 6. RELATIONSHIP BETWEEN $C_D A_D \frac{\sqrt{G}}{r_o}$ AND y_i.

To predict ΔP_E one must know C_D and A_D under given conditions of flow. No analytical method is available for predicting these quantities, but an empirical correlation valid for the air-water system may be developed by use of the experimental data. The method of correlation is based on the assumption that A_D is dependent mainly on the amount of water present in the tube and to some extent upon the velocity of the air.

Since C_D will vary with the wave geometry and the gas velocity, it is combined with A_D in this correlation as the term $(C_D A_D)$, which may be computed directly from experimental pressure-drop data. It was found from experimental data that $(C_D A_D)$ is proportional to $u_A^{-\frac{1}{2}}$ and also dependent upon y_i. This relationship is graphically shown in Figure 6, a plot of $C_D A_D \frac{\sqrt{G}}{r_o}$ vs. y_i. By use of Figure 6 in conjunction with Equation (36) below, the pressure drop due to profile drag can be determined if air rate and density, tube diameter, and water-film thickness are known.

$$\Delta P_E = \left(\frac{G}{r_o}\right)^{3/2}\left(\frac{\rho_G}{(60\pi)^2 2g}\right)\left(C_D A_D \frac{\sqrt{G}}{r_o}\right)\frac{2Z}{r_o} \qquad (36)$$

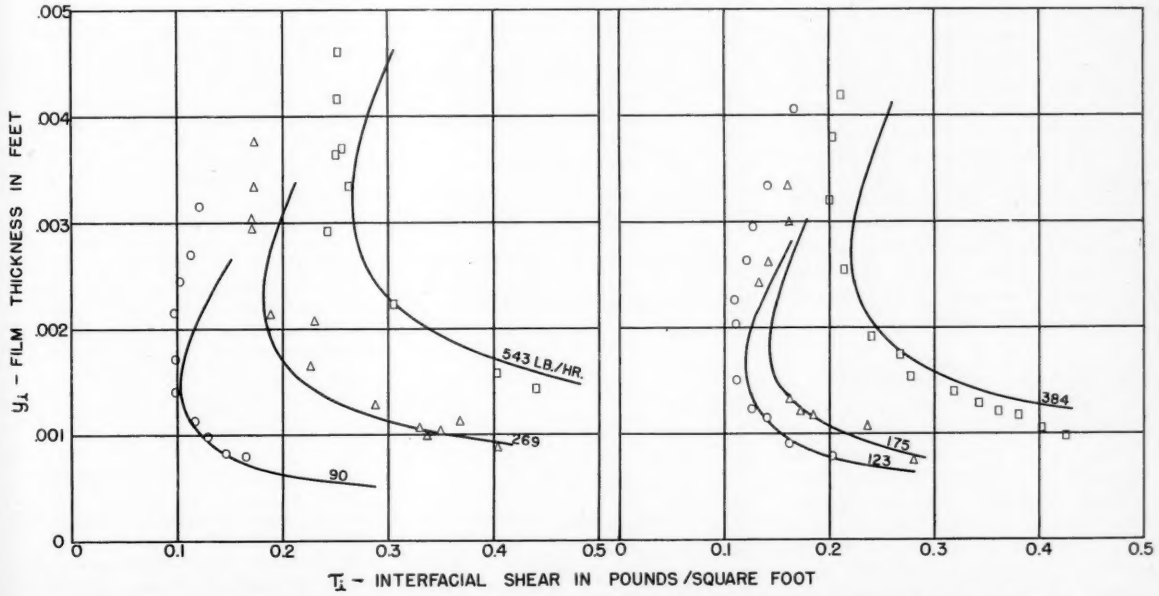

FIG. 7. PREDICTED WATER-FILM THICKNESS VS. INTERFACIAL SHEAR FOR SEVERAL WATER RATES IN A 1.05-IN. I.D. SMOOTH TUBE COMPARED WITH EXPERIMENTAL POINTS.

To summarize the method of computing pressure drop for annular flow if y_i, G, ρ_G, μ_G, and r_o are known, the following procedure is given

1. Determine ΔP_D by the friction-factor method for the flow rate of G through a dry tube of radius r_o.
2. Determine ΔP_E by use of Equation (36) and Figure 6.
3. Add ΔP_E and ΔP_D to get ΔP_W, the pressure drop for annular flow.

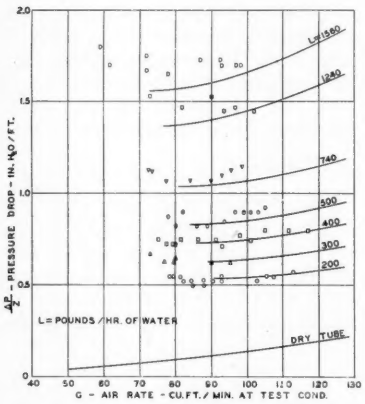

FIG. 8. COMPARISON OF EXPERIMENTAL WITH PREDICTED RELATIONSHIPS BETWEEN PRESSURE DROP, AIR RATE, AND WATER RATE FOR ANNULAR FLOW.

COMPARISON OF PREDICTED WITH EXPERIMENTAL WATER-FILM THICKNESS

The mathematical definition of vertical liquid-film flow was employed to predict water-film thickness as a function of interfacial shear and water-flow rate. The predictions for 90, 123, 175, 269, 384, and 543 lb. of water/hr. in a 1-in. I.D. tube are compared in Figure 7 with experimentally determined values. In the region of annular flow, that is, for film thicknesses smaller than those at the point of minimum shear, there is close agreement between the observed and predicted values.

COMPARISON OF PREDICTED WITH EXPERIMENTAL PRESSURE DROP

Values of pressure drop as a function of air rate for the flow of 200, 300, 400, 500, 740, 1,240, and 1,560 lb. of water/hr. in a 2-in. I.D. tube were predicted by means of the method described. The predicted values are shown along with experimentally observed points on Figure 8, a plot of pressure drop vs. air rate with water rate as the parameter. The solid lines representing predicted values are discontinued at air rates lower than the minimum for annular flow.

CONCLUSION

The agreement between prediction and observation for both film thickness and pressure drop is sufficient to establish the validity of the methods of prediction. The deviation of both observed pressure drop and film thickness from the predicted values at high water rates is probably due to the occurrence of wave entrainment.

ACKNOWLEDGMENT

The authors gratefully acknowledge the permission of Dr. B. A. Radford to use his data on the holdup of liquid in two-phase flow.

NOTATION

A = area, sq.ft.
A_o = projected area for drag, sq.ft./sq.ft.
B = width of film, ft.
C_D = drag coefficient
C = a constant
D = diameter, ft.
F = drag force, lb.
f = friction factor
G = mass velocity, lb./(hr.)(sq.ft.)
g = acceleration of gravity
$k = l/y$
l = Prandtl mixing length, ft.
L = volume rate of flow
N = a constant
ΔP = pressure drop lb./sq.ft.
ΔP_E = pressure drop due to drag, lb./sq.ft.
ΔP_S = stagnation pressure drop, lb./sq.ft.
Re = Reynolds number
r = radius, ft.
u = velocity in axial direction at point y
y = distance from solid boundary, ft.
y_i = film thickness, ft.
Z = height of film, ft.

Subscripts

A = annular flow
C = critical or transition of laminar to turbulent flow
D = dry tube
E = in profile drag
G = gas phase
i = gas-liquid interface
L = liquid phase
lam = laminar flow
o = tube wall
s = single-phase flow
t = turbulent flow
w = wet tube

Greek letters

δ = thickness of turbulent layer
μ = absolute viscosity
ρ = density
τ = shear

LITERATURE CITED

1. Bakhmeteff, B. A., "The Mechanics of Turbulent Flow," Princeton University Press (1941).
2. Bergelin, O., *Chem. Eng.*, **56**, 104 (1949).
3. Boelter, C. M. R., and R. H. Kepner, *Ind. Eng. Chem.*, **31**, 426 (1939).
4. Cromer and Huntington, *Trans. Am. Inst. Mining Met. Engrs.*, **136**, 79 (1940).
5. Dukler, A. E., Ph.D. Thesis, Univ. Delaware (1951).
6. Fallah, R, T. G. Hunter, and A. W. Nash, *J. Soc. Chem. Ind.*, **53**, 367, T-379T (1934).
7. Friedman, S. J., and C. O. Miller, *Ind. Eng. Chem.*, **33**, 885 (1941).
8. Gazley, C., Ph.D. Thesis, Univ. Delaware (1948).
9. Gosline, J. E., *Trans. Am. Inst. Mining Met. Engrs.*, **118**, 56 (1936).
10. Jesser, B. W., and J. C. Elgin, *Trans. Am. Inst. Chem. Engrs.*, **39**, 277 (1943).
11. Keulegan, G. H., *Natl. Bur. Standards Sci. Technol.* Paper 2040, **43** (November, 1949).
12. Kinney and Abramson, *Natl. Advisory Comm. Aeronaut. Tech. Mem.* E51C13 (May, 1951).
13. Laufer, J., *Natl. Advisory Comm. Aeronaut. Tech. Note* 2123 (1950).
14. Martinelli, R. C., J. A. Putnam, and R. W. Lockhart, *Trans. Am. Inst. Chem. Engrs.*, **42**, 681 (1946).
15. Martinelli, R. C., L. M. K. Boelter, T. H. M. Taylor, E. G. Thomsen, and E. H. Morrin, *Trans. Am. Soc. Mech. Engrs.*, **66**, 139 (1944).
16. O'Brien, M. P., and J. E. Gosline, *Ind. Eng. Chem.*, **27**, 1436 (1935).
17. Prandtl, L., and O. G. Tietjens, "Applied Hydro- and Aerodynamics," McGraw-Hill Book Company, Inc., New York (1934).
18. Radford, B. A., M.S. Thesis, University of Alberta (1949).
19. Schlichting, H., *Natl. Advisory Comm. Aeronaut., Tech. Mem.* 823 (1937).
20. Stanton, T., *Proc. Roy. Soc. (London)*, A 137, 283 (1932).
21. Tillman, W., *Natl. Advisory Comm. Aeronaut. Tech. Mem.* 1299 (1944).
22. Uren, L. C., P. P. Gregory, R. A. Hancock, and G. V. Feskov, *Trans. Am. Inst. Mining Met. Engrs.*, **86**, 209 (1930).

(Presented at A.I.Ch.E. Toronto meeting)

ENTHALPY-CONCENTRATION DIAGRAMS OF BINARY AQUEOUS MIXTURES OF HYDRAZINE, SODIUM CARBONATE, AND GLYCERINE

MACK TYNER
University of Florida, Gainesville, Florida

Generally an enthalpy-concentration diagram for a system is prepared for fixed pressure, and to be complete it should include data on the solid, liquid, and vapor phases. Such charts are useful for calculations involving heat balances with accompanying concentration changes. This article outlines the steps in the preparation of a diagram and includes the diagrams for aqueous solutions of hydrazine, sodium carbonate, and glycerine.

Calculation of heat effects accompanying concentration changes in binary solutions can be quickly and easily performed by use of an enthalpy - concentration diagram. Such charts have been called Merkel diagrams after Merkel (*1*), who was the first to give a thermodynamic analysis of the chart and who emphasized the use of it in heat-balance calculations. Zeisberg (*2*) was perhaps the first to compute enthalpy charts of binary mixtures. Ponchon (*3*) and Savarit (*4*) were the first to use the chart for calculating the number of theoretical plates in a rectifying column. Others have contributed to the use of the chart such as Hirsch (*5*), who applied it to single- and multiple-effect evaporators, and McCabe (*6*), who presented the sodium hydroxide-water diagram and reviewed its use in heat-balance calculations. Probably the most complete development of its use was due to Bosnjakovic (*7*). He recently applied the diagram to heat-exchange processes in sugar solutions (*8*) and to chemical processes such as ammonia synthesis (*9*). In summary it might be said that the chart may be used to solve any binary-mixture problem involving the first law of thermodynamics. The second law of thermodynamics is involved only in the phase-equilibrium portions of the diagram.

The principles involved in constructing an enthalpy-concentration diagram, given by Dodge (*10*), will be illustrated here by the construction of a diagram for the hydrazine-water system at 1 atm. The construction requires a complete set of thermochemical data for the pure substances and their mixtures over the temperature range desired for the diagram. Lack of such data is the chief reason that there are so few of these diagrams available to industry today. The data required are as follows:

1. Complete enthalpy-temperature data for the pure substances.
2. Heat of solution or dilution data for the binary mixtures.
3. Heat-capacity data for the binary mixtures.
4. Phase-equilibria data for the system if the solid or vapor phases are to be included in the diagram.

As temperatures are frequently measured on the centigrade scale and heat quantities are given in calories in the scientific literature, the most convenient way to report heat quantities or enthalpies is in calories per gram of system or, for engineering use, the equivalent, which is centigrade heat units per pound (C.h.u.). The enthalpy results in these units may be converted to British thermal units per pound by multiplying by 1.8.

Enthalpy of Pure Substances

The enthalpy data for water are available in tabular form from the work of Keenan and Keyes (*11*); the enthalpy data for solid, liquid, and gaseous hydrazine are given in equation form by Audrieth and Ogg (*12*). Generally the enthalpy of a pure substance must be calculated from heat capacity and latent-heat data after suitable enthalpy reference conditions have been selected. The enthalpy reference conditions used here are zero enthalpy for liquid water and solid hydrazine at 0°C. Then the enthalpy of hydrazine liquid at any temperature between its melting point (2.0°C.) and its boiling point (113.5°C.) is given by

$$H_{liq} = \int_0^2 Cp_{solid}\,dt + \lambda_{fusion} + \int_2^t Cp_{liq}\,dt = 95.5 + \int_2^t Cp_{liq}dt \quad (1)$$

and its enthalpy in the vapor region at 1 atm. is given by

$$H_{vapor} = H_{liq}\ (\text{at } 113.5^\circ\text{ C.}) + \lambda_{vapor} + \int_{113.5}^t Cp_{vapor}\,dt = 485.0 + \int_{113.5}^t Cp_{vapor}\,dt \quad (2)$$

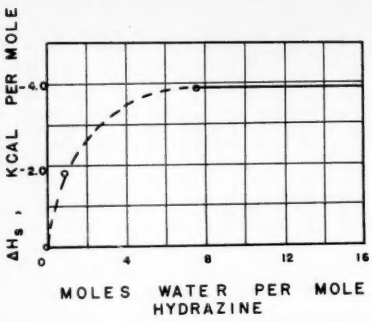

FIG. 1. HEAT OF SOLUTION OF HYDRAZINE (*12*) IN WATER AT 25° C.; THE VALUE AT 7.5 MOLES WATER/MOLE HYDRAZINE WAS ESTIMATED BY ANALOGY WITH AMMONIA.

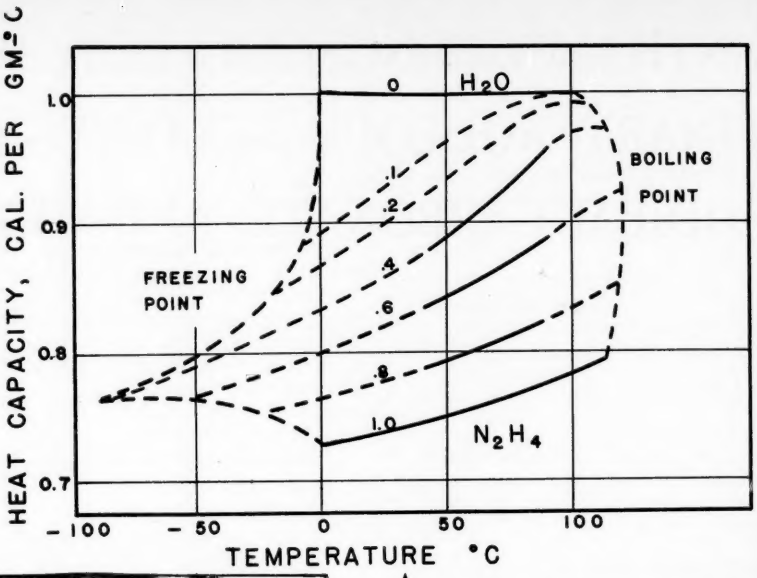

FIG. 2. HEAT CAPACITY OF AQUEOUS HYDRAZINE AT CONSTANT WEIGHT FRACTIONS OF HYDRAZINE. SOLID LINES REPRESENT EXPERIMENTAL DATA OF SAGE ET AL. (*14*).

FIG. 3. PHASE DIAGRAM FOR THE HYDRAZINE-WATER SYSTEM AT 1 ATM. (*15, 16, 17*).

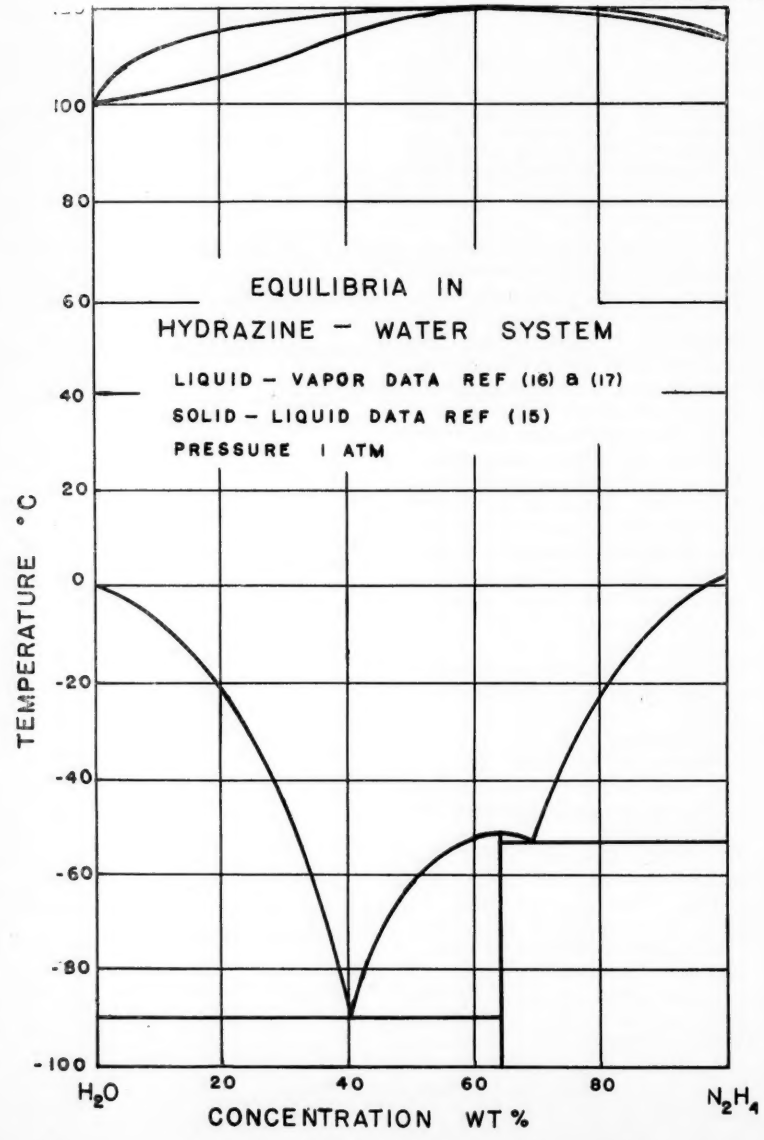

The enthalpy-temperature curves for the pure substances are shown in Figure 5 as the lines in the two *H-t* planes representing pure water and pure hydrazine. Figure 5 is an isometric drawing representing the complete *H-t-x* surface in space.

Since the effect of pressure on the enthalpy of solids, liquids, and gases at low pressures is very small, no attempt has been made here to correct the enthalpy values from the equilibrium vapor pressure of the various phases to 1 atm., the pressure for the diagram.

Heat of Solution or Dilution

The heat of solution of hydrazine in water is given by Audrieth and Ogg (*12*) at 25°C. for infinite dilution and for a concentration of 1 mole water/mole hydrazine. By analogy with ammonia, the hydrazine infinite dilution value is plotted at 7.5 moles water/mole hydrazine, since ammonia has realized its infinite dilution value at this concentration. These data are plotted in Figure 1 and a smooth curve has been put through the points for the purpose of reading intermediate heat-of-solution values for various quantities of water added. The enthalpy of binary mixtures at 25°C. relative to the pure substances having zero enthalpy at 0°C. is given by Equation (3) from Dodge (*10*).

$$H = (1-x)\,H_{H_2O} + x\,H_{N_2H_4} + x\,\Delta H_{soln} \qquad (3)$$

where H is the enthalpy in C.h.u. per pound of binary mixture at 25°C. of weight fraction x in hydrazine and (1—x) in water; H_{H_2O} and $H_{N_2H_4}$ are the enthalpies of water and hydrazine at 25°C. relative to zero values at 0°C. ΔH_{soln} is the heat of solution of hydrazine in water in calories per gram hydrazine (numerically the same as C.h.u. per pound) read from Figure 1 for the various compositions. Thus Equation (3) together with Figure 1 determines the 25°C. isotherm shown on the $H - x$ diagram in Figure (4). If heat-of-dilution data are available, the calculations are very similar. For more details on using heat-of-dilution data the reader is referred to McCabe(*6*) or Dodge(*10*).

Heat Capacity of Binary Mixtures

The enthalpy of a constant-composition mixture at various temperatures relative to the pure substances at the reference conditions is obtained by adding the integral of the heat capacity of the mixture with respect to temperature from 25°C. to t °C. to the enthalpy of that mixture at 25°C., as indicated by Equation (4), where the subscript x indicates constant composition.

$$(H_t)_x = (H_{25})_x + \int_{25}^{t} Cp_x \, dt \quad (4)$$

Frequently the heat-capacity data are not available over the range of temperature and composition desired, and so it is necessary to use some method of estimating these data. Bushnell, Hughes, and Gilbert(*13*) give heat-capacity data for very dilute aqueous hydrazine solutions at 25°C. and Hough, Mason, and Sage(*14*) have data on various compositions from 40 wt. % to pure hydrazine at several temperatures. These data together with those of pure water were plotted against composition at various constant temperatures, and smooth curves were drawn through the points. Then the heat-capacity-temperature plots at constant composition shown in Figure 2 were made by cross plot from the original data curves. The dotted portions of the curves indicate estimated data. Freezing points and boiling points of the various compositions are also indicated on Figure 2.

Figure 4 shows the complete enthalpy-concentration diagram for hydrazine and water. The 25°C. isotherm, which was established from heat-of-solution data, is the starting point for calculating all the other isotherms on the diagram.

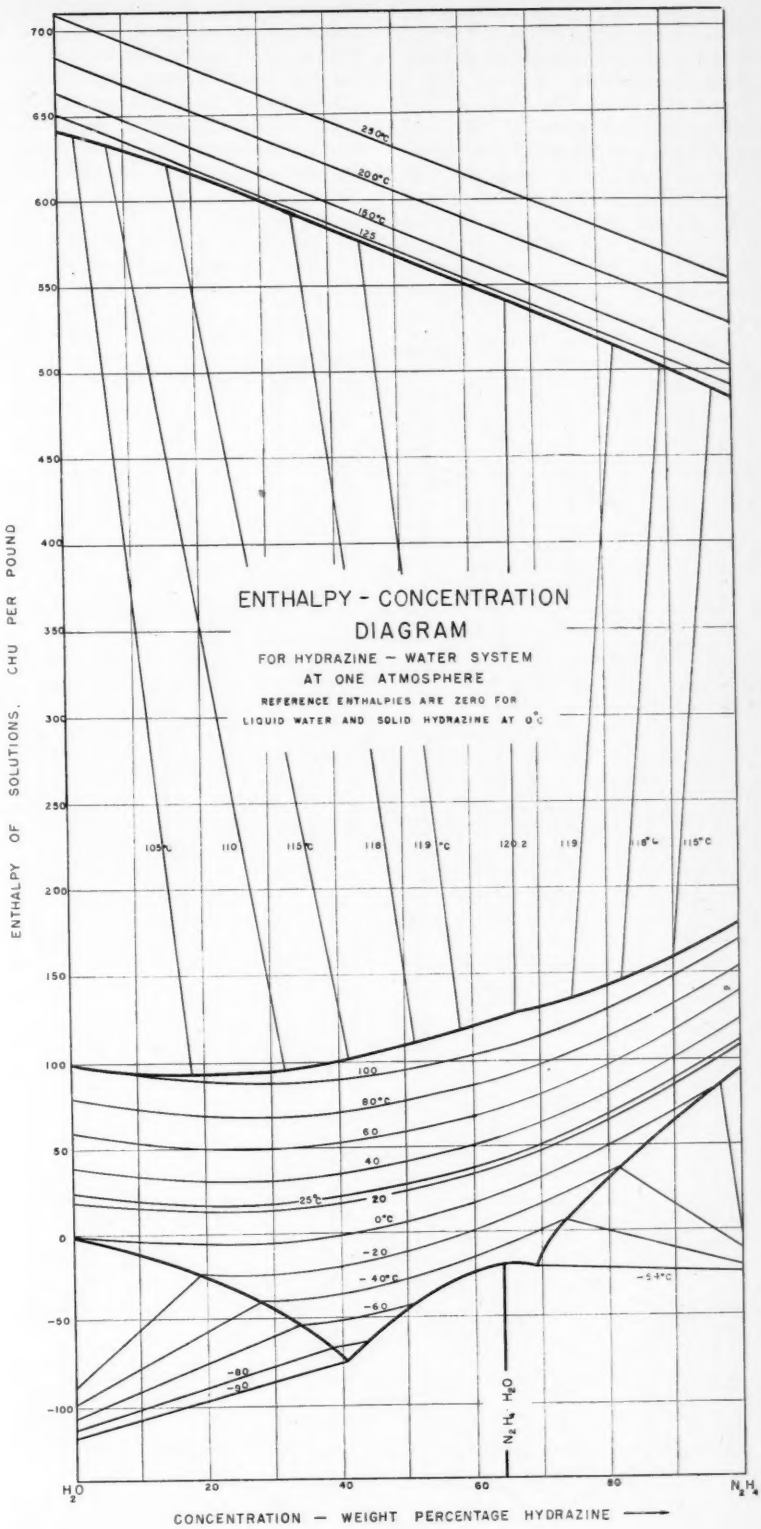

FIG. 4.

Isotherms in the liquid region were established by integrating the heat-capacity data in Figure 2 at constant composition between temperature limits (25° and t°C.) and adding the value of that integral to the enthalpy of that composition at 25°C., as indicated by Equation (4), to obtain the enthalpy of that composition at t°C. The value of the integral is positive for temperatures above 25°C. and negative for isotherms below 25°C. In this manner isotherms were calculated and plotted as shown in Figure (4) for temperatures up to the boiling point and down to the freezing point of the various compositions at 1 atm. pressure. The phase diagram for the system at 1 atm. furnishes data on the equilibrium-phase compositions and transition temperatures.

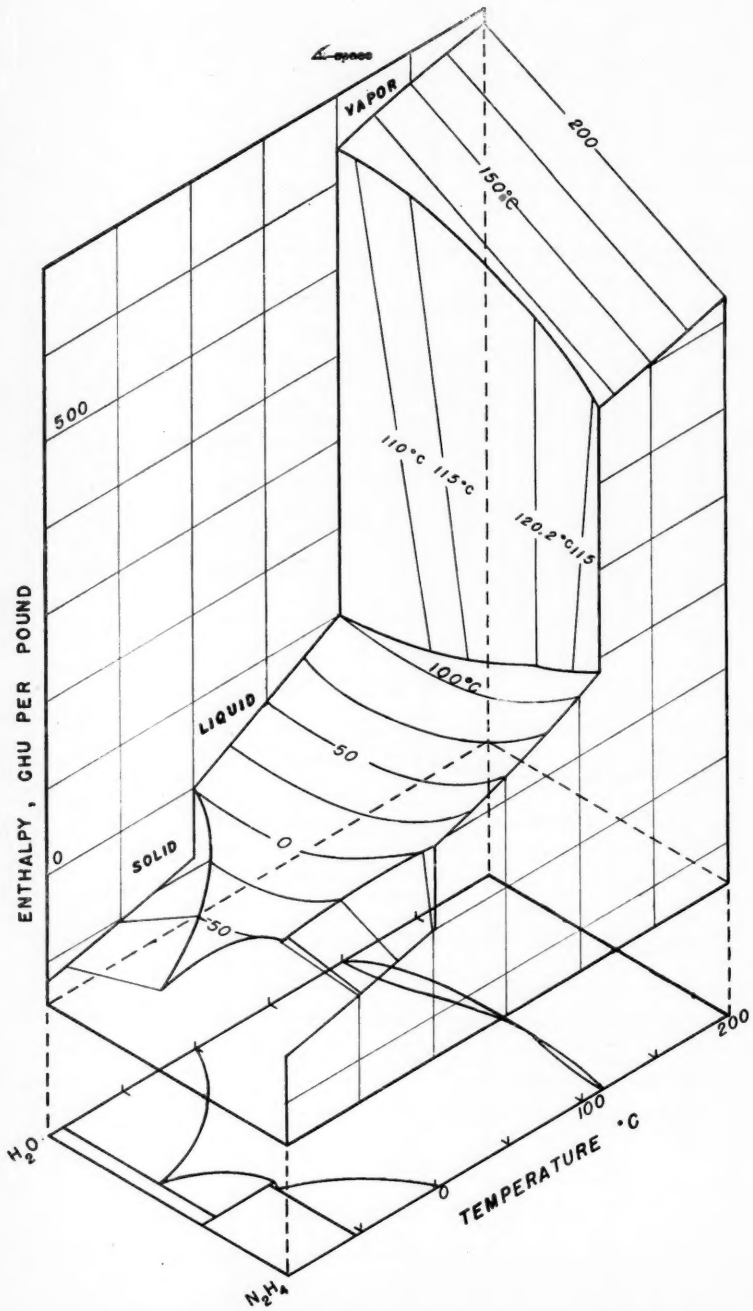

FIG. 5. ISOMETRIC VIEW OF H-x-t SURFACE IN SPACE.

Phase Diagram for Binary Mixtures

Data on the phase relationships in the binary system are necessary if the enthalpy-concentration diagram is to include enthalpy data on the system in the solid and vapor phases. The data of Hill and Sumner(*15*) in the solid-liquid region and those of Björkman(*16*) and Uchida, Ogawa, and Yamaguchi (*17*) in the liquid-vapor region are the most recent measurements on the hydrazine-water system. They are shown in Figure 3. The system has one solid compound, $N_2H_4 \cdot H_2O$, which melts at —51.7°C., and an azeotrope containing 66.6 wt.% hydrazine, which boils at 120.2°C. at 1 atm. pressure. In the solid-liquid-equilibrium region the diagram shows that hydrazine hydrate forms eutectic compositions with both water and hydrazine and also it indicates that the solid hydrate is not soluble in either solid water (ice) or solid hydrazine.

Completion of the Diagram

The procedure for establishing isotherms throughout the liquid region was shown above. The liquid-region boundaries are determined from the phase diagram. In the two phase regions enthalpies are additive (no heat effect is observed on mixing equilibrium phases), and so isotherms in these areas are straight lines connecting the enthalpies of the two phases at the equilibrium temperature. Three phases in a two-component system at constant pressure occur at invariant temperatures on the phase diagram and appear as isothermal triangular areas on the enthalpy-concentration diagram with the corners of the triangle located at the enthalpy value of each phase at the invariant temperature.

Isotherms in the vapor region are straight lines since there is little or no heat effect observed on mixing nonreactive vapors. The solid region in this diagram is incomplete since no information is available on the heat capacity and heat of fusion or heat of formation of the hydrazine monohydrate solid.

Figure 4 is the complete diagram including solid, liquid, and vapor regions at 1-atm. pressure. Figure 5 is an isometric plot showing the H-x-t diagram of Figure 4 in space. It is not so useful for calculation

purposes as is Figure 4, but it illustrates how the *H-t* diagrams for the pure substances and the system phase diagram fit together. Note that the *H-t* diagrams for the pure substances form the composition boundaries on the figure, and the phase diagram is the projection of all the phase boundaries onto the *t-x* plane.

In view of the approximations involved in Figures 1 and 2 and the scale of plotting used in Figure 4, it is probable that the errors in an enthalpy value read from Figure 4 may be as much as ± 2 C.h.u./lb. of solution; however, it is believed that the chart is sufficiently accurate for most engineering calculations.

AQUEOUS SODIUM CARBONATE

Sodium carbonate is a widely used industrial chemical. In 1948 the estimated national consumption was 4,880,000 short tons. Since most processes involving the manufacture and use of sodium carbonate are carried out in aqueous solution, the thermal properties of these solutions are of utmost importance. An enthalpy-concentration diagram is indispensable for calculating the amount of heat necessary to warm or cool batches of solutions and mixtures of solids and solutions.

Recently Kobe and Sheehy(*18*) reviewed and also collated the thermochemical data on sodium carbonate and its hydrates and solutions. Their results and the tabulations by Rossini et al.(*19*) for the heat of formation of the hydrates and the heat of solution of the anhydrous salt are in essential agreement. Kobe and Sheehy's data were used in the construction of Figure 6. The thermal properties of water were taken from Keenan and Keyes(*11*).

The heat capacities of the monohydrate and septahydrate salts are unknown, but they have been estimated from the known heat capacities of the anhydrous and decahydrate salts on the assumption that the heat capacity of the various hydrates is directly proportional to the moles of water in the salt; thus

Na_2CO_3 (s)	26.38	
$Na_2CO_3 \cdot H_2O$ (s)	36.5	(est.)
$Na_2CO_3 \cdot 7\,H_2O$ (s)	97.1	(est.)
$Na_2CO_3 \cdot 10\,H_2O$ (s)	127.40	

An enthalpy-concentration diagram using the data sources discussed above is shown in Figure 6. As enthalpy changes at constant pressure are heat quantities, the diagram may be used at atmospheric pressure to find the resulting temperature for any adiabatic mixing process occurring in this system or the amount of heat (*a*) to be removed in any sodium carbonate crystallization process, (*b*) to change the temperature of any mixture in this system, and (*c*) to keep any solution process in this system at constant temperature. Positive enthalpy changes mean that heat is gained by the system and negative values mean heat lost from the system.

AQUEOUS GLYCERINE

Glycerine and its aqueous solutions are used in the quick-freeze and refrigerating industries. They are particularly useful in the food industry because glycerine is edible and has an agreeable, sweet taste; consequently accidental contamination of food with the refrigerant is not completely objectionable. Glycerine solutions are also used in cold plates to act as a thermal buffer. Hospital ice bags filled with a 10 to 15% solution can be permanently sealed and frozen in a refrigerator to be used when needed. The thermal buffering capacity of an aqueous glycerine mixture is found by subtracting the enthalpy of the system at its original temperature from its enthalpy at the final temperature.

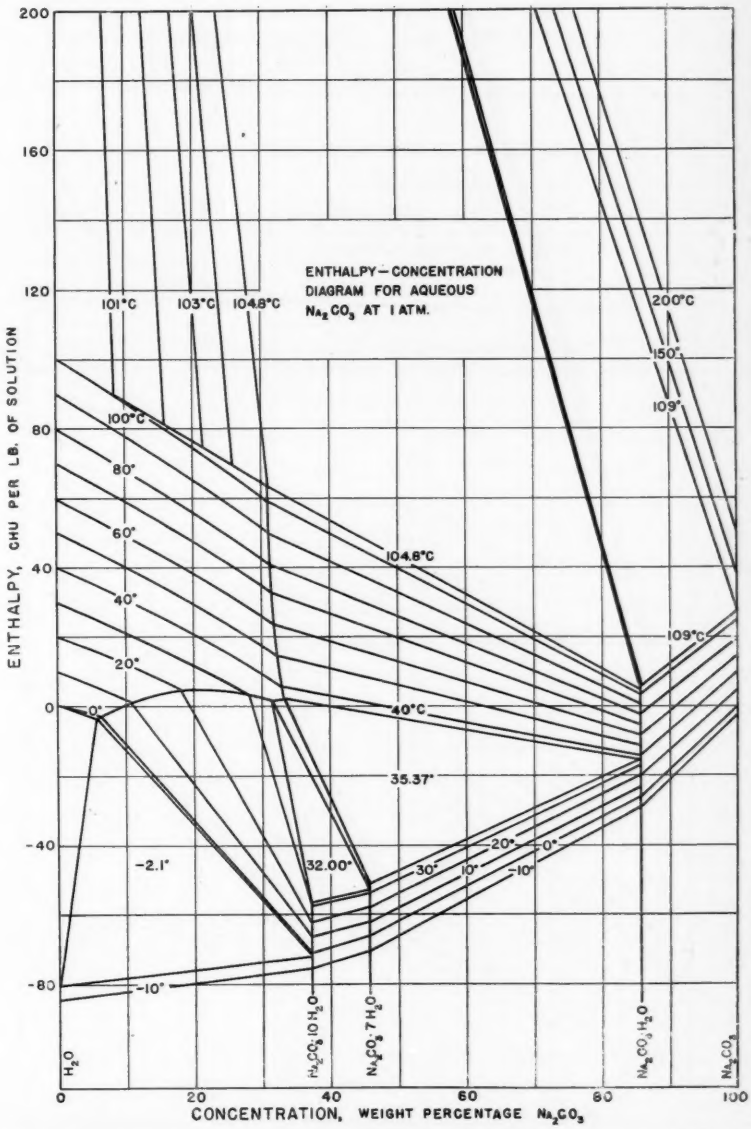

FIG. 6. ENTHALPY-CONCENTRATION DIAGRAM FOR SODIUM CARBONATE AND WATER AT 1 ATM. REFERENCE ENTHALPIES ARE ZERO FOR LIQUID WATER AND SOLID SODIUM CARBONATE AT 0°C.

The reference conditions for the enthalpy-concentration diagram in Figure 7 are zero enthalpies for pure liquid water and solid glycerine at 0°C. The enthalpy data for water were obtained from Keenan and Keyes (*11*) and Hodgman (*20*). The enthalpy data for glycerine were calculated from heat-capacity data from Hodgman (*20*). Heat-of-solution data for the system at 20°C. were obtained from the International Critical Tables (*21*). Heat-capacity data for aqueous solutions are given by Perry (*22*) at 15° and 32°C. and by Gucker and Marsh (*23*) down to —30°C. Gucker and Marsh give heat-capacity data in the two-phase (solid-liquid) region and also a tabulation of the heat required to heat 1 lb. of glycerine-water mixture from various temperatures to 0°C. From these data and the solid-liquid phase diagram of Lane (*24*) the diagram was extended to the eutectic temperature. Below the eutectic temperature the phases are pure solid water and solid glycerine and the isotherms are straight lines connecting the enthalpies of the pure materials.

Isotherms above 20°C. were constructed by adding the temperature integral of the heat capacity to the 20°C. value. In this manner isotherms up to the boiling point may be constructed. Heat-capacity data at 25°C. and normal boiling temperatures of the aqueous solutions were obtained from Miner and Dalton (*25*).

Figure 7 gives the diagram complete in the solid and liquid regions. The liquid-vapor and vapor regions are not included because sufficient experimental data are not available to establish this portion of the diagram.

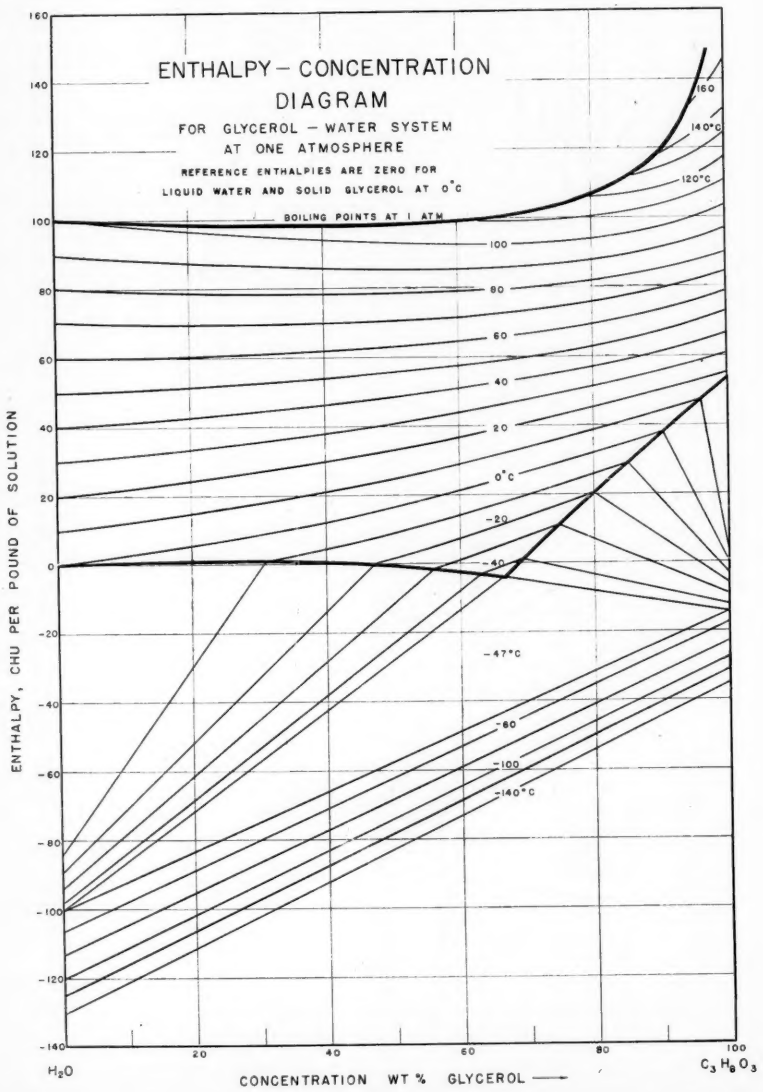

FIG. 7.

LITERATURE CITED

1. Merkel, F., *Arch. Wärme Wirtsch.*, **10**, 13 (1929).
2. Zeisberg, F. C., *Trans. Am. Inst. Chem. Engrs.*, **14**, 1 (1922).
3. Ponchon, M., *Tech. mod.*, **13**, 20, 55 (1921).
4. Savarit, R., *Chemie and Industrie*, special numbers, p. 737 (May 1923).
5. Hausbrand-Hirsch, "Verdampfen, Kondensieren, und Kuhlen," 7 ed., Julius Springer, Berlin (1931).
6. McCabe, W. L., *Trans. Am. Inst. Chem. Engrs.*, **31**, 129 (1935).
7. Bosnjakovic, F., "Technische Thermodynamik," I and II, T. Steinkopf, Leipzig (1935).
8. ———, *Z. Ver. deut. Ing. Beiheft*, No. 6, 169 (1939).
9. ———, *Forsch. Gebiete Ingenieurw.*, **10**, 256 (1939).
10. Dodge, B. F., "Chemical Engineering Thermodynamics," McGraw Hill Book Co., Inc., New York (1944).
11. Keenan, J. H., and F. G. Keyes, "Thermodynamic Properties of Steam," John Wiley and Sons, New York (1936).
12. Audrieth, L. F., and B. A. Ogg, "The Chemistry of Hydrazine," John Wiley and Sons, New York (1951).
13. Bushnell, V. C., A. M. Hughes, and E. C. Gilbert, *J. Am. Chem. Soc.*, **59**, 2142 (1937).
14. Hough, E. W., D. M. Mason, B. H. Sage, *J. Am. Chem. Soc.*, **72**, 5774 (1950).
15. Hill, T. C. H., and J. F. Sumner, *J. Chem. Soc.*, p. 838 (1951).
16. Björkman, A., *Svensk, Kem, Tidskr.*, **59**, 211 (1947).
17. Uchida, S., S. Ogawa, M. Yamaguchi, *Japan Sci. Rev., Ser.* **1**, No. 2, 41 (1950).
18. Kobe, K. A., and T. M. Sheehy, *Ind. Eng. Chem.*, **40**, 99 (1948).
19. Rossini, F. D., D. D. Wagman, W. H. Evans, S. Leirne and I. Jaffe, *Natl. Bur. Standards (U. S.), Circ.* 500 (1952).
20. Hodgman, C. D., "Handbook of Chemistry and Physics," 32 ed. Chemical Rubber Publishing Co., Cleveland (1950).
21. International Critical Tables, 5, 157, McGraw-Hill Book Company, Inc., New York (1929).
22. Perry, J. H., "Chemical Engineers' Handbook," 3 ed., McGraw-Hill Book Company, Inc., New York (1950).
23. Gucker, F. T., and G. A. Marsh, *Ind. Eng. Chem.*, **40**, 908 (1948).
24. Lane, L. B., *Ind. Eng. Chem.*, **17**, 924 (1925).
25. Miner, C. S., and N. N. Dalton, "Glycerol," Reinhold Publishing Corp., New York (1953).

This is the first issue of the

A.I.Ch.E. JOURNAL

a new technical magazine
published quarterly by the
American Institute of Chemical Engineers.

Subscriptions are available to members of the Institute at $4.50 for one year, $7.50 for two years; to nonmembers at $9.00 for one year.

A subscription form is on the reverse side.

CHEMICAL ENGINEERING PROGRESS

monograph

1. **Reaction Kinetics by Olaf A. Hougen**
(74 pages; $2.25 to members, $3.00 to nonmembers)

2. **Atomization and Spray Drying by W. R. Marshall, Jr.**
(122 pages; $3.25 to members, $4.25 to nonmembers)

& symposium

MINERAL ENGINEERING TECHNIQUES

Papers on the tools and techniques of the mineral industry are here assembled for the use of the chemical engineer who may wish to adapt them to his own field. Presented here are theoretical backgrounds, operating experience, design and cost considerations, and test procedures in various separation techniques. (Symposium Series No. 15, Vol. 50, 100 pages; $2.50 to members; $3.75 to nonmembers)

OTHER VOLUMES

1. **Ultrasonics—two symposia**
(87 pages; $2.00 to members, $2.75 to nonmembers)
2. **Phase-Equilibria—Pittsburgh and Houston**
(138 pages; $3.75 to members, $4.75 to nonmembers)
3. **Phase-Equilibria—Minneapolis and Columbus**
(122 pages; $3.75 to members, $4.75 to nonmembers)
4. **Reaction Kinetics and Transfer Processes**
(125 pages; $3.75 to members, $4.75 to nonmembers)
5. **Heat Transfer—Atlantic City**
(162 pages; $3.25 to members, $4.25 to nonmembers)
6. **Phase-Equilibria—Collected Research Papers for 1953**
(113 pages, $3.25 to members, $4.25 to nonmembers)
7. **Applied Thermodynamics**
(163 pages; $3.25 to members, $4.25 to nonmembers)
8. **Communications**
(57 pages; $1.00 to members, $1.50 to nonmembers)
9. **Heat Transfer—Research Studies for 1954**
(67 pages; $1.50 to members, $2.25 to nonmembers)
10. **Collected Research Papers—for Spring 1954**
(142 pages; $3.25 to members, $4.25 to nonmembers)
11. **Nuclear Engineering—Part I**
(280 pages; $3.25 to members, $4.25 to nonmembers)
12. **Nuclear Engineering—Part II**
(259 pages; $3.25 to members, $4.25 to nonmembers)
13. **Nuclear Engineering—Part III**
(274 pages; $3.25 to members, $4.25 to nonmembers)
14. **Ion Exchange**
(121 pages; $3.25 to members, $4.25 to nonmembers)

Price of each volume depends on number printed. Series subscriptions, which allow a 10% discount, make possible larger runs and consequently lower prices.

series

MAIL THIS COUPON

AMERICAN INSTITUTE OF CHEMICAL ENGINEERS, 25 West 45 Street, New York 36, N. Y.

☐ Please enter my subscription to the CEP Symposium and Monograph Series. I will be billed at a subscription discount of 10% with the delivery of each volume.

Please send:

☐ copies of *Ultrasonics.*
☐ copies of *Phase-Equilibria—Pittsburgh and Houston.*
☐ copies of *Phase-Equilibria—Minneapolis and Columbus.*
☐ copies of *Reaction Kinetics and Transfer Processes.*
☐ copies of *Heat Transfer—Atlantic City.*
☐ copies of *Phase-Equilibria—Collected Research Papers for 1953.*
☐ copies of *Applied Thermodynamics.*
☐ copies of *Communications.*
☐ copies of *Heat Transfer—Research Studies for 1954.*
☐ copies of *Collected Research Papers—for Spring 1954.*
☐ copies of *Nuclear Engineering—Part I.*
☐ copies of *Nuclear Engineering—Part II.*
☐ copies of *Nuclear Engineering—Part III.*
☐ copies of *Ion Exchange.*
☐ copies of *Mineral Engineering Techniques.*
☐ copies of *Reaction Kinetics.*
☐ copies of *Atomization and Spray Drying.*
☐ Bill me.
☐ Check enclosed (add 3% sales tax for delivery in N. Y. City).

☐ Enclosed is my check ..... money order ..... for $..... for a one-year, ... two year ..... subscription to the A.I.Ch.E. Journal.

Name ..... Address .....

.....

☐ Member ☐ Associate Member ☐ Affiliate ☐ Student ☐ Nonmember

ENRICHMENT CALCULATIONS IN GASEOUS DIFFUSION: Large Separation Factor

ROBERT W. NAYLOR and PAUL O. BACKER
Vitro Corporation of America, West Orange, New Jersey

A general method has been devised for calculating gaseous-diffusion-stage requirements to separate gases of widely differing molecular weights. For such a mixture the actual separation factor is shown to be less than the ideal separation factor, depending on the undiffused-gas composition and the ratio of absolute pressures on each side of the barrier. The equilibrium relationship between the compositions of the diffused- and undiffused-gas streams leaving any stage is also derived by means of the Rayleigh concept. Application of the method is illustrated with a diagram, like that of McCabe and Thiele for distillation, on which are stepped off the required number of theoretical stages to separate a particular hydrogen-nitrogen mixture.

Enrichment in gaseous diffusion results from the preferential effusion of the low-molecular-weight component through a barrier whose pore diameter is small with respect to the molecular mean free paths. A cascade of stages in series is used to enrich the mixture repeatedly until desired terminal compositions are achieved. In spite of inherent low thermodynamic efficiencies, the successful separation of uranium isotopes by gaseous diffusion has demonstrated the large-scale workability of the process for cases where product worth or other special considerations justify its use. Outside the field of isotope separation, gaseous diffusion might compete with low-temperature processes particularly for the separation of hydrogen from heavier gases. In such a case a high separation factor might reduce plant-size and energy requirements sufficiently to make the process economically attractive. It is to investigate such possibilities that the work of this paper was done.

In connection with their work on rubber and plastic membranes, Weller and Steiner (*4, 5*) have presented an exact and an approximate method for calculating membrane or barrier area and enriched-gas composition for a single stage when permeability coefficients and undiffused exit-gas composition are known. Although the method herein presented does not include determination of barrier area, it is believed to be a somewhat simpler and more general approach to calculation of stage requirements. Benedict (*1, 2*), Cohen (*3*), and others have developed the cascade enrichment calculations for isotope separation where the ideal separation factor is very close to unity so that certain approximations are permissible to gain simplification in the cascade calculations. Furthermore, with the relatively slight enrichment per stage and the consequent large number of stages in an isotope-separation cascade, it is permissible to treat the composition at any point in the cascade as a continuous function of stage number. Analytical methods involving conventional integration are then used to calculate the number of stages in the stripping and enriching sections of the cascade. This paper presents a method for enrichment calculations where the separation factor is considerably greater than one and the approximations of the isotope cascade are therefore not applicable.

The ideal separation factor for perfect effusion of a gas mixture into a total vacuum is given by

$$\alpha^* = \sqrt{\frac{m_H}{m_L}} \qquad (1)$$

Benedict (*2*) has shown that for the case of isotope separation the actual separation factor is independent of concentration, but it is lower than the ideal separation factor because of finite back pressure. The relationship is

$$\alpha - 1 = \left(\sqrt{\frac{m_H}{m_L}} - 1\right)\left(1 - \frac{P''}{P'}\right) \qquad (2)$$

For an ideal separation factor considerably greater than one, the actual separation factor is shown below to depend on composition as well as on the pressure ratio. Then by use of the Rayleigh concept to handle changes in composition across a stage, a relationship is derived between the composition of the two streams leaving any stage. The required number of theoretical stages is found by using a diagram like that of McCabe and Thiele for distillation. The method is illustrated by determining the number of theoretical stages necessary to separate a feed of 25 mole% hydrogen in nitrogen into an overhead of 99 mole% hydrogen and a bottoms of 99 mole% nitrogen.

ACTUAL SEPARATION FACTOR

For effusive flow through a barrier the pore size of which is small with respect to the molecular mean free path, the molar flow rate is defined by Knudsen's law of molecular effusion:

$$N = \sqrt{\frac{g}{2\pi m\, RT}}\left(\frac{\lambda d}{W}\right)(P' - P'') \qquad (3)$$

For a particular barrier at a certain operating temperature, the barrier permeability may be defined by

R. W. Naylor is at present with The M. W. Kellogg Company, Jersey City, New Jersey and P. O. Backer is with International Business Machines Company, New York, New York.

$$\phi = \sqrt{\frac{g}{2\pi RT}}\left(\frac{\lambda d}{W}\right) \qquad (4)$$

By use of the appropriate mole fractions, Knudsen's law may be written for each component of a mixture as follows:

$$N_L = \frac{\phi}{\sqrt{m_L}}\,[P'x - P''y] \qquad (5)$$

$$N_H = \frac{\phi}{\sqrt{m_L}}[P'(1-x) - P''(1-y)] \qquad (6)$$

Dividing (5) by (6); substituting α^*, the ideal separation factor, for $\sqrt{\frac{m_H}{m_L}}$; and letting $P = \frac{P''}{P'}$ give:

$$\frac{N_L}{N_H} = \alpha^*\left[\frac{x - Py}{(1-x) - P(1-y)}\right] \qquad (7)$$

The actual separation factor is defined by

$$\alpha = \frac{y/1-y}{x/1-x} \text{ or } y = \frac{\alpha x}{1+(\alpha-1)x} \qquad (8)$$

Consideration of the flow reaching the low-pressure side of the barrier shows

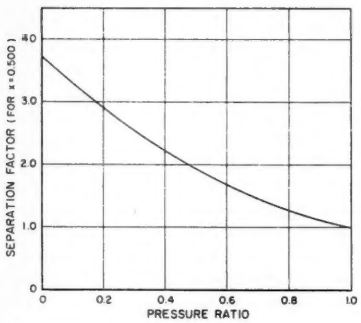

FIG. 1. VARIATION OF SEPARATION FACTOR WITH PRESSURE RATIO FOR EQUIMOLAR H_2-N_2 MIXTURE.

$$\frac{N_L}{N_H} = \frac{y}{1-y} \qquad (9)$$

Substituting (9) through (8) into (7) and solving for α gives †

$$\alpha = \frac{\alpha^*\left(\frac{1-x}{1-y}\right)}{\left(\frac{1-x}{1-y}\right) + P(\alpha^*-1)} \qquad (10)$$

Using (8) to eliminate y from (10) and then solving for α give‡.

$$\alpha = \frac{\alpha^*+1}{2} - \frac{P(\alpha^*-1)}{2x} - \frac{1}{2x} + \sqrt{\left(\frac{\alpha^*-1}{2}\right)^2 + \frac{(\alpha^*-1) - P[(\alpha^*)^2-1]}{2x} + \left[\frac{P(\alpha^*-1)+1}{2x}\right]^2} \qquad (11)$$

CHOOSING PRESSURE RATIO FOR H_2-N_2 CASCADE

For the case of H_2-N_2

$$\alpha^* = \sqrt{\frac{m_H}{m_L}} = \sqrt{\frac{2(14.008)}{2(1.008)}} = 3.7284 \qquad (12)$$

and so (11) becomes

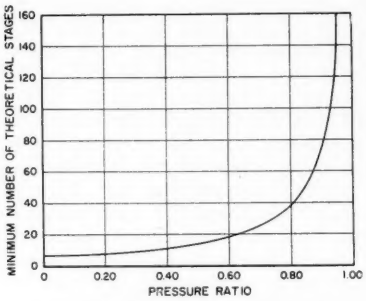

FIG. 2. MINIMUM NUMBER OF THEORETICAL STAGES VS. PRESSURE RATIO, BASED ON α FOR $x = 0.500$ IN THE H_2-N_2 EXAMPLE.

$$\alpha = 2.364 - 1.3642\frac{P}{x} - \frac{1}{2x} + \sqrt{1.860 + \frac{2.728 - 12.897P}{2x} + \left(\frac{1+2.728P}{2x}\right)^2} \qquad (13)$$

To examine the effect of the pressure ratio on the separation factor, x in (13) is fixed at 0.500. This is equivalent to assuming that the separation factor corresponding to $x = 0.500$ at any pressure ratio is a reasonable average value for the entire concentration span. Making this substitution in (13) reduces that equation to

$$\alpha_{(x=0.500)} = 1.364 - 2.7284P + \sqrt{7.442P^2 - 7.442P + 5.588} \qquad (14)$$

The curve of Figure 1 represents Equation (14). For the case of effusion into a perfect vacuum, $P = 0$ and α becomes α^*, the ideal separation factor; when the back and fore pressures are equal and P is unity, α falls to 1, indicating no enrichment.

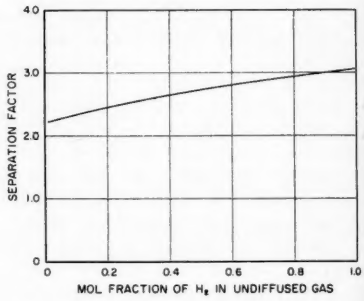

FIG. 3. VARIATION OF SEPARATION FACTOR WITH MOLE FRACTION H_2 IN UNDIFFUSED GAS FOR $P = 1/4$.

The Fenske equation for the minimum number of theoretical stages at total reflux is

$$S_{min} = \frac{\ln\left[\frac{y_D(1-x_B)}{x_B(1-y_D)}\right]}{\ln \alpha} \qquad (15)$$

The effect of the pressure ratio on the length of the cascade may be judged by plotting the ratio against the minimum number of theoretical stages required to span the concentration range from $x_B =$

† For isotope separation where (α^*—1) is much less than unity and $\left(\frac{1-x}{1-y}\right)$ is nearly unity because enrichment per stage is small, (10) becomes identical with (2), which was derived by Benedict (2).

‡ Numerical work shows that the positive root must be used.

0.010 to $y_D = 0.990$. Figure 2 is such a plot for the H_2N_2 cascade of the example as calculated from Equations (14) and (15). The nearly horizontal portion of this curve serves to indicate the range of P values in which a cascade might economically be operated. Other engineering considerations, such as the type of compressors and the actual fore pressure to be used, will aid in fixing the particular value of P for cascade operation. For further calculations of the example H_2N_2 cascade, $P = 0.25$ has been chosen. This lies toward the upper end of the nearly level portion of the curve and represents a compression ratio of four, which is attainable with single-stage compressors.

The selected value of P may be substituted into Equation (13) to get the relationship of separation factor to mole fraction of H_2 for the system operating at a back-to-fore pressure ratio of 0.25:

$$\alpha = 2.364 - \frac{0.84105}{x} + \sqrt{1.860 - \frac{0.2481}{x} + \frac{0.70728}{x^2}} \quad (16)$$

Figure 3 represents Equation (16) graphically; α varies from 2.222 for $x = 0.010$ upward toward a limit of 3.046 as x approaches unity.†

RELATION OF x AND y

Figure 4 is a schematic sketch of a gaseous-diffusion stage. It is evident that to achieve any enrichment some, but not all, of the entering stream must pass through the barrier; and there must be a concentration gradient between the undiffused gas entering and leaving the stage. If the stage is designed to give complete turbulence so that all the undiffused gas in the stage is of the same composition as that leaving, the situation becomes analogous to that assumed in conventional distillation calculations for a small column, where liquid mixing by the rising vapor negates any effect of liquid gradient on the plate. For such a case compositions of the effluent streams from the stage are correctly related by Equation (8) by use of separation factors from (11) or, for the example cascade, from (16). However in gaseous diffusion the undiffused gas must travel along the barrier while undergoing continual depletion of the light component. Good stage design to minimize film thickness at the barrier requires turbulence at any cross section of the axis of flow, but because there is a gradual composition gradient along the axis of flow, which is analogous to the liquid composition gradient observed in large distillation columns, it is proper to assume constant composition only within an element like that of Figure 4. A material balance around the element is

$$\frac{dq}{q} = \frac{dx}{y-x} \quad (17)$$

For such an element Equation (8) correctly relates the compositions across the barrier. Substituting ϵ for $(\alpha\text{-}1)$ allows (17) therefore to be rewritten as

$$\frac{dq}{q} = \left[\frac{1 + \epsilon x}{\epsilon\, x(1-x)}\right] dx \quad (18)$$

Although the separation factor has been shown to vary with composition, it is assumed that the variation across any *one* stage is small enough that ϵ may be treated as a constant between x_1 and x_0. If the value of α corresponding to x_0 is used, the error may be taken on the conservative side and thus made to compensate in part for errors from depletion of the film adjacent to the barrier. Under the assumption of constant separation factor, (18) may be integrated from the element of Figure 4 to the exit:

$$q = [(1\text{-}\theta)Q]\left[\left(\frac{x}{x_o}\right)^{1/\epsilon}\left(\frac{1-x_o}{1-x}\right)^{\sigma}\right] \quad (19)$$

In (19) θ, the cut, represents the fraction of the gas entering the stage which passes through the barrier, and σ is the ratio α/ϵ or $\alpha/(\alpha\text{-}1)$.

The composition of the enriched stream leaving any stage may be written

$$y_o = \frac{\int_{x_1}^{x_o} y\, d\, q}{\int_{x_1}^{x_o} d\, q} = -\frac{1}{\theta\, Q}\int_{x_1}^{x_o} y_{dq} \quad (20)$$

The term ydq may be written in terms of x by multiplying the right-hand sides of Equations (8), (18), and (19). Making this multiplication, canceling, rearranging, and noting that Q, $(1\text{-}\theta)$, and x_o are constant permit writing (20) as

$$y_o = -\sigma\left(\frac{1-\theta}{\theta}\right)\frac{(1-x_o)}{x_o^{\,1/\epsilon}} \int_{x_1}^{x_o} \frac{x^{\,1/\epsilon}}{(1-x)^{\sigma+1}}\, dx \quad (21)$$

Integrating (21) after appropriate changes of variables and canceling and rearranging give

$$y_o = x_o^{-1/\epsilon}\left(\frac{1-\theta}{\theta}\right)\left[(1-x_o)^{\sigma}\left(\frac{x_1}{1-x_1}\right)^{\sigma} - x_o^{\,\sigma}\right] \quad (22)$$

With reference again to Figure 4, a material balance around the stage is

$$\theta\, y_o + (1-\theta)\, x_o = x_1 \quad (23)$$

Since conventional enrichment calculations deal with the compositions of streams leaving a stage, Equation (23) may be used to eliminate x_1, from (22), and the subscripts are then no longer neces-

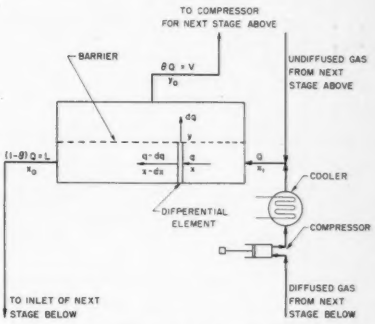

FIG. 4. SCHEMATIC SKETCH OF A GASEOUS-DIFFUSION STAGE.

TABLE 1.—EQUILIBRIUM DATA FOR THE H_2-N_2 EXAMPLE CASCADE

x	α (P=1/4)	y θ=0.3471	y θ=0.5833
0.010	2.222	0.029	
.025	2.241	.070	
.035	2.253	.098	
.050	2.270	.136	
.075	2.298	.197	
.100	2.326	.252	
.150	2.374	.351	
.200	2.437	.438	0.507
.250	2.490	.512	.579
.300	2.542	.579	.639
.400	2.641		,735
.500	2.730		.807
.600	2.809		.863
.700	2.880		.907
.800	2.942		.944
.900	2.985		.974
.950	3.022		.988

From Equations (16) and (27)

†Numerical data for Figure 3, calculated from (16), are included in Table 1.

sary. Thus the x-y relationship for any stage is

$$y = x^{-1/\epsilon}\left(\frac{1-\theta}{\theta}\right)\left\{(1-x)^{\sigma}\right.$$

$$\left.\left[\frac{\theta\, y + (1-\theta)\, x}{1-(\theta\, y + (1-\theta)\, x)}\right]^{\sigma} - x^{\sigma}\right\} \quad (24)$$

Once the cut is fixed for each section of the cascade and the separation factor is fixed as a function of the undiffused-gas composition, Equation (24) may be used to construct an x-y diagram to permit making enrichment calculations by the method of McCabe and Thiele for distillation. It should be noted that (24) is divergent for the purpose of iteration. Therefore a result calculated from a first approximation should not be used as a second approximation in the trial-and error solution, because the computed result is farther from the actual root than is the assumed value of y.

SELECTION OF CUT

From Figure 4 it is evident that for any stage

$$\frac{L}{V} = \frac{1-\theta}{\sigma} \quad (25)$$

Thus for total reflux where $L = V$ the cut must be 1/2 ; and for any finite product rate it must be greater than 1/2 in the rectifying section and less than 1/2 in the stripping section of the cascade. If the L/V ratio for either section or the V/D ratio for the cascade is known, then θ is fixed and the x-y curve may be calculated. A reasonable approximation of the continuously tapered ideal cascade which minimizes total flow may be made by using Equation (24) with $\theta = 1/2$ and the appropriate equations of Benedict(*2*). Economics would probably dictate squaring off the rectifying and stripping sections of the optimum cascade into several parts each operating at a constant L/V to achieve standardization of equipment. Once this is done Equation (24) may be used to determine the x-y curve appropriate to each part of the cascade.

With separation factors as great as those for H_2N_2, a square cascade having constant L/V ratios throughout the stripping and enriching sections would probably be chosen. For the continuation of the H_2-N_2 example a square cascade has been chosen with $V/D = 3.5$ for the rectifying section. From material balances and Equation (25) the cut for the rectifying section is calculated to be 0.5833. For a square cascade the following material balances may be written:

$$y_n = x_{n+1}\left(\frac{L}{V}\right)_N + y_D\left(\frac{D}{V}\right)_N \quad (26a)$$

$$y_m = x_{m+1}\left(\frac{L}{V}\right)_M - x_B\left(\frac{B}{V}\right)_M \quad (26b)$$

$$\left(\frac{D}{V}\right)_N = 1 - \left(\frac{L}{V}\right)_N \quad (27a)$$

$$\left(\frac{B}{V}\right)_M = \left(\frac{L}{V}\right)_M - 1 \quad (27b)$$

At the feed stage one may set $y_n = y_m$ and $x_{n+1} = x_{m+1} = x_F$ and so the foregoing equations may be combined to give

$$(y_D - x_B) - (y_D - x_F)\left(\frac{L}{V}\right)_N = (x_F - x_B)\left(\frac{L}{V}\right)_M \quad (28)$$

Using (25) to substitute for (L/V) in terms of the cuts yields the following after solution for θ_M:

$$\theta_M = \frac{(x_F - x_B)\theta_N}{2(y_D - x_B)\theta_N - (y_D - x_F)} \quad (29)$$

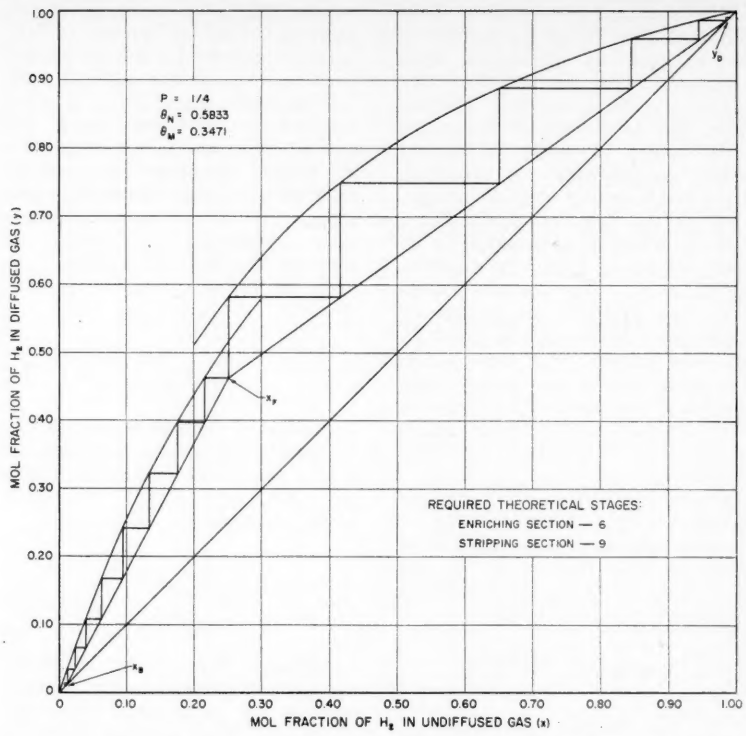

FIG. 5. ENRICHMENT DIAGRAM FOR THE H_2-N_2 CASCADE OF THE EXAMPLE.

The cut for the stripping section of the example cascade is then readily calculated as 0.3471.

EQUILIBRIUM CURVES FOR THE EXAMPLE CASCADE

Substituting the cuts into (24) gives the equations of the equilibrium curves for the two sections of the cascade:

Rectifying Section

$$y = 0.7143\, x^{-1/\epsilon}\left\{(1-x)^{\sigma}\right.$$

$$\left.\left[\frac{0.5833\, y + 0.4167\, x}{1-(0.5833\, y + 0.4167\, x)}\right]^{\sigma} - x^{\sigma}\right\} \quad (30a)$$

Stripping Section

$$y = 1.8810\, x^{-1/\epsilon}\left\{(1-x)^{\sigma}\right.$$

$$\left.\left[\frac{0.3471\, y + 0.6529\, x}{1-(0.3471\, y + 0.6529\, x)}\right]^{\sigma} - x^{\sigma}\right\} \quad (30b)$$

Solution of these equations by trial for various values of x by use of corresponding values of α from Equation (16) defines the equilibrium curves for the cascade of the example.†

† Equilibrium x-y values, calculated from (30), are presented in Table 1.

ENRICHMENT DIAGRAM FOR H_2-N_2 CASCADE

Equations (26*a*) and (26*b*) represent the material balances respectively for the enriching and stripping sections of a square cascade. For the cascade of H_2-N_2 example these equations become

$$y_n = 0.7143\, x_{n+1} + 0.2829 \quad (31a)$$

$$y_m = 1.8810\, x_{m+1} - 0.0088 \quad (31b)$$

If Equation (30) is used for the equilibrium lines and (31) for the operating lines, a diagram like that of McCabe and Thiele for distillation may be constructed and the number of stages determined in the usual manner. Figure 5 is such a diagram for the H_2-N_2 cascade of the example; it shows that a cascade of fifteen theoretical stages is needed to effect the separation under the conditions used for this example.

LIMITATIONS OF THE METHOD

Utilization of this method for gaseous-diffusion enrichment calculations is subject to certain inaccuracies and limitations. The use of Knudsen's law of molecular effusion implies a barrier capable of producing effusive flow to the exclusion of ordinary mass flow, which is nonseparative. It is probable that some mass flow would take place through an actual barrier unless the fore pressure were very low.

Good stage design requires high turbulence of the undiffused gas to minimize depletion of light component from the film immediately adjacent to the barrier. This effect is neglected in the derivation of Equation (24) by the assumption of constant composition in the differential element of Figure 4 around which (17) is written.

In the integration of Equation (21) the separation factor is assumed constant across any one stage. Figure 3 shows the actual variation for the cascade of the example; however, since α is calculated from (16) based on the composition x leaving the stage, the value used is actually the lowest separation factor encountered within the stage. This should tend to compensate, at least in part, for losses in enrichment from the friction pressure drop in the undiffused-gas stream and from the other factors discussed above.

The nature of the method, however, makes very simple the use of an individual or over-all stage efficiency to account for the effects discussed here. Relatively small-scale experiments with the barrier material and stage design of choice should yield this information. Scale-up to production scale should then be possible with a minimum of intermediate development.

SUMMARY

The successful separation of uranium isotopes by gaseous diffusion has demonstrated the large-scale workability of the process for cases where product worth or other special considerations justify the high energy expenditure. In spite of inherent low thermodynamic efficiencies gaseous diffusion might compete economically with processes utilizing very low temperatures to separate gases of widely differing molecular weights.

A general method of calculating gaseous-diffusion-stage requirements for separating gases of widely differing molecular weights has been devised. For the separation of such gases by gaseous diffusion the actual separation factor is shown to depend on the ideal-separation factor (square root of the molecular weight ratio), the ratio of absolute pressures on each side of the barrier, and the undiffused-gas composition. The relationship is derived from Knudsen's law of molecular effusion, and its similarities to that for isotope separation are pointed out. By use of the Rayleigh concept, the equilibrium relationship between the compositions of the diffused- and undiffused-gas streams leaving any stage is also derived. Application of these equations is illustrated by determination of the required number of theoretical stages to separate a particular H_2-N_2 mixture. A diagram similar to that of McCabe and Thiele for distillation is used. Certain limitations of the method are pointed out, and the use of a stage efficiency is suggested to account for them.

NOTATION

B = cascade bottoms withdrawal rate, moles/min.
D = cascade overhead withdrawal rate, moles/min.
d = average diameter of barrier pores, in.
g = acceleration from gravity, ft./min^2.
L = interstage downflow rate, moles/min.
m = molecular weight
N = molar velocity through the barrier, moles/(sq.ft.)(min.)
$P = P''/P'$ = ratio of back pressure to fore pressure across barrier
P' = fore pressure (undiffused gas), lb./sq.ft.
P'' = back pressure (diffused gas), lb./sq. ft.
Q = gas rate entering a stage, moles/min.
q = undiffused-gas rate along the barrier at any cross section, moles/min.
R = universal gas constant, ft.-lb./(mole)(°R.)
S_{min} = minimum number of theoretical stages
T = cascade operating temperature, °R
V = interstage upflow rate, moles/min.
W = thickness of barrier, in.
x = mole fraction of light component in undiffused gas
y = mole fraction light component in diffused gas

Greek

α = separation factor
α^* = ideal separation factor = $\sqrt{m_H/m_L}$
$\varepsilon = (\alpha - 1)$
θ = cut, the fraction of gas entering a stage which diffuses through the barrier
λ = fraction of barrier area open to flow
$\sigma = \alpha/\varepsilon = \alpha/(\alpha - 1)$
ϕ = barrier permeability, defined by Equation (4)

Subscripts

B = bottoms
D = overhead
F = feed
H = heavy component
1 = entering a stage
L = light component
M = stripping section
m = any stage of stripping section
N = enriching section
n = any stage of enriching section
o = leaving a stage

LITERATURE CITED

1. Benedict, M., *Chem. Eng. Progr.*, 43, No. 2, 41 (1947).
2. Kirk, R. E., and D. F. Othmer, ed., "Encyclopedia of Chemical Technology," pp. 124-8, Interscience Publishing Company, New York (1950).
3. Cohen, K., "Theory of Isotope Separation," McGraw-Hill Book Company, Inc., New York (1951).
4. Weller, S., and W. A. Steiner, *J. Appl. Phys.*, 21, 279 (1950).
5. ———, *Chem. Eng. Progr.*, 46, 585 (1950).

Use of the Redlich and Kwong Equation of State in Calculating Thermodynamic Properties of Gases from Experimental Compressibility Data

HENDRICK C. VAN NESS Purdue University, West Lafayette, Indiana

Convenient and accurate methods of calculating the thermodynamic properties of gases from experimental compressibility-factor data through the use of the Redlich and Kwong equation of state are presented. Analytical and graphical methods are combined. As an example, fugacity and activity coefficients are calculated for the nitrogen-ethylene system at 50°C. for pressures up to 500 atm.

There are two problems in the determination of thermodynamic properties of gases; one is the experimental problem of getting accurate data, and the other is the problem of calculating properties from these data. This paper deals with the latter problem and assumes that adequate compressibility-factor data are available. The general equations relating thermodynamic properties to pressure by use of compressibility factors (defined by the equation $pV = CnRT$) are well known (*10*):

$$H - H^* = \Delta H =$$

$$-RT^2 \int_{p^*}^{p} (\partial C/\partial T) \frac{dp}{p} \quad (1)$$

$$\ln (f/p = \int_{p^*}^{p} (C-1) \frac{dp}{p} \quad (2)$$

$$S - S^* = \Delta S =$$

$$-R \int_{p^*}^{p} \left[C + T (\partial C/\partial T) \right] \frac{dp}{p} \quad (3)$$

Equation (3) does not need to be solved independently, for it can readily be put in a form involving the integrals of Equations (1) and (2). Making the logical substitutions reduces it to

$$S - S^* = \Delta S = -R \ln (f/p)$$

$$+ \Delta H/T - R \ln (p/p^*) \quad (4)$$

It should be noted that an asterisk is used to denote the zero-pressure state, where all gases are assumed to obey the ideal-gas law. This state is a satisfactory reference for enthalpy and fugacity, but it is inconvenient in the case of entropy because S^* is infinite. In this case the reference state is taken as the ideal-gas state at 1 atm. The entropy in this state is designated as S°, and Equation (4) becomes

$$S - S^\circ = -R \ln (f/p)$$

$$+ \Delta H/T - R \ln (p) \quad (5)$$

This reference state for entropy is particularly convenient, because absolute values of entropy can be calculated for it by statistical methods. In the case of enthalpy, absolute values are not known, and an arbitrary value must be assigned at a selected temperature in the reference state. By definition, fugacity and pressure are taken as equal in the zero-pressure reference state. The influence of temperature on thermodynamic properties is not considered in this paper, for this cannot be determined from compressibility data alone; moreover, it does not present a calculational problem comparable to that of determining the effect of pressure.

The application of Equation (5) is obvious once Equations (1) and (2) have been solved. The problem reduces then to one of evaluating the integrals in these two equations. There are two straightforward methods for doing this. The first is to perform the required operations of differentiation and integration directly by graphical methods based on the experimental compressibility-factor data. To obtain accurate results by this method, one must make exceedingly large graphs. Furthermore, graphical differentiation is inherently inaccurate, and the subsequent integration accumulates the errors.

The other method is to represent the compressibility-factor data by a very accurate equation, essentially an equation of state, and to perform the required operations entirely analytically. This is a highly desirable method, but at the present time no equation of state sufficiently accurate over wide ranges of temperature and pressure is known; moreover, such an equation would probably be highly complex and difficult to use.

A less straightforward method, but one which combines the advantages of both the foregoing methods, is the use of an approximate but simple equation of state for the calculation of approximate results, plus the use of residuals for the graphical calculation of correction factors. This general method is by no means new. It allows the analytical calculation of the major part of the result and restricts the graphical part to the determination of small numbers which can be plotted with the required accuracy on a normal-size sheet of graph paper.

CALCULATIONS

To carry out this method, one defines the residual, ΔC, as the

difference between the experimental value of the compressibility factor and the value predicted by the equation of state at the same temperature and pressure, i.e.,

$$\Delta C = C - C' \qquad (6)$$

Substitution for C by Equation (6) in Equations (1) and (2) gives

$$\Delta H = -RT^2 \int_{p^*}^{p} (\partial C'/\partial T) \frac{dp}{p} - RT^2 \int_{p^*}^{p} (\partial \Delta C/\partial T) \frac{dp}{p} \qquad (7)$$

$$\ln (f/p) = \int_{p^*}^{p} (C' - 1) \frac{dp}{p} + \int_{p^*}^{p} (\Delta C) \frac{dp}{p} \qquad (8)$$

The first terms of these equations are determined analytically using an equation of state since C' is the "equation" value of the compressibility factor. The second terms are small correction factors and are usually determined graphically. The ease of the analytical calculations will of course depend on the simplicity of the equation of state; on the other hand, the size of the graphical correction factors will depend on the success with which the equation of state approximates the experimental data. Simplicity and high accuracy have not yet been combined in an equation of state. An excellent compromise however has been attained for gases by the Redlich and Kwong equation (*9*):

$$C' = 1/(1-h) - (A^2/B)(h/1+h) \qquad (9)$$

and

$$h = Bp/C' \qquad (10)$$

For a given gas or gas mixture, A and B are constants which depend on temperature only, i.e.,

$$B = k/T \qquad (11)$$

and

$$A^2/B = k'/T^{1.5} \qquad (12)$$

By use of Equations (9) to (12), Equation (7) may be reduced to the form

$$\Delta H = -1.5RT\,(A^2/B) \ln (1+h) + RT(C'-1) - RT^2 \int_{p^*}^{p} (\partial \Delta C/\partial T) \frac{dp}{p} \qquad (13)$$

Although this equation was not presented by Redlich and Kwong (*9*), they did develop the analytical expression for the first integral of Equation (8). Using their result reduces Equation (8) to

$$\ln (f/p) = (C'-1) - \ln (C'-C'h) - (A^2/B) \ln (1+h) + \int_{p^*}^{p} (\Delta C) \frac{dp}{p} \qquad (14)$$

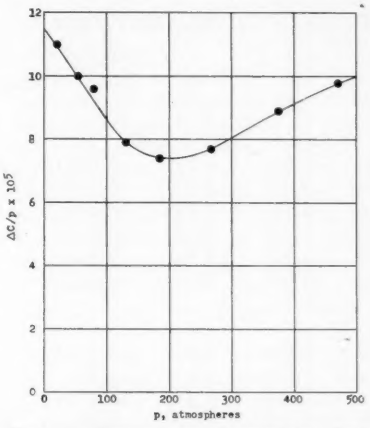

FIG. 1. CURVE FOR GRAPHICAL INTEGRATION; 59.7% N_2; NITROGEN-ETHYLENE MIXTURE, 50°C.

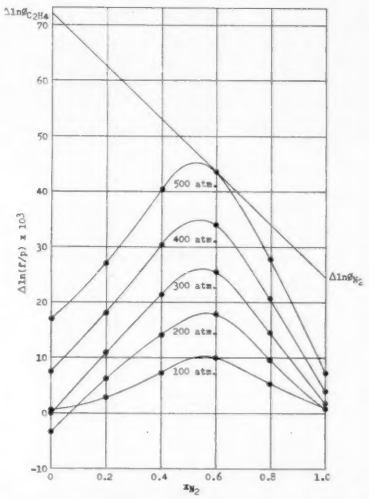

FIG. 2. CURVES FOR GRAPHICAL DIFFERENTIATIONS; NITROGEN-ETHYLENE MIXTURES, 50°C.

For the application of Equations (9), (10), (13), and (14), values of the constants B and A^2/B must be selected. This should be done with care. Probably the most satisfactory method involves a trial procedure: first, an arbitrary value of B is selected; as a starting approximation a value may be calculated from the equation given by Redlich and Kwong (*9*):

$$B = 0.0867 T_c/p_c T \qquad (15)$$

Then for a given temperature a series of values of pressure covering the range being considered is used together with the corresponding experimental values of C for substitution in Equation (10) for the calculation of a series of values of h. Equation (9) is then used with these results and the corresponding experimental values of C to calculate a series of values of A^2/B. The optimum result would be values of A^2/B, which are nearly constant; one might repeat the foregoing procedure with different values of B until one was found that led to the lowest deviation of the values of A^2/B from the mean. A better procedure however is to find by trial the value of B which leads to a very nearly constant value of A^2/B at low pressure with increasing deviations at high pressures, and it is this constant low-pressure value of A^2/B which should be used together with the value of B which leads to it in Equations (9) and (10) and those which follow. The reason for this is that the integral in Equation (14) is evaluated graphically by plotting $\Delta C/p$ vs. p and determining the area under the curve. By having ΔC small at low pressures and increasing with p, values of $\Delta C/p$ will always be reasonably small, and the graphical integration will be facilitated. It should be mentioned that although ΔC and p both approach zero at zero pressure, $\Delta C/p$ remains finite, and its value is the slope of the curve of ΔC vs. p at the origin. Once the values of B and A^2/B have been selected, they are used in Equations (9) and (10) to calculate values of C' at pressures for which experimental values of C are available. Values of C' must of course be calculated (a trial procedure) with the same precision as that for which C is known. Equation (6) is then used to calculate the required values of ΔC. From this point the applications of Equations (13), (14), and (5) are obvious and do not need to be illustrated here.

Much more difficult than the foregoing calculations are the determinations of fugacity coefficients and activity coefficients of the components of gaseous mixtures. The former are defined (*9*) by the equation

$$\phi_i = \bar{f}_i/x_i p \qquad (16)$$

where $\bar{f}_i$ is the fugacity of component i in a mixture whose mole fraction in i is x_i. It may be shown that (*3*):

TABLE 1.—CONSTANTS FOR THE REDLICH AND KWONG EQUATION AT 50°C.

	A	B	A^2/B
Pure C_2H_4	0.076850	0.0014300	4.1300
19.8% N_2	0.063083	0.0013508	3.4315
40.1% N_2	0.059094	0.0012696	2.7506
59.7% N_2	0.050416	0.0011912	2.1338
79.6% N_2	0.041604	0.0011116	1.5571
Pure N_2	0.032571	0.0010300	1.0300

TABLE 2.—CALCULATED VALUES

x_{N_2}	$\Delta\ln\frac{f}{p}$	Approx. $\ln\phi_{N_2}$	$\Delta\ln\phi_{N_2}$	ϕ_{N_2}	γ_{N_2}	Approx. $\ln\phi_{C_2H_4}$	$\Delta\ln\phi_{C_2H_4}$	$\phi_{C_2H_4}$	$\gamma_{C_2H_4}$	$\ln\frac{\gamma_{N_2}}{\gamma_{C_2H_4}}$
100 atm.										
0	0.0006	0.5859	0.0064	1.808	1.793	—0.5099	0.0007	0.6010	1.000	0.584
0.198	0.0028	0.2437	0.0163	1.297	1.287	—0.4772	—0.0007	0.6202	1.032	0.222
0.401	0.0073	0.1085	0.0230	1.141	1.132	—0.4226	—0.0032	0.6533	1.088	0.038
0.597	0.0101	0.0465	0.0053	1.053	1.044	—0.3616	0.0166	0.7083	1.178	—0.120
0.796	0.0054	0.0164	0.0005	1.017	1.008	—0.2941	0.0244	0.7637	1.270	—0.229
1.000	0.0008	0.0074	0.0007	1.008	1.000	—0.2172	0.0226	0.8232	1.370	—0.316
200 atm.										
0	—0.0034	0.6854	0.0465	2.079	2.007	—0.8516	—0.0035	0.4253	1.000	0.696
0.198	0.0062	0.4221	0.0419	1.590	1.534	—0.8189	—0.0028	0.4397	1.034	0.394
0.401	0.0142	0.2204	0.0343	1.290	1.247	—0.7379	0.0005	0.4784	1.125	0.103
0.597	0.0179	0.1073	0.0122	1.127	1.088	—0.6262	0.0260	0.5488	1.292	—0.170
0.796	0.0097	0.0511	—0.0007	1.052	1.016	—0.4998	0.0497	0.6377	1.500	—0.390
1.000	0.0007	0.0345	0.0007	1.036	1.000	—0.3597	0.0382	0.7251	1.705	—0.533
300 atm.										
0	0.0001	0.6713	0.0553	2.068	1.910	—0.9832	0.0000	0.3742	1.000	0.647
0.198	0.0108	0.4629	0.0534	1.676	1.547	—0.9590	0.0002	0.3834	1.024	0.412
0.401	0.0214	0.2844	0.0523	1.400	1.292	—0.8837	0.0005	0.4135	1.104	0.156
0.597	0.0255	0.1654	0.0161	1.199	1.108	—0.7669	0.0394	0.4836	1.292	—0.152
0.796	0.0145	0.0990	0.0016	1.106	1.021	—0.6140	0.0645	0.5773	1.543	—0.412
1.000	0.0016	0.0778	0.0016	1.083	1.000	—0.4362	0.0645	0.6896	1.843	—0.611
400 atm.										
0	0.0075	0.6842	0.0578	2.100	1.831	—1.0237	0.0076	0.3621	1.000	0.604
0.198	0.0180	0.5011	0.0633	1.758	1.532	—1.0041	0.0067	0.3689	1.019	0.407
0.401	0.0303	0.3406	0.0682	1.505	1.312	—0.9346	0.0046	0.3946	1.089	0.186
0.597	0.0341	0.2257	0.0202	1.279	1.116	—0.8194	0.0541	0.4653	1.285	—0.140
0.796	0.0206	0.1561	0.0044	1.174	1.025	—0.6612	0.0829	0.5609	1.550	—0.412
1.000	0.0040	0.1333	0.0039	1.147	1.000	—0.4615	0.0857	0.6868	1.898	—0.640
500 atm.										
0	0.0169	0.7181	0.0594	2.176	1.773	—1.0154	0.0168	0.3685	1.000	0.572
0.198	0.0270	0.5506	0.0737	1.867	1.522	—0.9965	0.0152	0.3749	1.017	0.404
0.401	0.0404	0.4012	0.0815	1.620	1.321	—0.9329	0.0129	0.3986	1.081	0.200
0.597	0.0437	0.2911	0.0242	1.371	1.117	—0.8222	0.0719	0.4723	1.281	—0.136
0.796	0.0278	0.2213	0.0081	1.258	1.026	—0.6621	0.1041	0.5724	1.552	—0.415
1.000	0.0072	0.1976	0.0071	1.227	1.000	—0.4518	0.1087	0.7076	1.925	—0.653

$$\ln(f/p) = x_a \ln\phi_a + x_b \ln\phi_b + x_c \ln\phi_c + \ldots \quad (17)$$

where f is the fugacity of the mixture, defined exactly as the fugacity of a pure gas. When Equation (17) is compared with the general equation for a property of a mixture (2):

$$G = x_a\bar{G}_a + x_b\bar{G}_b + x_c\bar{G}_c + \ldots \quad (18)$$

we see that $\ln\phi_a$, $\ln\phi_b$, $\ln\phi_c$, etc., are related to $\ln(f/p)$ exactly as partial molal properties are related to the total property. Thus the usual equations for partial molal properties may be used to calculate values of the terms $\ln\phi_i$. Thus (2)

$$\ln\phi_i = \ln(f/p) - x_a\frac{\partial\ln(f/p)}{\partial x_a} - x_b\frac{\partial\ln(f/p)}{\partial x_b} - x_c\frac{\partial\ln(f/p)}{\partial x_c} \quad (19)$$

In this equation the ith term is omitted, and the differentiations are carried out with all x's constant except x_i and the x with respect to which the term is differentiated.

The values of $\ln(f/p)$ determined from Equation (14) can be divided into two parts: the part calculated analytically and the part calculated by graphical integration. This latter part is represented by the integral in Equation (14), and it will be defined equal to

$\Delta\ln(f/p)$, i.e.,

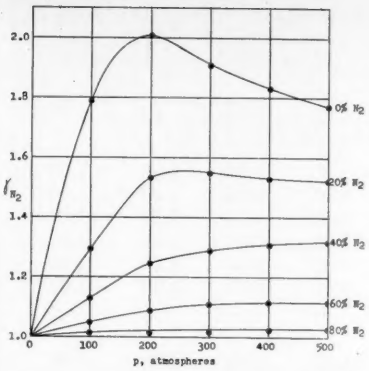

FIG. 3. ACTIVITY COEFFICIENTS FOR NITROGEN; NITROGEN-ETHYLENE MIXTURES, 50°C.

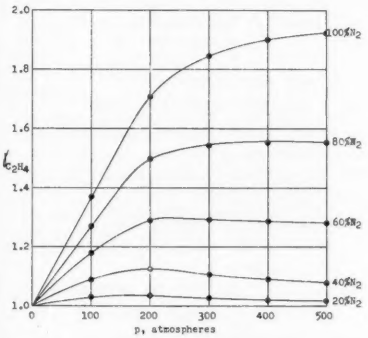

FIG. 4. ACTIVITY COEFFICIENTS FOR ETHYLENE; NITROGEN-ETHYLENE MIXTURES, 50°C.

$$\Delta \ln (f/p) = \int_{p^*}^{p} (\Delta C) \frac{dp}{p} \quad (20)$$

Substitution of the two parts of Equation (14) into Equation (19) divides it also into two parts, one of which may be evaluated analytically and the other graphically. The analytical solution was given by Redlich and Kwong(*9*), and their equation therefore gives approximate values of $\ln \phi_i$:

$$\text{approximate } \ln \phi_i = (B_i/B)(C'-1) - \ln (C'-C'h) - (A^2/B)\left[\frac{2A_i}{A} - \frac{B_i}{B}\right] \ln (1+h) \quad (21)$$

All quantities in this equation are for the mixture except those bearing the subscript *i*. *A* and *B* for the mixture are calculated by(*9*):

$$A = x_a A_a + x_b A_b + x_c A_c + \ldots$$

and

$$B = x_a B_a + x_b B_b + x_c B_c + \ldots \quad (22)$$

The corrections to be added to Equation (21) are determined according to the following equation, which comes directly from Equation (19):

$$\Delta \ln \phi_i = \Delta \ln (f/p) - x_a \frac{\partial \Delta \ln (f/p)}{\partial xa} - x_b \frac{\partial \Delta \ln (f/p)}{\partial x_b} - x_c \frac{\partial \Delta \ln (f/p)}{\partial x_c} \ldots \quad (23)$$

Again $\Delta \ln \phi_i$ corresponds to a partial molal quantity and again in this equation the *i*th term is omitted and the differentiations are carried out with all *x*'s constant except x_i and the x with respect to which the term is differentiated. These differentiations are ordinarily performed graphically.

For the final calculation of the logarithm of the fugacity coefficient:

$$\ln \phi_i = \text{approximate } \ln \phi_i + \Delta \ln \phi_i \quad (24)$$

Activity coefficients are readily calculated from fugacity coefficients by the following equation:

$$\gamma_i = \frac{\bar{f}_i}{x_i f_i} = \frac{\bar{f}_i / x_i p}{f_i / p} = \frac{\phi_i}{f_i / p} \quad (25)$$

APPLICATION TO THE NITROGEN-ETHYLENE SYSTEM

Since these calculations are somewhat involved, they will be illustrated by applying them to the binary system, nitrogen-ethylene. The calculations can be checked against the values reported by Bennett(*1*), who calculated activity coefficients for this system from the same data by an entirely graphical method. It should be noted however that the method illustrated here is inherently more accurate than a purely graphical method; hence exact agreement between the results cannot be expected.

Data for four nitrogen-ethylene mixtures were reported by Hagenbach and Comings(*5*). Data for pure nitrogen and pure ethylene were taken from Michels, Michels, and Wouters(*7*) and Michels and Geldermans(*6*). The pressure range covered is from 0 to 500 atm. at a temperature of 50°C.

The constants for use in the Redlich and Kwong equation for the pure components were selected according to the method already described. Constants for the mixtures, calculated by Equation (22), are listed in Table 1.

For each composition a series of values of ΔC covering the pressure range was calculated using Equations (6), (9), and (10). It is to be noted that no value of ΔC exceeded 0.053. Graphs of $\Delta C/p$ vs. p were then prepared for each composition as illustrated in Figure 1 for the mixture containing 59.7% N_2. Values of $\Delta \ln (f/p)$

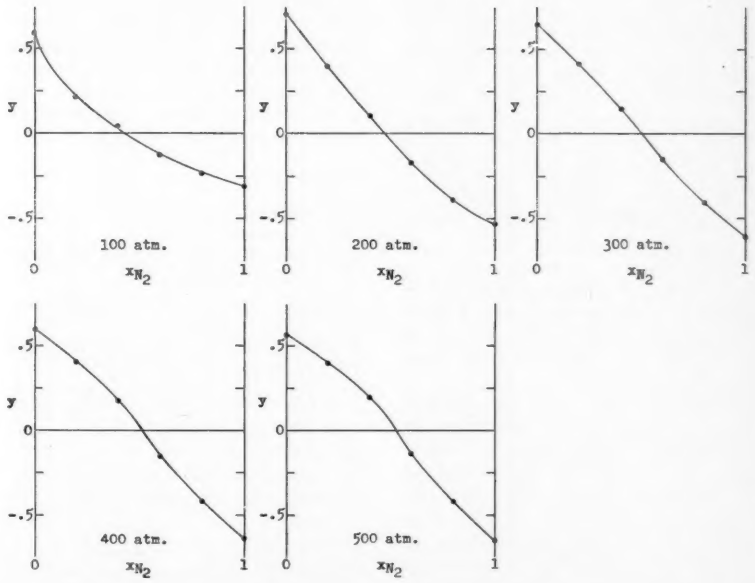

FIG. 5. NITROGEN-ETHYLENE MIXTURES, 50°C.; TESTS FOR THERMODYNAMIC CONSISTENCY. $y = \ln (\gamma_{N_2}/\gamma_{C_2H_4})$.

TABLE 3.—COMPARISON OF RESULTS WITH THOSE OF BENNETT (*1*).

p, atm.	$x_{N_2} = 0.0$		$x_{N_2} = 0.2$		$x_{N_2} = 0.4$		$x_{N_2} = 0.6$		$x_{N_2} = 0.8$		$x_{N_2} = 1.0$	
	γ_c	γ_b	γ_c	γ_b	γ_c	γ_b	γ_c	γ_b	γ_c	γ_b	γ_c	γ_b
Nitrogen												
0	1.00	1.00	1.00	1.00	1.00	1.00	1.00	1.00	1.00	1.00	1.00	1.00
100	1.79	1.45	1.30	1.27	1.13	1.14	1.05	1.06	1.01	1.01	1.00	1.00
200	2.01	1.85	1.53	1.48	1.25	1.25	1.09	1.10	1.02	1.02	1.00	1.00
300	1.91	1.99	1.55	1.55	1.29	1.28	1.10	1.11	1.02	1.03	1.00	1.00
400	1.83	1.99	1.53	1.55	1.31	1.28	1.20	1.11	1.02	1.03	1.00	1.00
500	1.77	1.99	1.52	1.55	1.32	1.28	1.20	1.11	1.02	1.03	1.00	1.00
Ethylene												
0	1.00	1.00	1.00	1.00	1.00	1.00	1.00	1.00	1.00	1.00	1.00	1.00
100	1.00	1.00	1.03	1.01	1.09	1.06	1.18	1.14	1.27	1.27	1.37	1.45
200	1.00	1.00	1.04	1.02	1.12	1.10	1.29	1.25	1.50	1.48	1.71	1.85
300	1.00	1.00	1.03	1.03	1.11	1.11	1.29	1.28	1.55	1.55	1.84	1.99
400	1.00	1.00	1.02	1.03	1.09	1.11	1.29	1.28	1.56	1.55	1.90	1.99
500	1.00	1.00	1.02	1.03	1.08	1.11	1.28	1.28	1.56	1.55	1.92	1.99

γ_c = activity coefficients calculated in this paper; γ_b = smoothed activity coefficients reported by Bennett.

were then determined by graphical integration [see Equation (20)] at pressures of 100, 200, 300, 400, and 500 atm. These values are listed in Table 2 and are shown on Figure 2, which is a plot of $\triangle \ln (f/p)$ vs. x_{N2} with pressure as parameter. The graphical determination of values of $\triangle \ln \phi_i$ by Equation (23) is particularly convenient for a binary mixture because the method of intercepts (*4*) can be used, as is illustrated in Figure 2 for the 59.7% N_2 mixture at 500 atm. Values of $\triangle \ln \phi_i$ determined in this way are listed in Table 2. The analytical part of the calculation was carried out by use of Equations (9) and (10) to calculate values of C' and h at even pressures of 100, 200, 300, 400, and 500 atm. for each composition. These values were then used in Equation (21) to calculate values of approximate $\ln \phi_i$ which are also listed in Table 2. The true values of $\ln \phi_i$ were then found by Equation (24). Activity coefficients were calculated by Equation (25).

RESULTS

Values of ϕ_i and γ_i are listed in Table 2, and Figures 3 and 4 show the activity coefficients plotted as a function of pressure with composition as parameter.

These results may be checked for thermodynamic consistency by the method of Redlich and Kister (*8*), which requires that a plot of $\ln (\gamma_{N2}/\gamma_{C2H4})$ vs. x_{N2} cut off equal areas on both sides of the zero ordinate. That this requirement is satisfied by the results presented in this paper is evident from the graphs shown in Figure 5. The data are from Table 2.

A comparison of these results with those of Bennett (*1*) is given in Table 3. The agreement is not perfect, but this is probably largely accounted for by the inherent inaccuracies of the straight graphical method.

CONCLUSIONS

A convenient and accurate method of calculating thermodynamic properties of gases from experimental compressibility measurements through the use of the Redlich and Kwong equation of state has been presented. The method was demonstrated for the usually troublesome calculation of fugacity and activity coefficients of the components of a gaseous mixture. The calculated activity coefficients are believed to be correct in the second decimal place, indicating an error of less than ±0.5%.

NOTATION

A = a constant
B = a constant
C = experimental value of compressibility factor
C' = equation value of compressibility factor
f = fugacity of a gaseous mixture
f_i = fugacity of pure i
$\overline{f}_i$ = fugacity of component i in a gaseous mixture
G = general property
$\overline{G}$ = general partial molal property
h = defined as being equal to Bp/C'
H = enthalpy
k, k' = constants
n = number of moles
p = pressure, atm.
p_c = critical pressure, atm.
R = universal gas-law constant
S = entropy
$S°$ = entropy in the ideal-gas state at 1 atm.
T = absolute temperature
T_c = absolute critical temperature
V = volume
x_i = mole fraction of component i
γ_i = activity coefficient of component i
ϕ_i = fugacity coefficient of component i
* = the zero-pressure state

LITERATURE CITED

1. Bennett, C. O., *Chem. Eng. Progr. Symposium Series* No. 7, **49**, 45 (1953).
2. Dodge, B. F., "Chemical Engineering Thermodynamics," pp. 105, 106, McGraw-Hill Book Co., Inc., New York (1944).
3. Gamson, B. W, and K. M. Watson, *Natl. Petroleum News, Tech. Sec.* **36**, R623 (1944).
4. Glasstone, S., "Thermodynamics for Chemists," p. 430, D. Van Nostrand Co., Inc., New York (1947).
5. Hagenbach, W. P., and E. W. Comings, *Ind. Eng. Chem.*, **45**, 606 (1953).
6. Michels, A., and M. Geldermans, *Physica*, **9**, 967 (1942).
7. Michels, A., C. Michels, and H. Wouters, *Proc. Roy. Soc. (London)*, **A153**, 214 (1935).
8. Redlich, O., and A. T. Kister, *Ind. Eng. Chem.*, **40**, 345 (1948).
9. Redlich, O., and J. N. S. Kwong, *Chem. Revs.*, **44**, 233 (1949).
10. Smith, J. M., "Introduction to Chemical Engineering Thermodynamics," pp. 168, 170, 278, McGraw-Hill Book Co., Inc., New York (1949).

Controlling Mechanism in the Aqueous Absorption of Nitrogen Oxides

M. S. PETERS, C. P. ROSS, AND J. E. KLEIN, University of Illinois, Urbana, Illinois

The reactions involved in the removal of nitrogen oxides from gases by reaction with water are reversible and proceed at a finite rate. It is possible therefore that the over-all process is controlled by the rate of the chemical reactions. On this basis an analysis of the process has been developed by the application of chemical kinetics, with consideration of reactions involving both nitrogen dioxide and dinitrogen tetroxide. The resulting differential equation has been simplified and integrated to give a final equation which can be tested experimentally.

Theoretical methods are presented for predicting the extent of absorption of nitrogen oxides at various gas rates and concentrations and are compared with the experimental results.

The paper presents some new concepts of the factors which control the rate of absorption of nitrogen dioxide and dinitrogen tetroxide in water. An understanding of the controlling factors in the process should indicate methods for improving the design of absorption towers in nitric acid plants and aid in the design of scrubbers for removing nitrogen oxides from waste gases.

The removal of nitrogen oxides from gaseous mixtures is important in the production of nitric acid and in the cleaning of certain stack gases. The removal may be accomplished by the reaction of nitrogen dioxide (NO_2) or dinitrogen tetroxide (N_2O_4) with water to give nitric acid and nitric oxide (NO). Although the chemical reactions of the various nitrogen oxides with themselves, with oxygen, and with water have been investigated extensively during the past 40 years, very little work has been done on the actual mechanisms involved in the removal of nitrogen oxides from gaseous mixtures.

Most industrial units for the production of nitric acid use bubble-cap-plate towers or packed towers for contact between water and the gases containing nitrogen oxides, but these towers are very inefficient when the concentration of nitrogen oxides in the gases is low. Development of improved methods for recovering the oxides requires an understanding of the controlling mechanisms in the oxide-recovery process.

The nitrogen oxides of importance in processes involving reactions with aqueous solutions are NO_2, N_2O_4, and NO. Small amounts of N_2O_3 and N_2O_5 are also present in the gases, but according to Verhoek and Daniels(*9*) and Smith and Daniels(*7*) these compounds rapidly come to equilibrium with NO and NO_2 and represent only a small fraction of the total oxides at room temperatures or above.

The essential chemical reactions occurring in the removal process may be written as follows:

$$2\,NO_2\ (\text{or}\ N_2O_4) + H_2O \longrightarrow HNO_3 + HNO_2 \qquad (A)$$

$$2\,HNO_2 \longrightarrow H_2O + NO + NO_2\ (\text{or}\ 1/2\ N_2O_4) \qquad (B)$$

$$2\,NO + O_2 \longrightarrow 2\,NO_2\ (\text{or}\ N_2O_4) \qquad (C)$$

$$2\,NO_2 = N_2O_4 \qquad (D)$$

Reaction (D) reaches equilibrium very rapidly(*8*), and the equilibrium constant for this reaction is known as a function of temperature between 0° and 90°C.(*6, 9, 10*). The oxidation of NO proceeds relatively slowly although the reaction goes essentially to completion. Reaction-rate constants for the oxidation reaction have been determined by Bodenstein(*1*).

The decomposition of nitrous acid in the liquid phase does not occur rapidly unless the liquid is well agitated. Under ordinary conditions, however, this reaction is not the controlling factor in determining the rate of oxides removal, for analyses of the liquid product obtained in this work indicated only small amounts of nitrous acid relative to the amount of nitric acid.

GAS- AND LIQUID-PHASE REACTION

In the past, most workers dealing with the reactions between nitrogen oxides and water have assumed that the reactions occur in the liquid phase. They have assumed that NO_2 and N_2O_4 diffuse into the liquid where the reaction with H_2O occurs; that nitrous acid formed decomposes into NO_2, H_2O, and NO; that this NO_2 reacts with more water and the NO is partially oxidized to NO_2 by absorbed oxygen in the liquid phase; and that most of the NO is desorbed from the liquid and oxidized to NO_2 in the gas phase.

The liquid-phase reaction undoubtedly occurs to some extent. However, the results of the present work and those of Chambers and Sherwood(*3*) definitely indicate that a gas-phase reaction does occur. Perhaps the strongest support of the gas-phase reaction lies in the observable formation of a mist when gases containing NO_2 and N_2O_4 are brought into contact with a gas containing appreciable amounts of water vapor. The mist formation has been observed repeatedly in this work and was reported by Chambers and Sherwood.

In carefully controlled experimental tests carried out in conjunction with the present investigation, gaseous N_2O_4 and NO_2 were admitted to a bulb containing nitrogen and water vapor. No droplets of liquid were present in the bulb in any form before the admittance of the nitrogen oxides. As soon as

Mr. Ross is now associated with E. I. DuPont de Nemours and Co., North Augusta, South Carolina.

the oxides entered the bulb, a mist was formed which quickly spread throughout the entire bulb. The same type of mist was observed when N_2O_4 and NO_2 were brought into contact with liquid water, with the mist having the greatest density just above the water surface.

The mist is undoubtedly composed of droplets containing nitric acid and water. The saturation vapor pressure of HNO_3 is very low over dilute mixtures of HNO_3 in water. It is conceivable, therefore, that the vapor-phase reaction could produce enough HNO_3 vapor to cause the formation of droplets of dilute nitric acid.

Caudle and Denbigh (*2*) in experiments with a wetted-wall column found that neither increasing the gas-space volume nor increasing the bulk liquid volume had any effect on the rate of removal of nitrogen oxides by liquid water. The rate of removal was proportional to the interfacial area between the gas and the liquid. The controlling resistance, therefore, must lie in the gas film or in the liquid film.

Under these conditions the following over-all mechanism can be postulated for the absorption process. Some of the gaseous NO_2 and N_2O_4 reacts with H_2O vapor in the gas film to form HNO_3 and HNO_2. Most of the HNO_3 diffuses into the liquid phase, and some H_2O and HNO_3 condense in the form of a mist containing small droplets of dilute nitric acid. Part of the HNO_2 decomposes in the vapor space to give NO, NO_2, and H_2O and the rest diffuses into the liquid, where the same decomposition products are obtained. Some of the NO_2 and N_2O_4 diffuses into the liquid phase before reacting with water.

DIFFUSION AS THE CONTROLLING FACTOR IN THE OVER-ALL MECHANISM

The rate of the over-all process by which nitrogen oxides are removed from gaseous mixtures by chemical reaction with water could be controlled by (*a*) diffusional resistances, (*b*) the speed of the chemical reactions, or (*c*) a combination of diffusional resistance and chemical reaction rate.

Chambers and Sherwood (*3*) assumed the controlling mechanism to be the physical diffusion of NO_2 and N_2O_4 through the gas film; consequently the following expression for the absorption rate, expressed as gram moles of equivalent combined nitrogen [i.e., moles of NO_2 + 2(moles of N_2O_4)] per second per square centimeter of gas-liquid interfacial area, may be derived:

$$N_{eNO_2} = \frac{2D_{N_2O_4}}{x_f}\Delta C_{N_2O_4} + \frac{D_{NO_2}}{x_f}\Delta C_{NO_2} \qquad (1)$$

Instantaneous attainment of equilibrium between NO_2 and N_2O_4 is assumed in the derivation of Equation (1). The result is the same as for the diffusion of NO_2 and N_2O_4 under conditions in which the two gases have no effect on each other.

According to the experimental results of this work and the results of Caudle and Denbigh (*2, 4*), the rate of nitrogen oxides removal (N_{eNO_2}) at any given gas rate is directly proportional to the concentration of N_2O_4. The ratio $D_{NO_2}/D_{N_2O_4}$ is 1.43 (*3*), and the NO_2 concentration in all the experimental runs was higher than the N_2O_4 concentration; therefore, as NO_2 and N_2O_4 may be assumed to be always in equilibrium, ΔC_{NO_2} was greater than $\Delta C_{N_2O_4}$. Under these conditions Equation (1) is not supported by the experimental results, for Equation (1) shows that the absorption rate should be determined to a large extent by the NO_2 concentration; therefore, it can be concluded that the diffusion of NO_2 and N_2O_4 through the gas film is not the controlling factor in the over-all mechanism.

By the employment of a method similar to that of Hatta (*5*), differential equations based on combined diffusional resistance and chemical-reaction rate as the controlling factor in the over-all mechanism have been derived. These equations either could not be integrated or did not agree with the experimental data. A similar approach based on the two-film theory was attempted by Caudle and Denbigh using methods such as those described by Van Krevelen and Hoftijzer (*8*). They were unable to develop any applicable relationships including diffusion as a controlling factor.

CHEMICAL-REACTION RATES AS THE CONTROLLING FACTOR IN THE OVER-ALL MECHANISM

The reactions involved in the removal of nitrogen oxides from gases by reaction with water are reversible and proceed at a finite rate. It is possible, therefore, that the rate of aqueous absorption is controlled by the rate of the chemical reactions. On this basis, an analysis of the process can be developed by the application of chemical kinetics, and the results agree closely with the experimental data.

The important chemical reactions involved in the removal of NO_2 and N_2O_4 from gaseous mixtures by reaction with water can be written as follows:

$$N_2O_4 + H_2O \underset{k_2}{\overset{k_1}{\rightleftarrows}} HNO_2 + HNO_3 \quad (a)$$

$$2\,NO_2 + H_2O \underset{k_4}{\overset{k_3}{\rightleftarrows}} HNO_2 + HNO_3 \quad (b)$$

$$2\,HNO_2 \underset{k_6}{\overset{k_5}{\rightleftarrows}} NO + 1/2\,N_2O_4 + H_2O \quad (c)$$

$$2\,HNO_2 \underset{k_8}{\overset{k_7}{\rightleftarrows}} NO + NO_2 + H_2O \quad (d)$$

$$2\,NO_2 = N_2O_4 \quad \text{(continuous equilibrium)} \quad (e)$$

By summation of reactions (*a*) and (*c*),

$$3/2\,N_2O_4 + H_2O \rightarrow 2\,HNO_3 + NO \quad (f)$$

By summation of reactions (*b*) and (*d*),

$$3\,NO_2 + H_2O \rightarrow 2\,HNO_3 + NO \quad (g)$$

The *k*'s in the preceding equations represent the reaction-rate constants for the forward and reverse reactions.

Equilibrium between NO_2 and N_2O_4 is attained very rapidly, and in the following derivation these two materials are assumed to be continuously in equilibrium. Reactions (*a*), (*b*), and (*e*) occur simultaneously, and reactions (*c*) and (*d*) are consecutive to reactions (*a*) and (*b*). Reaction (*a*), being a bimolecular reaction, should proceed at a faster rate than reaction (*b*), which is trimolecular; however, reaction (*b*) cannot be neglected because it may become important when the concentration of NO_2 is large relative to the N_2O_4 concentration.

At low total concentrations of equivalent NO_2 ($C_{eNO_2} = C_{NO_2} + 2C_{N_2O_4}$), only a small fraction of the total oxides is in the form of N_2O_4. For example, at 25°C. and a total pressure of 1 atm., a gaseous mixture containing 0.1 mole % eNO_2 has only 1.3% of the equivalent

oxides in the form of N_2O_4. At the same temperature and pressure, however, a gaseous mixture containing 10 mole % $_eNO_2$ has 43% of the equivalent oxides in the form of N_2O_4. This effect of total oxides concentration on fraction of oxides present as N_2O_4 is shown in Figure 1. As the total concentration of gaseous nitrogen oxides decreases, the efficiency of the removal process should decrease because of the reduction in the fraction of total oxides present as N_2O_4.

The reaction between NO and O_2 to yield NO_2 and N_2O_4 proceeds at a relatively slow rate. This reaction has not been considered here because the analysis deals only with the nitrogen oxides removal which can be accomplished by a one-stage contact with water. The NO oxidation does not proceed at a rate sufficient to cause an appreciable change in the NO_2 concentration while in contact with the liquid on a bubble-cap plate. This conclusion has been verified experimentally in the bubble cap column used for this work by substituting nitrogen for air in the entering gases.

In the following derivation C represents the concentration in gram moles per cubic centimeter and the subscript on the C represents the particular material to which the concentration refers. The symbol t represents time in seconds. According to reaction (a),

$$-\left(\frac{dC_{N_2O_4}}{dt}\right)_a = k_1 (C_{N_2O_4})(C_{H_2O}) - k_2 (C_{HNO_2})(C_{HNO_3}) \quad (2)$$

According to reaction (c),

$$\left(\frac{dC_{N_2O_4}}{dt}\right)_c = \frac{k_5}{4}(C_{HNO_2})^2 - k_6 (C_{NO})(C_{N_2O_4})^{\frac{1}{2}}(C_{H_2O}) \quad (3)$$

Therefore, the rate of change in N_2O_4 concentration caused by reaction (a) followed by reaction (c) is

$$-\left(\frac{dC_{N_2O_4}}{dt}\right)_{a+c} = k_1 (C_{N_2O_4})(C_{H_2O}) - k_2 (C_{HNO_2})(C_{HNO_3}) + k_6 (C_{NO})(C_{N_2O_4})^{\frac{1}{2}}(C_{H_2O}) - \frac{k_5}{4}(C_{HNO_2})^2 \quad (4)$$

In a continuous process involving consecutive reactions, a so-called "stationary state" may be reached in which the concentrations of the intermediate reacting materials are essentially constant. Unless reaction (c), or (d), is extremely slow, a stationary state will be obtained very rapidly in this process and the HNO_2 concentration will change very slowly. Under these conditions reaction (f) applies, and 1 mole of NO is formed [by reaction (c)] for every 3/2 moles of N_2O_4 which disappear [net N_2O_4 loss by reactions (a) and (c)]. Therefore according to reaction (f),

$$-\left(\frac{dC_{N_2O_4}}{dt}\right)_{a+c} = \frac{3}{2}\left(\frac{dC_{NO}}{dt}\right)_c \quad (5)$$

According to reaction (c),

$$\left(\frac{dC_{NO}}{dt}\right)_c = \frac{k_5}{2}(C_{HNO_2})^2 - 2k_6 (C_{NO})(C_{N_2O_4})^{\frac{1}{2}}(C_{H_2O}) \quad (6)$$

If Equations (4), (5), and (6) are combined,

$$-\left(\frac{dC_{N_2O_4}}{dt}\right)_{a+c} = \frac{3}{4}k_1 (C_{N_2O_4})(C_{H_2O}) - \frac{3}{4}k_2 (C_{HNO_2})(C_{HNO_3}) \quad (7)$$

Because NO_2 and N_2O_4 are continuously in equilibrium, a change in N_2O_4 concentration is caused by reaction (e). The rate of this concentration change may be represented by $(dC_{N_2O_4}/dt)_e$. The net rate of change in N_2O_4 concentration caused by reactions (a), (c), and (e) is

$$-\left(\frac{dC_{N_2O_4}}{dt}\right)_{net} = -\left(\frac{dC_{N_2O_4}}{dt}\right)_{a+c+e} = \frac{3}{4}k_1 (C_{N_2O_4})(C_{H_2O}) - \frac{3}{4}k_2 (C_{HNO_2})(C_{HNO_3}) - \left(\frac{dC_{N_2O_4}}{dt}\right)_e \quad (8)$$

By applying the same reasoning as was used for developing Equation (8), one can obtain the following equation representing the net rate of change in NO_2 concentration caused by reactions (b), (d), and (e):

$$-\left(\frac{dC_{NO_2}}{dt}\right)_{net} = -\left(\frac{dC_{NO_2}}{dt}\right)_{b+d+e} = \frac{3}{4}k_3 (C_{NO_2})^2(C_{H_2O}) - \frac{3}{2}k_4 (C_{HNO_2})(C_{HNO_3}) - \left(\frac{dC_{NO_2}}{dt}\right)_e \quad (9)$$

The rate of change in N_2O_4 concentration caused by reaction (e) must be one half the rate of change in NO_2 concentration due to this reaction, or

$$-\left(\frac{dC_{N_2O_4}}{dt}\right)_e = \frac{1}{2}\left(\frac{dC_{NO_2}}{dt}\right)_e \quad (10)$$

As reaction (e) is always at equilibrium,

K_e = equilibrium constant =

$$\frac{C_{N_2O_4}}{(C_{NO_2})^2} \quad (11)$$

$$dC_{NO_2} = \frac{dC_{N_2O_4}}{2\sqrt{K_e C_{N_2O_4}}} \quad (12)$$

Combination of Equations (8), (9), (10), (11), and (12) gives

$$-\frac{4}{3}\left(\frac{dC_{N_2O_4}}{dt}\right)_{net} - \frac{1}{3\sqrt{K_e C_{N_2O_4}}}\left(\frac{dC_{N_2O_4}}{dt}\right)_{net} = (k_1 + \frac{k_3}{2K_e})(C_{N_2O_4})(C_{H_2O}) - (k_2 + k_4)(C_{HNO_2})(C_{HNO_3}) \quad (13)$$

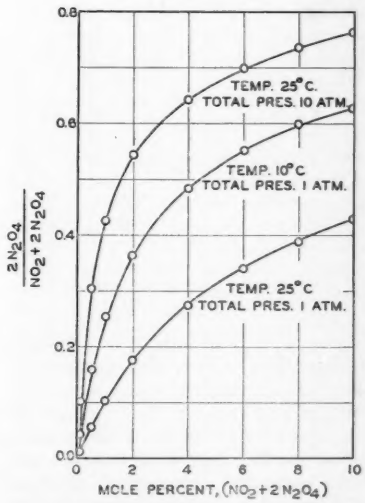

FIG. 1. EFFECT OF eNO_2 CONCENTRATION OF TOTAL OXIDE PRESENT AS N_2O_4.

Only three assumptions have been made in the derivation of Equation (13). They are (1) NO_2 and N_2O_4 are in continuous equilibrium, (2) the reactions as indicated represent the important chemical process, and (3) a stationary state is rapidly obtained. All these assumptions appear to be justified on the basis of results obtained in this work and by other investigators. It should be noted that Equation (13) could also have been derived from Equations (*a*), (*b*), (*e*), (*f*), and (*g*) on the basis of rate of change in HNO_3 concentration.

SIMPLIFICATION AND INTEGRATION OF RATE EQUATIONS

If the net chemical reactions (*f*) and (*g*) are essentially irreversible, the last term in Equation (13) may be neglected. If the irreversible reaction occurs in the gas film, the concentration of HNO_3 will be very small since it diffuses rapidly into the liquid phase. Under any conditions if the reactions are irreversible the concentration of HNO_2 will be very small. The concentration of H_2O may be assumed as constant at any given temperature. If the reactions occur in the gas film, the H_2O concentration will be directly proportional to the H_2O vapor pressure, and if the reactions occur in the liquid film the H_2O concentration (or activity) will be essentially constant unless there is a large change in the acid concentration. With these two simplifications Equation (13) may be written as follows:

$$-\left(\frac{dC_{N_2O_4}}{dt}\right)_{net} - \frac{1}{4\sqrt{K_c\, C_{N_2O_4}}}\left(\frac{dC_{N_2O_4}}{dt}\right)_{net} = A\,(C_{N_2O_4}) \qquad (14)$$

where

$$A = \frac{3}{4}\left(k_1 + \frac{k_3}{2K_c}\right)(C_{H_2O})$$

For gas concentrations less than about 10% eNO_2, the volumetric flow rate remains essentially constant, and under this condition Equation (14) may be integrated directly. The equation may be rearranged and integrated between the limits of zero time (corresponding to an original N_2O_4 concentration of $C_{oN_2O_4}$) and the time (t) any

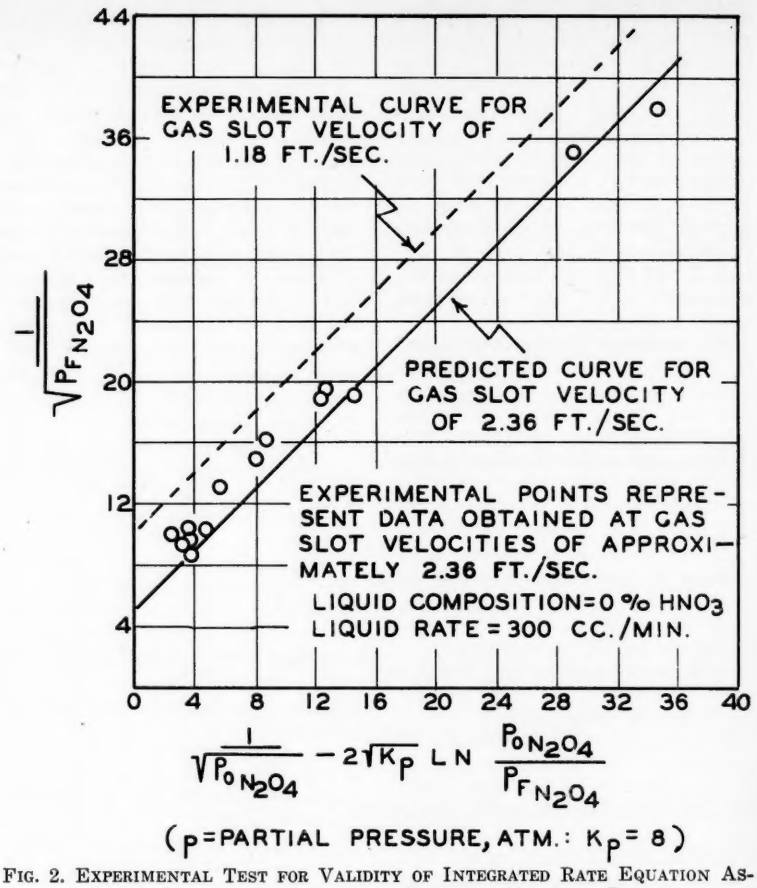
EXPERIMENTAL CURVE FOR GAS SLOT VELOCITY OF 1.18 FT./SEC.
PREDICTED CURVE FOR GAS SLOT VELOCITY OF 2.36 FT./SEC.
EXPERIMENTAL POINTS REPRESENT DATA OBTAINED AT GAS SLOT VELOCITIES OF APPROXIMATELY 2.36 FT./SEC.
LIQUID COMPOSITION=0 % HNO3
LIQUID RATE = 300 CC./MIN.
1/√PFN2O4
1/√PoN2O4 − 2√KP LN PoN2O4/PFN2O4
(P=PARTIAL PRESSURE, ATM.: KP= 8)
0 4 8 12 16 20 24 28 32 36 40
4 12 20 28 36 44

FIG. 2. EXPERIMENTAL TEST FOR VALIDITY OF INTEGRATED RATE EQUATION ASSUMING PROCESS CONTROLLED BY CHEMICAL REACTION RATES.

portion of the gas is in contact with the liquid (corresponding to a final N_2O_4 concentration of $C_{fN_2O_4}$).

$$-\int_{C_{o_{N_2O_4}}}^{C_{f_{N_2O_4}}} \frac{dC_{N_2O_4}}{C_{N_2O_4}} - \frac{1}{4\sqrt{K_c}}\int_{C_{o_{N_2O_4}}}^{C_{f_{N_2O_4}}} \frac{dC_{N_2O_4}}{(C_{N_2O_4})^{3/2}} = A\int_0^t dt \qquad (15)$$

Integration, substitution of the limits and rearrangement give

$$\frac{1}{(C_{f_{N_2O_4}})^{1/2}} = \frac{1}{(C_{o_{N_2O_4}})^{1/2}} - 2\sqrt{K_c}\,\ln\frac{C_{o_{N_2O_4}}}{C_{f_{N_2O_4}}} + 2A\sqrt{K_c}\;t \qquad (16)$$

At partial pressures of eNO_2 less than 0.1 atm. perfect-gas deviations are small and the concentration terms in Equation (16) can be expressed in more convenient units of partial pressure to give the following simplified equation:

$$\frac{1}{(P_{f_{N_2O_4}})^{1/2}} = \frac{1}{(P_{o_{N_2O_4}})^{1/2}} - 2\sqrt{K_p}\,\ln\frac{P_{o_{N_2O_4}}}{P_{f_{N_2O_4}}} + B\,t \qquad (17)$$

where

P = partial pressure, atm.

K_p = equilibrium constant = $\frac{P_{N2O4}}{P_{NO2}}$, atm.$^{-1}$

B = a constant at any temperature

Equation (17) shows that a plot of

$$\frac{1}{(P_{f_{N_2O_4}})^{1/2}} \text{ vs. } \left[\frac{1}{(P_{o_{N_2O_4}})^{1/2}} - 2\sqrt{K_p}\,\ln\frac{P_{o_{N_2O_4}}}{P_{f_{N_2O_4}}}\right]$$

TABLE 1.—EXPERIMENTAL DATA

Bubble-cap-plate Column

Total pressure = 1 atm.

Run	Plate temp., °C	Ent. liq. comp., wt. % HNO_3	Exit liq. rate, cc./ min.	Exit liq. comp., wt. % HNO_3 $\times 10^2$	Ent. gas rate, cu. ft./ min.	Entering-gas composition, mole %			Exit-gas composition, mole %		
						$NO_2 + 2N_2O_4$	NO_2	N_2O_4	$NO_2 + 2N_2O_4$	NO_2	N_2O_4
1	19.8	0	292	0.615	1.22	0.454	0.420	0.0171	0.422	0.392	0.0150
2	23.0	0	301	0.845	1.18	0.534	0.497	0.0185	0.491	0.459	0.0159
3	18.2	0	298	0.900	1.21	0.622	0.554	0.0340	0.578	0.518	0.0298
4	23.6	0	302	2.08	1.18	0.685	0.628	0.0286	0.576	0.534	0.0206
5	19.4	0	286	1.84	1.21	0.699	0.622	0.0388	0.611	0.550	0.0306
6	23.0	0	311	1.61	1.18	0.741	0.672	0.0344	0.656	0.602	0.0272
7	21.1	0	304	1.81	1.21	0.794	0.707	0.0435	0.696	0.627	0.0347
8	18.8	0	306	2.23	1.21	0.800	0.697	0.0515	0.686	0.608	0.0393
9	18.4	0	306	2.16	1.21	0.821	0.710	0.0554	0.714	0.628	0.0430
10	24.0	0	288	3.12	1.20	0.831	0.752	0.0394	0.681	0.626	0.0276

based on experimental data should be a straight line with a slope equal to 1.0 if the reactions occur irreversibly and all concentration values are determined at approximately the same temperature and a constant value of t. Experimental conditions in which the reactions occur essentially irreversibly may be obtained by contacting gases containing only NO_2 and N_2O_4 (plus air or nitrogen as a diluent) with dilute nitric acid or with pure water. Experimental data at various N_2O_4 concentrations have been obtained under these conditions maintaining constant gas rates (i.e., constant t) and constant temperature (i.e., constant values of A, B, and K_p). These data are plotted as

$$\frac{1}{(P_{f_{N_2O_4}})^{1/2}} \text{ vs. } \left[\frac{1}{(P_{o_{N_2O_4}})^{1/2}} - 2\sqrt{K_p} \ln \frac{P_{o_{N_2O_4}}}{P_{f_{N_2O_4}}}\right]$$

in Figure 2. It can be seen that a straight line with a slope of 1.0 is obtained in agreement with Equation (17).

EXPERIMENTAL EQUIPMENT AND PROCEDURE

A bubble-cap-plate column containing one plate was used for obtaining the experimental data. The bubble-cap plate was made of Lucite and was equipped with seven Lucite bubble caps. One bubble cap was located in the center of the plate, and the other six caps were arranged peripheral to the center cap. Eight equally spaced circular slots of 5/16-in. diam. were drilled in the center cap, and four slots in each of the peripheral caps, these slots being directed toward the center to reduce wall effects. The total slot area was 2.46 sq. in. The total depth of liquid on the plate was 1 in., and the tops of the slots were 1/2 in. below the liquid surface. A stainless steel cooling coil was also immersed in the liquid on the plate. The inside diameter of the glass column was 7 1/2 in., and the bubble-cap plate was 12 in. from both the top and bottom plates.

Water or aqueous nitric acid was fed to the plate from a constant-head tank through Tygon tubing. The product liquid was delivered from a downcomer to a 20-liter bottle. Liquid samples were taken through a glass side tube fitted with a stopcock. The liquid flow rate was determined by a rotameter and checked by volumetric measurements.

Gaseous nitrogen oxides, obtained from cylinders containing NO_2 and N_2O_4, were diluted with nitrogen or air and admitted at a steady rate to the lower section of the column. The inlet and exit gases were sampled by means of evacuated Gaillard bulbs. The gas-flow rates were measured by calibrated Venturi meters. Pressures at the top and bottom of the column were measured by open-tube manometers containing α-bromonaphthalene. The indicating fluid in the Venturi manometers was also α-bromonaphthalene, which is not strongly reactive with NO_2. Temperatures at the following points were measured by means of copper-constantan thermocouples: (1) liquid on bubble-cap plate, (2) entering liquid, (3) exit liquid, (4) entering gas, (5) exit gas.

Runs were made at liquid-flow rates of 300 and 600 cc/min., gas-slot velocities of 1.18 and 2.36 ft./sec., entering liquid compositions of 0 and 15 wt. % HNO_3, and gas compositions of 0.45 to 11.6 vol. % eNO_2. All runs were carried out at atmospheric pressure. Nitrogen was used as the diluent for the first series of runs, which was checked by use of air at the same flow conditions, and no significant difference in results was found; consequently, air was used for the remainder of the runs. If more than one bubble-cap plate had been used or if NO had been admitted to the column with the NO_2, there would have been a significant difference in the nitrogen and air results because air would have supplied oxygen for the oxidation of NO to NO_2.

At the start of a run the liquid- and air-flow rates were set and blank samples of each taken. Then the NO_2 was admitted at the desired flow rate and the equipment was run until steady-state conditions were attained. The liquid flow from the column was then diverted to the collecting bottle, and liquid was collected for 10 to 20 min. while the flow rates were carefully held constant. The pressures and temperatures were read, and entering- and exit-gas samples, as well as liquid samples, were taken near the beginning and near the end of the timing period. The liquid samples were analyzed for HNO_3 by titrating a known volume with standard $NaOH$ solution.

The gas samples were taken in evacuated bulbs containing hydrogen peroxide. The amount of sample was found by weighing, and the amount of nitrogen oxides present was determined by titrating the HNO_3 formed by the reaction between H_2O_2 and NO_2, N_2O_4, or NO. In order to analyze the exit gases for the NO content, a second sampling bulb containing potassium permanganate in sulfuric acid was used. The excess permanganate was back titrated with ferrous sulfate, and the results obtained from the hydrogen peroxide bulb and the permanganate bulb were used to determine the NO content in the exit gases. The observed exit-gas analyses differed considerably from the calculated values based on the liquid analysis. Collection of liquid sampes in H_2O_2 determined that a slight discrepancy was caused by NO being given up by the liquid; however, a large error in the exit-gas analyses was due to the admittance of a significant amount of mist to the sampling bulbs. It was not possible to determine the amount of mist to make the necessary corrections. The

mist also obviated the possibility of analyzing the exit gases by photometric methods because it would have critically interfered with the cell readings. All results consequently were reported on the basis of the liquid-flow rate, the entering- and exit-liquid analyses, the air-flow rate, and the entering-gas analysis.

The fraction of the oxides which theoretically could be converted to HNO_3 according to the over-all reaction

$$3\,NO_2 + H_2O \rightarrow 2\,HNO_3 + NO$$

was calculated by the method of Sherwood and Pigford(*6*) by use of extrapolated values of the equilibrium constant. When water (0% HNO_3) was used as the absorbent and the entering gases contained only NO_2 (with N_2O_4) and nitrogen or air, the calculated theoretical conversion was practically 66 2/3% based on the total gaseous oxides. This indicates that the reaction is essentially irreversible under these conditions because 1 mole of NO theoretically can be liberated for every 3 moles of equivalent NO_2 entering the system.

The relative amounts of NO_2 and N_2O_4 in the entering and exit gases were determined from the equilibrium constants for the reaction(*6*)

$$2\,NO_2 = N_2O_4\,.$$

INTERPRETATION OF RESULTS*

Table 1 presents a sample of the experimental results. The runs were all carried out under conditions in which the chemical reactions involved were essentially irreversible. All the runs at a slot velocity of 1.18 ft./sec. were at approximately the same temperature. Under these conditions, if the chemical reaction rate is the controlling mechanism in the over-all process, Equation (17) should apply, and a plot of

$$\frac{1}{(P_{f_{N_2O_4}})^{1/2}} \text{ vs. } \left[\frac{1}{(P_{o_{N_2O_4}})^{1/2}} - 2\sqrt{K_p}\ln\frac{P_{o_{N_2O_4}}}{P_{f_{N_2O_4}}}\right]$$

should be a straight line with a slope of 1.0. Figure 2 indicates that Equation (17) agrees with the experimental data. This plot covers a 150-fold change in N_2O_4 concentration in the entering gases and gives strong support to the theory that the rates of the chemical reactions involving N_2O_4 and NO_2 control the over-all removal process. The sensitivity of the correlation was checked by making calculations for conversions other than the reported values, and it was found that the correlation was quite sensitive to changes in the experimental results, especially at high eNO_2 concentrations.

The intercept of the straight line at

$$\left[\frac{1}{(P_{o_{N_2O_4}})^{1/2}} - 2\sqrt{K_p}\ln\frac{P_{o_{N_2O_4}}}{P_{f_{N_2O_4}}}\right]$$

equal to zero is Bt. The numerical value of the intercept can be used to predict the line for a similar plot at the same temperature with a different contact time, assuming the effective gas-liquid interfacial area does not change appreciably. This was done for a contact time equivalent to a gas-slot velocity of 2.36 ft./sec., and the predicted curve is shown in Figure 3. The experimental data fall slightly above the predicted curve probably because the effective contact area between the gas and liquid varies somewhat with gas rate.

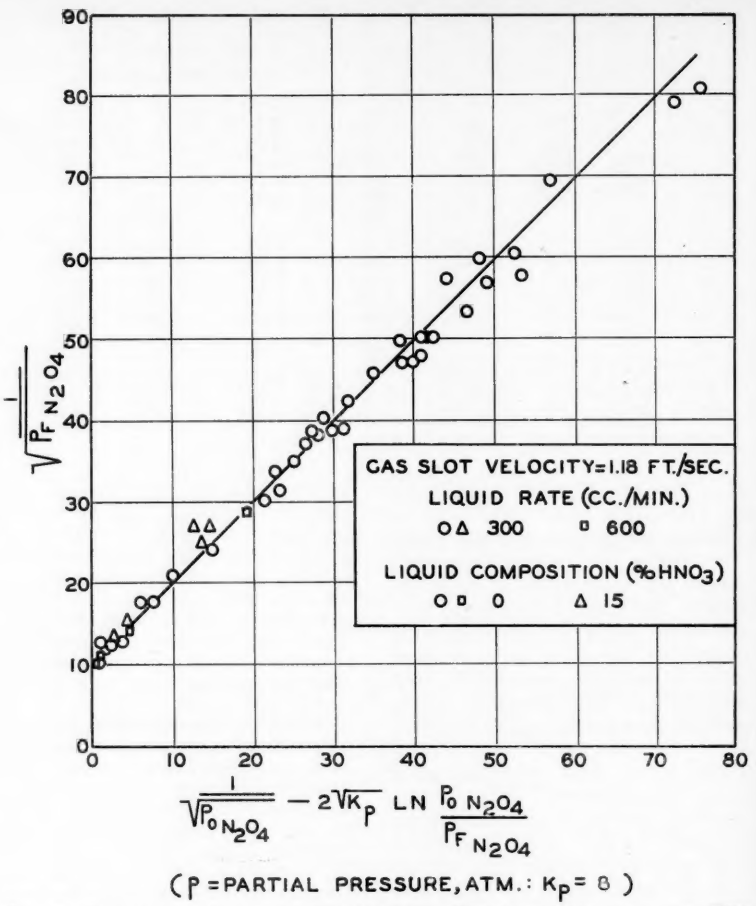
GAS SLOT VELOCITY=1.18 FT./SEC.
LIQUID RATE (CC./MIN.)
○△ 300 ▫ 600
LIQUID COMPOSITION (%HNO3)
○▫ 0 △ 15
1/√PF N2O4
1/√PO N2O4 − 2√Kp LN PO N2O4 / PF N2O4
(P = PARTIAL PRESSURE, ATM.: Kp = 8)

FIG. 3. PREDICTED CURVE FOR RELATIONSHIP BETWEEN ENTERING AND EXIT N_2O_4 CONCENTRATIONS.

The individual plate efficiency for the removal process may be expressed as the actual amount of nitrogen oxides removed from the gases divided by the amount of oxides which would have been removed if the plate were theoretically perfect. A plot of plate efficiency vs. percentage of eNO_2 in the entering gases at constant gas rate is shown in Figure 4. The plate efficiency decreases as the percentage of eNO_2 in the entering gases decreases. This effect would be expected if the factor which controls the over-all mechanism is the rate of the chemical reactions since the fraction of total oxides present as N_2O_4 decreases with reduced eNO_2 concentrations.

The change in removal efficiency with change in total gaseous oxides concentration must be recognized when systems for the aqueous absorption of nitrogen oxides are designed. As is indicated in Figure 1, an increase in pressure at any given composition of the gases causes a larger fraction of the total

*Complete tabulations of the experimental data are on file with the Photoduplication Service, American Documentation Institute, Library of Congress, Washington 25, D. C., as Document 4423, which may be ordered for $1.25 for microfilm or photoprints.

nitrogen oxides to be present in the form of N_2O_4. Consequently, higher plate efficiencies may be obtained by increasing the total pressure of the gases.

The experimental data obtained with the bubble-cap column showed that an increase in the gas rate caused a decrease in the fraction of entering oxides converted to nitric acid, but a twofold change in the liquid-flow rate had no appreciable effect on the fractional conversion.

SUMMARY

The factor which controls the over-all mechanism in the removal of nitrogen oxides from gaseous mixtures by contact with water is the rate of the chemical reactions involved. The rate of removal of the nitrogen oxides is proportional to the concentration of N_2O_4 in the gases. As the fraction of total oxides present as N_2O_4 is low when the concentration of gaseous oxides is low, the individual plate efficiencies for removal of nitrogen oxides from dilute gases are poor; however improved plate efficiencies can result with high total pressure.

The chemical reactions between nitrogen oxides and water occur partially in the gas phase or in the gas film, as evinced by the formation of a mist when NO_2 and N_2O_4 are in vapor.

The fraction of the entering oxides which are converted to nitric acid decreases as the contact time between the gas and liquid decreases. If experimental data for the equipment are available at one gas rate, the integrated kinetic equations can be used for an estimation of the effect of change in gas-liquid contact time.

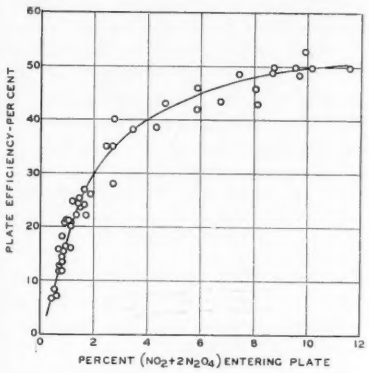

FIG. 4. EFFECT OF eNO_2 CONCENTRATION IN ENTERING GASES ON ABSORPTION EFFICIENCY (BUBBLE-CAP COLUMN AT 1 ATM. TOTAL PRESSURE; GAS-SLOT VELOCITY OF 1.18 FT./SEC.)

ACKNOWLEDGMENT

This work has been conducted in the Engineering Experiment Station of the University of Illinois as part of Contract AT(30-3)-28, United States Atomic Energy Commission, H. F. Johnstone, technical director. Detailed information concerning the theory and experimental results are available as Technical Report 10, COO-1011, Technical Information Service, United States Atomic Energy Commission, Oak Ridge, Tennessee.

NOTATION

A = constant at any temperature
B = constant at any temperature
C = concentration, gram moles/cc.
C_f = final concentration, gram moles/cc.
C_o = original concentration, gram moles/cc.
D = diffusivity, sq. cm./sec.
eNO_2 = equivalent NO_2 = $NO_2 + 2\ N_2O_4$
k = reaction-rate constant, units depending on reaction involved
K = equilibrium constant for the reaction, $2\ NO_2 = N_2O_4$
N_{eNO_2} = rate of nitrogen oxides removal based on equivalent NO_2 removal, gram moles/(sec.) (sq. cm.)
P = partial pressure, atm.
P_f = final partial pressure, atm.
P_o = original partial pressure, atm.
t = time, sec.
x_f = effective film thickness, cm.
ΔC = differences in concentration between main body of gas and gas-liquid interface, gram moles/cc.

LITERATURE CITED

1. Bodenstein, M., *Helv. Chim. Acta*, 18, 743 (1935).
2. Caudle, P. G., and K. G. Denbigh, *Trans. Faraday Soc.*, 49, 39 (1953).
3. Chambers, F. S., and T. K. Sherwood, *Ind. Eng. Chem.*, 29, 1415 (1937).
4. Denbigh, K. G., and A. J. Prince, *J. Chem. Soc.*, 790 (1947).
5. Hatta, S., *Tech. Repts. Tôhoku Imp. Univ.*, 10, 119 (1932).
6. Sherwood, T. K., and R. L. Pigford, "Absorption and Extraction," 2 ed., McGraw-Hill Book Company, Inc., New York (1952).
7. Smith, J. H., and F. Daniels, *J. Am. Chem. Soc.*, 69, 1735 (1947).
8. Van Krevelen, D. W., and P. J. Hoftijzer, *Rec. trav. chim.*, 66, 49, 67 (1947); 67, 133 (1948); 68, 221 (1949).
9. Verhoek, F. H., and F. Daniels, *J. Am. Chem. Soc.*, 53, 1250 (1931).
10. Wenner, R. R., "Thermochemical Calculations," McGraw-Hill Book Company, Inc., New York (1941).

(Presented at A.I.Ch.E. Washington meeting)

APPROXIMATE EQUATIONS FOR TIME OF BATCH FRACTIONATION

A. I. JOHNSON, CHEN-JUNG HUANG, and F. D. F. TALBOT

University of Toronto, Toronto, Ontario

Analytical expressions are obtained for the calculation of the time required for batch rectification of binary feeds which may be treated by assuming constant relative volatility and no column holdup. The equations cover constant reflux operations and varying reflux constant product operations for the two cases involving either a large or a small number of theoretical stages. The latter type of calculation has hitherto been possible only by tedious graphical methods. This paper introduces novel pseudo-equilibrium curves which lead to simple equations of considerable accuracy. The equations obtained may be rearranged or modified so that other factors such as sharpness of fractionation may be represented analytically.

An accurate method for the design of equipment for the batch distillation and fractionation of binary liquid mixtures of constant overhead product composition with varying reflux ratio was presented by Bogart(*1*). However, the method covered only the case of constant distillate composition with varying reflux ratio and involved a rather tedious graphical integration. Many subsequent papers have dealt with modifications of assumptions made by Bogart, notably the inclusion of the effect of holdup.

These papers are summarized in a recent excellent paper by Rose and Johnson(*5*), who also list all the variables which must be considered in any accurate computation method.

Another recent paper which is relevant to the present work is that of Chu(*2*). Analytical expressions are derived for calculating the yield of distillate obtainable in a batch distillation carried out with increasing reflux to a predetermined value.

The present paper discusses approximate analytical methods for constant-reflux and constant-overhead-composition batch distillations for binary systems with constant relative volatility. The equations derived permit the calculation of the time required, θ, to reduce the initial composition in the pot, x mole fraction more volatile, to a final composition x mole fraction in an apparatus containing n theoretical plates.

Depending on the number of plates, two situations arise. When n is large, the intersection of the operating line and equilibrium curve is usually at the same composition abscissa as is the pot composition for all practical purposes. The equations for θ may be derived easily, as outlined. However, when n is small, this assumption is considerably in error. For this case pseudoequilibrium curves are developed leading to equations for θ.

In addition to constant relative volatility all the usual simplifying assumptions made in applying the McCabe-Thiele method are employed: ideal plates, constant molal vaporization and overflow in the column at any instant, and an adiabatic column. The equations neglect holdup of liquid and vapor in the column and condenser.

DERIVATION OF EQUATIONS

Batch Operation Including a Large Number of Theoretical Plates. *Constant Reflux Ratio.* For constant relative volatility of α, the equation of the equilibrium curve is

$$y = \frac{\alpha x}{1 + (\alpha - 1)x} \qquad (1)$$

As the number of theoretical stages is large, the intersection of the operating line

$$y = \frac{R}{R+1}x + \frac{1}{R+1}x_D \qquad (2)$$

and the equilibrium curve [Equation (1)] is for all practical purposes at the same composition abscissa as is the pot-liquid composition (*see* Figure 1). Eliminating y between Equations (1) and (2) gives the corresponding distillate composition, obtained as a function of pot-liquid composition x,

$$x_D = \frac{\dfrac{\alpha x}{1 + (\alpha - 1)x} - \dfrac{R}{R+1}x}{\dfrac{1}{R+1}} \qquad (3)$$

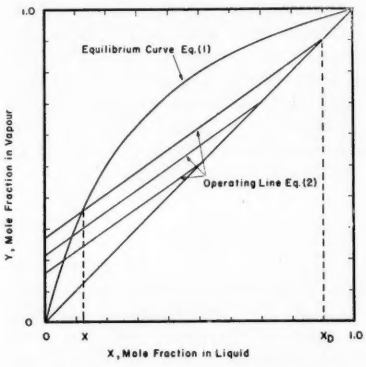

FIG. 1. CASE 1*a*, BATCH FRACTIONATION WITH CONSTANT REFLUX RATIO —LARGE NUMBER OF PLATES.

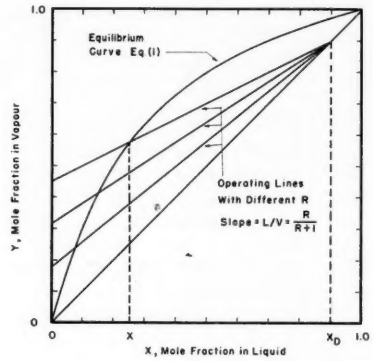

FIG. 2. CASE 1*b*, BATCH FRACTIONATION PRODUCING CONSTANT COMPOSITION OF DISTILLATE—LARGE NUMBER OF PLATES.

When this is substituted in the basic Rayleigh equation (4) or batch distillation,

$$\int_W^{W_i} \frac{dW}{W} = \int_x^{x_i} \frac{dx}{x_D - x} \qquad (4)$$

and integrated,

$$\frac{W_i}{W} = \left[\frac{\dfrac{(1-x_i)^\alpha}{x_i}}{\dfrac{(1-x)^\alpha}{x}}\right] - \frac{1}{(\alpha-1)}\,\frac{1}{(R+1)} \qquad (5)$$

This equation gives the relationship between the initial and final number of moles in the pot W_i and W and the initial and final pot-liquid compositions x_i and x. If the vaporizing rate is V moles/hr., the time required for this operation is

$$\theta = (R+1)\frac{W_i}{V}\left\{1 - \left[\frac{\dfrac{(1-x_i)^\alpha}{x_i}}{\dfrac{(1-x)^\alpha}{x}}\right]\frac{1}{(\alpha-1)}\,\frac{1}{(R+1)}\right\} \qquad (6)$$

Variable Reflux Ratios, Producing Distillate of Constant Composition. For this case as the distillation proceeds, the reflux ratio must be increased to maintain a given product purity x_D, which is held constant. If the initial pot-liquid composition is x_i, the initial value of L/V (and therefore the initial reflux ratio) is obtained from Equation (3) by substitution of x_i for x. The initial reflux ratio required is

$$R_i = \frac{x_D + (\alpha-1)\,x_i\,x_D - \alpha x_i}{(\alpha-1)\,x_i\,(1-x_i)} \qquad (7)$$

The total time for any binary distillation producing distillate of constant composition has been developed by Bogart(*1*):

$$\theta = \frac{W_i\,(x_D - x_i)}{V}\int_x^{x_i} \frac{dx}{(1 - \frac{L}{V})\,(x_D - x)^2} \qquad (8)$$

The slope of the operating line (*see* Figure 2) may be expressed as

$$\frac{L}{V} = \frac{x_D - y}{x_D - x} \qquad (9)$$

and imposing constant relative volatility from Equation (1) enables Bogart's equation [Equation (8)] to be integrated to

$$\theta = \frac{W_i\,(x_D - x_i)}{V(\alpha-1)\,x_D\,(1-x_D)}\left\{(1-x_D)\ln\frac{x_i}{x} + [1+(\alpha-1)x_D]\right.$$

$$\ln \frac{x_D - x}{x_D - x_i} + \alpha x_D \ln \frac{1 - x_i}{1 - x} \Bigg\} \quad (10)$$

Batch Operation Involving a Small Number of Theoretical Plates. *Constant Reflux Ratio.* The proposed method for calculation involving a small number of theoretical plates and constant reflux ratio is based on the use of a pseudoequilibrium curve and the application of the method previously described.

The pseudoequilibrium curve is to relate pot composition and overhead composition for constant-reflux-ratio distillation. Furthermore, it should reflect the relative volatility of the system, the number of theoretical plates in the column, and the reflux ratio. A curve which does this with sufficient accuracy for engineering calculations may be developed as follows (*see* Figure 3).

Following is a consideration of the geometry corresponding to $x = 0.5$. This abscissa was chosen as a starting point because of the simple value of the ordinate, $y = \frac{\alpha}{\alpha + 1}$, on the true equilibrium curve *BEGD*. For the true equilibrium curve the pseudoline *FD* is substituted. This line also has a rather simple equation

$$y = \frac{2}{\alpha + 1} x + \frac{\alpha - 1}{\alpha + 1} \quad (11)$$

or

$$y = m_2 x + b_2 \text{ where } m_2 = \frac{2}{\alpha + 1} \text{ and } b_2 = \frac{\alpha - 1}{\alpha + 1} \quad (12)$$

The equation of the operating line corresponding to the fixed reflux ratio and to the pot-liquid composition $x_n = 0.5$ may be

$$y = m_1 x + b_1 \quad (13)$$

where $m_1 = \frac{R}{R + 1}$

$$b_1 = \frac{x_D}{R + 1}$$

A relationship between x_n and x_D can be developed by a method similar to that of Smoker(7). Corresponding to $x_n = 0.5$, the composition of equilibrium vapor is $\alpha/(\alpha + 1)$.

From Equation (13),

$$x_{n-1} = \frac{y_n - b_1}{m_1} = \frac{\frac{\alpha}{\alpha + 1} - b_1}{m_1} \quad (14)$$

By substitution in Equation (12),

$$y_{n-1} = m_2 x_{n-1} + b_2 =$$

$$\frac{m_2}{m_1} \left(\frac{\alpha}{\alpha + 1} - b_1\right) + b_2 \quad (15)$$

When this operation is continued from plate to plate and $r = \frac{m_2}{m_1}$

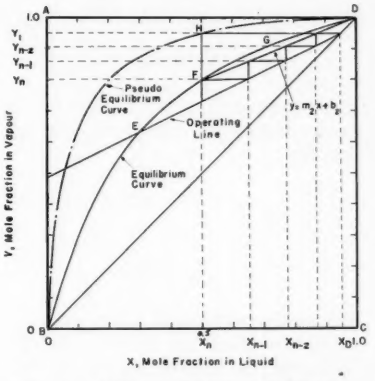

FIG. 3. CASE 2*a*, BATCH FRACTIONATION WITH CONSTANT REFLUX RATIO —SMALL NUMBER OF PLATES.

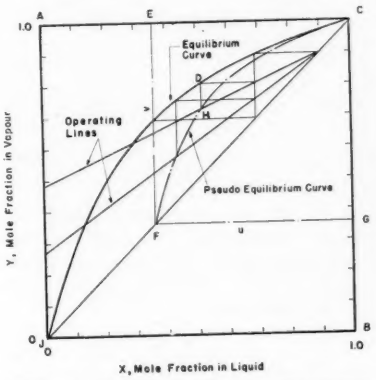

FIG. 4. CASE 2*b*. BATCH FRACTION PRODUCING CONSTANT COMPOSITION OF DISTILLATE — SMALL NUMBER OF PLATES.

$$y_{n-h} = r^h \left(\frac{\alpha}{\alpha + 1}\right) - b_1 (r^h + r^{h-1} + r^{h-2} + \ldots + r) + b_2 (r^{h-1} + r^{h-2} + \ldots + 1) \quad (16)$$

If n is the number of equilibrium stages including the pot and if h is the number of theoretical plates in the column, then y_{n-h} is equal to y_1, the composition of the vapor from the first plate.

Summing the geometric series:

$$y_1 = \frac{r^h \left(\frac{\alpha}{\alpha + 1}\right) + b_2 \left(\frac{1 - r^h}{1 - r}\right)}{1 + \left(\frac{r}{R + 1}\right)\left(\frac{1 - r^h}{1 - r}\right)} \quad (17)$$

This gives one of the y values on the pseudoequilibrium curve *BHD*, the proposed curve relating the pot composition to the overhead composition for constant reflux ratio distillation for the given conditions. It is called a pseudoequilibrium curve because the constant relative volatility α' associated with it is to be used in the simple Rayleigh batch fractionation equation. The ordinates on the curve are denoted as y' to associate them with α'.

Again since the abscissa is still 0.5 for point *H*, the pseudorelative volatility α' is obtained from the ordinate.

$$\frac{\alpha'}{\alpha' + 1} = \frac{r^h \left(\frac{\alpha}{\alpha + 1}\right) + b_2 \left(\frac{1 - r^h}{1 - r}\right)}{1 + \left(\frac{r}{R + 1}\right)\left(\frac{1 - r^h}{1 - r}\right)} \quad (18)$$

where

$$r = \frac{\frac{2}{\alpha + 1}}{\frac{R}{R + 1}} = \frac{2(R + 1)}{R(\alpha + 1)} \quad (19)$$

The pseudorelative volatility α' is now used in the same manner as true relative volatility in simple distillation. Mathematically, the pseudoequilibrium curve can be expressed in the equation

$$y' = \frac{\alpha' x}{1 + (\alpha' - 1) x} \quad (20)$$

By this development therefore the composition of distillate x_D corresponding to the liquid composition x in the pot at the same time is equal to the pseudovapor composition y' which is in equilibrium with the same liquid composition x. The closeness with which a curve so drawn follows the actual curve relating these compositions is indicated in the example shown in Figure 4. The dashed line *OJKHMD* was drawn here to relate actual pot compositions to overhead compositions for three theoretical plates. The curve *OEGFD* corresponds to an α' value based on Equation (18). Actually, at high values of x, y' will be found to be lower than x_D, as can be seen from Figures 3 and 5 and at lower x values y' will be greater than x_D. Nevertheless, for most applications the fit is sufficiently close for the results obtained to be useful. Equation (20) yields the approximation

$$x_D = \frac{\alpha' x}{1 + (\alpha' - 1)\, x} \qquad (21)$$

Substituting Equation (21) in the basic Rayleigh equation [Equation (4)] yields the relationship between the initial and final amounts of liquid in the pot:

$$\frac{W_i}{W} = \left[\frac{\dfrac{(1 - x_i)^{\alpha'}}{x_i}}{\dfrac{(1 - x)^{\alpha'}}{x}} \right]^{\frac{1}{\alpha' - 1}} \qquad (22)$$

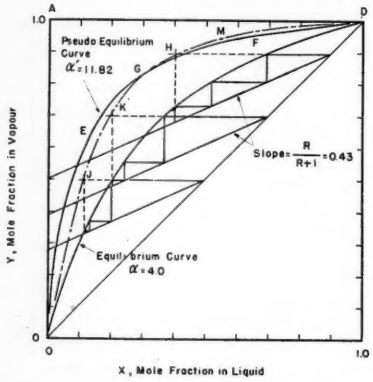

FIG. 5. SAMPLE CALCULATION OF CASE 2*a*.

And therefore the time required to reduce the liquid composition in pot from x_i to x is

$$\theta = (R + 1) \left(\frac{W_i}{V} \right) \left\{ 1 - \left[\frac{\dfrac{(1 - x_i)^{\alpha'}}{x_i}}{\dfrac{(1 - x)^{\alpha'}}{x}} \right]^{\frac{1}{\alpha' - 1}} \right\} \qquad (23)$$

Variable Reflux Ratio Producing Distillate of Constant Composition. Development of Equation (10) was made possible by the assumption that the operating line and equilibrium curve intersect at the abscissa corresponding to the pot composition. If the number of theoretical stages is relatively small, the composition of liquid in pot will correspond to a larger abscissa than this point of intersection. In the proposed method a pseudoequilibrium curve is set up which may be used in the same manner as for Equation (10) but which will reflect the small number of equilibrium stages. The pseudoequilibrium curve also includes the relative volatility of the system.

The method of introducing the pseudoequilibrium curve, illustrated in Figure 5, is to hold up to total reflux, and so the concentration of the pot liquid for the case of total reflux, a, is first obtained from the Fenske equation (*3*).

$$a = \frac{x_D}{\alpha^n (1 - x_D) + x_D} \qquad (24)$$

The pseudoequilibrium curve is now constructed based on the relations

$$u = (1 - a)x \qquad (25)$$

$$v = (1 - a)y \qquad (26)$$

The u-v coordinates now refer to a reduced diagram $EFGC$; the origin can be located as $x = a$ and $y = a$. The pseudoequilibrium curve is obtained by substituting u, v from above in Equation (1) to give

$$v = \frac{\alpha u}{1 + \dfrac{(\alpha - 1)}{1 - a} u} = \frac{\alpha u}{1 + \beta\,(\alpha - 1)u} \qquad (27)$$

where

$$\beta = \frac{1}{1 - a} \qquad (28)$$

It should be emphasized that for this construction u-v and x-y coordinates adopt the same modulus. When it is desired to use x-y axes as a reference

$$x = u + a \qquad (29)$$

$$y = v + a \qquad (30)$$

Substituting these values in Equation (27) yields the correct form of the pseudoequilibrium curve referred to in the diagram $AOBC$ (x-y coordinates):

$$y = \frac{\alpha(x - a)}{1 + \beta\,(\alpha - 1)\,(x - a)} + a \qquad (31)$$

If one eliminates y between Equations (31) and (2) and solves for $(R + 1)$,

$$R + 1 = \frac{(x_D - x)\,[1 + \beta(\alpha - 1)X]}{(\alpha - 1)\,X\,(1 - \beta X)} \qquad (32)$$

where $X = x - a$

Equation (32) is the mathematical expression relating the reflux ratio, R, with the composition of pot liquid, x, for the case of a small number of theoretical stages and of distillate of constant composition. As

$$1 - \frac{L}{V} = \frac{1}{R + 1} \qquad (33)$$

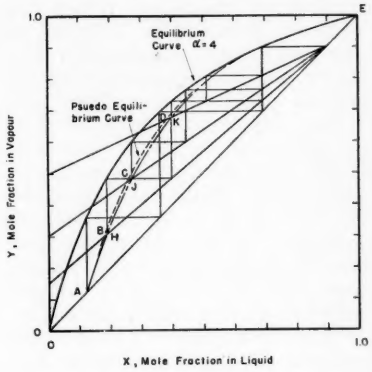

FIG. 6. SAMPLE CALCULATION OF CASE 2*b*.

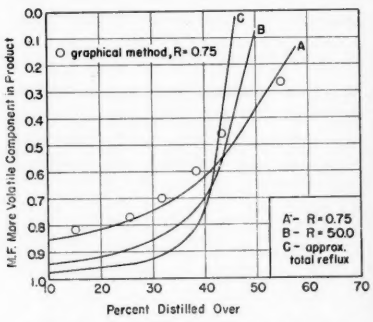

FIG. 7. SHARPNESS OF SEPARATION.

the proper substitutions can be made into Bogart's equation [Equation (8)] to yield finally

$$\theta = \frac{W_i\,(x_D - x_i)}{V\,(\alpha - 1)} \left[\frac{1}{m} \ln \frac{X_i}{X} + \frac{\alpha\beta}{m\beta - 1} \ln \frac{1 - \beta X}{1 - \beta X_i} + \frac{1 + m\beta\,(\alpha - 1)}{m\,(m\beta - 1)} \ln \frac{m - X_i}{m - X} \right] \qquad (34)$$

where

$$X = x_i - a$$
$$X = x - a$$
$$m = x_D - a$$

SHARPNESS OF FRACTIONATION FOR CONSTANT REFLUX RATIO AND A SMALL NUMBER OF PLATES

A sharpness of fractionation curve is a plot of the average dis-

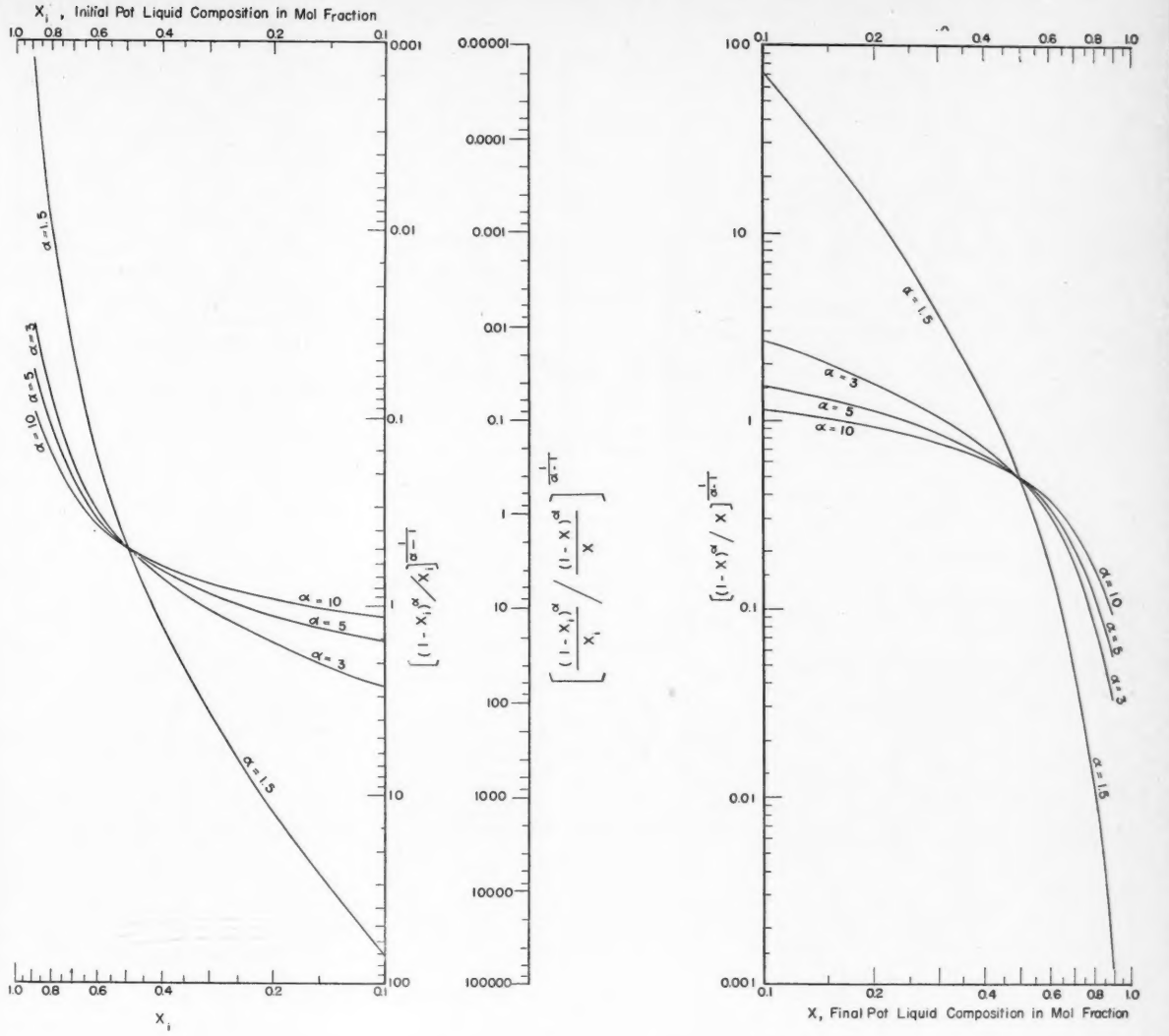

FIG. 8. NOMOGRAM FOR $\left[\dfrac{(1-x_i)^{\alpha}}{x_i} \Big/ \dfrac{(1-x)^{\alpha}}{x}\right]^{\frac{1}{\alpha-1}}$

tillate composition against the percentage of moles distilled. Rose and Welshans (*6*) have presented analytical methods for calculating sharpness curves for the case of constant relative volatility, any given number of stages, no holdup, and essentially total reflux.

Equation (22) will permit sharpness curves to be drawn for any reflux ratio, thus extending the work of Rose and Welshans. The pseudorelative volatility α' is calculated from Equation (18) as before. Figure 7 shows a series of curves corresponding to increasing reflux ratio to illustrate the calculation. Curve A is for a reflux ratio of 3 corresponding to the example of Figure 5; the circle points were calculated graphically for this example and show excellent agreement with the analytical results.

The calculations for curve A are shown as an appendix.

NOMOGRAMS

The final equations may be solved by combinations of nomograms of the usual type; however, there is little time advantage in using these, and for greater accuracy the use of the equations with a calculating machine is recommended.

Figure 8 is a nomograph for calculating

$$\left[\frac{\dfrac{(1-x_i)^{\alpha}}{x_i}}{\dfrac{(1-x)^{\alpha}}{x}}\right]\frac{1}{\alpha-1}$$

which appears in Equations (6) and (23).

Figure 9 is a nomogram for calculating a based on Equation (24) and $\beta = \dfrac{1}{1-a}$. These values are required for the calculations utilizing Equation (34).

SAMPLE CALCULATIONS

As an illustration, the results of sample calculations are shown in Tables 1 and 2 and are compared with those obtained by graphical integration.

SUMMARY

The equations for approximate calculation to determine the time required to reduce the composition of liquid in the pot from x_i to x are summarized as follows:

I. Batch Operation Involving a Large Number of Theoretical Plates

a. Constant reflux ratio

$$\theta = (R+1)\frac{W_i}{V}\Bigg\{1 - \left[\frac{\dfrac{(1-x_i)^{\alpha}}{x_i}}{\dfrac{(1-x)^{\alpha}}{x}}\right]^{\frac{1}{\alpha-1}\frac{1}{R+1}}\Bigg\} \quad (6)$$

b. Variable Reflux Ratio, Producing Distillate of Constant Composition

$$\theta = \frac{W_i\,(x_D - x_i)}{V(\alpha-1)x_D\,(1-x_D)}\Bigg\{(1-x_D)\ln\frac{x_i}{x} + [1+(\alpha-1)x_D]\ln\frac{x_D - x}{x_D - x_i} + \alpha x_D \ln\frac{1-x_i}{1-x}\Bigg\} \quad (10)$$

II. Batch Operation Involving a Small Number of Theoretical Plates

a. Constant Reflux Ratio

$$\theta = (R+1)\frac{W_i}{V}\Bigg\{1 - \left[\frac{\dfrac{(1-x_i)^{\alpha'}}{x_i}}{\dfrac{(1-x)^{\alpha'}}{x}}\right]^{\frac{1}{\alpha'-1}}\Bigg\} \quad (23)$$

where

$$\frac{\alpha'}{\alpha'+1} = \frac{r^h\left(\dfrac{\alpha}{\alpha+1}\right) + b_2\left(\dfrac{1-r^h}{1-r}\right)}{1 + \left(\dfrac{r}{R+1}\right)\left(\dfrac{1-r^h}{1-r}\right)}$$

$$r = \frac{2(R+1)}{R(\alpha+1)}, \text{ and } b_2 = \frac{\alpha-1}{\alpha+1}$$

b. Variable Reflux Ratio, Producing Distillate of Constant Composition

$$\theta = \frac{W_i\,(x_D - x_i)}{V(\alpha-1)}\left[\frac{1}{m}\ln\frac{X_i}{X} + \frac{\alpha\beta}{m\beta - 1}\ln\frac{1-\beta X}{1-\beta X_i} + \frac{1+m\beta(\alpha-1)}{m(m\beta-1)}\ln\frac{m-X_i}{m-X}\right] \quad (34)$$

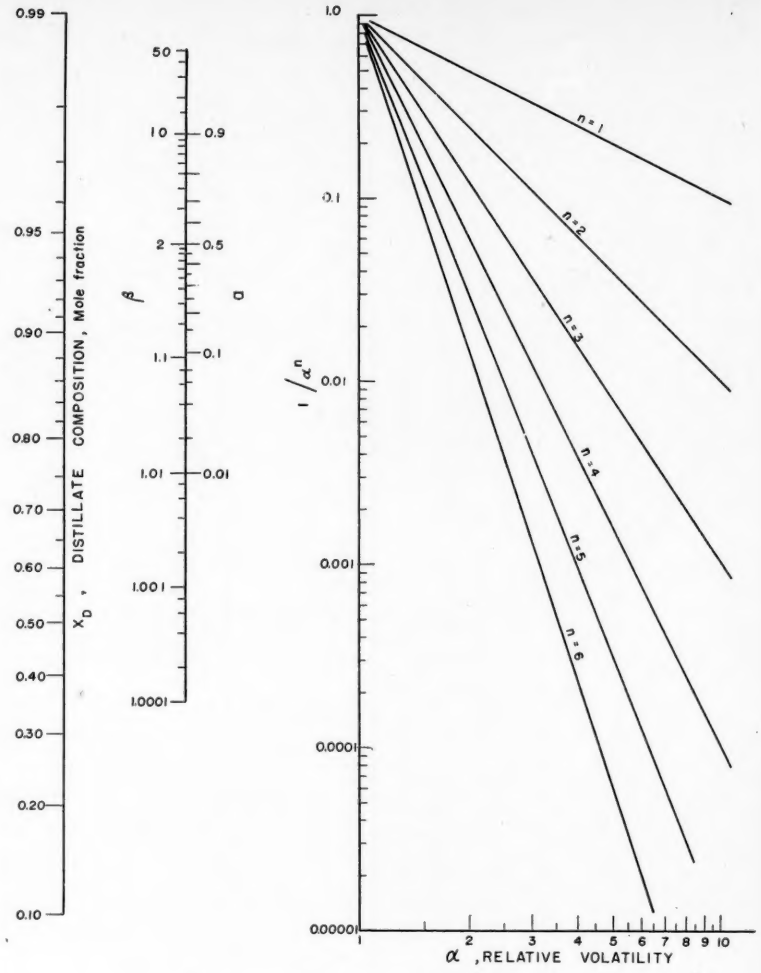

FIG. 9. NOMOGRAM FOR CONSTANTS α AND β.

where

$$X_i = x_i - a \qquad X = x - a$$

$$m = x_D - a \qquad \beta = \frac{1}{1-a}$$

and

$$a = \frac{x_D}{\alpha^n\,(1-x_D) + x_D}$$

TABLE 1.—BATCH OPERATIONS INVOLVING A LARGE NUMBER OF PLATES

Operating conditions and calculating results		Constant reflux ratio	Constant composition of distillate
Relative volatility	α	1.5	1.5
Initial amount of liquid in pot	W_i	100 moles	100 moles
Final composition of liquid in pot	x	0.05	0.05
Initial composition of liquid in pot	x_i	0.50	0.50
Rate of vaporization		50 moles/hr.	50 moles/hr.
Constant reflux ratio	R	3	
Initial reflux ratio	R_i	...	3
Constant composition of distillate	x_D	...	0.90
Composition of initial distillate	x_{D_i}	0.90	
Amount of liquid left in pot calculated by graphical integration	W	22.2 moles	
Amount of liquid left in pot calculated by proposed method [Equation (5)]	W	22.9 moles	
Time, calculated by graphical integration	θ	6.23 hr.	7.36 hr.
Time, calculated by proposed method		6.10 hr.	7.11 hr.

These equations involve novel pseudoequilibrium curves which may be useful in other applications, as illustrated by the example of sharpness of fractionation. It should be emphasized that these equations are approximate expressions only; however, they yield results which should aid in scheduling pilot-plant and industrial batch distillations and in evaluating the effect of the major factors—number of plates, relative volatility, vapor rates, and compositions on the times required for these distillations.

Some engineering discretion is required in the selection of equations. In general a small number of theoretical plates would be six or fewer and a large number ten or more. In border cases both equations should be applied for any given distillation.

NOTATION

W_i = Initial amount of liquid in pot, moles

W = Amount of liquid in pot, moles

x_i = Mole fraction of more volatile component of the initial liquid mixture in pot

x = Mole fraction of more volatile component of the liquid mixture in pot

α = Relative volatility

θ = Time required to reduce the initial liquid composition in pot, x_i, to the final composition, x, hr.

n = Number of theoretical stages

h = Number of theoretical plates in a distillation column

y = Vapor composition in mole fraction which is in equilibrium with liquid mixture of composition x

y' = Ordinate value on pseudo-equilibrium curve

R = Reflux ratio, L/D

R_i = Initial reflux ratio for the case of constant composition of distillate

V = Rate of vaporization, moles/hr.

L = Amount of reflux, moles/hr.

x_D = Mole fraction of more volatile component in the distillate

x_{D_i} = Mole fraction of more volatile component in the initial distillate for the case of constant reflux ratio

α' = Pseudorelative volatility determined by Equation (18)

a = Mole fraction of liquid calculated by Equation (24)

$\beta = 1/(1-a)$

$r = 2(R+1)/R(\alpha+1)$

$m_1 = R/(R+1)$

$m_2 = 2/(\alpha+1)$

$b_1 = x_D/(R+1)$

$b_2 = (\alpha-1)/(\alpha+1)$

$m = x_D - a$

$X_i = x_i - a$

$X = x - a$

LITERATURE CITED

1. Bogart, M. J., *Trans. Am. Inst. Chem. Engrs.*, **33**, 139 (1937).
2. Chu, Ju Chin, *Chem. Eng. Progr.*, **46**, 215 (1950).
3. Fenske, M. R., *Ind. Eng. Chem.*, **24**, 482 (1932).
4. Rayleigh, O. M., *Phil. Mag.*, 6th Series, **4**, No. 23, 521 (November, 1902).
5. Rose, A., and R. C. Johnson, *Chem. Eng. Progr.*, **49**, 15 (1953).
6. Rose, A., and L. M. Welshans, *Ind. Eng. Chem.*, **32**, 669, (1940).
7. Smoker, E. H., *Trans. Am. Inst. Chem. Engrs.*, **34**, 165 (1938).

TABLE 2.—BATCH OPERATION INVOLVING A SMALL NUMBER OF PLATES

Operating conditions and calculation results		Constant reflux ratio	Constant composition of distillate
Relative volatility	α	4.0	4.0
Initial amount of liquid in pot	W_i	100 moles	100 moles
Initial composition of liquid in pot	x_i	0.40	0.40
Final composition of liquid in pot	x	0.10	0.18
Rate of vaporization	V	50 moles/hr.	50 moles/hr.
Number of theoretical stages	n	3	3
Number of theoretical plates in the column	h	2	2
Constant reflux ratio	R	0.75	
Initial reflux ratio	R_i	...	0.75
Constant composition of distillate	x_D	...	0.90
Initial composition of distillate	x_{D_i}	0.90	
r, calculated from Equation (19)	r	0.934	
Slope of pseudoline of Equation (12)	m_2	0.40	
Slope of operating line of Equation (13)	m_i	0.43	
b_2 of Equation (12)	b_2	0.60	
Pseudo relative volatility	α'	11.82	
a of Equation (24)	a	...	0.123
β calculated by Equation (28)	..	...	1.140
$m = x_D - a$	m	...	0.777
$X_i = x_i - a$	X_i	...	0.277
$X = x - a$	x	...	0.057
Time, calculated by graphical integration	θ	1.66 hr.	1.62 hr.
Time, calculated by proposed method	θ	1.50 hr.	1.48 hr.

(Presented at A.I.Ch.E. Washington meeting)

APPENDIX

Sharpness of Fractionation Curves by the Analytical Method

W = 100 moles
x_i = 0.40
n = 3
α = 4.0

	$R=0.75$		$R=50.0$		Total reflux*	
x	W	y	W	y	W	y
0.35	91.0	0.858	91.8	0.950	92.1	0.972
0.30	82.6	0.824	84.0	0.930	85.2	0.966
0.25	75.2	0.784	78.0	0.910	79.3	0.956
0.20	68.5	0.732	73.0	0.884	74.0	0.942
0.15	62.1	0.656	67.0	0.845	69.1	0.920
0.10	56.2	0.548	62.8	0.770	64.8	0.878
0.08	53.8	0.487	61.0	0.725	63.2	0.848
0.06	50.8	0.410	58.8	0.665	61.5	0.804
0.04	48.1	0.282	56.8	0.558	59.8	0.728
0.02	43.8	0.182	54.6	0.382	58.0	0.567

*According to Rose, A., and L. M. Welshans, *Ind. Eng. Chem.*, *32*, 668 (1940).

Graphical Construction

W = 100 moles
x_i = 0.40
n = 3
α = 4.0

x	W	y
0.35	92.0	0.858
0.30	83.2	0.820
0.25	74.5	0.768
0.20	68.4	0.700
0.15	61.7	0.600
0.10	56.2	0.460
0.05	45.2	0.265

KINETICS OF THE CATALYZED AND UNCATALYZED LIQUID-PHASE HYDRATION OF PROPYLENE OXIDE

A. L. BENHAM and FRED KURATA
University of Kansas, Lawrence, Kansas

The kinetics of the catalytic and noncatalytic hydration of propylene oxide were studied in a continuous reactor. Both the catalytic and noncatalytic reaction were studied over a temperature range of 100° to 300°F. The feed ratios ranged from 2.5 to 10 lb. water/lb. propylene oxide. In the case of catalytic reaction, the catalyst concentration of sulfuric acid ranged up to 0.25 wt. % of the total feed.

The study showed the noncatalytic reaction to be pseudo first order with respect to propylene oxide, and an equation was found for the rate constant. The catalytic reaction was found to be pseudo second order with respect to propylene oxide, and the effect of the catalyst concentration is shown graphically.

Propylene glycol (1-, 2-propanediol), which was first prepared by Wurtz(*10*) in 1859 by hydrolysis of propylene glycol diacetate, was first produced on a commercial scale by Carbide and Carbon Chemicals Co. in 1931 via the chlorhydrin process. Curme and Johnston(*3*) state that the production of propylene glycol has become increasingly important, and in 1950 85,000,000 lb. was produced. In 1951 propylene glycol was being produced in five plants located in three states(*3*). Although the major portion of propylene glycol is manufactured by the chlorhydrin process, there is increasing interest in its production by the hydration of propylene oxide.

This investigation, made because of the lack of information on this reaction in the literature, was set up for study of the kinetics of this reaction. Some data on the distri-

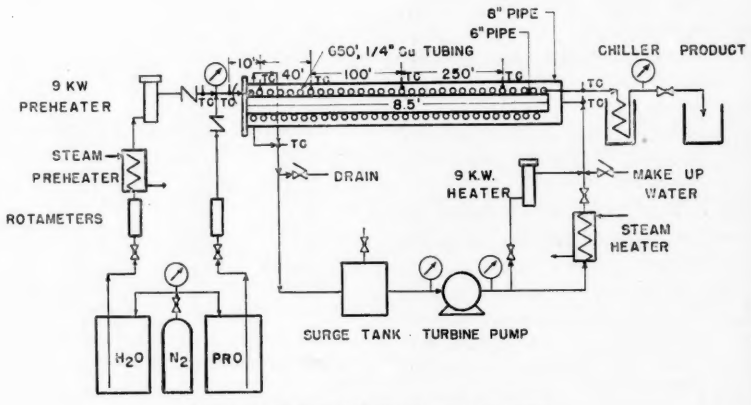

FIG. 1. FLOW DIAGRAM OF REACTOR.

A. L. Benham is at present with the University of Michigan, Ann Arbor, Michigan.

bution of products when propylene and dipropylene glycols are formed were also desired. The study was limited to a liquid-phase, homogeneous reaction, and both the uncatalyzed reaction and the reaction catalyzed with sulfuric acid were included in the study. The reaction was studied over a temperature range of 100° to 300° F.; the feed ratio was varied from 2.5 to 10 lb. water/lb. propylene oxide; and the catalyst concentration ranged up to 0.25 wt. % of the feed.

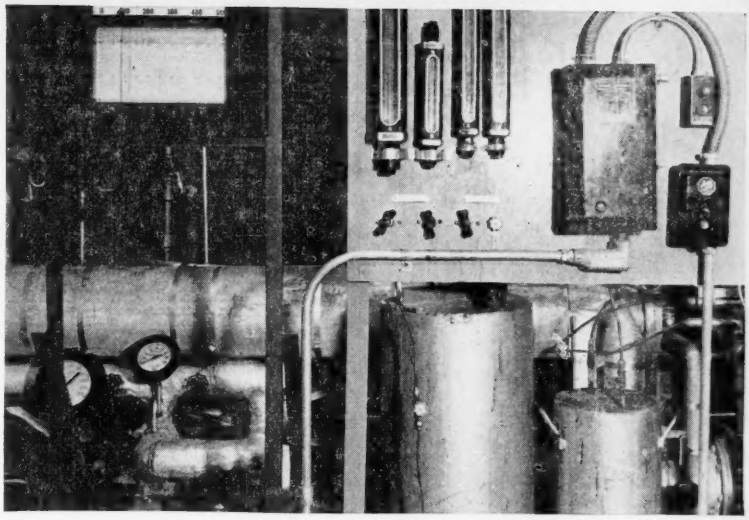

FIG. 2. REACTOR CONTROL PANEL.→

APPARATUS AND PROCEDURE

Apparatus. The reactor may be described with reference to the flow diagram shown in Figure 1 and the photographs in Figures 2, 3, and 4. In general the reactor consisted of a 650-ft. section of 1/4-in. copper tubing wound on the inside pipe of two concentric pipes with water circulating in the annulus to maintain the desired temperature. The coil was wound so that the water could circulate on both sides of the coil. The reactants mixed immediately before entering the reactor, and the reacted mass was quenched in an ice bath immediately after leaving the constant-temperature reactor.

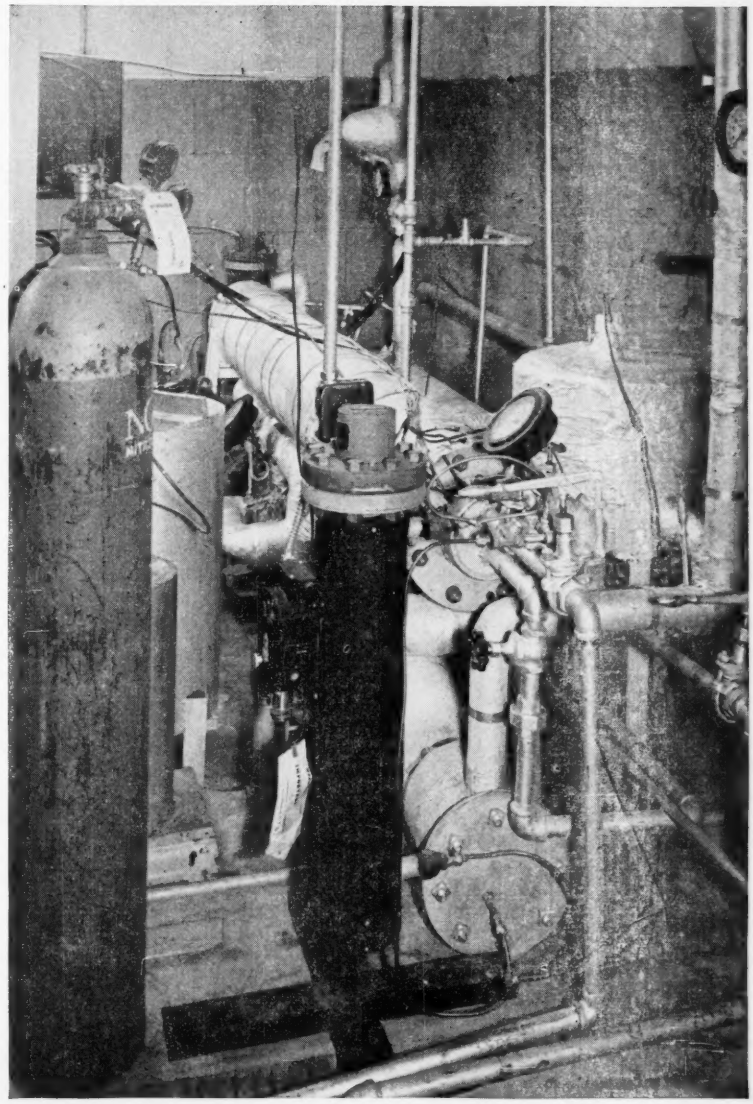

FIG. 4. OVERHEAD VIEW OF REACTOR.→

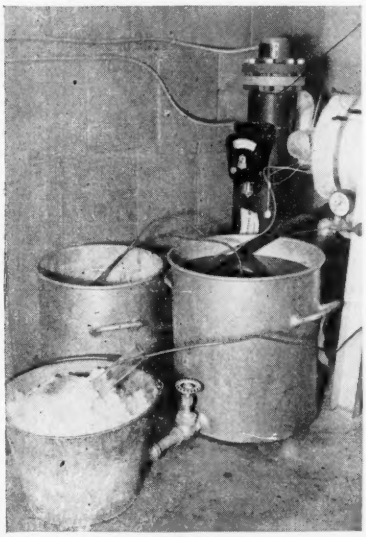

FIG. 3. SAMPLING THE REACTOR PRODUCT.

The two reactants were water and propylene oxide. The water was contained in a 20-gal. steel tank and the propylene oxide in a 5-gal. steel container. When catalytic runs were made, the sulfuric acid was mixed with the feed water. For these runs the steel feed-water tank was replaced by two 9-gal. stainless steel tanks. A nitrogen cylinder was connected to both the water and the propylene oxide containers and a pressure regulator maintained a constant pressure on them. The feed water left the tank through 1/4-in. copper tubing which led to a needle valve, then to a rotameter, a preheater consisting of a steam heat exchanger, a 9-kw. electric immersion preheater, and a check valve to the point where it mixed with propylene oxide. The propylene oxide was caused to flow through a needle valve, a rotameter, and a check valve to the point where it mixed with the feed water. The reactant solution then passed into the reactor proper. As a safety precaution, a rupture disk was placed in the mixing section. The reactor proper was made of 650 ft. of 1/4-in. copper tubing which was wound on an 8.5-ft. section of 6-in. pipe, which was then inserted coaxially in an 8-in. pipe. Water flowed in the annular space between two pipes in order to maintain the reaction mass at a constant temperature. This water was kept at a constant temperature by circulating it through an outside circuit where it flowed first into a surge tank, then through a turbine pump, through a heater, and back into the bath. Pressure was maintained in the bath circuit to keep the water in the liquid phase.

After the reactant mass had passed through the 650 ft. of tubing, it was immediately passed through an ice bath, where it was chilled in order effectively to stop the reaction. The solution was then passed through a pressure relief valve and was collected in a sample container.

A pressure gauge was placed in the line preceding the reactor section and one was placed following the quenching section. Nine thermocouples were included in the system in order to measure temperatures. Their locations were as follows:

1. Ten feet from the inlet in the reactor tubing
2. Fifty feet from the inlet in the reactor tubing
3. One hundred and fifty feet from the inlet in the reactor tubing
4. Four hundred feet from the inlet in the reactor tubing
5. Exit of circulating water from reactor
6. Inlet of circulating water to reactor
7. Six hundred and fifty feet from inlet in the reactor tubing just outside reactor
8. After preheater in feed water line
9. In the mixing section

Thermocouples 1 through 4 were soldered onto the outside of the reactor tube wall. Calculations showed that for the conditions chosen for this study, these thermocouples would indicate essentially the temperature of the fluid in the tube. The other thermocouples were placed in wells in the fluid stream. The temperatures in the various sections of the reactor never varied more than 1°F. from one point to another.

The reactants for this project were distilled water and propylene oxide, which was obtained from Carbide and Carbon Chemical Corp. The specifications for the propylene oxide (*2*) follow:

Acidity	0.05 wt. % max. as acetic acid
Water	1.0 wt. % max.
Residue	0.005 g./ml. max.
Color	15 pt-Co APHA units, max.
Suspended matter	Substantially free
Distillation at 760 mm.	I.b.p. 30.0°C. min.
	95 ml. 40.0°C. max.

Procedure. The circulating pump was started first and the reactor was heated to the desired temperature by controlling the heater in the circulation system. The reaction temperature was easily controlled within ± 1° F. for any given run. Feed water was then fed into the reactor system at a specified rate and the feed preheater was used to heat it a few degrees above the desired reaction temperature. Then cold propylene oxide was metered into the system and the water preheater was regulated to bring the temperature of the reactants, after mixing, to the desired reaction temperature. The individual flow rates were indicated by rotameters and controlled by needle valves. Pressure was maintained in the reactor by a pressure-relief valve downstream from the quenching zone so that the reactants were

TABLE 1.—UNCATALYZED REACTION-RATE CONSTANTS

Run	Reaction temp., °F.	Feed ratio, R_i lb. H_2O / lb. PrO	V_R/F (cu ft.) (sec.) / (lb. mole)	Fractional conversion of PrO, X	Reaction-rate constant, k_1, lb. mole / (cu. ft.) (sec.)
1	200	10.0	55.9	0.0357	0.000649
2	200	10.0	111.7	0.0572	0.000526
3	200	10.0	227.7	0.111	0.000511
17	200	10.0	219.2	0.120	0.000645
7	200	10.0	319.2	0.187	0.000593
18	200	10.0	312.7	0.173	0.000580
8	200	10.0	446.9	0.234	0.000604
				Representative	0.000625
14	200	5.0	217.0	0.081	0.000405
15	200	5.0	310.0	0.102	0.000331
16	200	5.0	867.7	0.232	0.000303
				Representative	0.00037
27	200	2.5	102.5	0.0454	0.000535
28	200	2.5	205.0	0.0550	0.000275
23	200	2.5	356.5	0.0760	0.000244
24	200	2.5	510.5	0.111	0.000242
				Representative	0.00024
4	250	10.0	55.9	0.154	0.00298
5	250	10.0	111.7	0.242	0.00247
6	250	10.0	223.5	0.460	0.00275
9	250	10.0	319.2	0.536	0.00239
19	250	10.0	319.2	0.502	0.00264
10	250	10.0	447.0	0.697	0.00216
				Representative	0.0025
20	250	5.0	215.9	0.280	0.00151
21	250	5.0	309.9	0.372	0.00148
22	250	5.0	867.3	0.724	0.00147
				Representative	0.00148
29	250	2.5	102.5	0.104	0.00060
30	250	2.5	205.0	0.139	0.00107
25	250	2.5	356.0	0.194	0.00073
				Representative	0.00087
11	300	10.0	55.9	0.392	0.00888
31	300	10.0	219.2	0.802	0.00728
32	300	10.0	319.2	0.916	0.00765
				Representative	0.0080
12	300	15.0	63.6	0.548	0.01242

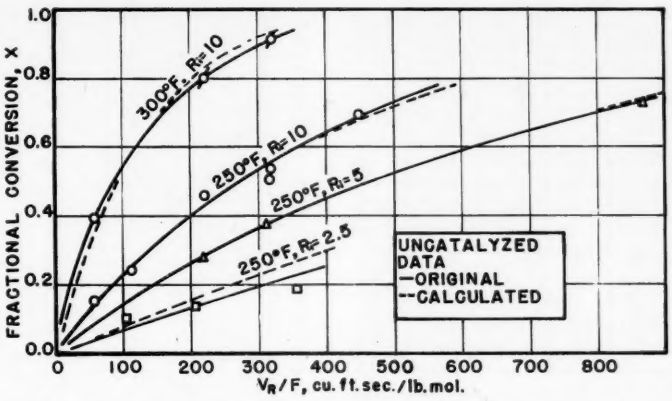

FIG. 5. UNCATALYZED DATA, CONVERSION OF PROPYLENE OXIDE TO GLYCOL, 250° AND 300°F.

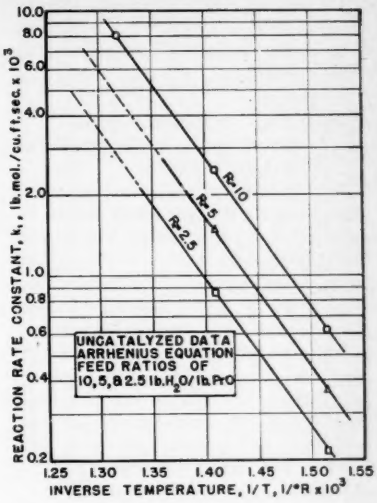

FIG. 6. ARRHENIUS EQUATION FOR UNCATALYZED REACTION.

maintained in the liquid phase. The reactor product was chilled after leaving the constant temperature zone and was collected in a sample bottle. A sample was not taken until after the flow rates and temperature had been maintained over a period of time which would allow the reactants to pass through the reactor. The sample was analyzed by the method used by Davis, Von Waaden, and Kurata(*4*).

When catalytic runs were made, the sulfuric acid catalyst was mixed with the feed water. In order to stop the reaction effectively, the product sample was immediately neutralized with sodium hydroxide.

Under certain conditions two liquid phases are possible for this system. The solubility data of Wickert, Tamplin, and Shank(*9*) were extended for use at higher temperatures. Conditions for study were then chosen which would ensure the reactant mass being in the single liquid phase.

RESULTS

Noncatalytic Reaction. The results of thirty noncatalytic runs are summarized in Table 1. The uncatalyzed reaction was found to be pseudo first order with respect to the propylene oxide concentration. The reaction-rate constants were calculated from the integrated equation below, which was derived from the basic assumption that the rate of reaction is proportional to the mole fraction of propylene oxide. The relationship between the measurable quantities (V_R, F, X, A') was further developed starting with the material balance over a differential section of the flow reactor, as suggested by Hougen and Watson(*5*).

$$CH_3 - C_2H_3O + H_2O \longrightarrow$$
$$CH_3 - CHOH - CH_2OH$$

$$A + B \longrightarrow C$$

or

$$\frac{V_R}{F} = \frac{1}{k_1}\left[(1-A')\ln\frac{1}{1-X} + A'X\right]$$

where

A' = initial concentration of propylene oxide, mole fraction

TABLE 2.—CONSTANTS CHARACTERISTIC OF UNCATALYZED REACTION

Arrhenius constants

$$k_1 = Ae^{\frac{-E}{RT}}$$

Feed ratio, R_i, lb. H_2O / lb. PrO	A, lb. mole / (cu. ft.) (sec.)	Energy of activation, E, B.t.u. / lb. mole
10.0	1.868×10^5	25.6×10^3
5.0	1.125×10^5	25.6×10^3
2.5	0.668×10^5	25.6×10^3

Concentration function

$$k_1 = a\,R_i^b$$

Reaction temperature, °F.	a, lb. mole / (cu. ft.) (sec.)	b, unitless
200	1.41×10^{-3}	¾
250	4.40×10^{-4}	¾
300	1.11×10^{-4}	¾

F = total feed rate, lb. moles/sec.
k_1 = first-order reaction-rate constant, lb. mole/(cu. ft.)(sec.)
V_R = reactor volume, cu. ft.
X = fractional conversion of propylene oxide

A representative reaction constant was found for each series of runs at a given temperature and feed ratio but with varying feed rates. The representative rate constant was found by fitting a calculated curve to the experimental points as shown in Figure 5. Similar procedures were carried out at other temperatures and feed ratios. The effect of temperature on the reaction-rate constant at three different feed ratios is shown in Figure 6.

The value of the reaction-rate constant was found to change with the initial propylene oxide concentration. This effect is correlated for three different reaction temperatures, as shown in Figure 7. The equation of the line is of the form

$$k_1 = aR_i^b$$

where

a = constant for a given temperature, lb. moles/(cu. ft.)(sec.)
b = constant for uncatalyzed reaction, unitless
k_1 = reaction-rate constant, lb. mole/(cu.ft.)(sec.)
R_i = feed ratio of reactants, lb. water/lb. propylene oxide

The values of the constants for the Arrhenius equation as obtained from Figure 6 and the constants obtained for the curves in Figure 7 are given in Table 2.

Catalytic Reaction. The summarized results of the reaction catalyzed with sulfuric acid are available elsewhere.* This reaction was found to be pseudo second order with respect to the mole fraction of propylene oxide. The rate constants were computed by use of the integrated form of the second-order rate expression for the reaction:

$$\frac{V_R}{F} = \frac{1}{k_2}\left[\frac{(1-A')^2}{A'}\left(\frac{X}{1-X}\right) + A'\,X + (A'-1)\ln(1-X)^2\right]$$

where

A' = initial concentration of propylene oxide, mole fraction

*Deposited with the Photoduplication Service, American Documentary Institute, Library of Congress, Washington 25 D.C., as document 4486, obtainable for $1.25 for microfilm or photoprints.

F = total feed rate, lb. moles/sec.
k_2 = second-order reaction-rate constant, lb. mole/(cu.ft.)(sec.)
N_A = concentration of propylene oxide at any time, mole fraction
V_R = reactor volume, cu.ft.
X = fraction conversion of propylene oxide

This expression was derived on the assumption that the rate of reaction is proportional to the square of the mole fraction of propylene oxide and that there is no competing reaction for propylene oxide. This latter asumption is true except for twelve of the catalytic runs in which detectable amounts of di-propylene glycol were formed. The results of these twelve runs are given in Table 3. It is seen from this table that the conversion of propylene oxide to di-propylene glycol did not exceed 2% and that the conversion to propylene glycol varied from 23 to 90%. The effect of the competing reaction upon the calculation of the rate constant was therefore negligible.

A representative reaction-rate constant was found for each series of runs at a given temperature, feed ratio, and catalyst concentration but at different throughput rates. The rate constant was found in the same manner as for the uncatalyzed reaction. Figure 8 shows the computed and the experimental curves of fractional conversion vs. V_R/F at 100°, 125°, and 150°F. for a feed ratio of 10 lb. water/lb. propylene oxide when the catalyst concentration is 0.05 wt. %. Similar curves were drawn for other catalyst concentrations and feed ratios.

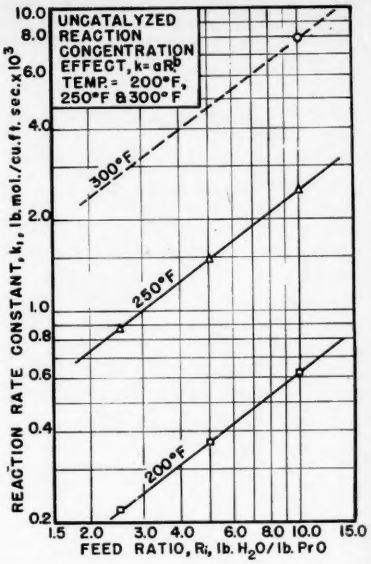

FIG. 7. CONCENTRATION EFFECT FOR UNCATALYZED REACTION.

The effect of temperature on the reaction-rate constant is shown in Figure 9 for different catalyst concentrations and feed ratios.

For conditions of constant temperature and acid concentration, the effect of the initial feed ratio on the rate constant was correlated as shown in Figure 10. The curve is of the form $k_2 = aR_i^b$.

The effect of the catalyst concentration on the rate constant at reaction temperatures of 100°, 125°, and 150°F. and with feed ratios of 5 and 10 is shown in Figures 11 and 12.

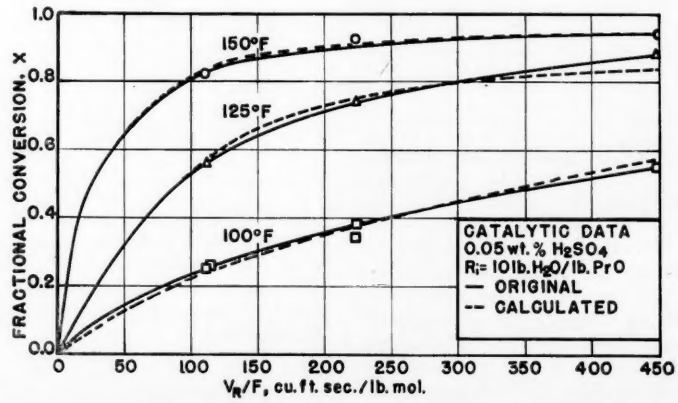

FIG. 8. CATALYTIC DATA, CONVERSION OF PROPYLENE OXIDE TO GLYCOL, 0.05 WT. % H_2SO_4, 10 LB. H_2O/LB. PrO.

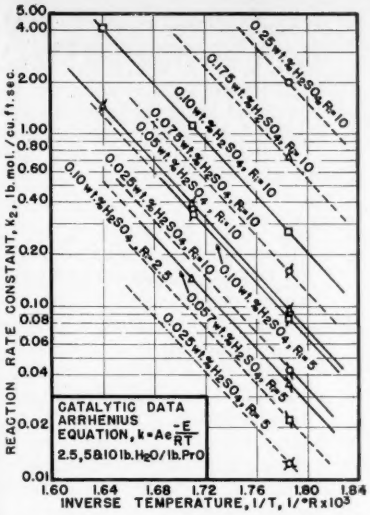

FIG. 9. ARRHENIUS RELATIONSHIP FOR CATALYZED REACTION.

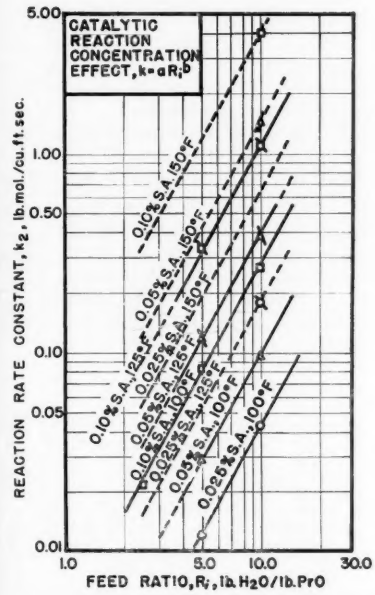

FIG. 10. CONCENTRATION EFFECT FOR CATALYZED REACTION.

The constants for the Arrhenius equation as obtained from Figure 9 and for the effect of the feed ratio as taken from Figure 10 are given in Table 4.

DISCUSSION OF RESULTS

A comparison of the correlation with the experimental data points has been made in order to estimate the accuracy of the correlation, which was used to calculate the experimental data points as shown by dashed lines in Figures 5 and 8.

For the uncatalyzed reaction the average percentage of deviation of the correlation from the experimental points was found to be 9.6, and the standard deviation was 0.024. The average percentage of deviation for the catalyzed reaction was 3.8 and the standard deviation was 0.026.

Since other experimental data for this reaction are not available in the literature, a direct comparison of this study cannot be made; however, data are available for a few other epoxide reactions.

Brönsted et al. (*1*) and Lichtenstein and Twigg (*6*) studied the liquid-phase hydration of ethylene oxide. Both groups found that the uncatalyzed reaction was first order with respect to ethylene oxide. This may be compared with the pseudo first-order rate found for the uncatalyzed reaction of this study. Brönsted et al. (*1*) studied the perchloric acid catalyzed hydration of ethylene oxide and found this reaction to be first order with respect to ethylene oxide and the rate to be proportional to the hydrogen ion concentration. In the present study such a simple dependence on the hydrogen ion was not found, and the catalytic reaction was found to be second order with respect to propylene oxide.

Lichtenstein and Twigg (*6*) studied the sodium hydroxide catalyzed reaction and found that the reaction-velocity constant could be expressed as follows: $k = a\,[OH^-] + b\,[OH^-]^2$. Smith, Wode, and Widhe (*8*) caried out kinetic studies on the liquid-phase hydration of ethylene oxide with perchloric and nitric acids as a catalyst. They found that the rate of this reaction was independent of the kind of acid used. Percorini (*7*), studying the reaction of propylene oxide with methanol to form 1-methoxy-2-propanol by use of a sodium hydroxide catalyst, found the effect of the sodium hydroxide to be one of direct proportionality.

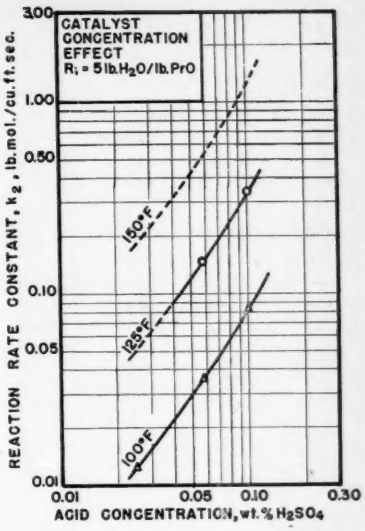

FIG. 11. EFFECT OF CATALYST CONCENTRATION UPON REACTION RATE.

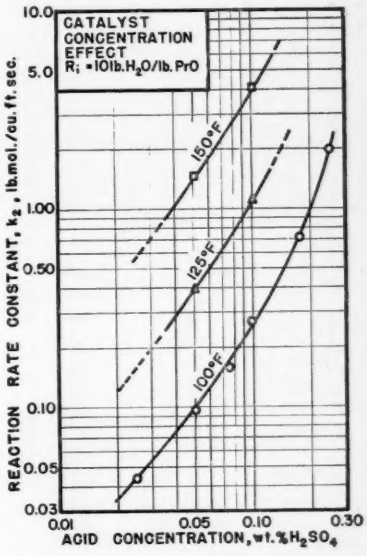

FIG. 12. EFFECT OF CATALYST CONCENTRATION UPON REACTION RATE.

CONCLUSIONS

The kinetics of the catalyzed and uncatalyzed homogeneous liquid-phase hydration of propylene oxide to form propylene glycol have been studied and the results correlated in a form convenient for the design of reactors.

The uncatalyzed reaction was found to be pseudo first order with respect to the concentration of propylene oxide. From the results of the uncatalyzed study, the reaction-rate constants for different initial propylene oxide concentrations have been expressed as a function of the feed ratio of water to propylene oxide.

The reaction catalyzed with sulfuric acid was found to be pseudo second order with respect to the concentration of propylene oxide. The rate constant for this reaction has been expressed as a function of the acid concentration, feed ratio, and temperature.

In order to check the accuracy of the correlations obtained from this

TABLE. 3.—DISTRIBUTION OF PRODUCTS FOR RUNS WHERE DIPROPYLENE GLYCOL WAS FORMED

Run	Reaction temp., °F.	Catalyst conc. H_2SO_4, wt. %	Feed ratio R_i, lb. H_2O / lb. PrO	V_R/F, cu. ft./ (sec.) (lb. mole)	Propylene oxide conversion, fraction to glycol X_1	to diglycol X_2	Total X_T
72	125	0.10	5.0	108.5	0.633	0.012	0.645
70	125	0.10	5.0	216.9	0.829	0.007	0.836
71	125	0.10	5.0	309.9	0.887	0.017	0.904
78	100	0.10	5.0	108.5	0.326	0.007	0.333
76	100	0.10	5.0	216.9	0.512	0.007	0.519
77	100	0.10	5.0	309.9	0.625	0.009	0.634
79	125	0.05	5.0	108.5	0.497	0.008	0.505
80	125	0.05	5.0	216.9	0.634	0.009	0.643
81	125	0.05	5.0	309.9	0.722	0.010	0.732
82	100	0.10	2.5	102.5	0.228	0.004	0.232
83	100	0.10	2.5	205.0	0.321	0.006	0.327
84	100	0.10	2.5	356.5	0.451	0.007	0.458

study, they were used to compute the conversion of propylene oxide. These calculated conversions were compared with the experimental conversions, and standard deviations and percentage errors were computed. The standard deviation for the uncatalyzed runs was 0.024 and the average percentage deviation was found to be 9.6. The catalytic data show a standard deviation of 0.026 and an average percentage deviation of 3.8.

ACKNOWLEDGMENT

Financial aid supplied by the University of Kansas Research Project 84 made this work possible. The cost of the reactor was contributed by Stone and Webster Engineering Corporation. Much of the credit for the laboratory work of operating the reactor and analyzing the samples must be shared with Joseph Christy, William Behrmann, John - Gerety, and George Daniels.

TABLE 4.—CONSTANTS CHARACTERISTIC OF CATALYZED REACTION

Arrhenius constants

$$k_2 = Ae^{\frac{-E}{RT}}$$

Feed ratio, R_i, lb. H_2O / lb. PrO	Catalyst concentration, H_2SO_4, wt. %	A, lb. mole / (cu. ft.) (sec.)	Energy of activation E, B. t. u. / lb. mole
10.0	0.025	1.09×10^{13}	36.9×10^3
10.0	0.050	2.42×10^{13}	36.9×10^3
10.0	0.075	4.04×10^{13}	36.9×10^3
10.0	0.100	6.82×10^{13}	36.9×10^3
10.0	0.175	18.2×10^{13}	36.9×10^3
10.0	0.250	50.5×10^{13}	36.9×10^3
5.0	0.025	0.318×10^{13}	36.9×10^3
5.0	0.057	0.909×10^{13}	36.9×10^3
5.0	0.100	2.10×10^{13}	36.9×10^3
2.5	0.100	0.555×10^{13}	36.9×10^3

Concentration function

$$k_2 = a R_i^b$$

Reaction temperature. °F.	Catalyst concentration, H_2SO_4, wt. %	a, lb. mole / (cu. ft.) (sec.)	b, unitless
100	0.10	0.00428	1.8
100	0.05	0.00155	1.8
100	0.025	0.000682	1.8
125	0.10	0.0174	1.8
125	0.050	0.00634	1.8
125	0.025	0.00285	1.8
150	0.10	0.0650	1.8
150	0.050	0.0230	1.8
150	0.025	0.0106	1.8

NOTATION

A = proportionality factor defined by the Arrhenius equation, lb. mole/ (cu.ft.) (sec.)
A' = initial concentration of propylene oxide, mole fraction
a = constant for a given temperature and catalyst concentration, units of k
b = constant for reaction, value depending only on whether a reaction is catalyzed, unitless
E = molal energy of activation, B.t.u./lb. mole
F = feed rate, lb. mole/sec.
k_1 = specific reaction-rate constant for first-order reaction, lb. mole/ (cu.ft.) (sec.)
k_2 = specific reaction-rate constant for second-order reaction, lb. mole/ (cu.ft.) (sec.)
N_A = propylene oxide concentration, mole fraction
R = gas-law constant, B.t.u./ (lb. mole) (°R.)
R_i = initial feed ratio of water to propylene oxide, lb./lb.
T = absolute temperature, °R.
V_R = volume of reactor, cu.ft.
X = fractional conversion of propylene oxide, lb. mole converted/lb. mole fed
PrO = propylene oxide

LITERATURE CITED

1. Brönsted, J. N., M. Kilpatrick, and M. Kilpatrick, *J. Am. Chem. Soc.*, 51, 428 (1940).
2. Carbide and Carbon Company, Inc., "Ethers and Oxide" (1949).
3. Curme, G. O., and F. Johnston, "Glycols," Reinhold Publishing Corp., New York (1952).
4. Davis, P. C., C. E. Von Waaden, and F. Kurata, *Chem. Eng. Progr. Symposium Series No. 4*, 48, 98 (1952).
5. Hougen, O. A., and K. M. Watson, "Chemical Process Principles," vol. 3, John Wiley and Sons, Inc., New York (1949).
6. Lichtenstein, H. J., and G. H. Twigg, *Trans. Faraday Soc.*, 44, 905 (1948).
7. Pecorini, H. A., Ph.D. Thesis, Univ. Michigan (1954).
8. Smith, L., G. Wode, and T. Widhe, *Z. Physik. Chem.*, 130, 154 (1927).
9. Wickert, J. N., W. S. Tamplin, and R. L. Shank, *Chem. Eng. Progr. Symposium Series No. 2*, 48, 92 (1952).
10. Wurtz, A., *Ann. chim. et phys.*, 55, (3), 438 (1859).

(Presented at A.I.Ch.E. New York meeting)

Performance of Small Herschel-Type Venturi Tubes

P. L. WALKER, JR., R. J. FORESTI, JR., F. RUSINKO, JR., and B. W. McCORMICK

The Pennsylvania State University, State College, Pennsylvania

The characteristics of five Herschel-type Venturi tubes with throat diameters ranging from 0.073 to 0.359 in. and throat-to-pipe—diameter ratios from 0.0882 to 0.4340 have been investigated.

Research on the performance of Venturis with small throats and low throat-to-pipe–diameter ratios has been practically ignored to the present. Their high value of frictional resistance and the low throat pressure produced, which can cause cavitation of the liquid, have been disadvantages which have kept these Venturis from being utilized as flow-measuring devices; however, recent research by two of the authors(*6*), among others, on the possibility of using the low throat pressure of the small Venturi to induce a secondary liquid stream (that is, to use the Venturi as a proportioner) pointed to the need for information on these Venturis. In this work the exhaustive data available on throat-to-pipe—diameter ratios above 0.25 have been extended down to a value of 0.0882. In addition, the performance of the Venturi at unusual operating conditions has been investigated with the pressure recovery being varied from close to 0 to 100% (the Venturi as a metering device has a pressure recovery of roughly 80%) in an attempt to determine the effect on flow rate and Venturi throat pressure, both important parameters if the Venturi is to be used as a proportioning device.

APPARATUS

The standard Venturi design discussed by Jorissen(*3, 4*) and presented in the British Standard Code(*1*) was adhered to in the construction. Figure 1 shows a drawing of the largest Venturi used. All Venturis utilized an entrance cone with an included angle of 21° and an exit cone with an angle of 7°. The length of the Venturi throat in all cases was nearly equal to the Venturi-throat diameter. At the middle of the throat a 1/32-in. pressure tap was located for pressure readings. A collector piezometer ring was not employed since for these small throats it was feared that too many pressure taps might severely distort the flow through the throat. The Venturis were made of Lucite acrylic resin so that flow conditions might be observed and pictures taken. The resin was very easily worked and was finished to a high polish. Sections of 17ST aluminum alloy were connected to the Venturi with hand tightening of the Venturi proper to these sections made possible by 1-in. machine threads. Extreme care was taken in machining to assure a smooth fit between these sections.

The manner in which the exit aluminum section was connected to the standard 3/4-in. (I.D. 53/64 in.) iron pipe is shown in Figure 2. The entrance section employed a similar connection. To join the Venturi unit smoothly to the pipe with no irregularities or surface roughness, a steel sleeve was soldered to both the entering and exit pipe and the internal surfaces were carefully polished. A good connection was then achieved by tightening the large hexagonal nut against a

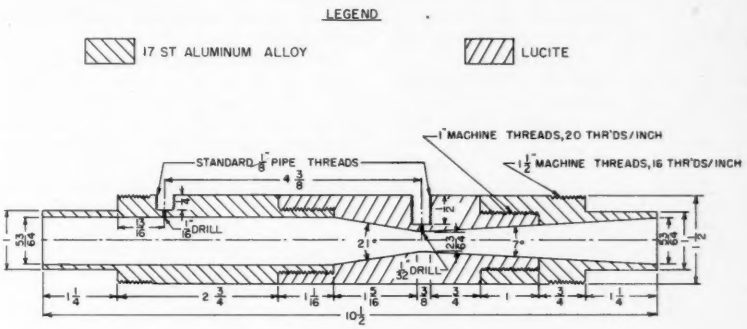

FIG. 1. VENTURI-METER DESIGN.

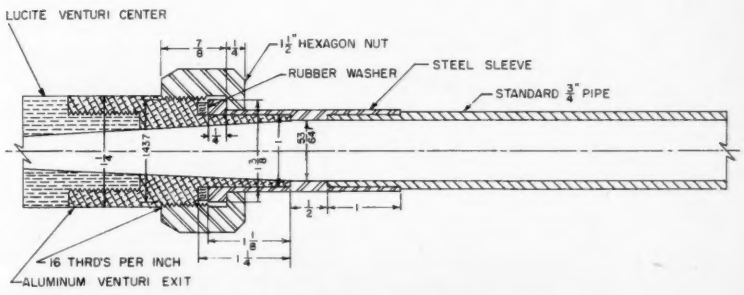

FIG. 2. CONNECTION DESIGN OF PIPING TO VENTURI METER.

R. J. Foresti, Jr., is at present with Monsanto Chemical Company, Dayton, Ohio.

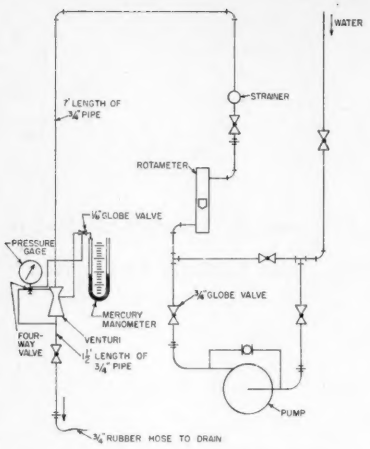

FIG. 3. VENTURI-METER FLOW SHEET.

rubber gasket. For most of the work only hand tightening was necessary.

Figure 3 shows the over-all flow sheet of the apparatus. An Aurora Pump Company pump with a capacity of 8.0 gal./min. at 275 lb./sq. in. gauge was used in the work. With the bypass system shown, flow rates could be easily adjusted and maintained. A high-pressure rotameter with a flow-rate range of 0.5 to 11.5 gal./min. was used, on which flow rates could be read to the nearest 0.1 gal. A strainer was placed in the line to remove any foreign matter which might conceivably lodge in the Venturi throat. Preceding the Venturi, a 7-ft. vertical section (100 pipe diameters) of new galvanized-iron pipe assured a well-developed flow pattern leading into the Venturi. The upstream pressure tap was in all cases a 1/16-in. hole located 3 1/2 pipe diameters ahead of the entrance cone. The pressure drop between this tap and the entrance to the Venturi tube was negligible. The downstream pressure tap was a 1/16-in. hole drilled in the 3/4-in. iron pipe and located 7 pipe diameters after the exit cone. A 3/4-in. globe valve was located 22 pipe diameters downstream from the exit cone and was used to vary the back or exit pressure of the Venturis.

Pressure readings at the Venturi throat were made on a 32-in. Hg manometer where possible. The inlet and outlet pressures, as well as high throat pressures, were read on a 6 3/4-in. face, 300 lb./sq.in. Crosby gauge.

The water used had an average temperature of 50°F.; it contained 8 p.p.m. of oxygen, 13 p.p.m. of nitrogen, 0.3 p.p.m. of chlorine, and negligible amounts of carbon dioxide in the form of dissolved gases.

EXPERIMENTAL PROCEDURE

The data were taken at selected values of inlet pressure, at which the outlet pressure was varied to produce different flow rates. At each condition, measurements were taken of the inlet, outlet, and throat pressure and of the flow rate. For each Venturi, data were obtained up to the maximum capacity of the pump, that being the pressure in the case of the small Venturi and flow rate for the larger Venturis. Duplicate runs gave excellent reproducibility of the data.

ANALYSIS OF RESULTS*

Discharge Coefficients. At each condition of inlet and outlet pressures, discharge coefficients and pipe Reynolds numbers were calculated for the five Venturis. The discharge coefficient C is defined by

$$Q = C \frac{A_t}{\sqrt{1-\beta^4}} \sqrt{\frac{2(p_i - p_t)}{\rho}} \quad (1)$$

The C is a measure of the deviation of throat velocity from the ideal-fluid case. In purely potential flow the value of C would be unity.

The calculated variation of the discharge coefficients with the pipe Reynolds number for the different Venturis is presented in Figure 4. An appreciable decrease in the discharge coefficient for the smallest Venturi as the Reynolds number decreased below 10,000 is observed. As is evident, there is considerable scatter in the data for the larger Venturis, particularly at the lower Reynolds numbers. The reasons for this are not entirely clear as the data were reproducible; however, it was observed that for the largest Venturi the pipe was not completely filled with water at the lower flow rates. In view of the experimental scatter, the major contribution of this paper is felt to be in presenting and analyzing the data obtained on the effects of cavitation and operation at extremely low Reynolds numbers and not in presenting quantitative values of the discharge coefficient in the Venturis. It is unfortunate that the limitations of the test equipment prevented operation of the smallest Venturi in the same range of Reynolds numbers as the larger Venturis.

The effect of Reynolds number appears to be conveniently presented as a "coefficient of correction," as given by Jorissen (3). This coefficient is the ratio of the discharge coefficient at any Reynolds number to the discharge coefficient at a relatively high Reynolds number (greater than 300,000) above which the discharge coefficient remains constant. According to Jorissen, the coefficient of correction does not depend to any extent upon the throat-pipe-diameter ratio. This coefficient was given by Jorissen down to a pipe Reynolds number of 10,000. By use of the curve of the discharge coefficient for the small Venturi as a function of

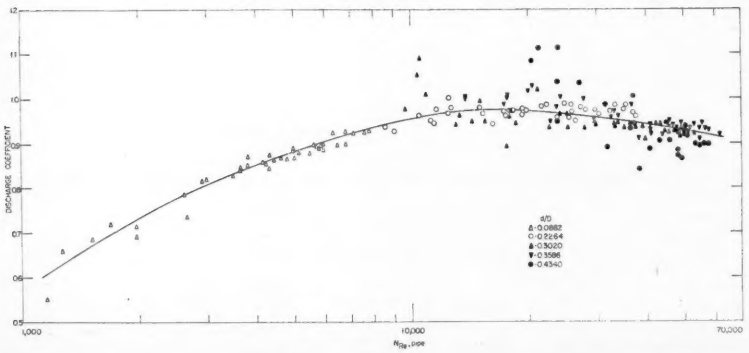

FIG. 4. DISCHARGE COEFFICIENT AS A FUNCTION OF PIPE REYNOLDS NUMBER FOR A SERIES OF VENTURIS.

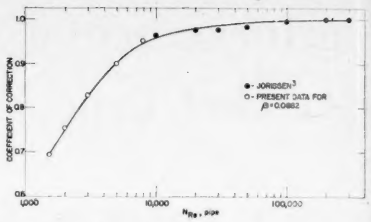

FIG. 5. COEFFICIENT OF CORRECTION AS A FUNCTION OF PIPE REYNOLDS NUMBER.

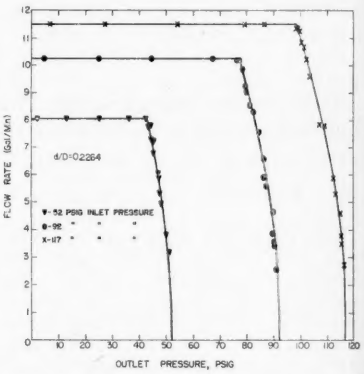

FIG. 6. EFFECT OF OUTLET PRESSURE ON WATER FLOW RATE THROUGH A VENTURI 3/16-IN.-DIAM. THROAT.

*The complete data are available as document 4477 from the A.D.I. Auxiliary Publications Project, Photoduplication Service, Library of Congress, Washington 25, D.C., at $1.25 for photoprints and $1.25 for 35-mm. microfilm.

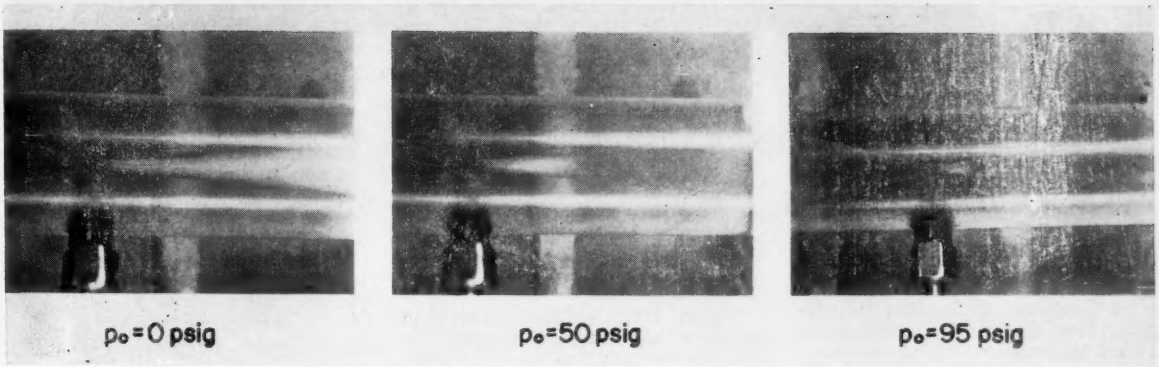

FIG. 7. EFFECT OF INCREASING OUTLET PRESSURE ON THE DEGREE OF CAVITATION IN VENTURI DIFFUSER: $\beta = 0.2264$, $p_i = 117$ LB./SQ. IN. GAUGE, $Q = 11.5$ GAL./MIN.

Reynolds number, Jorissen's coefficients of correction have been extended down to a Reynolds number of 1,500, as shown in Figure 5. The asymptotic value of the discharge coefficient was chosen so as to give the same value of the correction coefficient at a Reynolds number of 10,000 as was reported by Jorissen. It can be seen from Figure 5 that the effect of Reynolds number on the discharge coefficient becomes quite appreciable for Reynolds numbers much below 10,000. Whether or not this curve for the correction coefficient is independent of β for relatively low Reynolds numbers unfortunately cannot be determined by the data presented here.

Cavitation Inception. In addition to the discharge coefficients, considerable information was obtained on the effect of cavitation on the performance of the Venturis. For a fixed-inlet pressure, as the outlet pressure was reduced, a pressure and velocity would be reached at which cavitation would begin immediately following the throat. Any further reduction in outlet pressure produced no increase in the flow rate or the measured value of the throat pressure.

The occurrence of cavitation in the Venturi is closely linked with its performance. Figure 6 shows a typical variation of flow rate with outlet pressure for different inlet pressures with a β of 0.2264 for the Venturi. It can be seen that at a specific inlet pressure there is an outlet pressure below which the flow rate remains constant. This specific inlet pressure also represents the point of inception of cavitation; that is, as the inlet pressure is continually increased from zero to its critical value, the degree of cavitation in the diffuser section of the Venturi decreases. Upon reaching the critical outlet pressure for a constant inlet pressure, cavitation stops. Figure 7 clearly shows this phenomenon for the foregoing Venturi operating at a constant inlet pressure of 117 lb./sq. in. gauge. The three photographs from left to right represent 0, 50, and 95 lb./sq. in. gauge outlet pressures, respectively. When the "critical" outlet pressure of 98 lb./sq. in. gauge is reached, no cavitation is seen.

It is usually desirable to avoid cavitation in a Venturi for at least several reasons. First is the fact that the loss in total head across the Venturi increases considerably with cavitation present. This is obvious from Figure 6, which shows an appreciable decrease in the outlet pressure with no change in the inlet pressure and flow rate once cavitation occurs. Second, cavitation is undesirable from the standpoint of its accompanying noise and vibration. It is therefore expedient to predict when cavitation in a given Venturi will occur or, given a set of flow conditions in a pipe, to select the Venturi which will produce the largest differential pressure across the inlet nozzle without cavitating.

Cavitation is conveniently treated in terms of a parameter denoted as the cavitation index, σ, defined by (5):

$$\sigma = \frac{p_i - p_c}{1/2\ \rho\ (V_p)^2} \qquad (2)$$

This parameter can be defined in the general sense as an operating index; however, for a given geometrical configuration there will be one particular value of this index at which cavitation will begin. The value of σ for the inception of cavitation is referred to as the *critical cavitation index*, σ_{cr}. If σ is higher than σ_{cr}, there will be no cavitation present, but if σ is less than σ_{cr}, the critical pressure will have been reached and cavitation will occur. The value of p_c is usually taken to be the vapor pressure of the fluid although for extremely clear liquids it can be appreciably smaller, since it is generally accepted that nuclei of air or solid particles are needed about which the cavitation bubbles can grow.

The foregoing expression for the cavitation index can be rewritten in the form

$$\sigma = \frac{\left[\left(\frac{1}{\beta}\right)^4 - 1\right]}{C^2}\left(1 + \frac{p_t - p_c}{p_i - p_t}\right) \qquad (3)$$

If it is assumed, as is often done in elementary books on fluid mechanics (2), that the minimum pressure occurs at the throat, then at the inception of cavitation $p_t = p_c$ and σ_{cr} is given approximately by

$$\sigma_{cr} \cong \frac{\left(\frac{1}{\beta}\right)^4 - 1}{C^2} \qquad (4)$$

It was found that this approximation holds quite closely for all the β's tested except $\beta = 0.0382$. For this case the calculated flow rates for the inception of cavitation were in error by approximately 2 to 3%, when the approximation of Equation (4) was used. From the data obtained, the term $\frac{p_t - p_c}{p_i - p_t}$ for $\beta = 0.0882$ was measured as varying from 0.03 to 0.05, depending slightly upon Reynolds number. Since that term is small compared to unity, it is suggested that the critical cavitation index be calculated for this case from

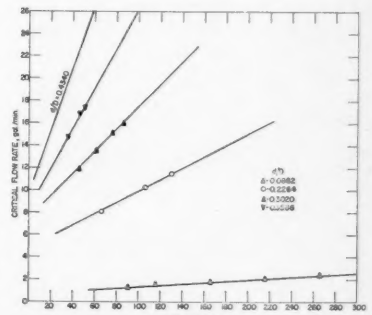

FIG. 8. COMPARISON OF PREDICTED AND EXPERIMENTAL CONDITIONS FOR INCEPTION OF CAVITATION FOR A SERIES OF VENTURIS.

$$\sigma_{cr} = 1.04 \frac{\left(\frac{1}{\beta}\right)^4 - 1}{C^2} \qquad (5)$$

Use of values of $\frac{p_t - p_c}{p_i - p_t}$ of less than 0.04 for intermediate values of β between 0.0882 and 0.2264 should result in predicted flow rates within 2% of the correct values.

Since C is a function of Reynolds number, which in turn is dependent upon the velocity to be obtained from σ_{cr}, the solution of Equation (5) for the critical velocity is an iterative one. As an example, $\beta = 0.0882$ and $p_i = 152$ lb./sq. in. gauge may be used. The problem is to find the flow rate at which cavitation will occur.

When it is assumed that $C = 1$, Equation (5) gives $\sigma_{cr} = 17{,}250$.

If V_p is solved for in Equation (2) and atmospheric pressure taken as 14 lb./sq. in. gauge (5) and $p_v = 0.5$ lb./sq. in. gauge

$$V_p = \sqrt{\frac{p_i - p_v}{1/2\rho\sigma}}$$

$$= \sqrt{\frac{144\ (152 + 14 - 0.5)}{0.97\ (17{,}250)}}$$

$$= 1.192 \text{ ft./sec.}$$

The pipe Reynolds number will then be

$$N_{Re,\ \text{pipe}} = \frac{V_p D}{\nu} = \frac{1.192(0.069)}{1.4 \times 10^{-5}} = 5{,}870$$

When the mean curve shown in Figure 4 is used, $C = 0.9$. Repeating the steps with this C gives $N_{Re,\ \text{pipe}} = 5{,}280$. For this Reynolds number $C = 0.89$, for which $N_{Re,\ \text{pipe}} = 5{,}220$. To the accuracy of Figure 4 the C for this Reynolds number is again 0.89. The velocity corresponding to this C is $V_p = 1.062$ ft./sec. The cross-sectional area of the pipe is 0.00373 sq. ft., and so the flow rate becomes $Q = 0.00396$ cu. ft./sec. or $Q = 1.78$ gal./min. This compares favorably with the measured flow rate of 1.80 gal./min. for the cavitating Venturi at this inlet pressure. The calculated and measured flow rates for the inception of cavitation for the five Venturis are compared in Figure 8. In these calculations, Equation (5) was used for the smallest Venturi and Equation (4) for the remainder. Good agreement is found between the calculated curves and the experimental points for the four smallest Venturis. For the largest Venturi, owing to the limitation in pump capacity, cavitation was not experimentally found; therefore, for this Venturi only the predicted variation in critical flow rate is presented.

Pressure Recovery. The efficiency of pressure recovery was computed for each set of data. This efficiency is defined as

$$\eta = \frac{p_o - p_t}{p_i - p_t} \qquad (6)$$

and represents approximately the percentage of the throat velocity head recovered as pressure head in the diffuser. It is desirable to maintain as high a value of this efficiency as possible in order to reduce the loss in total head attributable to the Venturi.

The variation of η with the pipe Reynolds number for the five Venturis tested is given in Figure 9. These curves are for the noncavitating conditions only. It can be seen from this figure that there is little or no scale effect on η for $\beta = 0.0882$ but for the larger Venturis the values of η appear to increase slightly with increasing Reynolds numbers.

The effect of cavitation on the pressure-recovery efficiency is marked. This is readily apparent from the fact that once cavitation is reached for a fixed inlet pressure, the throat pressure remains constant for further reductions in the outlet pressure.

CONCLUSIONS

It is concluded from the analysis of the tests of five small Venturi tubes that the discharge coefficient of a Venturi tube decreases appreciably with decreasing Reynolds number below a pipe Reynolds number of approximately 10,000.

The approximation that the minimum pressure in a Venturi occurs at the throat is shown to be satisfactory for predicting the occurrence of cavitation in all but the smallest Venturi tested. For this Venturi with a throat-to-pipe-diameter ratio of 0.0882, a 4% correction to the inlet-throat pressure difference is recommended for computing the critical flow rate for the inception of cavitation.

The pressure-recovery efficiency for noncavitating conditions is found to increase slightly with Reynolds number for the Venturis with the large throat-to-pipe–diameter ratios and to be nearly independent of Reynolds number for the smallest Venturi. This efficiency for a given Reynolds number decreases with decreasing throat-to-pipe ratio; however, the rate of decrease is not prohibitive to the use of very low ratios since the efficiency of the Venturi with a throat-to-pipe–diameter ratio of 0.0882 is still approximately 81%.

It should be emphasized that these conclusions are valid only for the range of Reynolds numbers considered herein.

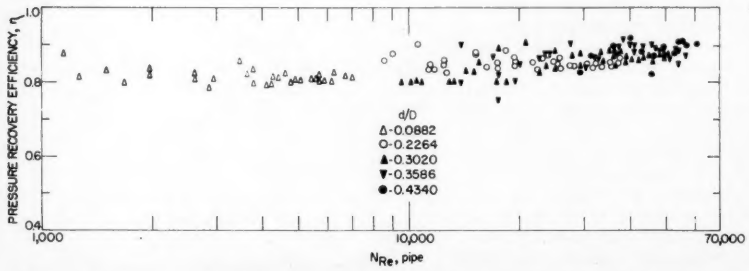

FIG. 9. PRESSURE RECOVERY EFFICIENCY AS A FUNCTION OF PIPE REYNOLDS NUMBER FOR A SERIES OF VENTURIS.

ACKNOWLEDGMENT

The authors are indebted to D. C. Whitmarsh for the interest which he has shown in this work.

NOTATION

A_t = throat area, sq. ft.
C = discharge coefficient
d = throat diameter, in.
D = pipe diameter, in.
p_c = critical pressure for inception of cavitation, usually taken to be vapor pressure of fluid, lb./sq. ft.
p_i = inlet pressure, lb./sq. ft.
p_o = outlet pressure, lb./sq. ft.
p_t = throat pressure, lb./sq. ft.
Q = rate of flow, cu. ft./sec.
V_p = flux average velocity in pipe, ft./sec.

Greek Letters

β = throat-to-pipe–diameter ratio d/D
η = efficiency of pressure recovery
ν = kinematic viscosity, sq. ft./sec.
ρ = fluid mass density, slugs/cu. ft.
σ = cavitation index
σ_{cr} = critical cavitation index, that is, at inception of cavitation

LITERATURE CITED

1. British Standard Code 1042 (1943).
2. Daugherty, R. L., "Hydraulics," pp. 151-159, McGraw-Hill Book Company, Inc. (1937).
3. Jorissen, A. L., *Trans. Am. Soc. Mech. Engrs.* **73**, 403 (1951).
4. Jorissen, A. L., *Trans. Am. Soc. Mech. Engrs.* **74**, 905 (1952).
5. Robertson, J. M., *Ordnance Research Laboratory Report, The Pennsylvania State Univ., Serial No. NOrd.* 7958-256 (1953).
6. Walker, P. L., Jr., and R. J. Foresti, Jr., *Chem Eng.*, **58**, 182 (1951).

A Note on the Additivity of Diffusional Resistances

T. K. SHERWOOD and K. F. GORDON

Massachusetts Institute of Technology, Cambridge, Massachusetts

The additivity of resistances to mass transfer between phases, as postulated by the Whitman two-film theory of 1923, has become an accepted concept in chemical engineering. In an experimental test of this principle, the authors recently reported a study (*1*) of the rate of transfer of fifteen different solutes between liter portions of isobutanol and water in a moderately stirred vessel under conditions such that the interface was essentially flat and of known area.

The over-all resistance (reciprocal of over-all coefficient K_W) was found to be a linear function of the distribution coefficient $1/m$, as called for by the theory, and individual coefficients were obtained from the intercepts and slopes of plots of $1/K_W$ vs. $1/m$.

Individual coefficients k_{IW} for isobutanol into water and k_{WI} for water into isobutanol were also obtained experimentally in extraction tests using water and dry isobutanol, with no third solute present. The agreement between these measured values and those obtained from the analysis of the data on over-all coefficients was only fair for k_{IW} and was poor for k_{WI}.

In analysis of the data to make this comparison it was necessary to correct for variations in molecular diffusivities, and values of both D_{IW} and D_{WI} were taken to be 10.0×10^{-6} sq. cm./sec., based on the estimation from the Wilke correlation (*6*) and on experimental data for the diffusivity of *n*-butanol into water (*3*) and water into *n*-butanol (*5*) taken for a dilute solution. All these gave values in the region of the value used.

Two sets of experimental values of diffusivities have recently become available, and it is worth while to recompute the comparison of individual coefficients. Heertjes, Holve, and Talsma (*2*) report values for D_{IW} and D_{WI} at 20°C. of 6.0×10^{-6} and 2.0×10^{-6} sq.cm./sec., and Lewis (*4*) has obtained values of 8.4×10^{-6} and 3.6×10^{-6} at the same temperature.

On the basis of these new values of diffusivity (adjusted to 25°C.) the values of k_{IW} and k_{WI} obtained from the over-all coefficients for various solutes (from intercepts and slopes of the resistance plot) show much better agreement with the values obtained by direct experiment:

	From over-all coefficients, cm./hr., by use of diffusivities from		By direct experiment cm/hr.	
k_{IW}....	8.0	9.4	9.6	8.36
k_{WI}....	5.4	7.2	11.0	5.9

The new values fall on both sides of those obtained by direct experiment. Evidently the poor comparison reported was due in large part to the use of incorrect values for D_{IW} and D_{WI}.

Figure 1 compares K_W as calculated from the two sources of values for the individual coefficients. Curves *A* and *B*, representing the comparison based on the new experimental values of diffusivities, straddle the solid line representing complete agreement, and both compare much better than curve *C*, previously presented on the basis of estimated values of D_{IW} and D_{WI}. As in the original paper, the transfer coefficients are assumed to be proportional to the square root of the molecular diffusivity.

The data on mass transfer of a number of solutes between stirred volumes of isobutanol and water not only support the additivity concept over a wide range of distribution coefficients, but now appear to agree with the data on individual coefficients.

LITERATURE CITED

1. Gordon, K. F., and T. K. Sherwood, *Chem. Eng. Progr. Symposium Series* No. 10, **50**, 15 (1954).
2. Heertjes, P. M., W. A. Holve, and Talsma, *Chem. Eng. Sci.*, **3**, 122 (1954).
3. Landolt-Bornstein Tabellen, 5 Auflage, Julius Springer, Berlin (1923).
4. Lewis, J. B. *A.E.R.E. C.E./R.* 1120, Atomic Energy Establishment, Harwell, England (1954).
5. Randall, M., B. Longtin, and H. Weber, *J. Phys. Chem.* **45**, 343 (1941).
6. Wilke, C. R., *Chem. Eng. Progr.*, 45, 218 (1949).

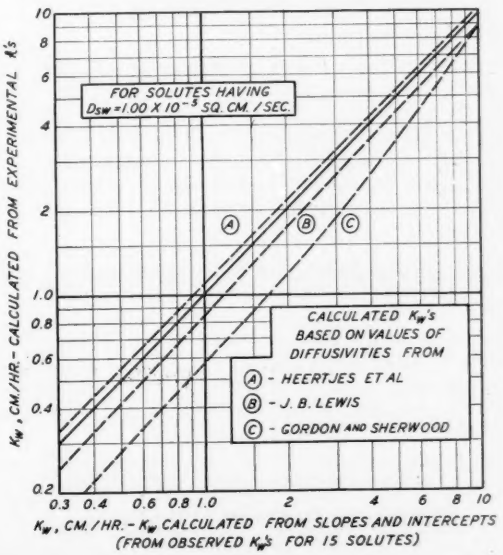
FOR SOLUTES HAVING
D_{SW} = 1.00 X 10⁻⁵ SQ. CM. / SEC.
CALCULATED K_W's BASED ON VALUES OF DIFFUSIVITIES FROM
(A) - HEERTJES ET AL
(B) - J. B. LEWIS
(C) - GORDON AND SHERWOOD
K_W, CM./HR. - CALCULATED FROM EXPERIMENTAL k's
K_W, CM./HR. - K_W CALCULATED FROM SLOPES AND INTERCEPTS
(FROM OBSERVED K_W's FOR 15 SOLUTES)

FIG. 1.

Recent Wiley Books for successful chemistry . . .

CHEMICAL PROCESS PRINCIPLES

Part I—Material and Energy Balances, 2nd Edition

By Olaf A. Hougen, *University of Wisconsin;* Kenneth M. Watson, *The Pure Oil Company; and* Roland A. Ragatz, *University of Wisconsin.* This key reference for solving industrial process problems has been revised and expanded to give a comprehensive, modern treatment of energy balances of chemical processes. Latest physical and chemical constants are included in a wide variety of tables. *1954. 525 pages. Illus. $8.50.*

SUCCESSFUL COMMERCIAL CHEMICAL DEVELOPMENT

Prepared by the Commercial Chemical Development Association. *Editor-in-Chief,* H. M. Corley, *Armour and Company.* "It is a remarkable compilation of the aggressive thinking and the experience of more than a hundred . . . leaders and pioneers in the commercial development of chemical products. . . contains a wealth of information and a variety of points of view seldom found between the covers of a single volume."—D. H. Killeffer, F.A.I.C., in *The Chemist. 1954. 374 pages. $7.75.*

The TECHNOLOGY of SOLVENTS and PLASTICIZERS

By Arthur K. Doolittle, *Carbide and Carbon Chemicals Company.* "Any laboratory or library devoted to the interests of those who specialize in organic coatings, inks, adhesives, plastics or synthetic fibers will find this work to be an invaluable source of information. It would be hard to know where else to turn in order to obtain such complete data presented in such a thorough manner on such a variety of solvents and plasticizers."—*Organic Finishing. 1954. 1056 pages. 461 illus. $18.50.*

SYNTHETIC RUBBER

Editor-in-Chief, G. S. Whitby, *University of Akron.* Prepared under the auspices of the American Chemical Society, this new work offers a first-hand account of the subject, phase by phase, by 37 top-ranking industrial technologists. As well as documenting what has been accomplished so far, it indicates the directions that new synthetics will take. *1954. 1044 pages. Illus. $18.00.*

ORGANIC COATING TECHNOLOGY

Vol. I: Oils, Resins, Varnishes and Polymers

By Henry Fleming Payne, *American Cyanamid Company and Polytechnic Institute of Brooklyn.* A. C. Elm, in *The Octagon,* writes: "It is refreshing to find in this book a new approach to the treatment of an old subject. . . . This book is what it promises in the preface, a compact treatment of current theory and practice of paint vehicle technology, and is highly recommended for careful study by every coatings technologist." *1954. 674 pages. Illus. $12.00*

ADHESION and ADHESIVES: Fundamentals and Practice

Papers read at a Conference held at the University of London (edited by F. Clark, *The Society of Chemical Industry), and at a Symposium held at the Case Institute of Technology (edited by* John E. Rutzler, Jr., *and* Robert L. Savage). *1954. 229 pages. Illus. $9.75.*

Send for your on-approval copies today.

JOHN WILEY & SONS, Inc.

440 Fourth Ave. New York 16, N. Y.

BOOKS

Chemical Process Principles-Part 1, Material and Energy Balances. O. A. Hougen, K. M. Watson, and R. A. Ragatz. Second Edition. John Wiley & Sons, Inc., New York (1954). 525 pages. $8.50.

Professor Ragatz has collaborated with the original authors of the *Chemical Process Principles* series to revise Part 1, "Material and Energy Balances." While retaining the many virtues of the original edition, the authors have increased its utility by the addition of discussions on stagewise extraction, ternary equilibria, and time lag in stirred vessels, and in recognition of the new era R. G. Taecker has contributed a brief section on the thermochemistry of nuclear reactions. Further, two new chapters are found in this edition, one devoted to mathematical procedures and conversion of units, the other to absorption. New methods of estimating physical properties and the latest thermal data are included.

Although the law of corresponding states and the concept of reduced properties are briefly treated in a prelude to the section on methods of estimated critical properties, the generalized compressibility-factor chart is not discussed. Thus the authors proceed from a treatment of ideal-gas behavior directly to reduced and critical properties, including a method of estimating critical compressibility factor, without reference to the most common application of the law of corresponding states. Continuity would seem to be sacrificed here. For example, an apparently promising method of predicting latent heats of vaporization is later in the book presented in terms of reduced properties and gas-liquid compressibility factors, the significance and limitations of which are lost to the student in his ignorance of the generalized compressibility chart. The merits of these chapters for reference purposes are obvious; however, it is the reviewer's experience that the pedagogic value of these portions of the text would have been enhanced by the early introduction of the generalized Z chart. The semimythical character of the ideal-gas concept would thus have been impressed upon the student's mind, and the value and intrinsic limitations of the law of corresponding states could have been made apparent in the light of the authors' discussion of the Lennard-Jones model and molecular polarity. The student must learn as early as possible that chemical engineering tools are not *de fide* truths.

Viewed in its entirety, this edition is a good revision of a good textbook. The authors are to be commended.

JAMES J. CARBERRY
YALE UNIVERSITY